Unconventional Superconductivity and Hybridized Correlated Fermion Systems

Marcin M. Wysokiński

Rozprawa doktorska
Promotor: **Prof. dr hab. Józef Spałek**
Promotor pomocniczy: **Dr Jan Kaczmarczyk**

Uniwersytet Jagielloński

Instytut Fizyki im. Mariana Smoluchowskiego
Zakład Teorii Materii Skondensowanej i Nanofizyki

Kraków 2015

Wydział Fizyki, Astronomii i Informatyki Stosowanej
Uniwersytet Jagielloński

Oświadczenie

Ja niżej podpisany Marcin M. Wysokiński (nr indeksu: 1014521) doktorant Wydziału Fizyki, Astronomii i Informatyki Stosowanej Uniwersytetu Jagiellońskiego oświadczam, że przedłożona przeze mnie roprawa doktorska pt. "Unconventional Superconductivity and Hybridized Strongly Correlated Fermion Systems" jest oryginalna i przedstawia wyniki badań wykonanych przeze mnie osobiście, pod kierunkiem prof. dr hab. Józefa Spałka. Pracę napisałem samodzielnie.

Oświadczam, że moja rozprawa doktorska została opracowana zgodnie z Ustawą o prawie autorskim i prawach pokrewnych z dnia 4 lutego 1994 r. (Dziennik Ustaw 1994 nr 24 poz. 83 wraz z późniejszymi zmianami).

Jestem świadom, że niezgodność niniejszego oświadczenia z prawdą ujawniona w dowolnym czasie, niezależnie od skutków prawnych wynikających z ww. ustawy, może spowodować unieważnienie stopnia nabytego na podstawie tej rozprawy.

Kraków, dnia 12.08.2015

.....
podpis doktoranta

Ze szczególną dedykacją dla mojej wspaniałej Rodziny: żony Anny i syna Jakuba

Contents

Acknowledgments

I would like to express my gratitude to Prof. Józef Spałek for suggesting the research subject that is presented in this Thesis and thorough supervision over the past 6 years (including M.Sc. studies). Especially, I appreciate pointing out to me that physicist should never forget that the Physics is an experimental science and that it is the Nature giving the final answer to the raised questions. Apart from that, I am very grateful to him for critical reading of this Thesis and the multitude of his corrections.

I am also grateful to my supporting advisor dr Jan Kaczmarczyk for his help and multiple advices on both technical and meritorical level during my PhD studies.

I would like to acknowledge collaboration with Marcin Abram with whom I have cooperated fruitfully and with great pleasure over the part of the presented work in this Thesis. The discussions with the Jörg Bünemann are also appreciated.

Furthermore, I would like to thank other members (present and former) of the Department of Condensed Matter Theory and Nanophysics: Dr hab. Andrzej Kapanowski, Dr hab. Adam Rycerz, Dr Danuta Goc-Jagło, Dr Jakub Jędrak, Dr Olga Howczak, Grzegorz Rut, Andrzej Kądzielawa, Ewa Kądzielawa-Major and Patryk Kubiczek for a nice and friendly atmosphere.

I also would like to thank my Father who has successfully injected in me the excitement in physics, and for countless scientific discussions, and to my Mother who is always extremely patient in listening to us. Moreover, I am grateful to both of them for their enormous support. I am also grateful to both of my Sisters and my Brother for helpful advices. Additional thanks are due to my Brother for first setting and then sending me citation alerts of my works.

Finally, and most importantly I would like to express my deep gratitude to my dearest and beloved Family, my Wife Ania and Son Jakub who are my inexhaustible source of support, inspiration, motivation, and love.

Funding

During three years of my PhD studies I was granted with the scholarship from the DOCTUS project of *Małopolskie Centrum Przedsiębiorczości*, co-funded by the European Union under the European Social Fund. The financial support from the Foundation for Polish Science (FNP) within project TEAM (2011-2015) and from the National Science Centre (NCN) under the project MAESTRO, Grant No. DEC-2012/04/A/ST3/00342, are gratefully acknowledged. This Thesis was completed as a part of all these projects.

List of Abbreviations and Symbols

- BCS theory - the Bardeen, Cooper, Schrieffer theory of conventional superconductivity
- GWF - Gutzwiller wave function
- DE-GWF - diagrammatic expansion for the Gutzwiller wave function
- GA - Gutzwiller approximation
- SGA - statistically consistent Gutzwiller approximation
- VMC - variational Monte Carlo method
- SC - superconductivity, superconducting
- FM - ferromagnetism, ferromagnetic
- FM1 - weak-ferromagnetic phase in UGe_2
- FM2 - strong-ferromagnetic phase in UGe_2
- HFS - heavy fermion systems
- ALM - Anderson lattice model, frequently referred to in the literature also as the periodic Anderson model
- HM - Hubbard model
- KLM - Kondo lattice model
- QCP - quantum critical point
- CEP - critical ending point
- TCP - tricritical point
- QCEP - quantum critical ending point

Selected used mathematical symbols

- $\langle\psi_0|...|\psi_0\rangle \equiv \langle...\rangle_0$
- $\frac{\langle\psi_G|...|\psi_G\rangle}{\langle\psi_G|\psi_G\rangle} \equiv \langle...\rangle_G$
- $\hat{\mathcal{P}}_G$ - Gutzwiller projection operator
- T_S - superconducting critical temperature
- T_N - Néel temperature
- T_K - Kondo temperature
- $\hat{c}^{(\dagger)}_{\mathbf{i},\sigma}$ - annihilation (creation) operator for conduction band Wannier state $|\mathbf{i}\sigma\rangle$
- $\hat{f}^{(\dagger)}_{\mathbf{i},\sigma}$ - annihilation (creation) operator for originally localized f-state $|\mathbf{i}\sigma\rangle$

Abstract

In this Thesis we model theoretically selected physical properties of strongly correlated materials. The particular emphasis is put on the heavy fermion systems revealing unconventional superconductivity and other interesting properties such as: (i) very large (and spin-direction-dependent) effective mass of the quasiparticles, (ii) itinerant magnetism connected with the unconventional superconductivity of the same electrons, (iii) classical and quantum criticalities, to name just a few examples. Wherever possible, we compare our theoretical results with experiment, either qualitatively or (semi)quantitatively. As an additional project, we also include other works connected with the analysis of thermoelectric transport in hybrid superconductor - normal metal junctions.

Our approach to correlated systems is based on the variational Gutzwiller wave function method, here applied to Hubbard (HM) and Anderson-lattice (ALM) models. We start with the analysis within the so-called *statistically consistent Gutzwiller approximation* (SGA) developed in our group in the last five years. Within this approach, here regarded as the zeroth-order approximation of the full Gutzwiller wave function solution, first we analyze three-dimensional HM on fcc lattice. On this basis we investigate general properties of neutral fermions in the applied magnetic field such as dependency of magnetization, specific heat, and spin-direction-dependent effective quasiparticle masses. Additionally, the critical comparison to the normal liquid ^{3}He is drawn. Within the same approach applied to ALM, we analyze in quantitative terms the magnetic properties of a moderate heavy fermion and ferromagnetic system UGe_2. The emphasis is put on classical and quantum criticalities and related two magnetic phase transitions, at temperature $T = 0$ and $T > 0$, respectively. Our work represents the first such complete analysis for UGe_2 within a microscopic model. We turn next to a systematic diagrammatic expansion for the Gutzwiller wave function (DE-GWF), developed earlier for the Hubbard and t-J models. Here we develop the method for ALM and show explicitly that unconventional d-wave superconductivity appears in the system induced solely by electronic correlations when we go beyond the zeroth-order. This result is the first of its kind.

Our additional project involves analysis of thermoelectrical transport through the junction consisting of superconductor and normal metal. We extend the so-called Blonder-Tinkham-Klapwijk formalism to incorporate an explicit energy dependence of the density of states around the Fermi level, resulting in nonzero thermopower across the hybrid normal metal - insulator - superconductor NIS junction. Our approach is used to analyze among others, the Seebeck effect in the graphene-based conductor - superconductor junction.

Keywords: strongly correlated systems, superconductivity, magnetism, ferromagnetism, heavy fermion systems, real-space pairing, Anderson lattice model, Hubbard model, Gutzwiller approximation, diagrammatic expansion for Gutzwiller wave function, variational approach, Ce-based systems, UGe_2, quantum critical points, classical critical points, normal liquid ^{3}He, spin-direction dependent quasiparticle effective masses, f-electron systems, f electron direct itineracy.

Streszczenie

Niniejsza rozprawa dotyczy opisu teoretycznego wybranych własności fizycznych dla układów silnie skorelowanych fermionów. Szczególna uwaga jest poświęcona związkom ciężko-fermionowym przejawiającym m.in.niekonwencjonalne nadprzewodnictwo, jak i inne interesujące zjawiska takie jak: (i) bardzo duże (zależne od kierunku spinu) kwazicząstkowe masy efektywne, (ii) magnetyzm pasmowy powiązany z nadprzewodnictwem tych samych elektronów, (iii) klasyczne i kwantowe punkty krytyczne. W większości wypadków znajdujemy jakościowe a w niektórych wypadkach ilościowe potwierdzenie naszych przewidywań teoretycznych z danymi eksperymentalnymi dotyczących ciekłego ^{3}He w stanie normalnym a także ciężkofermionowego nadprzewodnika UGe_2. Jako dodatkowy projekt dołączono do niniejszej rozprawy analizę transportu termoelektrycznego w hybrydowych nadprzewodzących złączach tunelowych metal-izolator-nadprzewodnik.

Metodą opisu własności silnie skorelowanych układów w pracach stanowiących tę rozprawę jest wariacyjna metoda bazująca na funkcji falowej Gutzwillera (GWF), zastosowana do modeli Hubbarda i sieci Andersona. Metoda przybliżonego rozwiązania, stanowiąca zerowy rząd rozwinięcia diagramatycznego dla GWF, tzw. *statystycznie konsystentne przybliżenie Gutzwillera* (SGA) została zastosowana do opisu własności magnetycznych skorelowanych fermionów takich jak, magnetyzacja, ciepło właściwe i zależne od kierunku spinu kwazicząstkowe masy efektywne w ramach modelu Hubbarda na sieci fcc. Przewidywania zostały porównane z danymi eksperymentalnymi dotyczącymi ciekłego ^{3}He w fazie normalnej. W ramach tej samej metody, zastosowanej do modelu sieci Andersona, przeanalizowane zostały magnetyczne właściwości ferromagnetycznego nadprzewodnika ciężkofermionowego UGe_2. Na tej podstawie skonstruowana została pierwsza mikroskopowa teoria wyjaśniająca powstawanie magnetyzmu w tym związku tłumacząca główne eksperymentalne pomiary, w szczególności obserwowane klasyczne i kwantowe punkty krytyczne. Dokładniejsza, w porównaniu do SGA, metoda diagramatycznego rozwinięcia dla funkcji falowej Gutzwillera, została z kolei sformułowana i zastosowana do modelu sieci Andersona i użyta do przewidzenia właściwości zhybrydyzowanych układów w stanach paramagnetycznym i nadprzewodzącym. Otrzymane niekonwencjonalne nadprzewodnictwo o symetrii *d-wave* parametru porządku dla modelu sieci Andersona jest jedynym takim rezultatem w literaturze światowej.

Dodatkowy projekt dotyczy analizy transportu termoelektrycznego poprzez złącza hybrydowe metal - izolator - nadprzewodnik. Formalizm Blondera-Tinkhama-Kalpwijka został rozszerzony o efekt zależnej od energii gęstości stanów w pobliżu poziomu Fermiego, którego uwzględnienie prowadzi do skończonego sygnału Seebecka w rozważanej klasie układów tunelowych. Opracowany rozszerzony formalizm użyty został także do obliczenia siły termoelektrycznej w nadprzewodzącym złączu hybrydowym na bazie grafenu.

Słowa kluczowe: silnie skorelowane układy, nadprzewodnictwo, magnetyzm, ferromagnetyzm, układy ciężko-fermionowe, układy f elektronów, parowanie w przestrzeni rzeczywistej, model sieci Andersona, model Hubbarda, przybliżenie Gutzwillera, diagramatyczne rozwinięcie dla funkcji falowej Gutzwillera, podejście wariacyjne, układy na bazie ceru, UGe_2, kwantowe punkty krytyczne, klasyczne punkty krytyczne, ciekły ^{3}He w fazie normalnej, spinowo-zależne kwazicząstkowe masy efektywne, bezpośrednia wędrowność f elektronów.

Chapter 1

Introduction and Motivation

1.1 Superconductivity

Over 100 years ago Heike Kamerlingh-Onnes observed[1] a complete loss of electrical resistance in solidified mercury after colling it down to the temperature $T_S = 2.17K$. This phenomenon called the superconductivity, subsequently turned out to occur in different metallic elements. Despite the engagement of the greatest minds of the first half of the twentieth century, such as Albert Einstein and Richard Feynman[2], for an almost fifty years the microscopic mechanism of superconductivity remained elusive.

Nevertheless, the understanding of the superconductivity was enlarged due to the phenomenological approaches, mainly by that by Vitaly Ginzburg and Lew Landau [1]. Their φ^4 theory with the genuine assumption of the global wave function being order parameter provided a successful explanation of many effects associated with superconductivity. For instance, on the basis of this approach Alexei Abrikosov provided the explanation of formation of hexagonal lattice of quantized vortices when a strong magnetic field is applied to the thin film of type II superconductor [2].

In 1957 the microscopic description of the superconductivity was formulated, the so-called BCS theory (from first letters of authors names: Bardeen, Cooper, Schriefer) [3]. It was explained that the phenomenon appears due to the phonon mediated attractive interaction between electrons. BCS theory being mean-field self-consistent approach turned out to accurately describe the thermodynamic and electromagnetic properties of the so-called conventional (type I) superconductors [4]. BCS theory was immediately explored and reformulated to the forms proved to be crucially important in the later developments. The extension to the spatial dependence of the superconducting order parameter was provided by Nikolaj Bogoliubov [5] and Pierre Giles de Gennes[4]: see also Valatin [6]. The derivation of the phenomenological Ginzburg-Landau approach from BCS theory was provided by Lew Gor'kov [7] using the Green's function approach. Adopting methodology of Lew Gor'kov, Gerasim Eliashberg formulated the microscopic theory of the superconductivity in the strong electron-phonon interaction limit [8].

When conventional superconductivity was claimed to be understood, new experi-

[1] To be precise, his technician did, but no information concerning his personal data are known.

[2] Einstein has claimed that superconductivity emerges due to the closed rings of electrons formation and supercurrent is flowing due to the cyclic shifts of charges. Before publishing his work, the experiment known today as Josephson effect was carried out and rebutted his theory. Feynman worked on the topic for several years using mainly perturbation theory with no success at all.

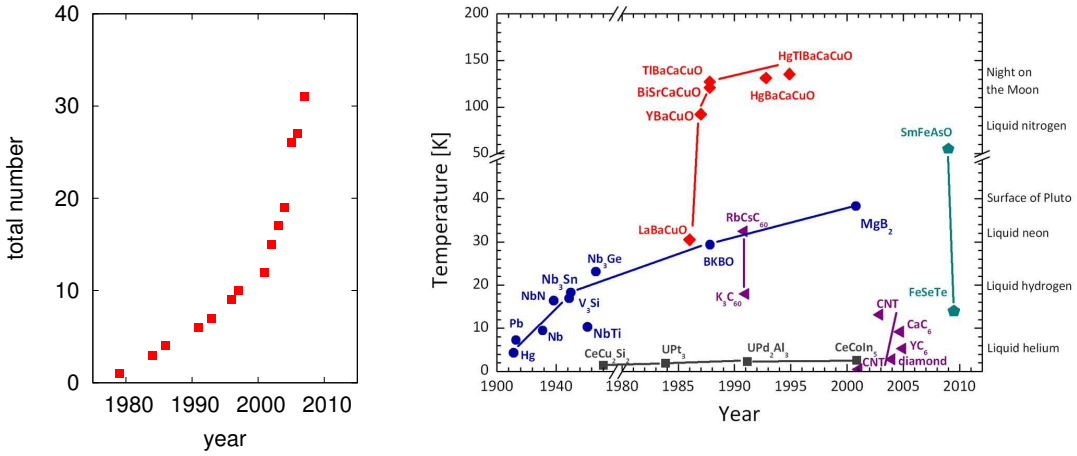

Figure 1.1: Left panel: Growth of the number of known heavy fermion superconductors with time up to 2009 (after Ref. [9]). Right panel: Superconducting critical temperature for selected materials with time up to 2010. Blue circles denote - conventional BCS systems, black squares - heavy fermion superconductors, red diamonds - high temperature cuprate superconductors, magenta triangles - organic superconductors, and sea green pentagons - iron-based high temperature superconductors (from *http : //dpmc.unige.ch/gr_gaps/index.html*). Not shown is the recently discovered (2014) sulfur hydride H_2S under pressure showing superconductivity at up to $203K$ [10].

mental discoveries have resulted in new issues that are still lacking a widely accepted theoretical interpretation. The first discovery was the transition to the superconducting phase below 1 K observed for the heavy fermion compound $CeCu_2Si_2$ in 1979 by Frank Steglich *et al.* [11] and second, the observation of the superconducting transition at unprecendentedly high critical temperature of about 30 K in LaBaCuO in 1986 by Johannes G. Bednorz and Karl A. Müller [12]. In both of these materials, due to the strong Coulomb interaction, the phonon mediated mechanism of pairing seems highly unlikely. In view of this fact, the conventional BCS theory has no application to this class of systems. Thus, the discoveries of the unconventional superconducting systems call for a new theory comprising the strong interactions (correlations) between electrons. The family of non-BCS systems, as termed *unconventional superconductors*, including both the superconducting heavy fermion systems and the high temperature superconductors, over time was enlarged with plenty of new members (cf. Fig.1.1). In this family also the organic [13] and iron-based [14] superconductors are included.

The ubiquity of the paired states in various compounds suggests that, in principle, superconductivity is rather a rule than exception. In fact, it is believed nowadays that the superconductivity is one of the few emergent phenomena that can be realized on all energy scales (cf. Fig. 1.2). What changes is the kind of particles and the origin of interaction that couples them. In the systems such as cuprates and heavy fermion systems the electrons are forming pairs with the nature of attraction between them is still not completely clear.

The novelty of the unconventional superconductivity is that, contrary to the conven-

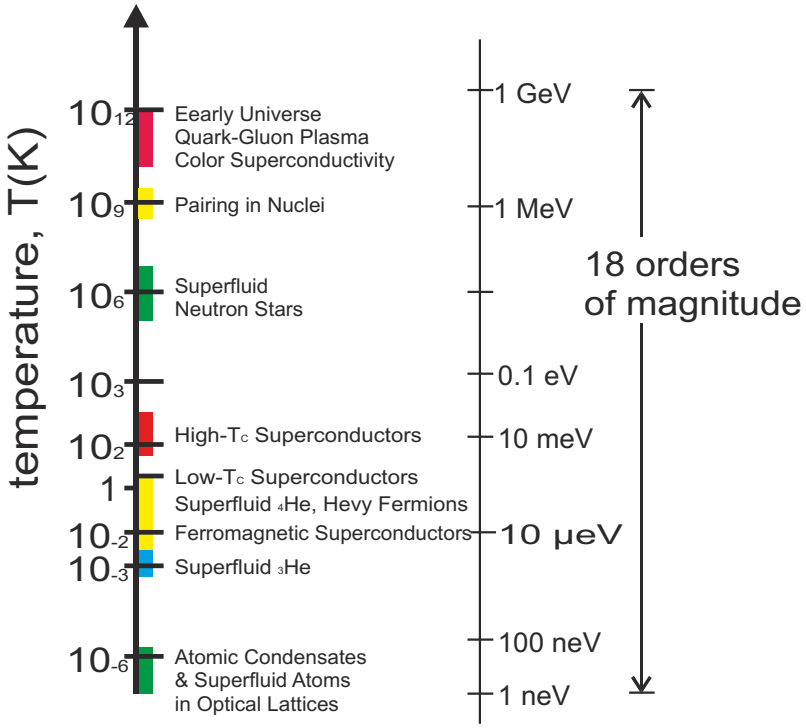

Figure 1.2: Schematic representation of the fundamental fact that superconductivity (superfluidity) is realized on all energy scales. (From [15])

tional BCS type, it appears in the systems with strong Coulomb interactions that for the conventional BCS theory is suggested to compete with the phonon-mediated attractive force [3, 16]. Also unconventional SC often happens to appear concomitantly with magnetism, either antiferro- or ferro-magnetism [9], either cooperating or competing. As a concrete example, the first observed coexistence of weak itinerant ferromagnetism and unconventional superconductivity in Y_9Co_7 by A. Kołodziejczyk, et al. [17, 18, 19] has the nature that points out to the mutual competition between those phases. On the other hand, twenty years later such exotic coexistence was discovered in the UGe_2 [20] and subsequently in URhGe [21] and UCoGe [22]. In these cases though, various experiments [9, 23, 24, 25] undoubtedly have indicated that both phases are strongly intertwined. It must be emphasized that by coexistence or competition between phases we mean here the states involving the same electrons.

However, what is certain and indisputable is that any theory pretending to resolve the issue of superconductivity mechanism particularly in the high temperature superconductors or heavy fermion systems, must account for the strong correlations between the relevant electrons. Moreover, as the Coulomb interaction represents the largest energy scale in those systems the repulsive interaction by itself can lead to the effective pairing. It naturally leads to the idea of *real-space pairing*, description of which on the example of the heavy fermion systems, is one of the aims of this Thesis.

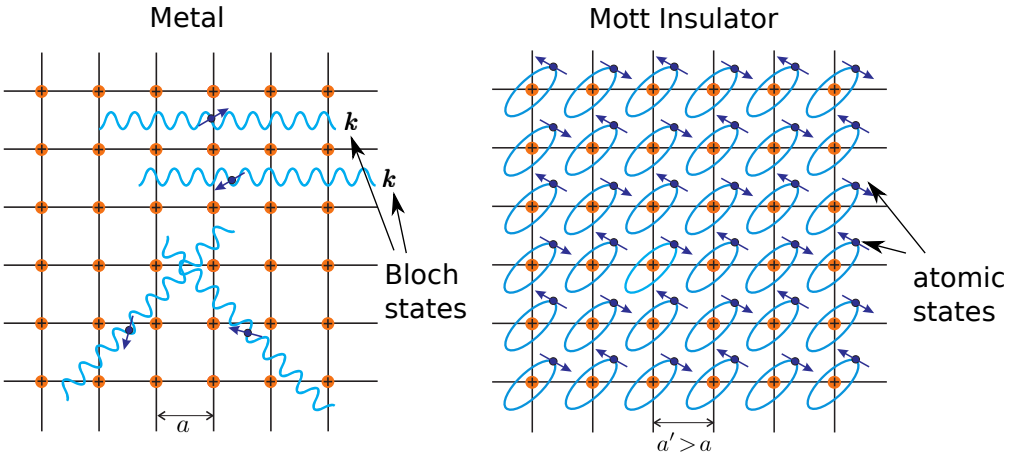

Figure 1.3: Schematic representation of a metallic (left) and the Mott-insulating (right) states on example of artificial hydrogen lattice containing only one valence electrons per atomic site (red points). (after Ref. [28])

1.2 Strongly Correlated Systems

In quantum mechanics only a limited number of problems can be solved exactly [26, 27]. However, one could systematically explore many problems in the approximate manner, among them by means of the perturbation theory. In general, this theory is useful when the Hamiltonian describing quantum system at hand can be divided into a solvable part and a significantly smaller perturbation.

Perturbation theory naturally is not applicable when the interaction is not small but comparable to the solvable part of the Hamiltonian. Such situation appears when one describes the class of systems called strongly correlated[3], i.e., when the interaction between particles is at least comparable to their kinetic (band) energy. From the competition of those two factors many nontrivial effects appear, some of which will be described on a selective basis in the following.

The archetypal system revealing sizable interactions is normal liquid ^{3}He with the total atomic spin $\frac{1}{2}$, thus can be treated as a quantum liquid of fermions. At low temperatures, $T \leq 4K$, the length of the thermal de Broglie wave of ^{3}He atoms in liquid state is of the same order as an average spacing between them. This was the first clue that normal liquid ^{3}He has quantum nature [29]. In fact, several non-trivial observations having their origin in the sizable van der Waals repulsive forces between atoms were made. One of them is the significant enhancement of the effective mass of the atoms roughly by factor of 3 at the ambient pressure, visible among others in their Fermi distribution from neutron scattering data [30] and the value of the linear specific heat coefficient [31, 32].

The first theory accounting for the sizable correlations and successfully provide semi-complete explanation of this quantum liquid (e.g. effective mass enhancement, second sound) was the seminal Landau's Fermi-liquid phenomenological theory [33]. Latter, a

[3] *Strongly interacting systems* would be more precise description. However, historically such term was already reserved for the high energy physics, therefore term *strongly correlated* was introduced instead.

microscopic model[4] was derived by John Hubbard [34, 35, 36, 37],

$$\hat{\mathcal{H}}_{HM} = \sum_{\mathbf{i},\mathbf{j},\sigma} t_{\mathbf{ij}} \hat{c}^{\dagger}_{\mathbf{i}\sigma} \hat{c}_{\mathbf{j}\sigma} + U \sum_{\mathbf{i}} \hat{n}_{\mathbf{i}\uparrow} \hat{n}_{\mathbf{i}\downarrow}, \tag{1.1}$$

and turned out to be one of the cornerstones in the physics of strongly correlated systems. The model comprises only the two parts: single particle (kinetic) energy of fermions on the lattice and the two-body intrasite Coulomb interaction. Hubbard model was treated by the approximate methods e.g. variational Gutzwiller approach [36, 38] and slave-boson method [39, 40], what has given enormous insight into the phenomena concerning physics of the strongly correlated systems.

One of the earliest concepts, first insightfully proposed by Nevill Mott [41] was the metal-to-insulator transition [42, 43, 44]. Configuration of the free electron gas on the lattice (assuming one electron per site) is limited only by the Pauli exclusion principle. By means of Bloch theorem one can make transformation to the momentum space providing appropriate set of the quantum numbers and consider system as a set of delocalized particles composing the metallic Fermi sea (cf. Fig. 1.3, left panel). If the Coulomb repulsive force between electrons is switched on adiabatically[5], the system for the critical interaction undergoes a phase transition to the insulating state, where all particles are localized (cf. Fig. 1.3, right panel). Roughly speaking, this transition can be understood as a blocking of electron mobility due to negative difference balance the gain from their kinetic energy and the cost of the Coulomb energy, when particles come close. The system believed originally to exhibit such physics was the normal liquid ^{3}He considered as an almost localized Fermi liquid [48]. Though, on the basis of comparing magnetization curve with the experimental measurements [49] such understanding may not to be fully justified [38].

In terms of Mott systems in solids, there exist materials that exhibit intermediate properties between ordinary metals and magnetic Mott insulators, such as V_2O_3, $La_{2-x}Sr_xCuO_4$, $NiS_{2-x}Se_x$, and SmS, where the transition from one state to the other can be triggered by temperature, pressure or alloy composition. Metals are well described by the Bloch theory, whereas $3d$ and $4f$ states in magnetic insulators by the atomic approaches based solely on the Heisenberg exchange interactions. Development of the approach bridging those states in a systematical manner was a challenging task. For instance, the phase diagram of the alloyed canonical system of $(V_{1-x}Cr_x)_2O_3$ was rationalized on the basis of Hubbard model with an inclusion of the antiferromagnetic exchange interactions [50, 51].

In parallel to the investigations of the Mott metal-to-insulator transition, Hubbard model was studied in terms of the ferromagnetic and antiferromagnetic instabilities. In the former case, one can derive the Stoner criterion for ferromagnetism appearance for itinerant electrons. On the other hand, for nearly half-filled band, an onset of antiferromagnetism turns to be energetically favorable against the paramagnetism.

Real interest in the problem of strongly correlated systems intensified after the discovery of unconventional superconductivity in the cuprates [12], where the onset of super-

[4]Here we provide only the simplest version of the Hamiltonian; a detailed discussion is given in the Sec. 1.5.

[5]The condition for the adiabatic change is necessary in order to ensure the ground state would be constantly in the equilibrium. The situation when the interaction is increased on the relevantly faster time scale is under the present study of the physics of the so-called quantum quenches in strongly correlated fermion systems [45, 46, 47].

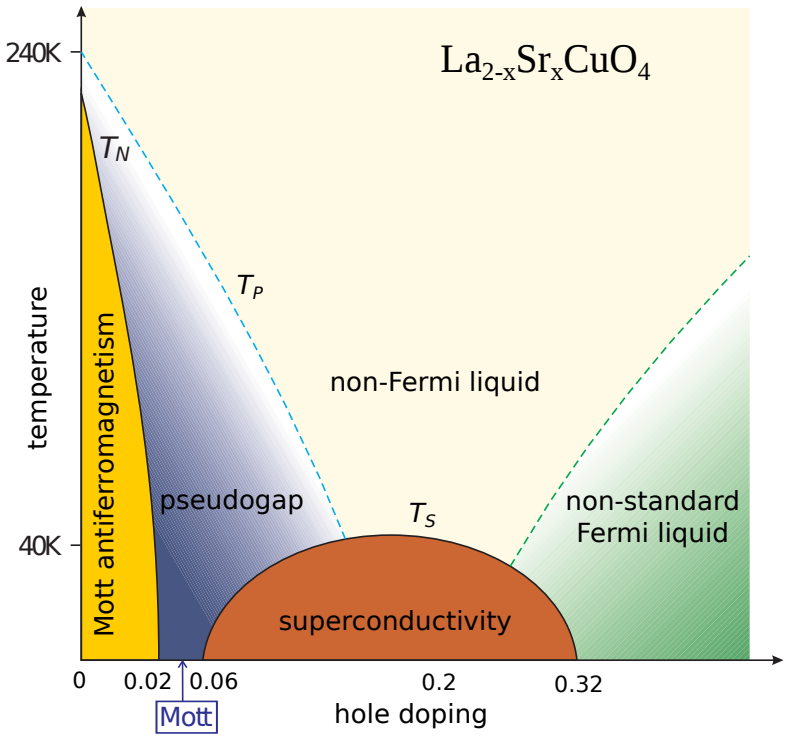

Figure 1.4: Schematic phase diagram on the hole doping - temperature plane for the high temperature superconductor $La_{2-x}Sr_xCuO_4$. The characteristic temperatures are: Néel temperature, T_N, superconducting critical temperature, T_S, and the temperature for the onset of the pseudogap, T_P. (From [28])

conductivity is in the vicinity of the Mott transition (cf. phase diagram of $La_{2-x}Sr_xCuO_4$ - Fig. 1.4). The repulsive interactions are here the largest energy scale in the system and are responsible for the superconducting instability. Despite intensive studies and understanding of several issues concerning high temperature superconductors [52, 53, 54], the nature of this unconventional paired phase itself and the mechanism responsible for its emergence is still not completely understood. Here we take the view that all discussed phenomena are induced by the strong correlations as the sole cause.

Main microscopic models believed to properly described phenomenon of high temperature superconductivity is the already mentioned Hubbard model [55] and its derivative [56, 57, 58], t-J model [59, 60].

In terms of a two dimensional Hubbard model, there are limited number of techniques that are able to properly treat superconducting correlations. These are: Variational Monte Carlo (VMC) [61], Dynamical Mean-Field Theory (DMFT) [62, 63], Dynamical Cluster Approximation (DCA) [64] and recently proposed Diagrammatic Expansion for the Gutzwiller Wave Function (DE-GWF) [55]. The t-J model is well suited for studying the superconductivity, as already on the level of the Hartree-Fock-type of approximation it reduces to the effective BCS-like Hamiltonian. Moreover, this model treated by so-called Renormalized Mean-Field Theory (RMFT) provides reasonable description of principal physical properties of high temperature superconductors [60]. Quite often, for a more realistic description of cuprates the extended version, the t-J-U model is con-

sidered [65]. In this case, the additional repulsive Hubbard term, in addition to the exchange interaction with exchange integral value J taken into account.

1.3 Heavy Fermion Materials

Heavy fermion (HF) materials are one of the principal classes of strongly correlated systems and are usually referred to as f electron systems. All those compounds belong to this group contain elements with partially filled $4f$ or $5f$ valence shell. The origin of the name *heavy fermions* has its origin in the unusually large enhancement of the electrons effective mass up to 1000 times as compared to that for free electron gas. Such behavior was first observed in $CeAl_3$ in 1975 [66] on the basis of strong renormalization of the linear specific heat coefficient. Apart from that, this type of result revealing the heavy fermion behavior appears also in the magnetic susceptibility, the electrical resistivity [67], and the de Haas-van Alphen oscillation [68] measurements. At the beginning, the strong mass renormalization was regarded as mere curiosity until the discovery of superconductivity in $CeCu_2Si_2$ which started an enormous interest in this class of materials. Heavy fermion systems were the first electron materials exhibiting non-BCS pairing,[6] and after this discovery a *new era* of unconventional superconductivity begun.

With the increasing number of the heavy fermion compounds unique scaling properties have been were observed. First of them was the Kadowaki-Woods scaling [70] (cf. Fig. 1.5, left panel) consisting of the linear relation between the linear-specific-heat coefficient, γ and the coefficient A for T^2 law for the resistivity, known earlier to hold for the transition metals [71]. Moreover, f-electron systems also follow a linear scaling of γ against the Pauli susceptibility $\chi(0)$, as predicted for the ideal electron gas - called the Wilson scaling (see e.g. [72]) (cf. Fig. 1.5, right panel).

Based on these scaling phenomena one can infer that apart from the mass renormalization the heavy fermions exhibit the behavior much alike the simplest ideal electron gas. However, they exhibit also highly non-trivial effects originating from an almost localized nature of electrons originating from the f shell. The most spectacular was already mentioned unconventional superconductivity, for discussion of which we devote the next section. The other phenomenon that attracted lots of attention in heavy fermions is the persistence of some features associated with the impurity, as e.g. Kondo effect [73]. Originally, it was studied as a way to understand anomalies of the increasing resistivity below the Kondo-temperature, T_K in the simple metallic materials containing a small amount of magnetic impurities. It was explained on the basis of coherent interaction of a single localized $\frac{1}{2}$ spin of the magnetic impurity with the spins of the Fermi sea of conduction electrons. In effect below T_K the groundstate of the system is the total spin singlet of the combined local system composed of magnetic moment and the spins from the conduction band, sometimes referred to as creation of the compensation cloud (cf. Fig. 1.6, left panel, A and B). The increase of the resistivity below T_K is due to the spin-flip scattering of carriers on the localized spin.

In the case of heavy fermions, the Kondo-like effect are much more complicated. Here the f electrons compose a periodically arranged lattice of magnetic impurities. Such system is frequently described by the Kondo lattice model (KLM) comprising of

[6] Precisely, the first unconventional superconductor was ^{3}He where superfluidity between neutral atoms emerges without the ionic lattice and is mediated by the spin-fluctuation exchange [69].

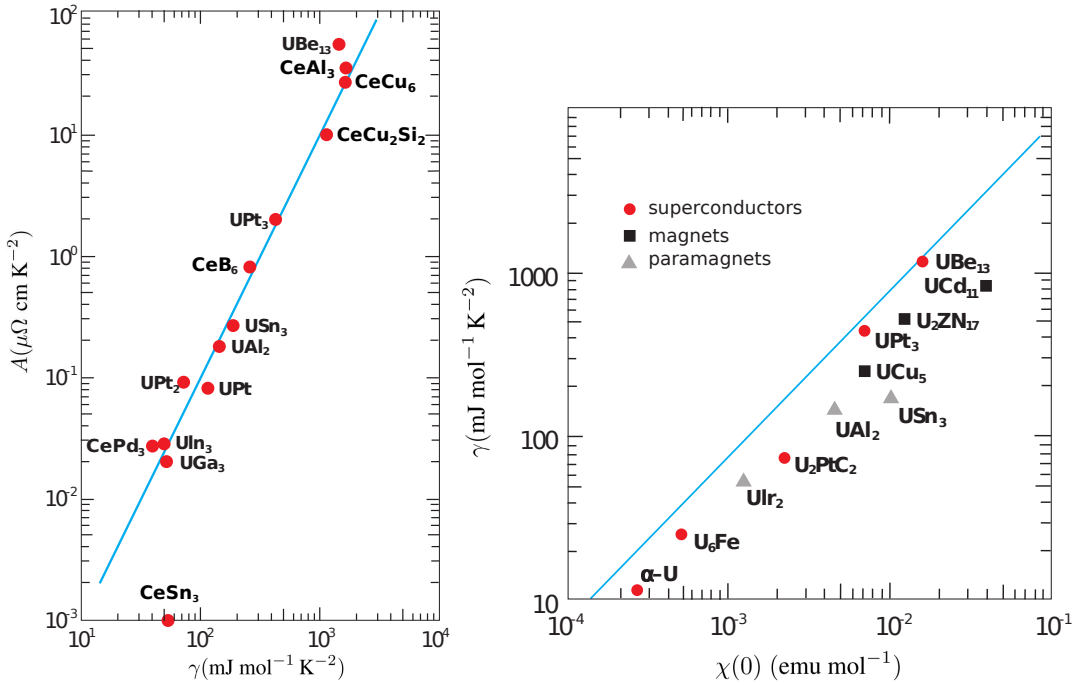

Figure 1.5: The Kadowaki-Woods (left panel) and the Wilson (right panel) scalings for the selected heavy fermion compounds. Both plots illustrate in a clean manner the Fermi-liquid properties for these systems with an extremely high effective masses of quasiparticles. (From [28], after [72])

the lattice of the localized f spins coupled by the effective antiferromagnetic (Kondo) exchange interaction with the conduction band[7], i.e.,

$$\hat{\mathcal{H}} \equiv \hat{\mathcal{H}}_{KLM} = \sum_{\mathbf{i},\mathbf{j},\sigma} t_{\mathbf{ij}} \hat{c}^{\dagger}_{\mathbf{i}\sigma} \hat{c}_{\mathbf{i}\sigma} - J^K \sum_{\mathbf{i}} \hat{S}_{\mathbf{i}} \cdot \hat{s}_{\mathbf{i}}, \tag{1.2}$$

where J^K is the value of the corresponding exchange integral[8]. This model leads, among others, to understanding of the heavy-Fermi-liquid behavior observed in HF systems. It turns out that by means of the Schrieffer-Wolff transformation [85] the above model can be derived from the more universal Anderson lattice model (ALM), which is defined and explained in detail in the following Sec. 1.5.

It is worth mentioning that although the Kondo-like effects within the class of strongly correlated systems is connected to the heavy fermion materials, indirectly have led to the better understanding of the whole range of systems with the strong interactions as such. It is due to the single Anderson impurity problem being at the heart of the dynamical mean field theory (DMFT) - one of the most successful approaches, among those not requiring large computing power, to treat the electronic strong correlations [86, 87, 88, 89, 90].

[7] In the following operators $\hat{c}^{(\dagger)}$ are responsible for creation (annihilation) of the electrons from conduction band, $\hat{s}$ is the spin operator for those electrons and $\hat{S}$ is the spin operator for f electrons.

[8] Such exchange apart from KLM explicitly appears in the context of other models, such as Anderson-Kondo and Kondo-Heisenberg lattice models, where it is frequently considered as a source of the superconducting pairing in HF materials [77, 78, 79, 80, 81, 82, 83, 84].

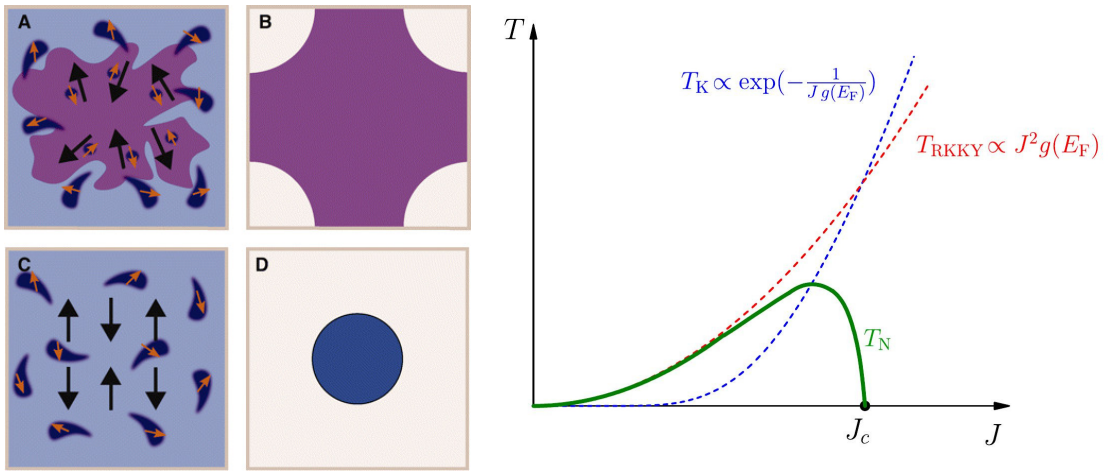

Figure 1.6: (Left panel) Simplistic visualization of the heavy Fermi liquid state due to Kondo interaction in the heavy fermion compounds (A) with resulting large Fermi surface (B) and antiferromagnetism due to the RKKY interaction (C) with resulting small Fermi surface (D) (after Ref. [74]). (Right panel) Schematic phase diagram proposed by Doniach [75] (after Ref. [76]). Antiferromagnetism is terminated for critical J_C and subsequently heavy Fermi liquid arises at $T < T_K$. This interpretation of the Kondo compensation can be regarded only as an illustration as it is based on the assumption of f-electron localization, which is not completely true in the heavy fermion case.

Apart from the Kondo interaction, also the so-called RKKY[9] interaction [91, 92, 93] can be crucially important in heavy fermion materials in which the spins are practically localized. On the basis of the fourth-order perturbation theory within ALM it can be shown that the f-electron magnetic moments couple with each other with the interaction mediated by the conduction electrons. The effective exchange integral oscillates with a distance, and in some cases it can lead to the antiferromagnetic interaction (cf. Fig. 1.6, left panel, C and D). As proposed by Doniach the comparison of the characteristic temperatures for the RKKY interaction and Kondo effect leads to a semi-universal phase transition in f electron systems between antiferromagnetism and the heavy-Fermi-liquid (cf. Fig. 1.6, right panel). However, the phase diagrams for heavy fermion systems are usually much more complicated than that proposed by Doniach. This is because in the *Doniach model* we assume explicitly that the f-spins are localized. This is not true in general [82, 94, 95, 96]. Furthermore, there are still many unresolved issues such as properties of the system due to the presence of quantum ciritical point and the origin of the unconventional superconductivity. The next section is devoted to a brief and selective overview of the experimental properties related to the latter issue.

1.4 Heavy Fermion Superconductors

Superconductivity in heavy fermion systems is unconventional due to the fact that (conventional) BCS theory based on the electron-phonon coupling has failed to describe

[9] After the first letters of the names: M.A. Ruderman, C. Kittel, T. Kasuya and K. Yosida.

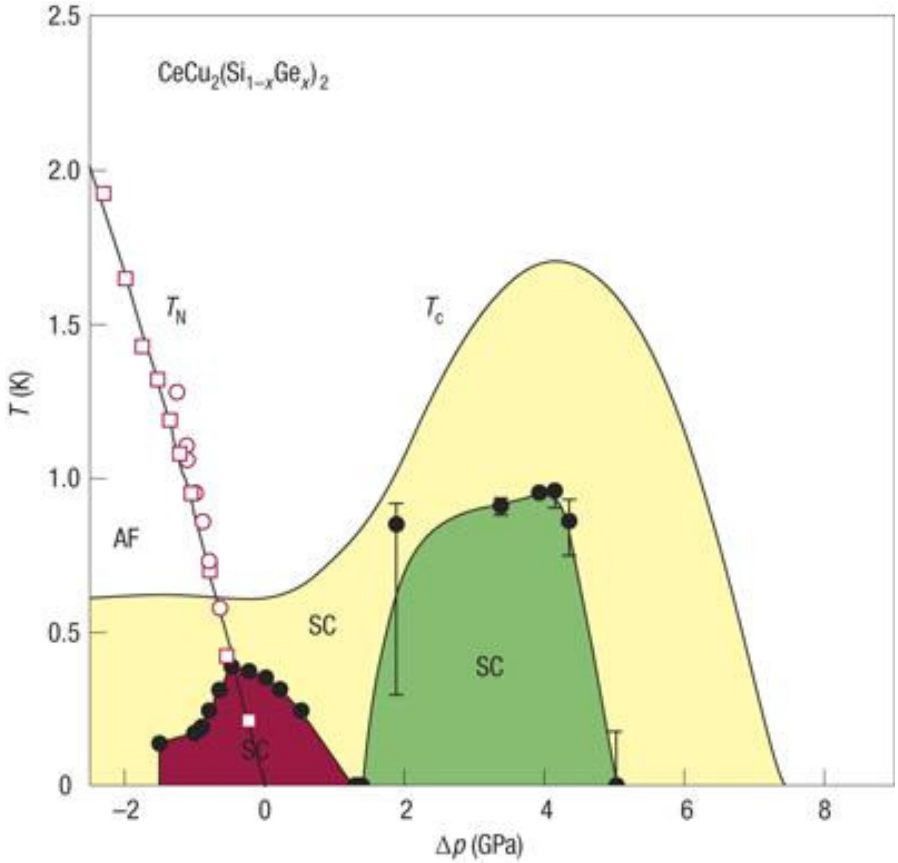

Figure 1.7: Phase diagram of the $CeCu_2(Si_{1-x}Ge_x)_2$ revealing two distinct superconducting domes (after Ref. [97]).

its properties in this case. Within the group of the so-called BCS superconductors magnetism plays a destructive role for the pairing. On the other hand, in the case of unconventional heavy-fermion superconductors the magnetism (frequently antiferro- or ferro-magnetism) is intrinsically intertwined with the appearance of the paired states. Consequently, the Cooper pairs are usually the *d*-wave spin singlets in an antiferromagnetic materials and the spin triplets in ferromagnetic case. This constitutes the reason of the division of the following into two subsections. In the first, the features for the phase diagrams would be sketched of the selected Ce-based superconductors at the border of antiferromagnetism, namely the families of CeM_2X_2 (Ce-122 series, here with M=Cu,Pd,Ni and X=Si,Ge) and $CeMIn_5$ (Ce-115 series, with M=Co,Ir,Rh). In the second,we describe the uranium-based superconducting ferromagnets.

1.4.1 Superconductivity at Border of Antiferromagnetism

The archetypal member in the Ce-122 series is the first discovered unconventional heavy fermion superconductor $CeCu_2Si_2$ [11]. The paired phase appears there at the border of antiferromagnetism [9, 103]. As the superconducting dome spreads to the both sides around the Néel critical temperature line designating second order phase transition, it is

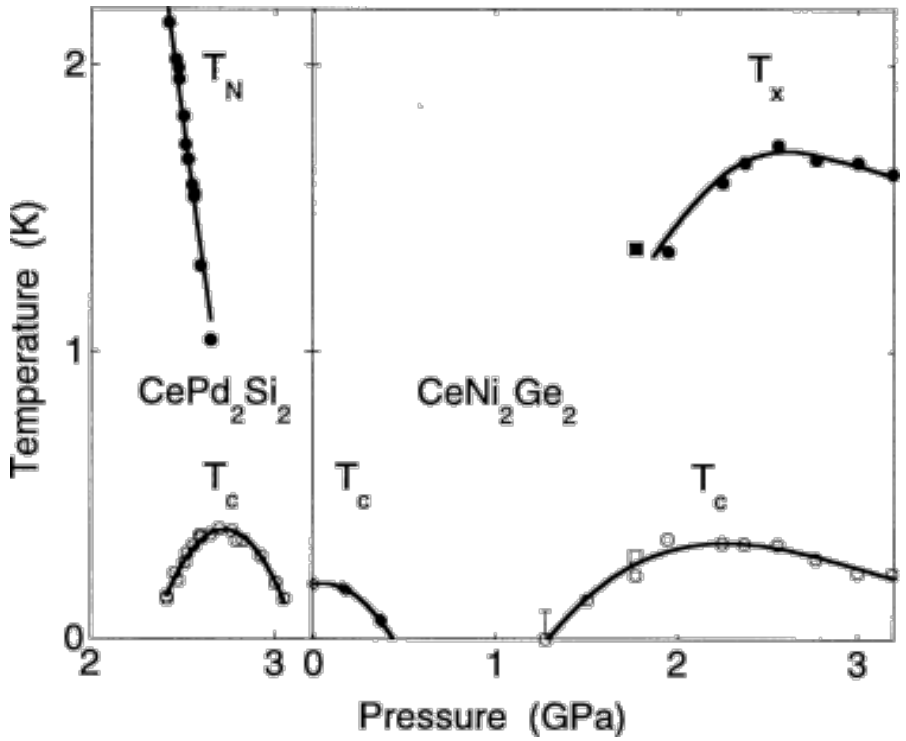

Figure 1.8: The combined phase diagram of the $CePd_2Si_2$ and $CeNi_2Ge_2$ heavy fermion superconductors (after Ref. [98])

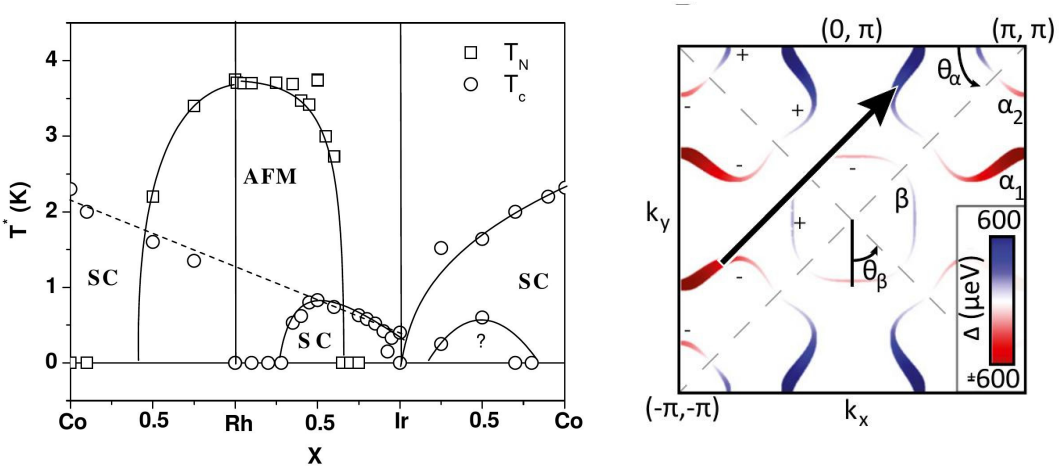

Figure 1.9: Left panel: Phase diagram of the heavy fermion family $CeMIn_5$, with M=Co, Rh or Ir, obtained by substitution of M elements (after Ref.[99]). Right panel: Measured with the help of the Bogoliubov quasiparticle spectroscopy superconducting gap nodal structure of the $CeCoIn_5$ - first experimental proof [100, 101, 102] for *d*-wave symmetry of SC order parameter among all HF superconductors (after Ref. [102]).

commonly believed that the origin of the pairing mechanism is the presence of a hidden antiferromagnetic quantum critical point. However, the specific shape of the SC dome divided into the two parts suggests two different pairing mechanisms. It was revealed by the experiments with $CeCu_2(Si_{1-x}Ge_x)_2$ that this is indeed the case, as alloying with germanium introduces pair breaking defects and thus splits the superconducting dome into two parts [104, 105] (cf. Fig. 1.7). Although, the common understanding of the origin of the second dome, far apart from antiferromagnetic quantum critical point is based on the valence-fluctuation mechanism [106, 105, 107] the recent experimental studies has questioned such description [108]. For that reason the question of underlying microscopic mechanism of pairing in this material remains still open. Quite similar behavior is observed on the phase diagram of the isostructural and isoelectronic compounds $CePd_2Si_2$ and $CeNi_2Ge_2$ [98] (cf. Fig. 1.8).

Another class of heavy fermions with superconductivity at the border of antiferromagnetism is the Ce-115 series, namely $CeMIn_5$, with M=Co, Rh or Ir. The phase diagram resulting from isovalent chemical substitution between M elements is presented in Fig. 1.9, left panel. The series member, $CeCoIn_5$, reflects the highest superconducting critical temperature of $T_S = 2.3$ K, among all known Ce-based compounds [109]. As cobalt is replaced by rhodium and subsequently rhodium by iridium, the unit cell volume increases but c/a ratio of the lattice constants decreases, tuning the system from the high T_S superconducting state through the antiferromagnetic to the low T_S superconducting phase. Conveniently, the alloying seems to be a good tuning parameter as it does not introduce substantial disorder to the system.

In terms of superconducting phase itself, the undoped $CeCoIn_5$ is the most promising material for theoretical studies. Due to recent advances in experimental techniques, particularly within the Bogoliubov quasiparticle interference spectroscopy, the symmetry of the order parameter, unprecedentedly among remaining Ce-based heavy fermions, is confirmed to be of mainly $d_{x^2-y^2}$ character [102, 100, 101] (cf. Fig. 1.9, right panel). Apart from the symmetry, the same experimental studies points to the emergence of superconductivity in more than one band.

1.4.2 Coexistence of Superconductivity with Itinerant Ferromagnetism

The coexistence of superconductivity with weak itinerant ferromagnetism was first discovered by A. Kołodziejczyk er al., in 1980, in the compound Y_9Co_7 [17, 18, 19]. Nonetheless, since the pairing in this compound is of the spin-singlet type, both orders are competing with each other. In UGe_2, 20 years later [20], the coexistence of superconductivity with the strong ferromagnetism ($\sim 1.48\mu_B$ per U atom) has been observed at high pressure. Observed high critical field has given strong argument for its spin-triplet type, as in this regime only the orbital effects should contribute to the Cooper-pair breaking [24].

Although, similar nature of the superconductivity has been subsequently discovered in ferromagnets with lower magnetization, in URhGe ($\sim 0.4\mu_B$ per U atom) [21] and UCoGe ($\sim 0.07\mu_B$ per U atom) [22], the coexistence in UGe_2 is regarded as unique and intriguing for several reasons. First, the superconductivity in UGe_2 for $T \to 0$ vanishes at the same critical pressure as ferromagnetism [20] (cf. Fig. 1.10). Second, the ferromagnetism is divided at low temperature into two phases, separated by first order transition, and the maximum of the superconducting dome coincides with this line [110] (cf. Fig. 1.10). Third, the abundance of the classical and quantum critical points on

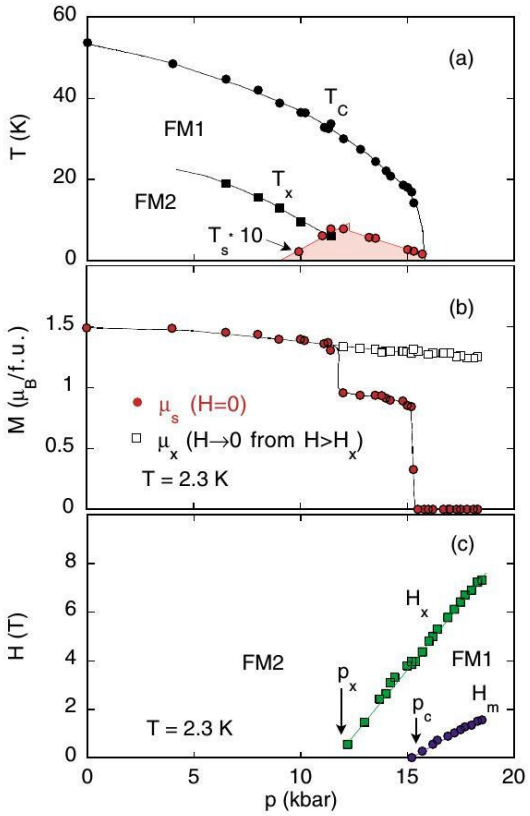

Figure 1.10: From top to bottom: Phase diagram of UGe_2 on temperature-pressure plane, magnetization curve as this compound is driven by the applied pressure undergoes two phase transition at low temperature, and its phase diagram on the magnetic field - pressure plane (after Ref. [110]).

the magnetic phase diagram [111, 112] (cf. Fig. 1.11) raise the question of a possible quantum critical behavior responsible for the superconductivity origin.

In spite of multiple attempts to understand the mechanism for the spin-triplet superconductivity, the origin of the phenomenon in U-based ferromagnets still remains open. In the case of UGe_2, the mentioned experimental findings strongly suggest that both magnetism and superconductivity are intertwined, and should be treated on an equal footing. Therefore, it seems that the origin of ferromagnetism itself with all the detailed features should be addressed first as its understanding should give strong evidence which processes are important in UGe_2 and where to search for the pairing mechanism. This is one of the main aims of th Thesis (cf. Ref. [113, 114] - articles A.2 and A.3).

1.5 Model Hamiltonians

A number of theoretical models are used to understand strongly correlated systems. Here we only refer to the most important ones which were of interest to us, namely the Hubbard (HM) and Anderson lattice (ALM) models (the latter also usually referred to as periodic Anderson model). The Hubbard model [34, 35, 36, 37] represents a microscopic

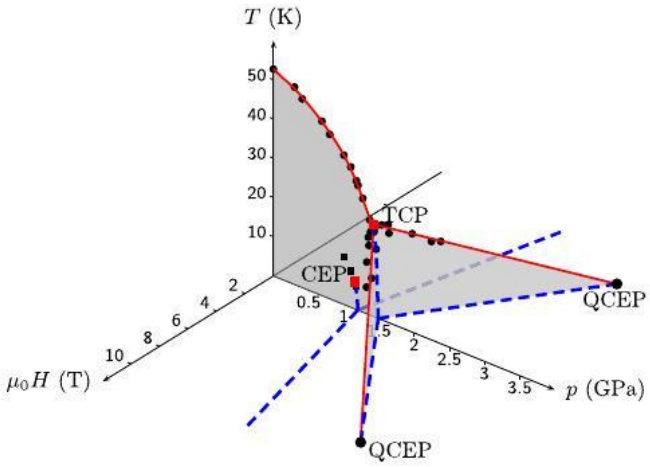

Figure 1.11: Tricritical wing structure of the phase boundaries in UGe_2 (after Ref. [111]).

playground for studies of the emergent phenomena due to strong electronic correlations. This simple microscopic model has been applied among others to the description of the mechanisms behind the Mott localization, band ferromagnetism, antiferromagnetism and eventually the high temperature superconductivity (cf. Sec. 1.2). On the other hand, ALM turned out to successfully incorporate the universal features of heavy fermion systems such as the large effective masses, the Kondo-type effects, and unconventional magnetism.

Formally, HM describes the itinerant electrons interacting with each other by means of the Coulomb repulsive interaction whenever two of them with opposite spins[10] are on the single site (cf. Fig. 1.12, left panel). Description of the materials in terms of the Anderson lattice model is more involved and the model provides a basic understanding of many features exhibited by the heavy fermion materials. In particular, it accounts for both localized and uncorrelated itinerant particles. Even though only localized electrons strongly interact with each other it is the hybridization which couples both subsystems leading to competition between localized and conduction electrons within an effective quasiparticle picture (cf. Fig. 1.12, right panel).

Specifically, the single-band Hubbard model (HM) reads

$$\hat{\mathcal{H}}_{HM} = \sum_{\mathbf{i},\mathbf{j},\sigma} t_{\mathbf{ij}} \hat{c}^{\dagger}_{\mathbf{i}\sigma} \hat{c}_{\mathbf{j}\sigma} + U \sum_{\mathbf{i}} \hat{n}_{\mathbf{i}\uparrow} \hat{n}_{\mathbf{i}\downarrow} - \sigma h \sum_{\mathbf{i},\sigma} \hat{n}_{\mathbf{i}\sigma}, \tag{1.3}$$

and the two-orbital Anderson lattice model,

$$\begin{aligned} \hat{\mathcal{H}}_{ALM} = & \sum_{\mathbf{i},\mathbf{j},\sigma} t_{\mathbf{ij}} \hat{c}^{\dagger}_{\mathbf{i}\sigma} \hat{c}_{\mathbf{j}\sigma} - \sum_{\mathbf{i},\sigma} \sigma h \; \hat{n}^{c}_{\mathbf{i}\sigma} + \sum_{\mathbf{i},\sigma} (\epsilon_f - \frac{g_f}{g} \sigma h) \hat{n}^{f}_{\mathbf{i}\sigma} + U \sum_{\mathbf{i}} \hat{n}^{f}_{\mathbf{i}\uparrow} \hat{n}^{f}_{\mathbf{i}\downarrow} \\ & + \sum_{\mathbf{i},\mathbf{j},\sigma} V_{\mathbf{ij}} (\hat{f}^{\dagger}_{\mathbf{i}\sigma} \hat{c}_{\mathbf{j}\sigma} + \hat{c}^{\dagger}_{\mathbf{i}\sigma} \hat{f}_{\mathbf{j}\sigma}), \end{aligned} \tag{1.4}$$

[10]The Pauli principle forbids configuration with two equal spin electrons on the same site (in the same Wannier state).

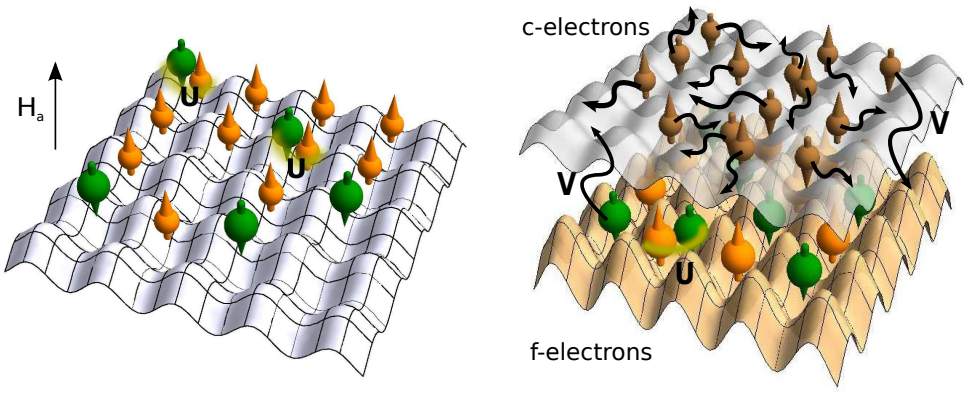

Figure 1.12: Schematic visualization of particles on lattice described by single-band Hubbard model (left panel) and those within a two-orbital Anderson lattice model (right panel). In the first case intersite hopping and f-c hybridization lead to a correlated state of fermions.

where in both models we include the Zeeman term in an applied magnetic field$h \equiv \frac{1}{2} g \mu_0 \mu_B H_a$. Both models are considered for a translationally invariant systems. We introduce the standard notation, for the spin quantum number $\sigma = \pm 1$ and $\{\mathbf{i}, \mathbf{j}\}$ being lattice position indices. The conduction band is described by the creation and annihilation operators, $\hat{c}^{\dagger}_{\mathbf{i}\sigma}$ and $\hat{\mathrm{c}}_{\mathbf{j}\sigma}$, respectively, and the and the hopping integral between the lattice sites, $t_{\mathbf{ij}}$. In HM, the repulsive on-site interaction exists between all electrons in the band, with the amplitude U. In case of ALM, the repulsive interaction is accounted for the f orbital, with initially localized f states placed at ϵ_f and coupled to the conduction band electrons by means of hybridization of amplitude $V_{\mathbf{ij}}$. The possible difference of the Landé factor for f-electrons, g_f different from the free electron value $g = 2$ is also taken into account. We have also defined the particle number operators for the respective orbitals, $\hat{n}^{c}_{\mathbf{i}\sigma} \equiv \hat{n}_{\mathbf{i}\sigma} \equiv \hat{c}^{\dagger}_{\mathbf{i}\sigma} \hat{c}_{\mathbf{i}\sigma}$ and $\hat{n}^{f}_{\mathbf{i}\sigma} \equiv \hat{f}^{\dagger}_{\mathbf{i}\sigma} \hat{f}_{\mathbf{i}\sigma}$. Those two models model respectively the correlated state in a representative band and in the hybridized system described by a two-orbital periodic system with correlations appearing originally only in one of them.

Hubbard model is generally used to describe strongly correlated systems comprising Mott insulating state. It is in particular the case among others for, in the mentioned in Sec.1.2, $(V_{1-x}Cr_x)_2O_3$ [50, 51] and cuprates, e.g. $La_{2-x}Sr_xCuO_4$ [53]. Applicability of this model was also suggested to the normal liquid ^{3}He [48] as the almost localized (crystallized) system.

Anderson lattice model is suitable for the description of the hybridized systems. Usually it concerns systems with the partially filled f-shell called heavy fermion systems. The crucial property of ALM model is the microscopic description of the delocalization of the initially at atomic states f-electrons by means of the hybridization to the conduction band with additional accounting for the strong Coulomb repulsion within f-orbital. Such picture leads to many nontrivial physical consequences as among others, itinerant magnetism, effective Kondo-type coupling and as derived within this Thesis unconventional superconductivity.

1.6 Aim and Scope of the Thesis

The general aim of this Thesis is to describe the selected physical properties of strongly correlated systems, i.e., those exhibiting strong electronic correlations, within theoretical models tackled with the variational Gutzwiller wave function approaches. We study mainly the hybridized systems, described by the Anderson lattice model (ALM) considered to capture most important features of the heavy fermion materials (HFS). We primary focus on the description of unconventional, heavy fermion superconductivity and related magnetism.

To achieve the original goal of this Thesis, which was the formulation of the theoretical framework with the correlation-induced superconductivity in ALM, we develop and implement a special variational method, namely the diagrammatic expansion for Gutzwiller wave function (DE-GWF) [55, 59, 115, 116, 117] for this model [118]. It is in particular important as, to the best knowledge of the author, up to now only one method for strongly correlated systems has enabled to analyze the microscopic mechanism of unconventional superconductivity in ALM [119]. Our framework of DE-GWF method within which we study d-wave symmetry of the order parameter in this light is the first investigation of its kind, and complete the picture of ALM describing principal properties of the heavy fermion systems.

The detailed problems addressed in the published articles as well as in those under the reviewing process constituting this Thesis, can be summarized in the following points:

- The behavior of the neutral fermions within the three dimensional Hubbard model on fcc lattice in the applied magnetic field: magnetization, specific heat, spin-direction dependent quasiparticle masses and their relevance for the canonical correlated system - normal liquid ^{3}He [38] - cf. Article A.1.

- Description of the magnetism of the ferromagnetic superconductor UGe_2 within two dimensional ALM for $T \to 0$ [113] - cf. Article A.2.

- Description of all the critical points, both classical and quantum which appear in UGe_2 and their possible relation to the onset of superconductivity [114] - cf. Article A.3.

- Studies on the accuracy of the quantitative fit of the 2nd order phase transition line joining tricritical point and quantum critical ending point in UGe_2 with respect to chosen total band filling and f-electron Landé factor [120] - cf. Article A.4..

- Derivation and implementation of the DE-GWF method to ALM: paramagnetic phase consideration including analysis of the specific features of emerging quasiparticle density of states [118] - cf. preprint of Article A.5.

- Extension of the DE-GWF method for the d-wave superconductivity description in ALM: determination of the general phase diagram [121] - cf. preprint of Article A.6.

As a additional project included in this Thesis, some additional problems concerning unconventional superconductivity[11] as such are studied, namely:

[11] Unconventional character is due to the fact that considered superconductivity is induced in the graphene layer by means of the proximity effect. Therefore, although the symmetry is conventional s-wave the paired phase is described by means of non-standard Dirac-Bogoliubov-De Gennes equations.

- Derivation of the extended Blonder-Tinkham-Klapwijk formula for the thermoelectrical transport through the superconducting hybrid junction (NIS - Normal conductor, Insulator, Superconductor) [122] - cf. Article B.1.
- Application of obtained theory for the case of the graphene based junction (NS) [123] - cf. Article B.2.
- Investigations of the impact of temperature on the conductance oscillations in the graphene based NIS junction [124] - cf. Article B.3.

The content of the Thesis is as follows. In Chapter 2 we have described in detail used variational methods based on the Gutzwiller wave function, including the implementation of SGA approach to Hubbard and Anderson lattice models, and DE-GWF technique as applied to Anderson lattice model, specifically for description of paramagnetic and the superconducting states. In Chapter 3 we describe the articles constituting the main part of this Thesis. In Chapter 3.8 we have additionally briefly refer to the additional project concerning thermoelectrical transport through superconducting hybrid junctions. Chapter 4 contains the Thesis summary and conclusions. The original articles are reproduced in Chapter 3. At the end, we list the bibliographical references quoted in the foregoing chapters.

Chapter 2

Gutzwiller Wave Function Variational Approaches

In the Hubbard Model considered for the translationally invariant lattice, one can narrow down the Fock space to four different local (on the site $\mathbf{i}$) spin configurations, $|\Gamma\rangle_{\mathbf{i}} \in \{|0\rangle_{\mathbf{i}}, |\uparrow\rangle_{\mathbf{i}}, |\downarrow\rangle_{\mathbf{i}}, |\uparrow\downarrow\rangle_{\mathbf{i}}\}$. In the case of the absence of the correlations all of those configuration are equally probable and the ground state is assumed as the Slater determinant, $|\psi_0\rangle$. In 1963 Gutzwiller [36] proposed the variational wave function which can accurately approximate true ground state when the interactions are significant by optimizing the probability of the onsite double (opposite) spin occupancy, $|\uparrow\downarrow\rangle_{\mathbf{i}}$. In the standard formulation Gutzwiller Wave Function (GWF), $|\psi_G\rangle$, is constructed in a following manner:

$$|\psi_G\rangle = \hat{\mathcal{P}}_G|\psi_0\rangle \equiv \prod_{\mathbf{i}} \hat{\mathcal{P}}_{G;\mathbf{i}}|\psi_0\rangle \equiv \prod_{\mathbf{i}} \Big(1-(1-g)\hat{n}_{\mathbf{i}\uparrow}\hat{n}_{\mathbf{i}\downarrow}\Big)|\psi_0\rangle, \tag{2.1}$$

where g is a variational parameter, and $\hat{\mathcal{P}}_G = \hat{\mathcal{P}}_G^{\dagger}$ is the so-called Gutzwiller projection operator. For $g = 1$ one recovers an uncorrelated ground state whereas the $g = 0$ case determines fully projected state with no double occupancies. Therefore, GWF enables to investigate both limits, as well as the intermediate regime within this single framework. In order to proceed with the variational treatment, one needs to calculate expectation value of the Hamiltonian with the GWF,

$$\langle\hat{\mathcal{H}}\rangle_G \equiv \frac{\langle\psi_G \mid \hat{\mathcal{H}} \mid \psi_G\rangle}{\langle\psi_G \mid \psi_G\rangle} = \frac{\langle\psi_0 \mid \hat{\mathcal{P}}_G\hat{\mathcal{H}}\hat{\mathcal{P}}_G \mid \psi_0\rangle}{\langle\psi_0 \mid \hat{\mathcal{P}}_G^2 \mid \psi_0\rangle}. \tag{2.2}$$

Despite of an apparently simple form of (2.2), its evaluation specifically for both the Hubbard and the Anderson lattice models is impossible for realistic two and three dimensional infinite lattices and arbitrary parameters[1]. Therefore, one needs to make some assumptions to circumvent this difficulty. Two approximate methods: the generalized GA in the statistically consistent form (called SGA) and Diagrammatic Expansion for the Gutzwiller Wave Function (DE-GWF) are addressed in this chapter. These methods are described in detail for the particular cases considered in the following chapter 3 - *Results*.

[1] Note, that there exists exact solutions for very specific situations [125, 126, 127, 128]

Despite some inaccuracies generated by various approximations generally GWF stands out with the physically transparent form and large flexibility which is reflected in a possible formulation for a range of different models and cases, e.g. [48, 129, 82, 130, 131, 132], and even enables for studying phenomena far from equilibrium [47].

2.1 Statistically-Consistent Gutzwiller Approximation (SGA)

One of the earliest, and still in use today, attempts to approach the hard task of calculating average values of the Hamiltonian with GWF is the so-called Gutzwiller Approximation (GA) which takes only leading, local projections into account. Namely, any product operator, $\hat{\mathcal{O}}_{\mathbf{i(j)}}$ acting on the site $\mathbf{i}$ (and $\mathbf{j}$) from considered Hamiltonian is projected only locally,

$$\hat{\mathcal{P}}_G \sum_{\mathbf{i(j)}} \hat{\mathcal{O}}_{\mathbf{i(j)}} \hat{\mathcal{P}}_G \approx \sum_{\mathbf{i(j)}} \hat{\mathcal{P}}_{G;\mathbf{i}} (\hat{\mathcal{P}}_{G;\mathbf{j}}) \hat{\mathcal{O}}_{\mathbf{i(j)}} (\hat{\mathcal{P}}_{G;\mathbf{j}}) \hat{\mathcal{P}}_{G;\mathbf{i}}. \tag{2.3}$$

Such approximation becomes the exact variational solution in infinite dimensions, but it is also believed to capture most important physics of the two- and three- dimensional systems as well.

2.1.1 Hubbard Model in Applied Magnetic Field

In this Section we formulate the SGA method for the single-band Hubbard Hamiltonian in its translationally-invariant form and the grand canonical ensemble forms. We also add the applied magnetic field H_a introduced via the Zeeman term. In effect,

$$\hat{\mathcal{H}}_{HM} = \sum_{<ij>,\sigma} t_{ij} \hat{c}^{\dagger}_{i\sigma} \hat{c}_{j\sigma} + U \sum_{i} \hat{n}_{i\uparrow} \hat{n}_{i\downarrow} - \sigma h \sum_{i,\sigma} \hat{n}_{i\sigma} - \mu \sum_{i,\sigma} \hat{n}_{i\sigma}, \tag{2.4}$$

where $h \equiv \frac{1}{2} g \mu_0 \mu_B H_a$ and μ is the system chemical potential (Fermi energy at $T = 0$). We use standard notation introduced earlier (cf. Sec. 1.5). The role of the chemical potential is important as it should be adjusted to preserve the number of fermions while evolving system, e.g. in the magnetic field or by undergoing transition to another phase.

The effect of the local Gutzwiller projection on the model (2.4) results in the following renormalized effective single particle Hamiltonian in the momentum space representation (cf. e.g., Refs. [50, 48, 38]),

$$\hat{\mathcal{H}}_{GA} = \sum_{\mathbf{k}\sigma} (q_\sigma(d, n, m) \epsilon_{\mathbf{k}} - \sigma h) \hat{c}^{\dagger}_{\mathbf{k}\sigma} \hat{c}_{\mathbf{k}\sigma} + LUd^2, \tag{2.5}$$

where $\epsilon_{\mathbf{k}}$ is the uncorrelated tight-binding single-particle dispersion relation and L - the number of lattice sites. Under projection, the interaction term can be evaluated by the average potential energy per lattice site in the system and is equal to Ud^2, where d^2 is the probability of having a doubly occupied site. On the other hand, the band resulting from tight-binding approach is significantly renormalized. The narrowing factor q_σ appears and can be evaluated on the basis of the combinatoric considerations (see e.g. Ref. [48]) which depends on the parameter d, total fermion band filling $n = n_{\mathbf{i}\uparrow} + n_{\mathbf{i}\downarrow}$, and in the case of spin-imbalance irrelevant if of the intrinsic or field-driven origin, on the spin magnetization $m = n_{\mathbf{i}\uparrow} - n_{\mathbf{i}\downarrow}$. The final result is:

$$q_\sigma = \frac{2\left[\sqrt{(n + \sigma m - 2d^2)(1 - n + d^2)} + \sqrt{(n - \sigma m - 2d^2)d^2}\right]^2}{(n + \sigma m)(2 - n - \sigma m)}. \tag{2.6}$$

The Zeeman term and coupling to the external reservoir remains unchanged under the Gutzwiller local projection since $\hat{\mathcal{P}}_{G;\mathbf{i}}\hat{n}_{\mathbf{i}\sigma}\hat{\mathcal{P}}_{G;\mathbf{i}} = \hat{n}_{\mathbf{i}\sigma}$.

In the usual Gutzwiller Approximation the expectation value of the Hamiltonian (2.5) is optimized with respect to variational parameter d - equivalent in terms of optimization procedure to g (used in Def. 2.1). Additional incorporation of the thermodynamic equations for the fixed number of particles and their magnetization leads then to the following set of self-consistent equations,

$$\begin{cases} d = -\dfrac{1}{2LU}\displaystyle\sum_{\mathbf{k}\sigma}\frac{\partial q_\sigma}{\partial d}f(E_{\mathbf{k}\sigma})\epsilon_{\mathbf{k}}, \\ m = \dfrac{1}{L}\displaystyle\sum_{\mathbf{k},\sigma}\sigma f(E_{\mathbf{k}\sigma}), \\ n = \dfrac{1}{L}\displaystyle\sum_{\mathbf{k},\sigma} f(E_{\mathbf{k}\sigma}), \end{cases} \tag{2.7}$$

with $f(E) = \frac{1}{e^{\beta(E-\mu)}+1}$ being Fermi - Dirac distribution function, $E_{\mathbf{k}\sigma} = q_\sigma\epsilon_{\mathbf{k}} - \sigma h - \mu$, and $\beta = 1/k_BT$ being the reduced inverse temperature.

However, when magnetization of the system is nonzero ($m \neq 0$)[2], its value calculated from (2.7) is not that in equilibrium. Explicitly, by changing the spin-resolved occupancies, the ground state energy can be further minimized. This provides an explicit evidence of the lack of the consistency [133] between solution of the self-consistent equations (2.7) and those obtained from a variational principle, ensuring that the system in equilibrium chooses possible the lowest energy state.

On the basis of such observations, the reinforcement of the statistical consistency was proposed [133] by means of the Lagrange multipliers added to the effective Hamiltonian $\hat{\mathcal{H}}_{GA}$ (2.5). Within the new formulation called *statistically consistent Gutzwiller approximation* (SGA), we ensure that both the magnetization and the particle concentration determined self-consistently and variationally, coincide. In effect, we introduce extended effective Hamiltonian in the following form,

$$\hat{\mathcal{H}}_{SGA} \equiv \hat{\mathcal{H}}_{GA} - \lambda_m(\sum_{\mathbf{i}\sigma}\sigma\hat{n}_{\mathbf{i}\sigma} - mL) - \lambda_n(\sum_{\mathbf{i}\sigma}\hat{n}_{\mathbf{i}\sigma} - nL), \tag{2.8}$$

with λ_m and λ_n being Lagrange multipliers. The set of the self-consistent equations is then enriched by the two additional equations resulting from optimization of the ground state energy with respect to Lagrange multipliers.

In order to account for the entropy part in the non-zero temperature considerations we define generalized Landau grand-potential functional,

$$\mathcal{F}^{SGA} = -\frac{1}{\beta}\sum_{\mathbf{k}\sigma} ln[1 + e^{-\beta E^{(SGA)}_{\mathbf{k}\sigma}}] + L(\lambda_n n + \lambda_m m + Ud^2), \tag{2.9}$$

where $E^{(SGA)}_{\mathbf{k}\sigma} = q_\sigma\epsilon_{\mathbf{k}} - \sigma(h + \lambda_m) - \mu - \lambda_n$. The new set of self-consistent equations for the equilibrium values of the parameters merged into a vector form, $\vec{\lambda} \equiv (m, d, n, \lambda_n, \lambda_m)$

[2]Either due to magnetic field or by an intrinsic mechanism such, as that on the basis of the Stoner theory.

and is determined from the condition of the optimal $\mathcal{F}^{SGA}$: $\left(\frac{\partial \mathcal{F}}{\partial \vec{\lambda}}\right)_0 = 0$. Explicitly,

$$\begin{cases} \lambda_n = -\dfrac{1}{L}\displaystyle\sum_{\mathbf{k}\sigma} \frac{\partial q_\sigma}{\partial n} f(E^{(SGA)}_{\mathbf{k}\sigma})\epsilon_{\mathbf{k}}, \\ \lambda_m = -\dfrac{1}{L}\displaystyle\sum_{\mathbf{k}\sigma} \frac{\partial q_\sigma}{\partial m} f(E^{(SGA)}_{\mathbf{k}\sigma})\epsilon_{\mathbf{k}}, \\ d = -\dfrac{1}{2LU}\displaystyle\sum_{\mathbf{k}\sigma} \frac{\partial q_\sigma}{\partial d} f(E^{(SGA)}_{\mathbf{k}\sigma})\epsilon_{\mathbf{k}}, \\ n = \dfrac{1}{L}\displaystyle\sum_{\mathbf{k}\sigma} f(E^{(SGA)}_{\mathbf{k}\sigma}), \\ m = \dfrac{1}{L}\displaystyle\sum_{\mathbf{k}\sigma} \sigma f(E^{(SGA)}_{\mathbf{k}\sigma}), \end{cases} \tag{2.10}$$

This procedure allows for a consistent analysis of the thermodynamic properties, as e.g. the specific heat. The grand-potential functional evaluated for the optimal values of the components of the vector $\vec{\lambda}$, and determined from (2.10) reduces to the physical grand potential Ω. Once we have determined the equilibrium thermodynamic potential, we can also determine all relevant thermodynamic quantities. For example, the entropy is

$$-S = \frac{d\Omega}{dT} = \Big(\frac{\partial \mathcal{F}}{\partial T}\Big)_0 + \Big(\frac{\partial \mathcal{F}}{\partial \vec{\lambda}}\Big)_0 \cdot \frac{\partial \vec{\lambda}}{\partial T}, \tag{2.11}$$

where subscript "0" labels the equilibrium values of variational parameters. Since $\left(\frac{\partial \mathcal{F}}{\partial \vec{\lambda}}\right)_0 = 0$, Eq. (2.11) simplifies to the form

$$S = -\Big(\frac{\partial \mathcal{F}}{\partial T}\Big)_0 = k_B \sum_{\mathbf{k}\sigma} \Big[ln(1 + e^{-\beta E^0_{\mathbf{k}\sigma}}) + \beta E^0_{\mathbf{k}\sigma} f(E^0_{\mathbf{k}\sigma}) \Big]. \tag{2.12}$$

The specific heat is then defined in the usual manner

$$c_V = T\frac{dS}{dT}\Big|_{n,T,h,V} \equiv -T\frac{\partial^2 \mathcal{F}}{\partial T^2}\Big|_0. \tag{2.13}$$

2.1.2 Anderson Lattice Model in Applied Magnetic Field

In this section the SGA method is implemented for the specific case of Anderson lattice model[3] with the magnetic field accounted by Zeeman term[4] and coupled to external reservoir with chemical potential μ,

$$\begin{aligned} \hat{\mathcal{H}}_{ALM} - \mu\hat{N} =& {\sum_{\mathbf{i},\mathbf{j},\sigma}}' t_{\mathbf{ij}} \hat{c}^\dagger_{\mathbf{i}\sigma}\hat{c}_{\mathbf{j}\sigma} - \sum_{\mathbf{i}\sigma}(\mu + \sigma h)\hat{n}^c_{\mathbf{i}\sigma} + \sum_{\mathbf{i},\sigma}(\epsilon_f - \mu - \sigma h)\hat{n}^f_{\mathbf{i}\sigma} \\ &+ U\sum_{\mathbf{i}} \hat{n}^f_{\mathbf{i}\uparrow}\hat{n}^f_{\mathbf{i}\downarrow} + \sum_{\mathbf{i},\sigma} V_{\mathbf{ij}}(\hat{f}^\dagger_{\mathbf{i}\sigma}\hat{c}_{\mathbf{i}\sigma} + \hat{c}^\dagger_{\mathbf{i}\sigma}\hat{f}_{\mathbf{i}\sigma}). \end{aligned} \tag{2.14}$$

The Gutzwiller operator acts in this case only on the correlated f-orbital [129]. Therefore, the projection leads to the renormalization of the hybridization and average

[3]The procedure is similar to the Hubbard model case, thus part of the general discussion is skipped.
[4]For simplicity, here the Landé factor for f electrons is equal to the free elctron value, $g_f = 2$.

potential energy, the latter is identical as in the case of the Hubbard model (LUd^2). Operator $\hat{n}^f_{\mathbf{i}\sigma}$ remains unchanged under the projection. Gutzwiller approximation together with additional terms enforcing necessary conditions leads to the following single particle effective Hamiltonian in the momentum space representation,

$$\begin{aligned}\hat{\mathcal{H}}_{SGA} \equiv \sum_{\mathbf{k},\sigma} \hat{\Psi}^\dagger_{\mathbf{k}\sigma} \begin{pmatrix} \epsilon^c_{\mathbf{k}} - \sigma h - \mu & \sqrt{q_\sigma} V \\ \sqrt{q_\sigma} V & \epsilon_f - \sigma h - \mu \end{pmatrix} \hat{\Psi}_{\mathbf{k}\sigma} + LUd^2 \\ - \lambda^f_n \Big(\sum_{\mathbf{k},\sigma} \hat{n}^f_{\mathbf{k}\sigma} - Ln_f \Big) - \lambda^f_m \Big(\sum_{\mathbf{k},\sigma} \sigma \hat{n}^f_{\mathbf{k}\sigma} - Lm_f \Big) \\ \equiv \sum_{\mathbf{k},\sigma} \hat{\Psi}^\dagger_{\mathbf{k}\sigma} \begin{pmatrix} \epsilon^c_{\mathbf{k}} - \sigma h - \mu & \sqrt{q_\sigma} V \\ \sqrt{q_\sigma} V & \epsilon_f - \sigma(h + \lambda^f_m) - \lambda^f_n - \mu \end{pmatrix} \hat{\Psi}_{\mathbf{k}\sigma} \\ + L(Ud^2 + \lambda^f_n n_f + \lambda^f_m m_f), \quad (2.15)\end{aligned}$$

where $\hat{\Psi}^\dagger_{\mathbf{k}\sigma} \equiv (\hat{c}^\dagger_{\mathbf{k}\sigma}, \hat{f}^\dagger_{\mathbf{k}\sigma})$, and q_σ is the narrowing factor in the standard form already defined in the previous section (2.6), with the difference that instead of the average magnetization and electron concentration for conduction electrons it is now dependent on the f electrons correspondents, $n_f = n^f_{\mathbf{i}\uparrow} + n^f_{\mathbf{i}\downarrow}$ and $m_f = n^f_{\mathbf{i}\uparrow} - n^f_{\mathbf{i}\downarrow}$. It is invoked in this manner due to the fact that only f electrons are correlated and factor q_σ appears as an effect of the Gutzwiller projection of the f-electron operators. Eigenvalues, $E_{\mathbf{k}\pm}$ of the above Hamiltonian are,

$$E^{(SGA)}_{\mathbf{k}\sigma a} = \xi^+_{\mathbf{k}\sigma} + a\sqrt{(\xi^-_{\sigma\mathbf{k}})^2 + q_\sigma V^2}, \quad (2.16)$$

where $a \equiv \pm 1$ differentiates between the two hybridized bands. For convenience, in above we defines

$$\begin{aligned}\xi^+_{\mathbf{k}\sigma} &\equiv \frac{\epsilon^c_{\mathbf{k}} + \epsilon^f_{\mathbf{k}} - \sigma(2h + \lambda^f_m) - 2\mu - \lambda^f_n}{2}, \\ \xi^-_{\mathbf{k}\sigma} &\equiv \frac{\epsilon^c_{\mathbf{k}} - \epsilon^f_{\mathbf{k}} + \sigma\lambda^f_m + \lambda^f_n}{2}.\end{aligned} \quad (2.17)$$

Rest of the discussion is in accordance to the Hubbard model with the difference that eventually we have to solve set of six self-consistent equations: five resulting from the optimization of $\mathcal{F}^{SGA}$ with respect to $\vec{\lambda} \equiv (m_f, d, n_f, \lambda^f_n, \lambda^f_m)$,

$$\begin{cases} \lambda^f_n = -\dfrac{1}{L} \displaystyle\sum_{\mathbf{k}\sigma a} \frac{\partial E^{(SGA)}_{\mathbf{k}\sigma a}}{\partial q_\sigma} \frac{\partial q_\sigma}{\partial n} f(E^{(SGA)}_{\mathbf{k}\sigma a}), \\ \lambda^f_m = -\dfrac{1}{L} \displaystyle\sum_{\mathbf{k}\sigma a} \frac{\partial E^{(SGA)}_{\mathbf{k}\sigma a}}{\partial q_\sigma} \frac{\partial q_\sigma}{\partial m} f(E^{(SGA)}_{\mathbf{k}\sigma a}), \\ d = -\dfrac{1}{2LU} \displaystyle\sum_{\mathbf{k}\sigma a} \frac{\partial E^{(SGA)}_{\mathbf{k}\sigma a}}{\partial q_\sigma} \frac{\partial q_\sigma}{\partial d} f(E^{(SGA)}_{\mathbf{k}\sigma a}), \\ n_f = -\dfrac{1}{L} \displaystyle\sum_{\mathbf{k}\sigma a} \frac{\partial E^{(SGA)}_{\mathbf{k}\sigma a}}{\partial \lambda^f_n} f(E^{(SGA)}_{\mathbf{k}\sigma a}), \\ m_f = -\dfrac{1}{L} \displaystyle\sum_{\mathbf{k}\sigma a} \frac{\partial E^{(SGA)}_{\mathbf{k}\sigma a}}{\partial \lambda^f_m} f(E^{(SGA)}_{\mathbf{k}\sigma a}), \end{cases} \quad (2.18)$$

and one additional adjusting the chemical potential in order to keep total number of particles fixed,

$$n = \frac{1}{L}\sum_{\mathbf{k}\sigma a} f(E^{(SGA)}_{\mathbf{k}\sigma a}). \tag{2.19}$$

Moreover, total magnetization of the system can be afterwards determined from,

$$m = \frac{1}{L}\sum_{\mathbf{k}\sigma a} \sigma f(E^{(SGA)}_{\mathbf{k}\sigma a}). \tag{2.20}$$

This method will be elaborated in detail in Articles A1-A4 (cf. Chapter 3).

2.2 Diagrammatic Expansion for Gutzwiller Wave Function (DE-GWF)

2.2.1 General formulation for Anderson lattice model

In this section the DE-GWF approach is formulated in detail for the Anderson lattice model:

$$\begin{aligned}\hat{\mathcal{H}}_{ALM} = &\sum_{\mathbf{i},\mathbf{j},\sigma}(t_{\mathbf{ij}} - \mu\delta_{\mathbf{i},\mathbf{j}})\hat{c}^{\dagger}_{\mathbf{i}\sigma}\hat{c}_{\mathbf{j}\sigma} + \sum_{\mathbf{i},\sigma}(\epsilon_f - \mu)\hat{n}^f_{\mathbf{i}\sigma} \\ &+U\sum_{\mathbf{i}}\hat{n}^f_{\mathbf{i}\uparrow}\hat{n}^f_{\mathbf{i}\downarrow} + \sum_{\mathbf{i},\mathbf{j},\sigma}(V_{\mathbf{ij}}\hat{f}^{\dagger}_{\mathbf{i}\sigma}\hat{c}_{\mathbf{j}\sigma} + V^{*}_{\mathbf{ij}}\hat{c}^{\dagger}_{\mathbf{i}\sigma}\hat{f}_{\mathbf{j}\sigma}),\end{aligned} \tag{2.21}$$

where we have used the standard notation (cf. Sec. 1.5).

Aim of the present approach is to systematically extend the Gutzwiller approximation-limit, where only local sites are projected (which is variationally exact only in infinite dimensions) and to approach the exact evaluation, where all sites are projected. The natural parameter to control the calculations is the number of projected sites taken into account. In the following we provide the formal reasoning towards this goal.

The Gutzwiller operator can be defined in a general form [115, 55, 59, 116, 117] as

$$\hat{P}_{G;\mathbf{i}} = \sum_{\Gamma}\lambda_{\Gamma} \mid \Gamma\rangle_{\mathbf{i}}\langle\Gamma \mid_{\mathbf{i}}, \tag{2.22}$$

with variational parameters $\lambda_{\Gamma} \in \{\lambda_0, \lambda_{\uparrow}, \lambda_{\downarrow}, \lambda_d\}$ characterizing weights of all the occupation probabilities for the four possible local (atomic) Fock states for the f orbital $\mid\Gamma\rangle_{\mathbf{i}} \in \{|0\rangle^f_{\mathbf{i}}, |\uparrow\rangle^f_{\mathbf{i}}, |\downarrow\rangle^f_{\mathbf{i}}, |\uparrow\downarrow\rangle^f_{\mathbf{i}}\}$. One can easily identify the explicit form of the operator projecting on the particular state $\mid\Gamma\rangle_{\mathbf{i}}\langle\Gamma\mid_{\mathbf{i}}$ as

$$\begin{aligned}|0\rangle^f_{\mathbf{i}}\langle 0|^f_{\mathbf{i}} &= (1-\hat{n}^f_{\mathbf{i}\downarrow})(1-\hat{n}^f_{\mathbf{i}\uparrow}), \\ |\sigma\rangle^f_{\mathbf{i}}\langle\sigma|^f_{\mathbf{i}} &= (1-\hat{n}^f_{\mathbf{i}\bar{\sigma}})\hat{n}^f_{\mathbf{i}\sigma}, \\ |\uparrow\downarrow\rangle^f_{\mathbf{i}}\langle\uparrow\downarrow|^f_{\mathbf{i}} &= \hat{n}^f_{\mathbf{i}\downarrow}\hat{n}^f_{\mathbf{i}\uparrow}.\end{aligned} \tag{2.23}$$

The operator $\hat{P}_{G;\mathbf{i}}$, alternative to standard GA form (but equivalent in terms of the variational approach) is selected to satisfy the following relation [134]

$$\hat{P}^2_{G;\mathbf{i}} = \mathbf{1} + x\hat{d}^{HF}_{\mathbf{i}}, \tag{2.24}$$

where for the translationally invariant system we define Hartree-Fock (HF) operators

$$\hat{d}^{HF}_{\mathbf{i}} \equiv \hat{n}^{HF}_{\mathbf{i}\uparrow}\hat{n}^{HF}_{\mathbf{i}\downarrow} = (\hat{n}^{f}_{\mathbf{i}\uparrow} - n^{f}_{0\uparrow})(\hat{n}^{f}_{\mathbf{i}\downarrow} - n^{f}_{0\downarrow}). \tag{2.25}$$

Here the expectation values of the number of f particles are taken with respect to the uncorrelated ($U = 0$) ground state (Slater determinant), to be defined later, $|\psi_0\rangle$, so that $n^{f}_{0\sigma} \equiv \langle \hat{n}^{f}_{\mathbf{i}\sigma}\rangle_0$. Strictly speaking, although, $\hat{d}^{HF}_{\mathbf{i}}$ has not the Hartree-Fock form of the double occupancy operator, the HF superscript has its meaning as the property, $\langle \hat{d}^{HF}_{\mathbf{i}}\rangle_0 \equiv 0$ is preserved. Effectively, relation (2.24) leads to relation between λ_Γ and x, derived by acting with operator $P^2_{G;\mathbf{i}}$ on the state $|\Gamma\rangle_{\mathbf{i}}$ with the use of both definitions (2.24) and (2.22),

$$\begin{aligned}
\lambda_0^2 &= 1 + x n^{f}_{0\bar{\sigma}} n^{f}_{0\sigma}, \\
\lambda_\sigma^2 &= 1 - x n^{f}_{0\sigma}(1 - n^{f}_{0\bar{\sigma}}), \\
\lambda_d^2 &= 1 + x(1 - n^{f}_{0\bar{\sigma}})(1 - n^{f}_{0\sigma}),
\end{aligned} \tag{2.26}$$

resulting in only one independent variational parameter. The choice of the parameter is generally arbitrary, but selecting x has its presentational strengths as it leads to an elegant power expansion of the expectation values with respect to GWF of any product operator with respect to GWF.

The key point of the variational procedure is the calculation of the ground state energy of (2.21) with GWF $|\psi_G\rangle$, i.e.,

$$\langle \hat{\mathcal{H}}\rangle_G \equiv \frac{\langle \psi_G \mid \hat{\mathcal{H}} \mid \psi_G\rangle}{\langle \psi_G \mid \psi_G\rangle} = \frac{\langle \psi_0 \mid \hat{P}_G \hat{\mathcal{H}} \hat{P}_G \mid \psi_0\rangle}{\langle \psi_0 \mid \hat{P}^2_G \mid \psi_0\rangle}. \tag{2.27}$$

The idea of the expansion can be visualized transparently on example of calculation of the GWF norm

$$\langle \psi_G \mid \psi_G\rangle = \langle \psi_0 \mid \prod_{\mathbf{l}} \hat{P}^2_{G;\mathbf{l}} \mid \psi_0\rangle = (*). \tag{2.28}$$

If the product would run over two sites, $\mathbf{l} \in \mathbf{l_1}, \mathbf{l_2}$ it could explicitly be written as

$$(*) = \langle 1 + x(\hat{d}^{HF}_{\mathbf{l}_1} + \hat{d}^{HF}_{\mathbf{l}_2}) + x^2(\hat{d}^{HF}_{\mathbf{l}_1}\hat{d}^{HF}_{\mathbf{l}_2} + \hat{d}^{HF}_{\mathbf{l}_2}\hat{d}^{HF}_{\mathbf{l}_1})\rangle_0. \tag{2.29}$$

In case of three sites taken into account, $\mathbf{l} \in \mathbf{l_1}, \mathbf{l_2}, \mathbf{l_3}$, the norm after execution of the product is

$$\begin{aligned}
(*) = {} & \langle 1 + x(\hat{d}^{HF}_{\mathbf{l}_1} + \hat{d}^{HF}_{\mathbf{l}_2} + \hat{d}^{HF}_{\mathbf{l}_3})\rangle_0 \\
& + \langle x^2(\hat{d}^{HF}_{\mathbf{l}_1}\hat{d}^{HF}_{\mathbf{l}_2} + \hat{d}^{HF}_{\mathbf{l}_2}\hat{d}^{HF}_{\mathbf{l}_1} + \hat{d}^{HF}_{\mathbf{l}_1}\hat{d}^{HF}_{\mathbf{l}_3} + \hat{d}^{HF}_{\mathbf{l}_3}\hat{d}^{HF}_{\mathbf{l}_1} + \hat{d}^{HF}_{\mathbf{l}_3}\hat{d}^{HF}_{\mathbf{l}_2} + \hat{d}^{HF}_{\mathbf{l}_2}\hat{d}^{HF}_{\mathbf{l}_3})\rangle_0 \\
& + \langle x^3(\hat{d}^{HF}_{\mathbf{l}_1}\hat{d}^{HF}_{\mathbf{l}_2}\hat{d}^{HF}_{\mathbf{l}_3} + \hat{d}^{HF}_{\mathbf{l}_2}\hat{d}^{HF}_{\mathbf{l}_3}\hat{d}^{HF}_{\mathbf{l}_1} + \hat{d}^{HF}_{\mathbf{l}_3}\hat{d}^{HF}_{\mathbf{l}_1}\hat{d}^{HF}_{\mathbf{l}_2} \\
& + \hat{d}^{HF}_{\mathbf{l}_1}\hat{d}^{HF}_{\mathbf{l}_3}\hat{d}^{HF}_{\mathbf{l}_2} + \hat{d}^{HF}_{\mathbf{l}_2}\hat{d}^{HF}_{\mathbf{l}_1}\hat{d}^{HF}_{\mathbf{l}_3} + \hat{d}^{HF}_{\mathbf{l}_3}\hat{d}^{HF}_{\mathbf{l}_2}\hat{d}^{HF}_{\mathbf{l}_1})\rangle_0.
\end{aligned} \tag{2.30}$$

Because operators $\hat{d}^{HF}_{\mathbf{l}_k}$ for different k commute with each other, it is easy to write down the general formula. namely for the case of infinite lattice the product extends to all sites and the closed expression for the norm reads

$$\langle \psi_G \mid \psi_G\rangle = \sum_{k=0}^{\infty} \frac{x^k}{k!} {\sum_{\mathbf{l}_1,\ldots,\mathbf{l}_k}}' \langle \hat{d}^{HF}_{\mathbf{l}_1,\ldots,\mathbf{l}_k}\rangle_0, \tag{2.31}$$

where $\hat{d}^{HF}_{\mathbf{l}_1,\ldots,\mathbf{l}_k} \equiv \hat{d}^{HF}_{\mathbf{l}_1} \cdots \hat{d}^{HF}_{\mathbf{l}_k}$. The primed multiple summation means that $\mathbf{l}_p \neq \mathbf{l}_{p'}$ for all p, p'. In terms of any product operator in (2.21): $\hat{\mathcal{O}}_{\mathbf{i(j)}} \equiv \{\hat{c}^{\dagger}_{\mathbf{i}\sigma}\hat{c}_{\mathbf{j}\sigma}, \hat{n}^{c}_{\mathbf{i}\sigma}, \hat{n}^{f}_{\mathbf{i}\sigma}, \hat{n}^{f}_{\mathbf{i}\uparrow}\hat{n}^{f}_{\mathbf{i}\downarrow}, \hat{f}^{\dagger}_{\mathbf{i}\sigma}\hat{c}_{\mathbf{j}\sigma}, \hat{c}^{\dagger}_{\mathbf{i}\sigma}\hat{f}_{\mathbf{j}\sigma}, \hat{f}^{\dagger}_{\mathbf{i}\sigma}\hat{n}^{HF}_{\mathbf{i}\bar{\sigma}}\hat{c}_{\mathbf{j}\sigma}\}$, above expansion can be generalized in a straightforward manner to the following form

$$\langle \psi_G \mid \hat{\mathcal{O}}_{\mathbf{i(j)}} \mid \psi_G \rangle = \Big\langle \hat{\tilde{\mathcal{O}}}_{\mathbf{i(j)}} \prod_{\mathbf{l}\neq\mathbf{i},\mathbf{j}} \hat{P}^2_{G;\mathbf{l}} \Big\rangle_0 = \sum_{k=0}^{\infty} \frac{x^k}{k!} {\sum_{\mathbf{l}_1,\ldots,\mathbf{l}_k}}' \langle \hat{\tilde{\mathcal{O}}}_{\mathbf{i(j)}} \hat{d}^{HF}_{\mathbf{l}_1,\ldots,\mathbf{l}_k} \rangle_0, \tag{2.32}$$

where $\hat{\tilde{O}}_{\mathbf{i(j)}} \equiv \hat{P}_{G;\mathbf{i}}(\hat{P}_{G;\mathbf{j}})\hat{\mathcal{O}}_{\mathbf{i(j)}}(\hat{P}_{G;\mathbf{j}})\hat{P}_{G;\mathbf{i}}$. Such power expansion in x enables for a systematic approach towards the full solution. For GA calculations of the expectation value with GWF invoke approximation that local, i.e., the *external* sites, $\mathbf{i}$ and $\mathbf{j}$ from the Hamiltonian (2.21) are correlated, while the remaining vertices are not. Here, in variance with GA, DE-GWF method additionally accounts that the processes between two local sites (or within the single one) that are affected by the correlated environment. For that reason the non-local, *internal* vertices, $\mathbf{l}_k$ are systematically one-by-one accounted for as correlated. It must be noted that x is not the expansion parameter but its power (k) is, denoting the number of *internal* correlated vertices taken into account. As it would be presented in the section concerning particular results, satisfactory convergence to the full GWF solution can be obtained already by accounting for three *internal* $(k = 3)$ correlated vertices $(\mathbf{l}_k)$ in addition to the *external* ones $(\mathbf{i}, \mathbf{j})$.

The expectation values with respect to the uncorrelated wave function $|\psi_0\rangle$ can be evaluated by means of the Wick's theorem [135], here applied in its real-space version. The respective contractions are transparently visualized by diagrams[5] of lines (two operator averages) connecting vertices (real space lattice sites). The choice of the studied phase, e.g. paramagnetic, ferromagnetic, antiferromagnetic or superconducting, are defined by contractions considered as nonvanishing.

By construction, in the case of the norm $\langle\psi_G|\psi_G\rangle$ we have eliminated all the diagrams with any local loop, the so-called *Hartree bubbles* due to trivial identity $\langle \hat{n}^{f}_{\mathbf{i}\sigma} - n^{f}_{0\sigma}\rangle_0 = 0$ for any vertex (site) $\mathbf{i}$. For the purpose of ensuring the same feature for the remaining expectation values, we rewrite the primary projected operators $(\hat{\tilde{O}}_{\mathbf{i(j)}})$ in the following forms,

$$\begin{aligned}
\hat{P}_{G;\mathbf{i}}\hat{d}_{\mathbf{i}}\hat{P}_{G;\mathbf{i}} &= \lambda_d^2[n^{f}_{0\bar{\sigma}}\hat{n}^{HF}_{\mathbf{i}\sigma} + n^{f}_{0\sigma}\hat{n}^{HF}_{\mathbf{i}\bar{\sigma}} + (1 - xd_0)\hat{d}^{HF}_{\mathbf{i}} + d_0\hat{P}^2_{G;\mathbf{i}}],\\
\hat{P}_{G;\mathbf{i}}\hat{n}^{f}_{\mathbf{i}\sigma}\hat{P}_{G;\mathbf{i}} &= \hat{n}^{HF}_{\mathbf{i}\sigma} + xm_{\sigma}\hat{n}^{HF}_{\mathbf{i}\bar{\sigma}} + \gamma_{\sigma}\hat{d}^{HF}_{\mathbf{i}} + n^{f}_{0\sigma}\hat{P}^2_{G;\mathbf{i}},\\
\hat{P}_{G;\mathbf{i}}\hat{f}^{(\dagger)}_{\mathbf{i}\sigma}\hat{P}_{G;\mathbf{i}} &= \alpha_{\sigma}\hat{f}^{(\dagger)}_{\mathbf{i}\sigma} + \beta_{\sigma}\hat{f}^{(\dagger)}_{\mathbf{i}\sigma}\hat{n}^{HF}_{\mathbf{i}\bar{\sigma}},
\end{aligned} \tag{2.33}$$

where for notation compactness we have defined the quantities

$$\begin{aligned}
\beta_{\sigma} &\equiv \lambda_{\bar{\sigma}}\lambda_d - \lambda_{\sigma}\lambda_0,\\
\alpha_{\sigma} &\equiv \lambda_{\sigma}\lambda_0 + \beta_{\sigma}n^{f}_{0\bar{\sigma}},\\
\gamma_{\sigma} &\equiv x(1 - 2n^{f}_{0\sigma}),\\
d_0 &\equiv n^{f}_{0\sigma}n^{f}_{0\bar{\sigma}},\\
m_{\sigma} &\equiv n^{f}_{0\sigma}(1 - n^{f}_{0\sigma}).
\end{aligned} \tag{2.34}$$

[5]The diagrams are drawn for the case of paramagnetic state in the following subsection (cf. Fig. 2.2).

Such procedure ensures the disappearance of *Hartree bubbles* for any correlated vertex, as the product of operators over the *internal* sites is additionally multiplied by a parameter or operators which also cancel out the diagrams with the loop at any vertex, due to trivial identity $\langle \hat{n}^f_{\mathbf{i}\sigma} - n^f_{0\sigma} \rangle_0 = 0$.

The last analytical step that significantly simplifies the proposed diagrammatic expansion is the division of the numerator of the expectation value by the norm in (2.27). It can be shown on example of normalized expectation value of arbitrary operator $\hat{\mathcal{O}}_{\mathbf{i(j)}}$, that

$$\frac{\langle \psi_G \mid \hat{\mathcal{O}}_{\mathbf{i(j)}} \mid \psi_G \rangle}{\langle \psi_G \mid \psi_G \rangle} = \frac{\sum_{k=0}^{\infty} \frac{x^k}{k!} \sum'_{\mathbf{l}_1,\ldots,\mathbf{l}_k} \langle \hat{\mathcal{O}}_{\mathbf{i(j)}} \hat{d}^{HF}_{\mathbf{l}_1,\ldots,\mathbf{l}_k} \rangle_0}{\sum_{k=0}^{\infty} \frac{x^k}{k!} \sum'_{\mathbf{l}_1,\ldots,\mathbf{l}_k} \langle \hat{d}^{HF}_{\mathbf{l}_1,\ldots,\mathbf{l}_k} \rangle_0} = (**). \tag{2.35}$$

By means of the linked cluster theorem [135] the summation restriction can be skipped and effectively the contribution to the norm cancels out all disconnected diagrams from the numerator, i.e.,

$$(**) = \frac{\sum_{k=0}^{\infty} \frac{x^k}{k!} \sum_{\mathbf{l}_1,\ldots,\mathbf{l}_k} \langle \hat{\mathcal{O}}_{\mathbf{i(j)}} \hat{d}^{HF}_{\mathbf{l}_1,\ldots,\mathbf{l}_k} \rangle_0}{\sum_{k=0}^{\infty} \frac{x^k}{k!} \sum_{\mathbf{l}_1,\ldots,\mathbf{l}_k} \langle \hat{d}^{HF}_{\mathbf{l}_1,\ldots,\mathbf{l}_k} \rangle_0} = \sum_{k=0}^{\infty} \frac{x^k}{k!} \sum_{\mathbf{l}_1,\ldots,\mathbf{l}_k} \langle \hat{\mathcal{O}}_{\mathbf{i(j)}} \hat{d}^{HF}_{\mathbf{l}_1,\ldots,\mathbf{l}_k} \rangle^c_0, \tag{2.36}$$

where the superscript c ($\langle ... \rangle^c_0$) symbolically denotes that fact.

The formalism enables for a systematic expansion of the order k by taking into account long-range correlations between k *internal* sites $(\mathbf{l}_1, ..., \mathbf{l}_k)$ and the *external* ones $(\mathbf{i}, \mathbf{j})$. Apart from that, the order of the expansion limitations, the real space cutoff is necessary to set for a possible direct expectation values evaluation. We assume that on the square lattice lines satisfying the relation $|\mathbf{i}-\mathbf{j}|^2 = (i_x-j_x)^2+(i_y-j_y)^2 \leq 10$ are taken into account (cf. Fig. 2.1). For comparison, an alternative technique, variational Monte Carlo (VMC) usually accounts for the lines corresponding to the largest hopping distance in the starting Hamiltonian. Therefore, by the construction, our method samples a richer variational space than VMC by including longer-range hopping components.

As the result of the described DE-GWF procedure, the expectation values of ALM Hamiltonian (2.21) can be expressed in the closed form by the diagrammatic sums $S \in \{T^{cc(1,1)}_{\mathbf{ij}\sigma}, T^{fc(1,1)}_{\mathbf{ij}\sigma}, T^{fc(3,1)}_{\mathbf{ij}\sigma}, I^{c(2)}_{\sigma}, I^{f(2)}_{\sigma}, I^{f(4)}\}$, defined as

$$S = \sum_{k=0}^{\infty} \frac{x^k}{k!} S(k). \tag{2.37}$$

with the k-th order contributions

$$T^{cc(1,1)}_{\mathbf{ij}\sigma}(k) \equiv \sum_{\mathbf{l}_1,\ldots,\mathbf{l}_k} \langle \hat{c}^{\dagger}_{\mathbf{i}\sigma} \hat{c}_{\mathbf{j}\sigma} \hat{d}^{HF}_{\mathbf{l}_1,\ldots,\mathbf{l}_k} \rangle^c_0, \tag{2.38}$$

$$T^{fc(1[3],1)}_{\mathbf{ij}\sigma}(k) \equiv \sum_{\mathbf{l}_1,\ldots,\mathbf{l}_k} \langle [\hat{n}^{HF}_{\mathbf{i}\bar{\sigma}}] \hat{f}^{\dagger}_{\mathbf{i}\sigma} \hat{c}_{\mathbf{j}\sigma} \hat{d}^{HF}_{\mathbf{l}_1,\ldots,\mathbf{l}_k} \rangle^c_0, \tag{2.39}$$

$$I^{c(2)}_{\sigma}(k) \equiv \sum_{\mathbf{l}_1,\ldots,\mathbf{l}_k} \langle \hat{n}^{c}_{\mathbf{i}\sigma} \hat{d}^{HF}_{\mathbf{l}_1,\ldots,\mathbf{l}_k} \rangle^c_0, \tag{2.40}$$

$$I^{(2)}_{\sigma}(k) \equiv \sum_{\mathbf{l}_1,\ldots,\mathbf{l}_k} \langle \hat{n}^{HF}_{\mathbf{i}\sigma} \hat{d}^{HF}_{\mathbf{l}_1,\ldots,\mathbf{l}_k} \rangle^c_0, \tag{2.41}$$

$$I^{(4)}(k) \equiv \sum_{\mathbf{l}_1,\ldots,\mathbf{l}_k} \langle \hat{d}^{HF}_{\mathbf{i}} \hat{d}^{HF}_{\mathbf{l}_1,\ldots,\mathbf{l}_k} \rangle^c_0. \tag{2.42}$$

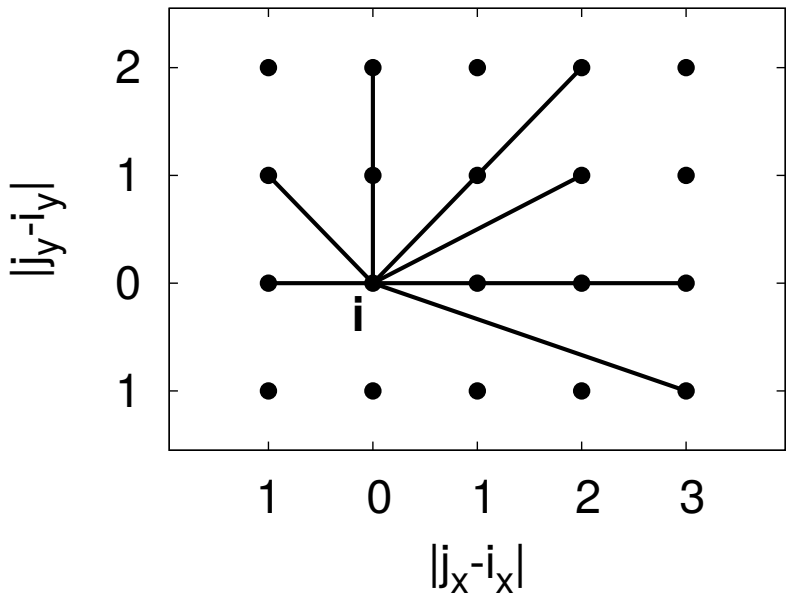

Figure 2.1: Schematic representation of the real-space cutoff on the lattice. The solid lines denote exemplary, in terms of distance, correlation functions (referred to as *lines*) taken into account between **i**-site (central vertex) and the **j**-sites (on the periphery).

The meaning of the first three consecutive terms is defined by the presence of the corresponding operators: $\hat{c}^{\dagger}_{\mathbf{i}\sigma}\hat{c}_{\mathbf{j}\sigma}$, $\hat{f}^{\dagger}_{\mathbf{i}\sigma}\hat{c}_{\mathbf{i}\sigma}$, and $\hat{n}^{c}_{\mathbf{i}\sigma}$. The resulting full expectation value of the Hamiltonian $\hat{\mathcal{H}}_{ALM}$ with GWF can be expressed as

$$\begin{aligned}\frac{\langle\hat{\mathcal{H}}_{ALM}\rangle_G}{L} &= \frac{1}{L}\sum_{\mathbf{i},\mathbf{j},\sigma} t_{\mathbf{ij}} T^{cc(1,1)}_{\mathbf{ij}\sigma} - \sum_{\sigma}\mu I^{c(2)}_{\sigma} + 2\sum_{\mathbf{i},\mathbf{j},\sigma} V_{\mathbf{ij}}\left(\alpha_{\sigma} T^{fc(1,1)}_{\mathbf{ij}\sigma} + \beta_{\sigma} T^{fc(3,1)}_{\mathbf{ij}\sigma}\right) \\ &+ \sum_{\sigma}(\epsilon_f - \mu)\left(n^{f}_{0\sigma} + I^{f(2)}_{\sigma} + x m_{\sigma} I^{f(2)}_{\bar{\sigma}} + \gamma I^{f(4)}\right) \\ &+ U\lambda_d^2\left(d_0 + n^{f}_{0\bar{\sigma}} I^{f(2)}_{\sigma} + n^{f}_{0\sigma} I^{f(2)}_{\bar{\sigma}} + (1 - x d_0) I^{f(4)}\right),\end{aligned} \tag{2.43}$$

where the trivial sum $\sum_{\mathbf{i}} = L$ have been already executed.

The final step of the whole approach is the self-consistent determination of the effective uncorrelated Hamiltonian and uncorrelated wave function $|\psi_0\rangle$. First, the expectation value $\langle\hat{\mathcal{H}}_{ALM}\rangle_G$ calculated with the diagrammatic technique is minimized with respect to the variational parameter x. Second the original model situation $\langle\hat{\mathcal{H}}_{ALM}\rangle_G$ is mapped onto the uncorrelated effective one, $\langle\psi_0|\hat{\mathcal{H}}^{\text{eff}}|\psi_0\rangle$, with the condition that the minima of the groundstate energies of both Hamiltonians coincide for the same equilibrium values of lines. This allows the determination of the parameters entering $\hat{\mathcal{H}}^{eff}$. The general scheme of DE-GWF method can be put into the following steps:

1. Choice of initial state $|\psi_0\rangle$.
2. Diagrammatic evaluation of $\langle\hat{\mathcal{H}}\rangle_G \equiv \frac{\langle\psi_G|\hat{\mathcal{H}}|\psi_G\rangle}{\langle\psi_G|\psi_G\rangle}$ for selected $|\psi_0\rangle$.
3. Minimization of $\langle\hat{\mathcal{H}}\rangle_G$ with respect to the variational parameter (here x).

4. Construction of the effective single particle Hamiltonian determined by $\delta\hat{\mathcal{H}}^{\text{eff}}(|\psi_0\rangle) = \delta\hat{\mathcal{H}}(|\psi_0\rangle)$.

5. Determination of $|\psi_0'\rangle$ as a ground state of the effective Hamiltonian.

6. Execution of the self-consistent loop: starting again from the step 1 with $|\psi_0'\rangle$ until a satisfactory convergence, i.e., $|\psi_0'\rangle = |\psi_0\rangle$, is reached.

The choice of $|\psi_0\rangle$ and construction of $\hat{\mathcal{H}}^{\text{eff}}$ vary for different phases. Therefore in the next subsections we analyze explicitly the cases of paramagnetic and superconducting phases. In each situation the notation may differ slightly and is caused to achieved a consistency with just published (or submitted) original articles.

2.2.2 Paramagnetic Phase

In this Section we consider paramagnetic ALM with onsite hybridization. As we consider spin isotropic phase, we set $n^f_{0\sigma} = n^f_{0\bar{\sigma}} \equiv n_{f0}$ and subsequently all the parameters defined in Eqs. (2.26) and (2.34) as well as evaluated order contributions to diagrammatic sums (2.42) becomes spin-independent . Diagrammatic sums, S for this case, up to the second order ($k = 2$) are depicted in Fig. 2.2, where the following spin-independent lines were taken into account

$$\begin{aligned} C_{\mathbf{ij}} &\equiv \langle \hat{c}^\dagger_{\mathbf{i}\sigma} \hat{c}_{\mathbf{j}\sigma} \rangle_0, \\ W_{\mathbf{ij}} &\equiv \langle \hat{f}^\dagger_{\mathbf{i}\sigma} \hat{c}_{\mathbf{j}\sigma} \rangle_0, \\ F_{\mathbf{ij}} &\equiv \langle \hat{f}^\dagger_{\mathbf{i}\sigma} \hat{f}_{\mathbf{j}\sigma} \rangle_0 - \delta_{\mathbf{ij}} n_{0f}. \end{aligned} \tag{2.44}$$

The effective uncorrelated Hamiltonian $\hat{\mathcal{H}}^{\text{eff}}$ is constructed in a manner to obey following relation

$$\begin{aligned} \delta\langle\hat{\mathcal{H}}^{\text{eff}}\rangle_0(C,F,W,n_{0f}) = \delta\langle\hat{\mathcal{H}}_{ALM}\rangle_G(C,F,W,n_{0f}) \\ = \frac{\partial\langle\hat{\mathcal{H}}_{ALM}\rangle_G}{\partial C}\delta C + \frac{\partial\langle\hat{\mathcal{H}}_{ALM}\rangle_G}{\partial W}\delta W + \frac{\partial\langle\hat{\mathcal{H}}_{ALM}\rangle_G}{\partial F}\delta F + \frac{\partial\langle\hat{\mathcal{H}}_{ALM}\rangle_G}{\partial n_{0f}}\delta n_{0f}, \end{aligned} \tag{2.45}$$

where for clarity we have skipped the lattice indices and the summations over them. It leads directly to the following form of the effective single-particle two-band Hamiltonian with non-local interband hybridization, i.e,

$$\hat{\mathcal{H}}^{\text{eff}} \equiv \sum_{\mathbf{i},\mathbf{j},\sigma} t^c_{\mathbf{ij}} \hat{c}^\dagger_{\mathbf{i}\sigma} \hat{c}_{\mathbf{j}\sigma} + \sum_{\mathbf{i},\mathbf{j},\sigma} t^f_{\mathbf{ij}} \hat{f}^\dagger_{\mathbf{i}\sigma} \hat{f}_{\mathbf{j}\sigma} + \sum_{\mathbf{i},\mathbf{j},\sigma} (V^{fc}_{\mathbf{ij}} \hat{c}^\dagger_{\mathbf{i}\sigma} \hat{f}_{\mathbf{j}\sigma} + \text{H.c.}) + const, \tag{2.46}$$

where the effective hopping and the hybridization parameters are derivatives with respect to lines, i.e.,

$$\begin{aligned} t^c_{\mathbf{ij}} &= \frac{\partial\langle\hat{\mathcal{H}}_{ALM}\rangle_G}{\partial C_{\mathbf{ij}}}, \qquad t^f_{\mathbf{ij}} = \frac{\partial\langle\hat{\mathcal{H}}_{ALM}\rangle_G}{\partial F_{\mathbf{ij}}}, \\ V^{fc}_{\mathbf{ij}} &= \frac{\partial\langle\hat{\mathcal{H}}_{ALM}\rangle_G}{\partial W_{\mathbf{ij}}}, \qquad t^f_{\mathbf{ii}} = \frac{\partial\langle\hat{\mathcal{H}}_{ALM}\rangle_G}{\partial n_{0f}}. \end{aligned} \tag{2.47}$$

In the following we would set the constant in definition (2.46) equal zero as it is trivial shift of the reference energy level. Note that now the f electrons acquire direct-hopping

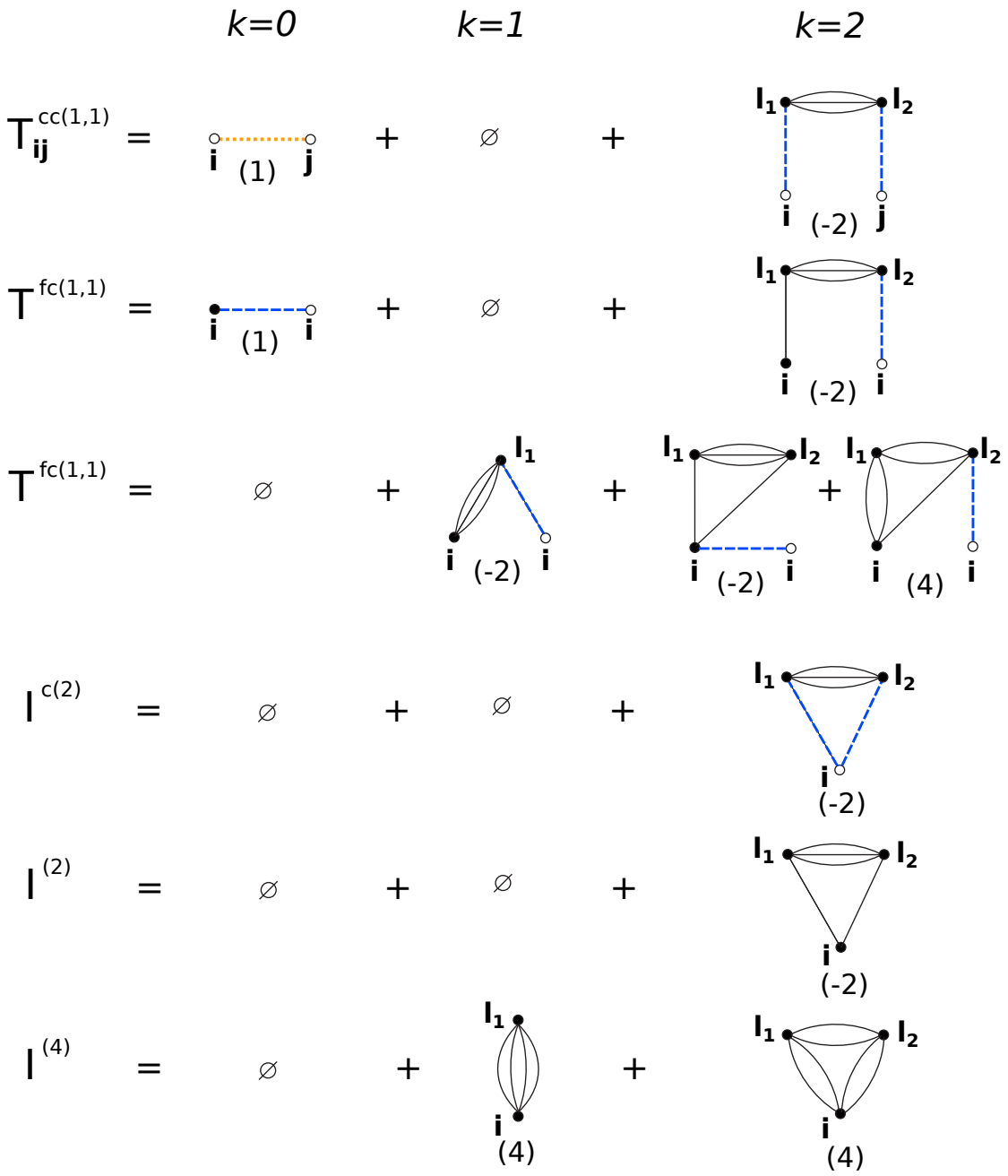

Figure 2.2: Diagrammatic sums up to the second order, $k = 2$, for the paramagnetic case and with the onsite hybridization. c- and f- orbital sites are denoted with empty and filled circles respectively. Solid (black), dotted (orange), and dashed (blue) connections, represents contractions between f orbitals, c orbitals, and mixed, respectively. The numbers (in brackets) under the diagrams stands for their multiplicity resulting from the application of Wick's theorem. The symbols $\varnothing$ denote the absence of contribution in given order of expansion, due to the cancellation of the diagrams consisting of loops at the given vertex - so-called *Hartree bubbles*.

property and the hybridization also an intersite contribution. In order to obtain the effective dispersion relations for c- and f-electrons and the $\mathbf{k}$-dependent hybridization we apply the usual lattice Fourier transform

$$\begin{aligned}\epsilon^{c(f)}_{\mathbf{k}} &= \frac{1}{L}\sum_{\mathbf{i},\mathbf{j}} e^{i(\mathbf{i}-\mathbf{j})\mathbf{k}} t^{c(f)}_{\mathbf{ij}},\\ V^{cf}_{\mathbf{k}} &= \frac{1}{L}\sum_{\mathbf{i},\mathbf{j}} e^{i(\mathbf{i}-\mathbf{j})\mathbf{k}} V^{cf}_{\mathbf{ij}}.\end{aligned} \tag{2.48}$$

In this manner, we reduce the many-body interacting model to the effective two-band Hamiltonian straightforwardly diagonalized to the effective single-quasiparticle picture. The 2x2 -matrix representation of (2.46) in k-space representation reads,

$$\begin{aligned}\hat{\mathcal{H}}^{\text{eff}} &= \sum_{\mathbf{k},\sigma} (\hat{c}^\dagger_{\mathbf{k}\sigma}\ \hat{f}^\dagger_{\mathbf{k}\sigma}) \begin{pmatrix} \epsilon^c_{\mathbf{k}} & V^{cf}_{\mathbf{k}} \\ V^{cf}_{\mathbf{k}} & \epsilon^f_{\mathbf{k}} \end{pmatrix} \begin{pmatrix} \hat{c}_{\mathbf{k}\sigma} \\ \hat{f}_{\mathbf{k}\sigma} \end{pmatrix} \\ &= \sum_{\mathbf{k},\sigma} (\hat{c}^\dagger_{\mathbf{k}\sigma}\ \hat{f}^\dagger_{\mathbf{k}\sigma}) \mathcal{T}^\dagger \begin{pmatrix} E_{\mathbf{k}+} & 0 \\ 0 & E_{\mathbf{k}-} \end{pmatrix} \mathcal{T} \begin{pmatrix} \hat{c}_{\mathbf{k}\sigma} \\ \hat{f}_{\mathbf{k}\sigma} \end{pmatrix},\end{aligned} \tag{2.49}$$

where the eigenvalues, $E_{\mathbf{k}\pm}$ of the above Hamiltonian are,

$$E_{\mathbf{k}a} = \xi^+_{\mathbf{k}} + a\sqrt{(\xi^-_{\mathbf{k}})^2 + (V^{cf}_{\mathbf{k}})^2}, \tag{2.50}$$

where $a \equiv \pm 1$ differentiates between the two hybridized bands. For convenience we also define

$$\xi^+_{\mathbf{k}} \equiv \frac{\epsilon^c_{\mathbf{k}} + \epsilon^f_{\mathbf{k}}}{2} \quad \text{and} \quad \xi^-_{\mathbf{k}} \equiv \frac{\epsilon^c_{\mathbf{k}} - \epsilon^f_{\mathbf{k}}}{2}. \tag{2.51}$$

$\mathcal{T}$ in (2.49) is unitary transformation matrix to the base in which the $\hat{\mathcal{H}}^{\text{eff}}$ is diagonal, defined as

$$\mathcal{T} = \begin{pmatrix} u_+ & u_- \\ u_- & -u_+ \end{pmatrix}, \tag{2.52}$$

where

$$u_\pm = \sqrt{\frac{1}{2}\left(1 \pm \frac{\xi^-_{\mathbf{k}}}{\sqrt{(\xi^-_{\mathbf{k}})^2 + (V^{cf}_{\mathbf{k}})^2}}\right)}, \tag{2.53}$$

Now, it is straightforward to determine explicitly the following correlation functions

$$\begin{aligned}\langle \hat{c}^\dagger_{\mathbf{k}\sigma}\hat{c}_{\mathbf{k}\sigma}\rangle_0 &= u^2_+\Theta(E_{\mathbf{k}+}) + u^2_-\Theta(E_{\mathbf{k}-}),\\ \langle \hat{f}^\dagger_{\mathbf{k}\sigma}\hat{c}_{\mathbf{k}\sigma}\rangle_0 &= u_+u_-\big(\Theta(E_{\mathbf{k}+}) - \Theta(E_{\mathbf{k}-})\big),\\ \langle \hat{f}^\dagger_{\mathbf{k}\sigma}\hat{f}_{\mathbf{k}\sigma}\rangle_0 &= u^2_-\Theta(E_{\mathbf{k}+}) + u^2_+\Theta(E_{\mathbf{k}-}),\end{aligned} \tag{2.54}$$

where $\Theta(E)$ denotes the Heaviside step function which plays the role of energy cutoff for the respective quasiparticle bands energies (2.50). Using the inverse Fourier trans-

formation we obtain the self-consistent equations for lines and n_{0f}:

$$\begin{aligned} C_{\mathbf{ij}} &= \frac{1}{L}\sum_{\mathbf{k}a}\langle \hat{c}^{\dagger}_{\mathbf{k}\sigma}\hat{c}_{\mathbf{k}\sigma}\rangle_0 \; e^{i(\mathbf{i}-\mathbf{j})\mathbf{k}}, \\ W_{\mathbf{ij}} &= \frac{1}{L}\sum_{\mathbf{k}a}\langle \hat{f}^{\dagger}_{\mathbf{k}\sigma}\hat{c}_{\mathbf{k}\sigma}\rangle_0 \; e^{i(\mathbf{i}-\mathbf{j})\mathbf{k}}, \\ F_{\mathbf{ij}} &= \frac{1}{L}\sum_{\mathbf{k}a}\langle \hat{f}^{\dagger}_{\mathbf{k}\sigma}\hat{f}_{\mathbf{k}\sigma}\rangle_0 \; e^{i(\mathbf{i}-\mathbf{j})\mathbf{k}}, \\ n_{0f} &= \frac{1}{L}\sum_{\mathbf{k}a}\langle \hat{f}^{\dagger}_{\mathbf{k}\sigma}\hat{f}_{\mathbf{k}\sigma}\rangle_0. \end{aligned} \tag{2.55}$$

Explicit formulas read,

$$C_{\mathbf{ij}} = \frac{1}{L}\sum_{\mathbf{k}a}\frac{\Theta(E_{\mathbf{k}a})}{2}\left(1+\frac{a\xi^{-}_{\mathbf{k}}}{\sqrt{(\xi^{-}_{\mathbf{k}})^2+(V^{cf}_{\mathbf{k}})^2}}\right)e^{i(\mathbf{i}-\mathbf{j})\mathbf{k}}, \tag{2.56}$$

$$W_{\mathbf{ij}} = \frac{1}{L}\sum_{\mathbf{k}a}\frac{\Theta(E_{\mathbf{k}a})}{2}\frac{aV^{cf}_{\mathbf{k}}}{\sqrt{(\xi^{-}_{\mathbf{k}})^2+(V^{cf}_{\mathbf{k}})^2}}e^{i(\mathbf{i}-\mathbf{j})\mathbf{k}}, \tag{2.57}$$

$$F_{\mathbf{ij}} = \frac{1}{L}\sum_{\mathbf{k}a}\frac{\Theta(E_{\mathbf{k}a})}{2}\left(1-\frac{a\xi^{-}_{\mathbf{k}}}{\sqrt{(\xi^{-}_{\mathbf{k}})^2+(V^{cf}_{\mathbf{k}})^2}}\right)e^{i(\mathbf{i}-\mathbf{j})\mathbf{k}}, \tag{2.58}$$

$$n_{0f} = \frac{1}{L}\sum_{\mathbf{k}a}\frac{\Theta(E_{\mathbf{k}a})}{2}\left(1-\frac{a\xi^{-}_{\mathbf{k}}}{\sqrt{(\xi^{-}_{\mathbf{k}})^2+(V^{cf}_{\mathbf{k}})^2}}\right). \tag{2.59}$$

To determine the properties of the model, we solve the system of Eqs. (2.47) and (2.55), together with the minimization of $\langle\hat{\mathcal{H}}_{ALM}\rangle_G$ with respect to x. As an additional constraint, we add the adjustment of the chemical potential in order to preserve fixed total number of particles in the system. For that purpose we use the self-consistent loop procedure [115, 55, 59, 116, 117] according to the general scheme pointed out in the previous subsection.

Finally, the ground state energy E_G is defined by

$$E_G = \langle\hat{\mathcal{H}}_{ALM}\rangle_G|_0 + n\mu, \tag{2.60}$$

where $\langle\hat{\mathcal{H}}_{ALM}\rangle_G|_0$ denotes the expectation value (2.43) of the starting Hamiltonian for the equilibrium values of the lines and the total number of particles $n \equiv 2\langle\hat{n}^{f}_{\mathbf{i}\sigma}+\hat{n}^{c}_{\mathbf{i}\sigma}\rangle_G$. The f-orbital filling separately is defined by $n_f \equiv 2\langle\hat{n}^{f}_{\mathbf{i}\sigma}\rangle_G$.

2.2.3 Superconducting Phase

In this Section we consider spin-singlet superconducting phase solution for the Anderson lattice model (2.21) with the nearest-neighbor intersite hybridization. In this case, we have to allow for appearance of both paramagnetic and superconducting contractions

(lines), which we define respectively as

$$\begin{aligned} P^{\alpha,\beta}_{\mathbf{l},\mathbf{l}'} &\equiv \langle \hat{\alpha}^{\dagger}_{\mathbf{l}\sigma}\hat{\beta}_{\mathbf{l}'\sigma}\rangle_0 - \delta_{\alpha,f}\delta_{\beta,f}\delta_{\mathbf{l},\mathbf{l}'}n_{0f}, \\ S^{\alpha,\beta}_{\mathbf{l},\mathbf{l}'} &\equiv \langle \hat{\alpha}^{\dagger}_{\mathbf{l}\sigma}\hat{\beta}^{\dagger}_{\mathbf{l}'\bar{\sigma}}\rangle_0, \end{aligned} \tag{2.61}$$

where $\alpha, \beta \in \{c, f\}$, and $\mathbf{l}, \mathbf{l}'$ are lattice sites. Note that although the spin indecies are important in the case of superconducting phase the lines as well as n_{0f} are spin-independent. We consider general nodal d-wave symmetry of the superconducting state. Therefore, we set to zero following superconducting contractions: $S^{\alpha,\beta}_{0,0} = 0$, $S^{\alpha,\beta}_{1,1} = 0$ and $S^{\alpha,\beta}_{2,2} = 0$ where we have defined $S^{\alpha,\beta}_{\mathbf{l},\mathbf{l}'} \equiv S^{\alpha,\beta}_{|l_x - l'_x|,|l_y - l'_y|}$ (cf. Fig. 2.1). Following the same procedure as in the preceding Subsection, the effective single particle Hamiltonian $\hat{\mathcal{H}}^{\text{eff}}$ for the uncorrelated wave function $|\psi_0\rangle$ is now determined from the condition

$$\begin{aligned} &\delta\langle\hat{\mathcal{H}}^{\text{eff}}\rangle_0(P^{\alpha,\beta}_{\mathbf{l},\mathbf{l}'}, S^{\alpha,\beta}_{\mathbf{l},\mathbf{l}'}, n_{0f}) = \delta\langle\hat{\mathcal{H}}_{ALM}\rangle_G(P^{\alpha,\beta}_{\mathbf{l},\mathbf{l}'}, S^{\alpha,\beta}_{\mathbf{l},\mathbf{l}'}, n_{0f}) \\ &= \frac{\partial\langle\hat{\mathcal{H}}_{ALM}\rangle_G}{\partial P^{\alpha,\beta}_{\mathbf{l},\mathbf{l}'}}\delta P^{\alpha,\beta}_{\mathbf{l},\mathbf{l}'} + \frac{\partial\langle\hat{\mathcal{H}}_{ALM}\rangle_G}{\partial S^{\alpha,\beta}_{\mathbf{l},\mathbf{l}'}}\delta S^{\alpha,\beta}_{\mathbf{l},\mathbf{l}'} + \frac{\partial\langle\hat{\mathcal{H}}_{ALM}\rangle_G}{\partial n_{0f}}\delta n_{0f}. \end{aligned} \tag{2.62}$$

Explicitly, the effective single particle Hamiltonian reads now

$$\begin{aligned} \hat{\mathcal{H}}^{\text{eff}} &= \sum_{\mathbf{i},\mathbf{j},\sigma}\left(t^{cc}_{\mathbf{ij}}\hat{c}^{\dagger}_{\mathbf{i}\sigma}\hat{c}_{\mathbf{j}\sigma} + t^{ff}_{\mathbf{ij}}\hat{f}^{\dagger}_{\mathbf{i}\sigma}\hat{f}_{\mathbf{j}\sigma} + t^{cf}_{\mathbf{ij}}(\hat{c}^{\dagger}_{\mathbf{i}\sigma}\hat{f}_{\mathbf{j}\sigma} + \text{h.c.})\right) \\ &+ \sum_{\mathbf{i},\mathbf{j},\sigma}\Delta^{cf}_{\mathbf{ij}}(\hat{c}^{\dagger}_{\mathbf{i}\sigma}\hat{f}^{\dagger}_{\mathbf{j}\bar{\sigma}} + \text{h.c.}) + \sum_{\mathbf{i},\mathbf{j}}\Delta^{ff}_{\mathbf{ij}}(\hat{f}^{\dagger}_{\mathbf{i}\uparrow}\hat{f}^{\dagger}_{\mathbf{j}\downarrow} + \text{h.c.}) + const., \end{aligned} \tag{2.63}$$

with effective microscopic parameters defined as

$$t^{\alpha\beta}_{\mathbf{ij}} = \frac{\partial\langle\mathcal{H}_{ALM}\rangle_G}{\partial P^{\alpha,\beta}_{\mathbf{i},\mathbf{j}}}, \qquad \Delta^{\alpha\beta}_{\mathbf{ij}} = \frac{\partial\langle\mathcal{H}_{ALM}\rangle_G}{\partial S^{\alpha,\beta}_{\mathbf{i},\mathbf{j}}}, \qquad t^{ff}_{\mathbf{ii}} = \frac{\partial\langle\mathcal{H}_{ALM}\rangle_G}{\partial n_{0f}}. \tag{2.64}$$

In (2.63) constant is set to zero as it causes only the trivial shift of the energy reference level. There is no effective pairing between the c-electrons due to the lack of lines $S^{c,c}_{\mathbf{i},\mathbf{j}}$ in any of the diagrams visualizing the Wick's contractions. By means of the Fourier transformation to the momentum space the effective Hamiltonian is brought to the Bogoliubov - de Gennes - Nambu form [4],

$$\hat{\mathcal{H}}^{\text{eff}} = \sum_{\mathbf{k}}\Psi^{\dagger}_{\mathbf{k}}\begin{pmatrix} \epsilon^{cc}_{\mathbf{k}} & 0 & \epsilon^{fc}_{\mathbf{k}} & \Delta^{fc}_{\mathbf{k}} \\ 0 & -\epsilon^{cc}_{\mathbf{k}} & \Delta^{fc}_{\mathbf{k}} & -\epsilon^{fc}_{\mathbf{k}} \\ \epsilon^{fc}_{\mathbf{k}} & \Delta^{fc}_{\mathbf{k}} & \epsilon^{ff}_{\mathbf{k}} & \Delta^{ff}_{\mathbf{k}} \\ \Delta^{fc}_{\mathbf{k}} & -\epsilon^{fc}_{\mathbf{k}} & \Delta^{ff}_{\mathbf{k}} & -\epsilon^{ff}_{\mathbf{k}} \end{pmatrix}\Psi_{\mathbf{k}}, \tag{2.65}$$

where we have defined $\Psi^{\dagger} \equiv (\hat{c}^{\dagger}_{\mathbf{k}\uparrow},\ \hat{c}_{-\mathbf{k}\downarrow},\ \hat{f}^{\dagger}_{\mathbf{k}\uparrow},\ \hat{f}_{-\mathbf{k}\downarrow})$ and

$$\begin{aligned} \epsilon^{\alpha\beta}_{\mathbf{k}} &= \frac{1}{L}\sum_{\mathbf{ij}} t^{\alpha\beta}_{\mathbf{ij}} e^{i(\mathbf{i}-\mathbf{j})\mathbf{k}}, \\ \Delta^{\alpha\beta}_{\mathbf{k}} &= \frac{1}{L}\sum_{\mathbf{ij}} \Delta^{\alpha\beta}_{\mathbf{ij}} e^{i(\mathbf{i}-\mathbf{j})\mathbf{k}}. \end{aligned} \tag{2.66}$$

By L we again denote number of the lattice sites. The system posses now two gaps and therefore the formalism contains 4x4 matrices. Parenthetically, the same type of formal expressions will appear for a two-band superconductor.

Hamiltonian (2.65) can be easily transformed into the diagonal form by unitary transformation $\mathcal{T}$ composed of its normalized eigenvectors. The respective averages of components of Ψ and $\Psi^\dagger$ can be expressed as

$$\langle \Psi_n^\dagger \Psi_m \rangle = \sum_j \mathcal{T}_{jn} \mathcal{T}_{jm} \Theta(E_j), \tag{2.67}$$

where E_j is j-th eigenvalue to the eigenvector $\phi_j = (\mathcal{T}_{j1}\ \mathcal{T}_{j2}\ \mathcal{T}_{j3}\ \mathcal{T}_{j4})$ of the Hamiltonian (2.65). By the inverse Fourier transform the formulas for the new lines read

$$\begin{aligned} P_{\mathbf{i},\mathbf{j}}^{\alpha,\beta} &= \frac{1}{L} \sum_{\mathbf{k}} \langle \hat{\alpha}_{\mathbf{k}}^\dagger \hat{\beta}_{\mathbf{k}} \rangle_0 e^{i(\mathbf{i}-\mathbf{j})\mathbf{k}}, \\ S_{\mathbf{i},\mathbf{j}}^{\alpha,\beta} &= \frac{1}{L} \sum_{\mathbf{k}} \langle \hat{\alpha}_{\mathbf{k}}^\dagger \hat{\beta}_{\mathbf{k}}^\dagger \rangle_0 e^{i(\mathbf{i}-\mathbf{j})\mathbf{k}}. \end{aligned} \tag{2.68}$$

Effectively, to determine equilibrium properties of the model the systems of Eqs. (2.64) and (2.68) need to be solved self-consistently together with minimization of $\langle \hat{\mathcal{H}}_{ALM} \rangle_G$ with respect to x [115, 55, 59, 116, 117]. We also adjust chemical potential to preserve total number of electrons in the system as we change other microscopic parameters of the model in the new phase. Finally the physical ground state energy of the system is obtained in the form

$$E_G = \langle \hat{\mathcal{H}}_{ALM} \rangle_G |_0 + n\mu, \tag{2.69}$$

where $|_0$ denotes the equilibrium value and $n \equiv 2\langle \hat{n}_{\mathbf{i}\sigma}^f + \hat{n}_{\mathbf{i}\sigma}^c \rangle_G$ is the total electron concentration.

The presented variational scheme determines thus both $\hat{\mathcal{H}}^{\text{eff}}$ and $|\psi_0\rangle$. The latter, in turn, allows for computing the superconducting correlation functions, i.e.,

$$\Delta_{G;i_x-j_x,i_y-j_y}^{\alpha\beta} \equiv \langle \hat{\alpha}_{\mathbf{i}}^\dagger \hat{\beta}_{\mathbf{j}}^\dagger \rangle_G = \langle \hat{\alpha}_{\mathbf{i}} \hat{\beta}_{\mathbf{j}} \rangle_G. \tag{2.70}$$

Interestingly, although there is no pairing term between c electrons in the effective Hamiltonian (2.63), $\Delta_{\mathbf{k}}^{cc} \equiv \langle \hat{c}_{\mathbf{k}}^\dagger \hat{c}_{\mathbf{k}}^\dagger \rangle_0 = \langle \hat{c}_{\mathbf{k}} \hat{c}_{\mathbf{k}} \rangle_0$, the corresponding superconducting correlation functions $\langle \hat{c}_{\mathbf{i}}^\dagger \hat{c}_{\mathbf{j}}^\dagger \rangle_G = \langle \hat{c}_{\mathbf{i}} \hat{c}_{\mathbf{j}} \rangle_G$ are finite. This means that the correlations induce also the pairing in the effective conduction band.

2.3 Appendix: Equivalence of zeroth order of DE-GWF with GA: Paramagnetic case

Here we show the equivalence of the zeroth order DE-GWF and the standard Gutzwiller approximation (GA) on the example of paramgnetic ALM. In both methods, DE-GWF in the zeroth order of expansion ($k = 0$) and GA the effect of the projection can be summarized by the expressions for evaluating following expectation values: $\langle \hat{n}_{\mathbf{i}\uparrow} \hat{n}_{\mathbf{i}\downarrow} \rangle_G$ and $\langle \hat{f}_{\mathbf{i}\sigma}^\dagger \hat{c}_{\mathbf{i}\sigma} + \text{H.c.} \rangle_G$. The remaining averages in ALM are unchanged under the projection.

Explicitly, in the DE-GWF for $k = 0$ the resulting averages are expressed as follows

$$\langle \hat{n}_{\mathbf{i}\uparrow} \hat{n}_{\mathbf{i}\downarrow} \rangle_G^{(k=0)} = \lambda_d^2 n_{0f}^2 \tag{2.71a}$$

$$\langle \hat{f}^{\dagger}_{\mathbf{i}\sigma}\hat{c}_{\mathbf{i}\sigma} + \text{H.c.}\rangle_G^{(k=0)} = \alpha\langle \hat{f}^{\dagger}_{\mathbf{i}\sigma}\hat{c}_{\mathbf{i}\sigma} + \text{H.c.}\rangle_0, \tag{2.71b}$$

where parameter α is defined as

$$\alpha \equiv (1-n_{0f})\lambda_0\lambda_s + n_{0f}\lambda_d\lambda_s. \tag{2.72}$$

On the other hand, in GA the resulting averages are expressed as[129]

$$\langle \hat{n}_{\mathbf{i}\uparrow}\hat{n}_{\mathbf{i}\downarrow}\rangle_G^{(GA)} = \langle n^f_{\mathbf{i}\uparrow}\hat{n}^f_{\mathbf{i}\downarrow}\rangle_0 \equiv d^2, \tag{2.73a}$$

$$\langle \hat{f}^{\dagger}_{\mathbf{i}\sigma}\hat{c}_{\mathbf{i}\sigma} + \text{H.c.}\rangle_G^{(GA)} = \sqrt{q_\sigma}\langle \hat{f}^{\dagger}_{\mathbf{i}\sigma}\hat{c}_{\mathbf{i}\sigma} + \text{H.c.}\rangle_0, \tag{2.73b}$$

where the parameter d^2 is the double occupancy probability, and q_σ is the so-called Gutzwiller factor reducing the hybridization amplitude, which for the equal number of particles for each spin is defined as

$$\sqrt{q} = \frac{\sqrt{(n_{0f}-d^2)(1-2n_{0f}+d^2)} + \sqrt{(n_{0f}-d^2)d^2}}{\sqrt{n_{0f}(1-n_{0f})}}. \tag{2.74}$$

If we identify double occupancy probabilities expressed by both methods in (2.73a) and (2.71a) to be equal: $d^2 = \lambda_d^2 n_{0f}^2$, then parameter α (2.72) exactly reduces to the parameter $\sqrt{q}$ (2.74).

GA procedure in the SGA formulation effectively, results in the effective single-particle Hamiltonian of the form

$$\begin{aligned}\hat{\mathcal{H}}_{GA} \equiv \sum_{\mathbf{k},\sigma} \hat{\Psi}^{\dagger}_{\mathbf{k}\sigma} \begin{pmatrix} \epsilon^c_{\mathbf{k}} - \mu & \sqrt{q_\sigma}V \\ \sqrt{q_\sigma}V & \epsilon_f - \mu \end{pmatrix} \hat{\Psi}_{\mathbf{k}\sigma} + LUd^2 \\ -\lambda^f_n\Big(\sum_{\mathbf{k}\sigma}\hat{n}^f_{\mathbf{k}\sigma} - Ln_{0f}\Big) - \lambda^f_m\Big(\sum_{\mathbf{k}\sigma}\sigma\hat{n}^f_{\mathbf{k}\sigma} - Lm_f\Big).\end{aligned} \tag{2.75}$$

In the above expressions the constraints for f-electron concentration and their magnetization are necessarily added in order to satisfy the consistency of the whole procedure [133, 129]. In effect, the whole variational problem is reduced to optimization of the Landau grand potential functional with respect to d^2, n_{0f}, m_f, and of the Lagrange multipliers λ^f_n and λ^f_m, playing the role of the effective molecular fields [133].

However, the effect of the constraint for f-electron magnetization is crucial in the case of magnetism consideration, either as intrinsic[113, 114] or induced by the applied magnetic field [38]. Here we discuss nonmagnetic state only and thus simply $m^f = \lambda^f_m = \lambda^f_n = 0$.

DE-GWF method guarantees by construction that the variationally obtained f-electron occupancy n_f coincides with that obtained self-consistently [116]. We have thus provided an analytical argument for the equivalence of DE-GWF method for $k = 0$ and the standard GA procedure. Also, by an independent numerical crosscheck we have seen that all the observables calculated within both methods indeed coincide in that situation.

Chapter 3

Articles Composing the Thesis with Summaries

3.1 A brief overview of the main results

During the four-year doctoral studies several problems concerning strongly correlated systems, mainly heavy-fermion compounds and unconventional superconductivity, have been tackled.

The first addressed problem was the metamagnetism and spin-dependent effective masses triggered by the applied magnetic field. We have analyzed it within the Hubbard model by using the statistically-consistent Gutzwiller approximation [38]. Although the motivation was to study the canonical correlated system, normal liquid ^{3}He without hybridized states as such it turned out that the predictions are quite universal and similar metamagnetic behavior afterwards was found in heavy fermion compound UPt_3 [136, 137].

The work on the Hubbard model was also the prelude to the investigations of the more complex hybridized two-orbital systems described within the Anderson lattice model, treated also by the SGA method. Specifically the magnetic phase diagram on the pressure - magnetic field - temperature planes of the spin-triplet superconductor UGe_2 was addressed [113, 114, 120]. We have provided a microscopic interpretation of the origin of two distinct ferromagnetic phases changing with the Fermi surface topology, and triggered by mutual competition of the Coulomb interaction and the hybridization. Our model not only has provided excellent quantitative agreement with the experimental data concerning emergence of the all observed critical points, both classical and quantum, but also predicted a new Lifshitz-type quantum critical point (QCP) in the close vicinity of the superconducting dome, that can be thus related to the pairing.

Nonetheless, the renormalized mean-field approach, SGA, fails to describe the heavy fermion superconductivity in the Anderson lattice model. For that reason we have applied to this model the recently proposed [115, 55, 59, 116, 117] variational technique, diagrammatic expansion for Gutzwiller wave function (DE-GWF) enabling us to carry out the systematic analysis approaching the full Gutzwiller-wave-function solution. By accounting for the correlations beyond the local sites, this technique indeed provides a stable superconducting solution.

As a starting point to the superconductivity investigations, we have first studied thoroughly the paramagnetic phase of the Anderson lattice model within DE-GWF [118].

In this case, with the inclusion of the higher orders of the expansion we have obtained enormous effective mass enhancement by determining the density of states at the Fermi level, as well as shown a formation of the f band out of initially localized atomic f states. The latter property leads to the proof of existence of the three universal disjoint heavy fermion regimes within a single framework. These are the mixed-valence regime, the almost-Kondo/Kondo insulator regime, and the Kondo-lattice regime.

On that basis we have finally addressed the issue of the correlation-driven microscopic mechanism of superconductivity [121]. Namely, we have enriched our previous considerations of the paramagnetism by the superconducting correlations, and obtained its stability in a wide range of the hybridization strength and total fillings. Determined paired phase reflects several features observed experimentally e.g. for $CeCoIn_5$ [102, 100, 101] such as mainly $d_{x^2-y^2}$-wave symmetry of the order parameter, two-gaped structure, and a reasonable value of the pairing condensation energy, together with its non-BCS features.

3.2 Article A.1, Properties of an almost localized Fermi liquid in an applied magnetic field revisited: a statistically consistent Gutzwiller approach

In this work we have studied the system of the neutral spin-$\frac{1}{2}$ fermions in the regime of the total number of particles close to the half filling. The motivation for this work was the attempt to reproduce within the Hubbard model the normal liquid ^{3}He magnetization measurements in high magnetic fields [49]. The previous theory of the the normal liquid ^{3}He as an almost localized system based on the standard Gutzwiller approach (GA) failed to do so as it predicts spectacular metamagnetic transition [48] which is not observed in experiment [49]. In our group, the statistical inconsistencies in GA were corrected when the magnetic field or spontaneous magnetization is accounted for [133]. The generalized approach, SGA (cf. Sec. 2.1) was implemented to the almost half-filled Hubbard model on the closed packed *fcc* three-dimensional lattice. The model was thoroughly studied in terms of the correlation induced features, specifically **(i)** spin dependent masses in the high magnetic fields universally observed in the heavy fermion systems [138, 139], and **(ii)** signs of a metamagnetic-like features determined from the magnetization and specific heat curves - recently similar behavior was observed in the case of UPt_3 [136, 137]. **(iii)** The critical discussion of our predictions when compared to the normal liquid ^{3}He case, has also been done. We have pointed out the problem that the good quantitative fit to the experimental data is performed at the cost of disagreement for the effective masses enhancement. This disagreement may meen that a careful analysis of higher order (beyond SGA) contributions should be carried out. The results are described in detail in article A.1.

The preliminary results of this work specifically concerning normal liquid ^{3}He were published in the Salerno Workshop Proceedings [140] and included in the authors Master Thesis 2011 [141].

IOP Publishing Journal of Physics: Condensed Matter
J. Phys.: Condens. Matter **26** (2014) 055601 (9pp) doi:10.1088/0953-8984/26/5/055601

Properties of an almost localized Fermi liquid in an applied magnetic field revisited: a statistically consistent Gutzwiller approach

Marcin M Wysokiński[1] **and Jozef Spałek**[1,2]

[1] Marian Smoluchowski Institute of Physics, Jagiellonian University, Reymonta 4, PL-30-059 Kraków, Poland
[2] Academic Centre for Materials and Nanotechnology (ACMiN) and Faculty of Physics and Applied Computer Science, AGH University of Science and Technology, Aleja Mickiewicza 30, PL-30-059 Kraków, Poland

E-mail: marcin.wysokinski@uj.edu.pl and ufspalek@if.uj.edu.pl

Received 22 October 2013, revised 22 November 2013
Accepted for publication 9 December 2013
Published 16 January 2014

Abstract
We discuss the Hubbard model in an applied magnetic field and analyze the properties of neutral spin-$\frac{1}{2}$ fermions within the so-called *statistically consistent Gutzwiller approximation*. The magnetization curve reproduces in a semiquantitative manner the experimental data for liquid ^{3}He in the regime of moderate correlations and in the presence of a small number of vacant cells, modeled by a non-half-filled band situation, when a small number of vacancies ($\sim$5%) is introduced in the virtual fcc lattice. We also present the results for the magnetic susceptibility and the specific heat, in which a *metamagnetic-like* behavior is also singled out in a non-half-filled band case.

Keywords: correlated fermions, statistically consistent Gutzwiller approach, liquid helium 3, almost-localized Fermi liquid, magnetic properties of Fermi liquid

(Some figures may appear in colour only in the online journal)

1. Introduction

In condensed matter physics, systems with moderate to strong local correlations, such as almost-localized electron systems, heavy-fermion metals, liquid ^{3}He, and selected cold atomic systems in optical lattices, have been extensively studied during the past decades. On the other hand, starting from the seminal Landau papers on the theory of Fermi liquids [1, 2] as a direct generalization of the concept of an electron gas, it became unquestionable that the interactions between fermions are the source of their non-trivial physical properties even before the Mott transition to the localized state takes place for either sufficiently strong interactions or low density. The original Landau formulation [1], despite being in essence phenomenological, provides a good qualitative rationalization of the observed effective mass enhancement of ^{3}He atoms in the liquid state [3–6] and that of electrons in metals. However, the Landau Fermi liquid theory turned out to be insufficient to account for specific, more sophisticated effects of the correlations, such as Mott (Mott–Hubbard) localization [7], the appearance of spin-dependent effective masses of quasi-particles [8], or the observation of metamagnetism of itinerant almost-localized and correlated fermions [9]. Note that by *correlated fermions* or a *correlated Fermi liquid* we understand a system for which the kinetic or Fermi energy (per particle) is comparable to or even smaller than the interaction energy per particle. Therefore, strictly speaking, one should term those systems *strongly interacting*; however, that particular phrase is reserved for high-energy interactions of elementary particles. Similar correlated states appear also there, such as, for exam-

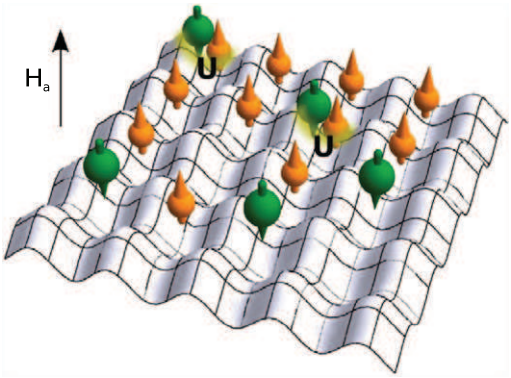

Figure 1. Schematic visualization of the division of a quantum-liquid state into an effective lattice system composed of cells (modeled by potential valleys with spin $\frac{1}{2}$ fermions). Every cell can contain up to two fermions with opposite spins, at the price of energy loss U. The number of fermions N_e is assumed in general to differ from the number of all sites N_L, i.e., $N_e < N_L$. Consequently, in the applied field the effective masses of the minority spin fermions are enhanced when compared to those of the spin-majority fermions, as discussed in the main text.

ple, the deconfinement transition of condensed hadron matter into the quark–gluon plasma contains the principal features of the Mott localization–delocalization transition [10, 11]. Hence the concept of an almost-localized Fermi liquid seems to have a universal meaning in condensed matter physics.

One of the basic microscopic models of correlated fermions for lattice systems is the Hubbard model, accounting for a balance between the kinetic energy of moving fermions (hopping energy) and the effective local repulsive interaction U, whenever two fermions with opposite spins (or other internal quantum number) occupy the same site (cell) and the same orbital (Wannier) state (see figure 1 for visualization of such state). Within this model, not only the principal predictions of the Landau Fermi liquid theory have been derived [9, 12], but also a unique explanation of the correlation-driven Mott metal–insulator transition [7] and the emergence of d-wave pairing have been discussed [13]. The importance of the Hubbard model manifests itself also as the basis of the derivation of the so-called t–J model, which turned out to be very successful in a description of the high-temperature superconductivity in the cuprates (see, for example, [14]).

An important approach to solving the Hubbard model is the variational Gutzwiller wave function (GWF) [15, 16] and its simplified version—the Gutzwiller approximation (GA) [7, 17]. Those methods are based on the paradigm of optimizing the number of doubly occupied sites (cells) which appear in both the local repulsive energy and the renormalized band energy. In effect, the simpler GA approach leads among others to a renormalized mass of the quasiparticles in a direct manner which becomes divergent at the point of Mott–Hubbard localization [18, 19], as well as leading concomitantly to the infinite zero-field magnetic susceptibility in the paramagnetic state [20]. Although the GA is, strictly speaking, exact only for a lattice of infinite dimensionality [7], it may provide a good description of almost-localized systems above the so-called upper critical dimensionality (as yet not determined) for fermions. Minimally, it plays the role of a mean-field theory. Among other techniques frequently applied to the Hubbard model are dynamical mean-field theory (DMFT) [21] and the quantum Monte Carlo (QMC) [22] method.

Recently, we have discovered statistical inconsistencies in the GA when one includes the magnetic field via the Zeeman term, and have provided the necessary correction to the GA approach. The extended approach, called the statistically consistent Gutzwiller approximation (SGA), was successfully applied also to the t–J [14, 23, 24], t–J-U [25] and periodic Anderson models [26] to describe both magnetism and superconductivity. The SGA is of the same class approach as the GA (exact in the infinite-dimension limit [7]), but is furthermore consistent from the statistical physics point of view, as explained in detail below (cf. appendix A).

The SGA method we are going to discuss here has its own merits. First, it is analytic and therefore can be applied to infinite-size systems. This means that it can also be compared directly with more numerically oriented approaches, where the lattice size is usually limited. Second, it generalizes the Landau concept of a quasiparticle, as well as providing the corresponding effective single-particle Hamiltonian. Third, it corrects the principal inconsistency of the GA while retaining its attractive qualitative features by providing a testable approach in the vicinity of the border between the moderate and the strong correlation limits. This is the most difficult regime, as here the kinetic and interaction energies are of comparable amplitudes.

In the present paper we have applied the SGA method to the almost-half-filled band situation, where the physics turns out to be non-trivially different from the half-filled case but where the almost-localized character of the system [27–30] is still seen, as discussed below. Such a situation with $N_e < N_L$ (there are fewer fermions than cells) is physically feasible for neutral fermions, whereas for charged fermions (e.g., electrons) a consideration of the non-half-filled band situation requires an additional justification of preserving the charge neutrality of the whole system unless a compensating charge reservoir is assumed. We discuss results concerning magnetization, magnetic susceptibility, and specific heat, as well as the spin-direction dependent effective masses of quasiparticles, in addition to metamagnetism. As an example of its concrete application we have also compared results from our approach for magnetization with the experimentally obtained magnetization curve [31] for liquid ^{3}He and found a good semiquantitative agreement. The fitting parameter U places this system in the moderate correlation regime at ambient pressure.

The structure of the paper is as follows. In section 2 we discuss the Hubbard model solution within the statistically consistent Gutzwiller approach (SGA). In section 3 we provide the main results concerning the dependence of the system properties on the applied magnetic field. Section 4 contains conclusions and a brief overview. Appendix A provides some details of the SGA.

A brief methodological remark is in place here. The description is applicable, strictly speaking, to neutral fermions, as we include the applied magnetic field only via the Zeeman term and ignore the Landau-level structure appearing for charged quantum particles. This approach may then be applied to the discussion of both liquid ^{3}He and to the neutral cold-atom systems of spin $\frac{1}{2}$ in optical lattice systems.

2. Modeling: statistically consistent Gutzwiller approach (SGA)

Our starting point is the single-band Hubbard Hamiltonian in its translationally invariant form and in an applied magnetic field H_a

$$\mathcal{H} = \sum_{\langle ij\rangle,\sigma} t_{ij}\hat{c}^{\dagger}_{i\sigma}\hat{c}_{j\sigma} + U\sum_{i}\hat{n}_{i\uparrow}\hat{n}_{i\downarrow} - \sigma h\sum_{i,\sigma}\hat{n}_{i\sigma}, \quad (1)$$

where the first term expresses single-particle hopping between sites i and j (with the hopping amplitude $t_{ij} < 0$) and the second describes the intra-atomic repulsive interaction characterized by the Hubbard parameter $U > 0$. The applied magnetic field is introduced via the Zeeman splitting (last term), with $h \equiv \frac{1}{2}g\mu_B H_a$, and for spin $\frac{1}{2}$ we have that $\sigma = \pm 1$. In the case of neutral fermions (atoms in either liquid ^{3}He or in an optical lattice) the magnetic field enters the Hamiltonian only via this term. Applying the variational GA procedure [23] we obtain the effective one-particle renormalized Hamiltonian in the form:

$$\mathcal{H}_{GA} = \sum_{\mathbf{k}\sigma}(q_\sigma(d,n,m)\epsilon(\mathbf{k}) - \sigma h)\hat{c}^{\dagger}_{\mathbf{k}\sigma}\hat{c}_{\mathbf{k}\sigma} + LUd^2 \quad (2)$$

where $\epsilon(\mathbf{k})$ is the single-particle dispersion relation, $L \equiv N_L$ is the number of lattice sites, d^2 is the probability of having a doubly occupied site, $n = n_\sigma + n_{\bar{\sigma}}$ is the band filling, and $m = n_\sigma - n_{\bar{\sigma}}$ is the uniform magnetic polarization per site. The band narrowing factor $q_\sigma(d,m,n)$ is derived from combinatorial calculations in the usual form (a transparent derivation is provided in [9] and [7])

$$q_\sigma = \frac{2[\sqrt{(n+\sigma m-2d^2)(1-n+d^2)}+\sqrt{(n-\sigma m-2d^2)d^2}]^2}{(n+\sigma m)(2-n-\sigma m)}. \quad (3)$$

However, in an applied magnetic field the standard self-consistent GA procedure is insufficient. To achieve statistical consistency one needs to introduce additional constraints. The essence of the SGA method is discussed in appendix A. In effect, we introduce a new effective Hamiltonian in the form

$$\mathcal{H}_{SGA} \equiv \mathcal{H}_{GA} - \lambda_m\left(\sum_{i,\sigma}\sigma\hat{n}_{i,\sigma} - mL\right) - \lambda_n\left(\sum_{i,\sigma}\hat{n}_{i,\sigma} - nL\right), \quad (4)$$

where the Lagrange multipliers λ_m and λ_n represent the constraints imposed on m and n that their values calculated self-consistently should coincide with those determined variationally. The diagonalization of (4) allows the calculation of the thermodynamic potential functional

$$\mathcal{F}^{SGA} = -\frac{1}{\beta}\sum_{\mathbf{k}\sigma}\ln[1+e^{-\beta E^{(SGA)}_{\mathbf{k}\sigma}}] + L(\lambda_n n + \lambda_m m + Ud^2), \quad (5)$$

where the eigenenergies of the quasiparticles are

$$E^{(SGA)}_{\mathbf{k}\sigma} = q_\sigma\epsilon_{\mathbf{k}} - \sigma(h+\lambda_m) - \mu - \lambda_n. \quad (6)$$

The functional (5) represents the effective Landau functional with order parameters and extra variables expressing the inter-particle correlations.

In order to achieve the condition where the polarization m and the chemical potential μ determined variationally coincide with those determined in a self-consistent manner, we have effectively introduced corresponding *effective fields* adding to both h and μ. In essence, this procedure assures the fulfilment of the Bogoliubov theorem, discussed originally in the Hartree–Fock approximation, stating that the introduced effective single-particle approach represents the optimal single-particle representation of the mean-field state. Note also that the Luttinger theorem for the Hamiltonian (4) is obeyed, so that the system is represented by a Fermi liquid, i.e., there is a one-to-one correspondence between the bare states (of energies $\epsilon_{\mathbf{k}}$) and the quasiparticle states ($E_{\mathbf{k},\sigma}$ for $h = 0$). However, a number of renormalizing factors ($q_\sigma, \lambda_m, \lambda_n$) appear; these are determined by the statistical consistency (equilibrium) conditions. The presence of these three parameters, determined either from self-consistency conditions or variationally, represent features which do not appear in the original Landau theory of Fermi liquids. This is the reason why it is termed either as a correlated or an almost-localized Fermi liquid.

The equilibrium values of the parameters and mean field are obtained from the following minimizing procedure of a generalized grand-potential functional (5) with respect to the variables assembled into a vector $\vec{\lambda} \equiv (m, d, n, \lambda_n, \lambda_m)$, representing all relevant quantities, determined from the necessary condition for the minimum

$$\left(\frac{\partial\mathcal{F}}{\partial\vec{\lambda}}\right)_0 = 0, \quad (7)$$

in combination with a comparison of $\mathcal{F}$ values for different possible solutions. Explicitly, the above conditions can be rewritten as a set of five self-consistent equations for the corresponding quantities

$$\begin{aligned}
\lambda_n &= -\tfrac{1}{L}\textstyle\sum_{\mathbf{k}\sigma}\frac{\partial q_\sigma}{\partial n}f(E^{(SGA)}_{\mathbf{k}\sigma})\epsilon_{\mathbf{k}},\\
\lambda_m &= -\tfrac{1}{L}\textstyle\sum_{\mathbf{k}\sigma}\frac{\partial q_\sigma}{\partial m}f(E^{(SGA)}_{\mathbf{k}\sigma})\epsilon_{\mathbf{k}},\\
d &= -\tfrac{1}{2LU}\textstyle\sum_{\mathbf{k}\sigma}\frac{\partial q_\sigma}{\partial d}f(E^{(SGA)}_{\mathbf{k}\sigma})\epsilon_{\mathbf{k}},\\
n &= \tfrac{1}{L}\textstyle\sum_{\mathbf{k}\sigma}f(E^{(SGA)}_{\mathbf{k}\sigma}),\\
m &= \tfrac{1}{L}\textstyle\sum_{\mathbf{k}\sigma}\sigma f(E^{(SGA)}_{\mathbf{k}\sigma}),
\end{aligned} \quad (8)$$

where $f(E)$ is the Fermi–Dirac distribution function. Note that the first two equations contain the derivatives of the band

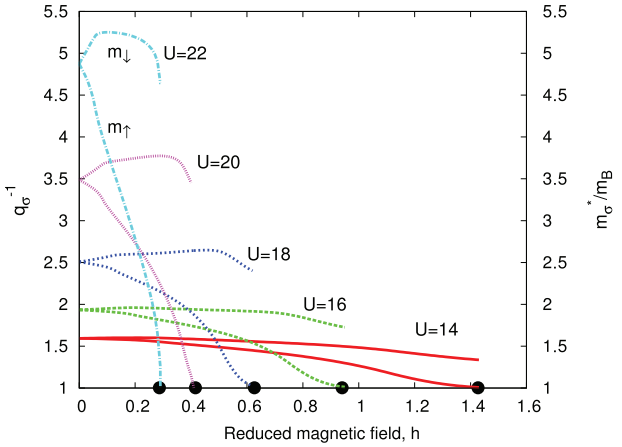

Figure 2. Spin-direction dependent effective quasiparticles masses as a function of the applied magnetic field for an almost-half-filled band ($n = 0.97$). The curves terminate when the magnetization saturates, i.e., when in the spin-majority subband the quasiparticle mass $m_\uparrow = m_B$ (the solid points on the horizontal axis). The evolution is spin asymmetric, since q_σ depends on m in this fashion, with respect to the spin direction $\sigma = \pm 1$.

narrowing factor with respect to the respective variables and would be absent in the ordinary Hartree–Fock approximation. In the case of GA, the fields $\lambda_m = \lambda_n \equiv 0$; this is the limit of weak coupling and represents one of the checks on the method's reliability. The grand-potential functional evaluated for the optimal values of the components of vector $\vec{\lambda}$, and determined from (8), reduces to the physical grand potential Ω. Once we have determined the equilibrium thermodynamic potential, we can also determine all relevant thermodynamic quantities. For example, the entropy is

$$-S = \frac{\mathrm{d}\Omega}{\mathrm{d}T} = \left(\frac{\partial \mathcal{F}}{\partial T}\right)_0 + \left(\frac{\partial \mathcal{F}}{\partial \vec{\lambda}}\right)_0 \cdot \frac{\partial \vec{\lambda}}{\partial T}, \tag{9}$$

where subscript '0' labels the equilibrium values of the variational parameters. Since $(\frac{\partial \mathcal{F}}{\partial \vec{\lambda}})_0 = 0$ from equation (7), equation (9) simplifies to the form

$$\begin{aligned} S &= -\left(\frac{\partial \mathcal{F}}{\partial T}\right)_0 \\ &= k_B \sum_{\mathbf{k}\sigma} [\ln(1 + \mathrm{e}^{-\beta E^0_{\mathbf{k}\sigma}}) + \beta E^0_{\mathbf{k}\sigma} f(E^0_{\mathbf{k}\sigma})]. \end{aligned} \tag{10}$$

The specific heat is then defined in the usual manner by

$$c_V = T \left.\frac{\mathrm{d}S}{\mathrm{d}T}\right|_{n,T,h,V} \equiv -T \left.\frac{\partial^2 \mathcal{F}}{\partial T^2}\right|_0. \tag{11}$$

Note that the variational parameters depend on temperature in a non-trivial manner. Therefore we have to determine the specific heat numerically. A detailed analysis of the results follows next.

3. Results and discussion

3.1. Principal physical properties

To obtain the equilibrium values from solutions of the set of equations (8), we have made use of the scientific library GSL under the GNU license [32]; the precision of the numerical results was 10^{-7}. In our calculations we set the energy scale in units of the nearest-neighbor hopping $|t|$. We consider a particular closed-packed structure, a three-dimensional face-centered cubic lattice of size $200 \times 200 \times 200$. If not otherwise specified, we have taken into account the second-nearest-neighbor hopping set as $t' = 0.25$, the band filling as $n = 0.97$, and the reduced temperature in the system as $\beta \equiv \frac{1}{k_B T} = 500$, which can be regarded practically as the $T \approx 0$ limit.

Both approaches, the GA as well as the SGA, automatically account for renormalization of the effective mass (m^*_σ) with respect to the bare band mass (m_B) in the form:

$$\frac{m^*_\sigma}{m_B} = q_\sigma^{-1} \equiv \left(\frac{\partial E_{\mathbf{k}}}{\partial \epsilon_{\mathbf{k}}}\right)^{-1}, \tag{12}$$

where q_σ is the optimized Gutzwiller band narrowing factor defined in (3). In the absence of an applied magnetic field, the effective mass for larger values of the interaction is renormalized appreciably, as detailed in figure 2. However, in an applied magnetic field, in an almost-half-filled band we observe strong asymmetric dependences with respect to the spin direction. This asymmetry with respect to the value of $\sigma = \pm 1$ is caused by the corresponding m dependence of q_σ. The curves terminate at the saturation point $m = n$, where simultaneously $m_\uparrow = m_B$ and the spin-minority quasiparticle subband becomes empty. Parenthetically, the saturation point may thus be used to determine the value of the bare band mass, m_B, as the Hubbard interaction is then switched off. This spin-dependent mass renormalization of quasiparticles in the strong correlation regime has been discussed extensively in the literature [30, 33–35], and observed experimentally by means of de Haas–van Alphen oscillations in strong magnetic fields [36, 37]. It thus represents a crucial new concept, which does not appear in the standard Landau Fermi liquid (LFL) theory.

In figure 3 we show a family of magnetization curves as a function of the reduced magnetic field ($h \equiv \mu_B H_a$). In comparison to the results obtained within the GA [9, 38] we do not observe any spectacular metamagnetic transition for $n < 1$. The magnetization curves, especially in the intermediate interaction regime, are rather smooth and saturate gradually. Nonetheless we observe a weak kink, which we qualify as metamagnetic-like behavior. Indeed, this kink can be singled out clearly on the field dependence of the magnetic susceptibility and the specific heat curves, as shown in figures 4 and 5, respectively.

One can say that the presence of both spin-dependent masses and the metamagnetic behavior signal the appearance of the so-called almost-localized Fermi liquid (ALFL) state, as such behavior is absent for the Landau Fermi liquid [38]. The

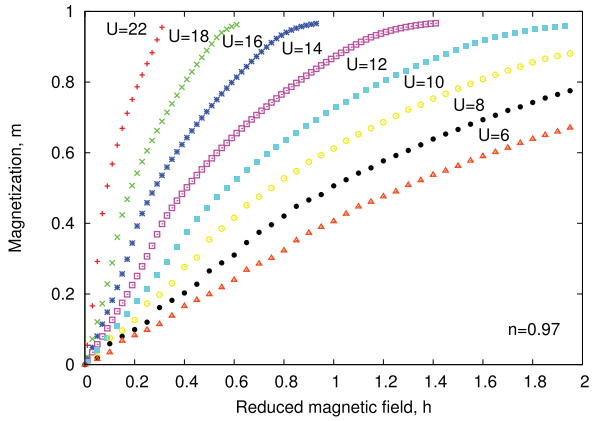

Figure 3. Magnetization curve for selected values of the Hubbard parameter U and fixed band filling $n = 0.97$. Even for very large values of U the curves show a metamagnetic-like transition in the form of a kink.

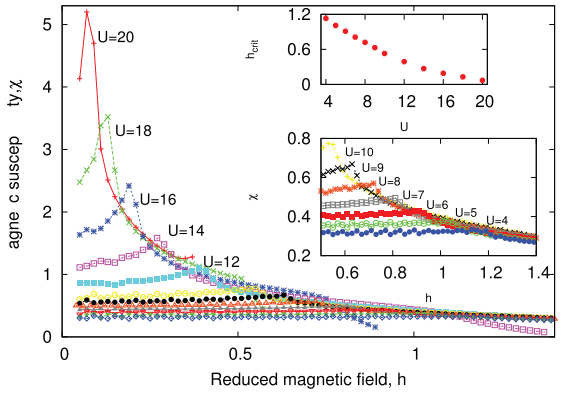

Figure 4. Magnetic susceptibility ($\chi = \frac{\partial m}{\partial h}$) as a function of the reduced magnetic field for selected values of the Hubbard parameter U. In the whole range of U values we observe a discontinuity, which we ascribe to the metamagnetic-like behavior. In the lower inset we plot the zoomed curves for smaller values of the U parameter. In the upper inset we present the dependence of the critical field ($h_{\rm crit}$) representing the metamagnetic-like point for selected values of the parameter U.

diminution of c_V with h is the sign of a combined decrease of both the effective-mass components, as well as of the decreasing population of the spin-minority subband.

3.2. Subsidiary quantities

The introduction of constraints results in additional self-consistent equations to be obeyed, which in turn restricts the parameter space to search for the true global minimum of the free-energy functional. Furthermore, the Lagrange multipliers λ_m and λ_n play the role of an effective field and a shift of the chemical potential, respectively. They are induced by the correlations in the sense that their presence is induced by the presence of q_σ and, more particularly, by its singular dependence on both m and n in the present situation. The fields λ_m and λ_n are determined within the variational/self-consistent procedure and represent the third factor distinguishing an

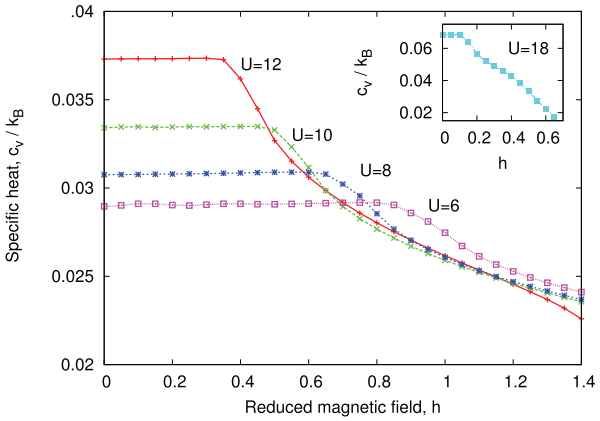

Figure 5. Specific heat (per site) as a function of the reduced magnetic field for selected values of U. The slope change occurs for the same values of h as the kinks in the magnetic susceptibility shown in figure 4. At lower fields the mass enhancements $\{m^*_\sigma\}$ are symmetric, so their contributions to the total density of states average out to a value roughly independent of h. The temperature was taken as $k_{\rm B}T = 0.04|t|$.

ALFL from a LFL. For the sake of completeness, in table 1 we provide exemplary values of the relevant quantities. Note that λ_n almost compensates μ, and in effect we obtain the effective value of the Fermi energy for the heavy quasiparticles.

In figure 6 we plot the spin-resolved density of states for the two values of $U = 8$ and 18 (in units of $|t|$) in an applied field. The spin subbands are shifted by an amount $h + \lambda_m$ and narrowed down asymmetrically by the spin-direction dependent factor q_σ. In figures 7(a)–(c) we have plotted λ_m, λ_n, and μ, all as functions of h. Furthermore, the field λ_m as a function of magnetization m is shown in figure 8. This effective field is a nonlinear function of both h and m, and represents a relatively fast growing quantity with increasing h. It is only weakly dependent on h in the moderate interaction limit. This means that the presence of λ_m will have an essential impact on the magnetic properties, while the relative constancy of μ and λ_n in the regime $h < h_{\rm crit}$ explains the flat behavior of $c_V(T)$ in that regime. It would be interesting to see if the presence of the effective field λ_m acting on the spin degrees of freedom only (in analogy to the Weiss molecular field) can be detected with the same accuracy as the spin splitting of the masses. Such a test would be a decisive step forward in defining an almost-localized Fermi liquid as a separate state from the Landau Fermi liquid. Note, however, that λ_m cannot be, strictly speaking, considered as a molecular Weiss field, since it is nonlinear in m.

3.3. Concrete example: liquid ^{2}He

Liquid ^{3}He is regarded as a canonical example of the Landau Fermi liquid (cf. e.g. [6]). It has also been regarded as an ALFL, as it undergoes a transition to the solid state at a pressure $p \simeq 34$ bar, with the localization of the ^{3}He atoms regarded as a fermions of spin $\frac{1}{2}$ [9, 12, 39]. Here we briefly discuss its behavior in an applied magnetic field at ambient pressure. We have compared the magnetization curve obtained

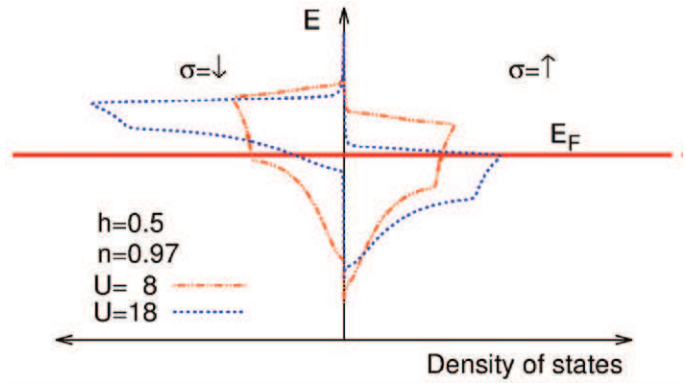

Figure 6. Spin-resolved density of states of quasiparticle states in the applied magnetic field $h = 0.5$ for the selected values of U. The spin (magnetic-moment)-minority subband is narrowed, whereas the spin-majority-spin subband is widened so that it acquires the bare bandwidth as the saturation state is reached in the strong-field limit.

Table 1. Values of the parameters obtained for $U = 12$, $t' = 0.25$, $n = 0.97$, $\beta = 500$ (in units where $|t| = 1$) for four values of the reduced magnetic field. The calculations were made for a fcc lattice of size $200 \times 200 \times 200$.

Quantity	$h = 0$	$h = 0.2$	$h = 0.5$	$h = 1$
$\mathcal{F}$	−6.475 2954	−6.476 5977	−6.435 4871	−6.051 8362
d	0.323 1845	0.319 33441	0.295 0449	0.237 0746
m	0	0.169 0908	0.448 3957	0.720 6020
μ	5.838 7352	5.822 7839	5.684 5669	4.981 5074
λ_n	−5.574 7470	−5.560 1127	−5.459 9753	−5.214 1073
λ_m	0	0.400 7685	1.141 0240	2.180 9003
$q_\uparrow$	0.725 0737	0.729 3968	0.748 2932	0.797 1271
$q_\downarrow$	0.725 0737	0.723 6794	0.730 7299	0.756 9461

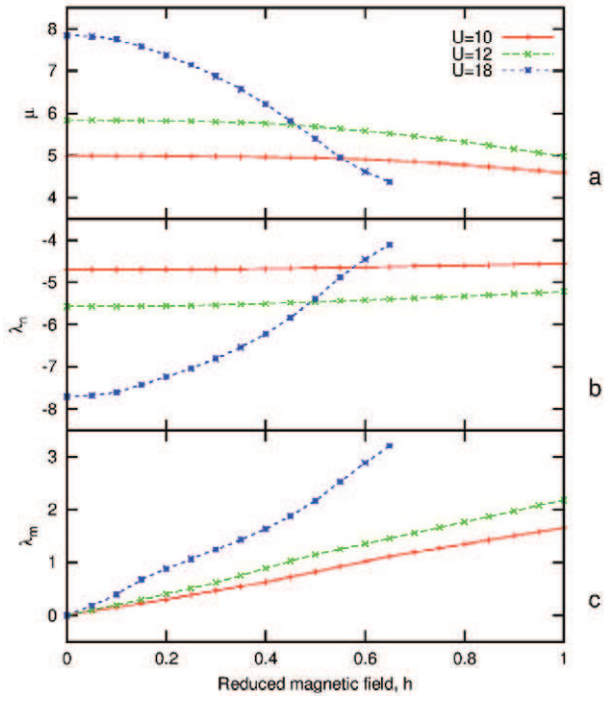

Figure 7. Panels (a)–(c) show the evolution of the fields λ_m and λ_n and the chemical potential μ with respect to the applied magnetic field. The field λ_m appears only in the spin polarized state, whereas λ_n is almost compensated by μ.

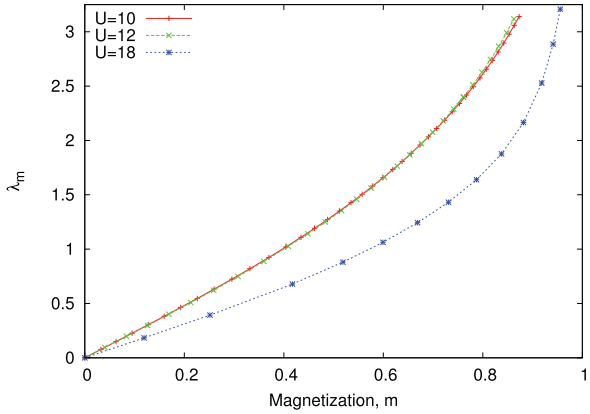

Figure 8. Effective field induced by correlations as a function of the magnetization; this illustrates its nonlinear character and in this manner it cannot be regarded as a Weiss molecular field.

from our model with the experimental magnetization [31] of the liquid ^{3}He, as shown in figure 9. We find a good overall agreement. Note that our results, obtained for $n < 1$, do not exhibit the discontinuous metamagnetic transition which disqualified the applicability of the standard GA to ^{3}He with $n = 1$ [9]. To avoid this discontinuity, we have introduced about 5% of vacancies in this virtual fcc lattice representing liquid ^{3}He. This number of vacant sites provides the best fit of our results to the experimental data. Furthermore, it is important to note that the relatively small number of holes introduced preserves the almost-localized nature of this quantum liquid. This note is important also in view of the circumstance that the detailed $m(h)$ dependence is very sensitive to the number of quantum vacancies. It is tempting to suggest that the effective

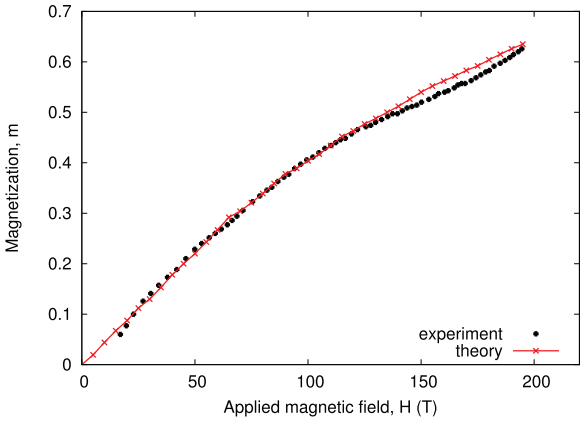

Figure 9. Magnetization in dimensionless units, $m \equiv n_\uparrow n_\downarrow$ versus the applied field H calculated within the SGA fitted to the experimental data [31]. The fitting parameters are: $U = 5|t|$, $n = 0.95$, $t' = 0.25|t|$, $|t| = 62.5$ K. A very weak, almost unnoticeable metamagnetic kink is present. The reason for the small deviation of the results from the data (for $H \gtrsim 125$ T) is not accounted for within the present approach.

empty-site content $\delta \equiv 1 - n$ of the order of a few percent can be interpreted as the presence of quantum vacancies in the liquid state, in direct analogy to the quantum Andreev vacancies postulated and observed in solid ^{3}He [40]. From a detailed analysis of the fitting procedure we conclude that the assumption of a non-half-filled lattice is necessary if either the GA, SGA or DMFT approaches and the Hubbard model are to emulate the magnetic behavior of liquid ^{3}He.

One important difficulty of the just discussed results (figure 9) should be raised at this point. Namely, a relatively small value of $U \sim 5|t| \ll W$ (where $W \equiv 24|t|$ is the bare band width) obtained from the $m(h)$ best fit places the liquid ^{3}He at ambient pressure as a moderately correlated system. This seemingly unexpected conclusion is also in agreement with the DMFT analysis [21]. In this way, the Hubbard model approach also squares qualitatively with the fundamental Fermi liquid theory assumption that the interaction between quasiparticles can be essentially limited to the region very close to the Fermi surface (U substantially smaller than W). Furthermore, the method for estimating the number of vacancies might be associated with a detailed study of the field dependence of the specific heat to determine a possible spin-direction dependence of the effective mass, though the weak effect for this moderate value of U may be prove decisive. Such an explicit spin-direction mass dependence is absent when we have the exactly half-filled situation (i.e., one atom per site, without any vacant cells).

Furthermore, in spite of this success in explaining $m(h)$ in a semiquantitative manner, there still is another problem concerning determination with the same set of parameters of a realistic value of the mass enhancement estimated from the $c_V(T)$ curves for $T \to 0$ [3, 4]. Namely, the value of the specific heat enhancement at $h = 0$ obtained for $U = 5|t| \sim W/5$ is far too small to provide the corresponding effective mass enhancement $m^* = 2.86 m_0$ at ambient pressure, where m_0 is the free ^{3}He atomic mass. This disagreement is common to the present and the previous [12, 21] treatments. A small mass enhancement within the GA, SGA or DMFT of the mass can be interpreted in two ways. First, the spin-fluctuation contribution can be very important [41]. In that situation, the SGA should be considered only as a saddle-point approximation to a more complete approach (cf. appendix B). This question certainly requires a detailed analysis. Second, one has to note that the m^*/m_0 ratio estimate from the experimental c_V data [3, 4], based on the relations to an ideal gas, may not be fully adequate either. Finally, our assumption that $N_e < N_L$ and $\delta \equiv 1 - n$, independent of h or pressure, may be analyzed further as well.

4. Conclusions

We have carried out a systematic study of a correlated Fermi liquid modeled by the Hubbard model on a fcc lattice, utilizing the statistically consistent Gutzwiller approach (SGA) [42] in an applied magnetic field and in an almost-half-filled regime. Within this method, the field and spin-direction dependent effective masses, the magnetization curve, the magnetic susceptibility, and the specific heat, were all calculated in a both self-consistent and variationally optimal manner. We have found a metamagnetic-like behavior, tracing the discontinuities which would appear for the half-filled band case (one particle per cell). In other words, we have not obtained any first-order metamagnetic transition which limits the applicability of the original Gutzwiller approach (GA) to real systems such as liquid ^{3}He (see also the discussion in [21]). Apart from that, the GA approach is not statistically consistent, as discussed in detail in the text. We have found a good overall agreement of our approach with experimental data for the magnetization of liquid ^{3}He. However, there remains the question of putting into mutual agreement the magnetization data and the magnitude of effective mass enhancement observed for that system in zero applied field. The quantitative analysis within the lattice-approach required the introduction of a small number (∼5%) of vacant cells to destroy the strong metamagnetism. A way of including the spin fluctuations is suggested (cf. appendix B), starting from the SGA state, which should then be regarded as a saddle-point state for a more complete analysis. In this manner, the SGA state replaces the Hartree–Fock state, regarded so far as a reference (saddle-point) state for further considerations concerning spatially inhomogeneous fluctuations [43–45], here of both spin and charge types.

In summary, our SGA approach, as well as the works carried within DMFT [21, 34, 35] provide a convergent quasiparticle language in the sense that the effective masses are dependent on the spin-direction in the magnetically polarized state. We also introduce a set of nonlinear effective fields, determined in a self-consistent manner, which renormalize both the chemical potential and the applied field magnitude experienced by the quasiparticles representing the almost-localized Fermi liquid. Our method of approach may be regarded as equivalent to the slave-boson approach in the saddle-point approximation [42], without involving the slave-boson fields which introduce spurious Bose-condensation phase transitions at nonzero temperature.

Acknowledgments

We would like to thank Marcin Abram, Jakub Jędrak and Jan Kaczmarczyk for very useful discussions and technical help. We also greatly acknowledge cooperation with Professor Włodzimierz Wójcik on the early stages of this work. The work has been partially supported by the Foundation for Polish Science (FNP) under the TEAM program, as well as by the National Science Centre (NCN) under the MAESTRO program, Grant No. DEC-2012/04/A/ST3/00342. Preliminary results of this work have been presented in proceedings of the XVI Training Course in the Physics of Strongly Correlated Systems [46].

Appendix A. Statistically consistent Gutzwiller approximation

As pointed out in the main text, it has been noticed (see [42, 46, 47] and references therein) that the Gutzwiller approximation which leads to the effective single-particle Hamiltonian (2) has a principal drawback. Namely, if we try to calculate the ground state energy from $E_{\rm G} \equiv \langle \mathcal{H}_{\rm GA} \rangle$, we have first to determine the average spin polarization m, the double occupancy probability d^2 and μ [48]. This can be achieved in two ways: either by minimizing the free-energy functional $\mathcal{F}$ for $T \geq 0$ (defined by equation (5) for $\lambda_m = \lambda_n = 0$) with respect to the variables (m, d^2, n) or by writing down the self-consistent equation of m and n and minimizing $\mathcal{F}$ with respect to d^2. Those two procedures should provide the same answers if (2) properly represents the defined single-particle Hamiltonian. In fact, the results do differ [42, 47], and this discrepancy is caused by the fact that the single-particle energies depend on q_σ, which depends on m and n in a non-analytic manner (see, for example, the limits $n \to 1$ and/or $m \to 1$). The presence of this discrepancy means that the GA violates the fundamental Bogoliubov theorem, stating that the effective single-particle states represent the optimal quasiparticle states in the variational sense, with the ordinary self-consistent procedure preserved at the same time.

To cure this principal defect one can choose an approach in which one imposes the constraints so that the consistency from the point of view of statistical mechanics is preserved. To carry through such a procedure one can utilize the maximum entropy method to derive the correct statistical distribution (with constraints) and then proceed further [47]. Here we have chosen a slightly different path. Namely, we have defined the generalized free-energy functional (5) with the constraints that the variationally calculated quantities m and n represent correct values. This is realized by adding two terms to $\mathcal{H}_{\rm GA}$, as written in equation (4). This last step amounts to introducing the statistically consistent Gutzwiller approximation (SGA). As a result, we have to minimize $\mathcal{F}$ given by (5) also with respect to λ_m and λ_n, and the procedure introduces two physically relevant fields (cf. (6)) which appear only in the correlated state ($q_\sigma < 1$) and vanish in the small-U limit, i.e., in the Hartree–Fock limit ($q_\sigma \to 1$). The last limiting situation thus represents a test for the correctness of our approach.

One should note that the SGA is essentially based on the GA, but provides additional essential consistency of the model by introducing two extra parameters into the approach. In summary, the self-consistent equations

$$\begin{aligned} \tfrac{1}{L}\textstyle\sum_{i,\sigma} \sigma \langle \hat{n}_{i\sigma} \rangle &= \tfrac{1}{L}\textstyle\sum_{\mathbf{k},\sigma} \sigma \langle \hat{n}_{\mathbf{k}\sigma} \rangle \equiv m, \\ \tfrac{1}{L}\textstyle\sum_{i,\sigma} \langle \hat{n}_{i\sigma} \rangle &= \tfrac{1}{L}\textstyle\sum_{\mathbf{k},\sigma} \langle \hat{n}_{\mathbf{k}\sigma} \rangle \equiv n, \\ \langle \hat{n}_{\mathbf{k}\sigma} \rangle &= \frac{1}{\mathrm{e}^{\beta(E_{\mathbf{k}\sigma}-\mu)}+1}, \end{aligned} \tag{A.1}$$

are consistent with the variational equations (7) derived within the SGA method.

Appendix B. SGA as a saddle-point approximation

Here we would like to sketch the method of extending the SGA approach. In this method SGA is regarded as a saddle-point approximation to a more complete theory which includes the quantum fluctuations.

In general, the constraints in (4) should be written in the local form

$$\begin{aligned} -\left\{ \sum_{i\sigma} \lambda_{mi} \sigma (\hat{n}_{i\sigma} - \langle \hat{n}_{i\sigma} \rangle) + \sum_{i\sigma} \lambda_{ni} (\hat{n}_{i\sigma} - \langle \hat{n}_{i\sigma} \rangle) \right\} \\ \equiv -\left\{ \sum_{i\sigma} (\lambda_{mi} \delta \hat{S}_i^z - \lambda_{ni} \delta \hat{n}_i) \right\}, \end{aligned} \tag{B.1}$$

with $\delta \hat{S}_i^z \equiv \hat{S}_i^z - \langle \hat{S}_i^z \rangle$ and $\delta \hat{n}_i \equiv \hat{n}_i - \langle \hat{n}_i \rangle$. In other words, in the system with fluctuating local quantities, the constraints should also be obeyed locally. Also, the charge fluctuations are expressed via the term

$$U \sum_i (\hat{n}_{i\uparrow} \hat{n}_{i\downarrow} - \langle \hat{n}_{i\uparrow} \hat{n}_{i\downarrow} \rangle). \tag{B.2}$$

The last term can be rewritten in the spin explicit form

$$\begin{aligned} \hat{n}_{i\uparrow} \hat{n}_{i\downarrow} &= \left(\frac{n_{i\uparrow} - \hat{n}_{i\downarrow}}{2} \right)^2 + \frac{\hat{n}_i^2}{4} \\ &= (\delta \hat{S}_i^z)^2 + 2 \langle \hat{S}_i^z \rangle \delta \hat{S}_i^z + \langle \hat{S}_i^z \rangle^2 + \frac{\hat{n}_i^2}{4}, \end{aligned} \tag{B.3}$$

where $\langle \hat{S}_i^z \rangle \equiv m$ and $\hat{n}_i \equiv \hat{n}_{i\downarrow} + \hat{n}_{i\uparrow}$. In effect, we have

$$U \sum_i \hat{n}_{i\uparrow} \hat{n}_{i\downarrow} = U \sum_i \delta (\hat{S}_i^z)^2 + U \sum_i \frac{\hat{n}_i^2}{4} + \text{const.} \tag{B.4}$$

One can reformulate the whole approach in the spin rotationally invariant form in a straightforward manner. In effect, we have linear and quadratic spin and charge fluctuations. We can thus define the part of the Hamiltonian responsible for fluctuations as

$$\mathcal{H} = \mathcal{H}^{\rm SGA} + \mathcal{H}^{\rm fluct} + \text{const}, \tag{B.5}$$

where

$$\begin{aligned} \mathcal{H}^{\rm fluct} \equiv &- \sum_i [\lambda_{mi} \delta \hat{S}_i^z - \lambda_{ni} \delta \hat{n}_i] \\ &+ U \sum_i [(\delta \hat{S}_i^z)^2 + \tfrac{1}{4} (\delta \hat{n}_i)^2]. \end{aligned} \tag{B.6}$$

This expression (B.6) (or their spin-rotation invariant correspondents) should be inserted into the expression for the energy expressed in the functional-integral form over the Fermi fields [48] and then evaluated explicitly, as it involves cumbersome calculations. Methodologically, it is analogous to the slave-boson approach [41]. However, the present approach involves only coherent physical Fermi $\{\hat{c}_{i\sigma}, \hat{c}^{\dagger}_{i\sigma}\}$ and Bose $\{\lambda_m, \lambda_n\}$ fields, without introducing condensing ghost slave-boson fields.

When the reference (saddle-point) system is represented by an almost-localized Fermi liquid, both the spin and charge fluctuations thus become relevant. This should lead to a renormalization of the thermodynamic properties and should be analyzed separately, as in the present paper we concentrate on the $T \to 0$ results. Nonetheless, inclusion of the fluctuations should lead to a further enhancement of the specific heat, as well as to the presence of the $T^3 \ln T$ term for $h = 0$ [41].

References

[1] Landau L 1956 *Zh. Exp. Teor. Fiz.* **30** 1058
Landau L 1957 *Sov. Phys.—JETP* **3** 920 (Engl. transl.)
[2] Landau L 1957 *Zh. Exp. Teor. Fiz.* **32** 59
Landau L 1957 *Sov. Phys.—JETP* **5** 101 (Engl. transl.)
[3] Greywall D S 1983 *Phys. Rev.* B **27** 2747
[4] Greywall D S 1986 *Phys. Rev.* B **33** 7520
[5] Mook H A 1985 *Phys. Rev. Lett.* **55** 2452
[6] Dobbs E 2000 *Helium Three* (Oxford: Oxford University Press)
[7] Gebhard F 1997 *The Mott Metal-Insulator Transitions* (Berlin: Springer)
[8] Spałek J and Gopalan P 1990 *Phys. Rev. Lett.* **64** 2823
[9] Vollhardt D 1984 *Rev. Mod. Phys.* **56** 99
[10] Castorina P, Gavani R V and Satz H 2010 *Eur. Phys. J.* C **69** 169
[11] Satz H 2012 *Acta Phys. Pol.* B **43** 587
[12] Vollhardt D, Wölfle P and Anderson P W 1987 *Phys. Rev.* B **35** 6703
[13] Scalapino D J 2012 *Rev. Mod. Phys.* **84** 1383
[14] Jędrak J and Spałek J 2011 *Phys. Rev.* B **83** 104512
[15] Bünemann J, Schickling T and Gebhard F 2012 *Europhys. Lett.* **98** 27006
[16] Kaczmarczyk J, Spałek J, Schickling T and Bünemann J 2013 *Phys. Rev.* B **88** 115127
[17] Gutzwiller M 1965 *Phys. Rev.* **137** A1726
[18] Bünemann J, Gebhard F and Thul R 2003 *Phys. Rev.* B **67** 075103
[19] Spałek J 1990 *J. Solid State Chem.* **88** 70
[20] Brinkman W F and Rice T M 1970 *Phys. Rev.* B **2** 4302
[21] Parihari D, Vidhyadhiraja N S and Taraphder A 2011 *J. Phys.: Condens. Matter* **23** 055602
[22] Jarrell M 1992 *Phys. Rev. Lett.* **69** 168
[23] Jędrak J and Spałek J 2010 *Phys. Rev.* B **81** 073108
[24] Kaczmarczyk J and Spałek J 2011 *Phys. Rev.* B **84** 125140
[25] Abram M, Kaczmarczyk J, Jędrak J and Spałek J 2013 *Phys. Rev.* B **88** 094502
[26] Howczak O and Spałek J 2012 *J. Phys.: Condens. Matter* **24** 205602
[27] Spałek J, Datta A and Honig J M 1987 *Phys. Rev. Lett.* **59** 728
[28] Spałek J, Kokowski M and Honig J M 1989 *Phys. Rev.* B **39** 4175
[29] Spałek J 2005 *Physica* B **654** 378
[30] Spałek J 2006 *Phys. Status Solidi* b **78** 243
[31] Wiegers S A J, Wolf P E and Puech L 1991 *Phys. Rev. Lett.* **66** 2895
[32] 0954612078Galassi M, Davies J, Theiler J, Gough B, Jungman G, Alken P, Booth M and Rossi F *GNU Scientific Library Reference Manual* 3rd edn
[33] Maśka M M, Mierzejewski M, Kaczmarczyk J and Spałek J 2010 *Phys. Rev.* B **82** 054509
[34] Bauer J and Hewson A C 2007 *Phys. Rev.* B **76** 035118
[35] Bauer J 2009 *Eur. Phys. J.* B **68** 201
[36] McCollam A, Julian S R, Rourke P M C, Aoki D and Flouquet J 2005 *Phys. Rev. Lett.* **94** 186401
[37] Sheikin I, Gröger A, Raymond S, Jaccard D, Aoki D, Harima H and Flouquet J 2003 *Phys. Rev.* B **67** 094420
[38] Korbel P, Spałek J, Wójcik W and Acquarone M 1995 *Phys. Rev.* B **52** R2213
[39] Spałek J 2000 *Eur. J. Phys.* **21** 511
[40] Andreev A 1976 *Zh. Eksp. Teor. Fiz.* **24** 608
Andreev A 1976 *JETP Lett.* **24** 564 (Engl. transl.)
[41] Wolfle P and Li T 1990 *Z. Phys.* B **78** 45
[42] Jędrak J, Kaczmarczyk J and Spałek J 2010 (arXiv:1008.0021)
[43] Hertz J 1976 *Phys. Rev.* B **14** 1165
[44] Moriya T 1985 *Spin Fluctuations in Itinerant Electron Magnetism* (Berlin: Springer)
[45] Millis A J 1993 *Phys. Rev.* B **48** 7183
[46] Wysokiński M, Jędrak J, Kaczmarczyk J and Spałek J 2012 *AIP Conf. Proc.* **1485** 319
[47] Jędrak J 2011 Real-space pairing in an extened *t–J* model *PhD Thesis* Jagiellonian University, Kraków
[48] Spałek J 2012 *Acta Phys. Pol.* A **121** 764 (cf. Appendix E)

3.3 Article A.2, Ferromagnetism in UGe_2: A microscopic model

In the work [113] we have proposed that the two dimensional Anderson lattice model with the magnetic field accounted for by the Zeeman term is able to accurately describe the magnetic and electronic properties of the f-electron ferromagnetic superconductor UGe_2 [20]. The proposed model correctly captures several features of this material: **(i)** the considerations of the two dimensional lattice is justified by the quasi-two-dimensional Fermi surface as determined by the band structure calculations [142]; **(ii)** the initially localized in the atomic states f electrons and lack of any direct hoppings between them considered in ALM is based on the fact that uranium atoms are distant well above the so-called Hill limit [9]; **(iii)** On the other hand, due to the coupling of f electrons to the conduction electrons via hybridization, their effective itineracy is supported by the measured paramagnetic moment per U is different from atomic value [20, 9].

By solving the model by SGA method in the limit of low temperature (cf. Sec. 2.1) we have obtained three competing solutions: the paramagnetic (PM) and two distinct ferromagnetic phases, of stronger (FM2) and weaker (FM1) magnetization. The ferromagnetism itself arises as an effect of competition between the Coulomb interaction and hybridization, whereas the splitting into two phases, separated by the metamagnetic transition, has its source in the characteristic two-peaked density of states with the hybridization gap with sharp borders at $T = 0$. Strictly speaking, both magnetic phases have different Fermi surface topology and FM1 phase is of the *half-metallic* nature.

In the specific range of the total number of electrons in the system, we have shown that with the increasing hybridization the FM2-FM1-PM sequence of the phases appears, with the transitions of the first order between them. By assuming that the main effect of the pressure applied to the real material can be modeled by the increasing hybridization amplitude we have reproduced qualitatively the characteristics of UGe_2 [110]: **(i)** As seen, among others in de Haas - van Alphen oscillations [143] and the resistivity measurements [144], the crucial property of the metamagnetic phase transition (FM2$\rightarrow$ FM1) is associated with the dramatic increase of the effective quasiparticle masses. In our model, this transition is linked to the chemical potential crossing the hybridization peak in the majority spin subband. The boost of the density of states at the Fermi level directly explains observed enhancement of effective quasiparticle mass; **(ii)** As FM1 is predicted by our model to be of the half-metallic type, we can rationalize the disappearance of some of the majority spin frequencies and a slight evolution of the spin-minority ones at the same metamagnetic phase transition as seen in the de Haas - van Alphen oscillations measurements [143]; **(iii)** Our model, in accord with the neutron scattering experiment [145], predicts that magnetization comes almost only from f-electrons; **(iv)** We have also favorably compared our results with the experiment in magnetic field and found that the pressure - applied field phase diagram of UGe_2 can be well reproduced by our theory. Here the most important feature is that the metamagnetic transition occurs for the same value of the magnetization irrespectively of the applied magnetic field strength [110] .

PHYSICAL REVIEW B **90**, 081114(R) (2014)

Ferromagnetism in UGe_2: A microscopic model

Marcin M. Wysokiński,* Marcin Abram,† and Józef Spałek‡
Marian Smoluchowski Institute of Physics, Jagiellonian University, Reymonta 4, PL-30-059 Kraków, Poland
(Received 25 July 2014; revised manuscript received 18 August 2014; published 26 August 2014)

The Anderson lattice model is used to explain the principal features of the heavy fermion compound UGe_2 by means of the *generalized Gutzwiller approach* (the statistically consistent Gutzwiller approximation method). This microscopic approach successfully reproduces the magnetic and electronic properties of this material, in qualitative agreement with experimental findings from magnetization measurements, neutron scattering, and de Haas–van Alphen oscillations. Most importantly, it explains the appearance, sequence, character, and evolution in an applied magnetic field of the observed in UGe_2 ferromagnetic and paramagnetic phases as an effect of a competition between the f-f electron Coulomb interaction energy and f-conduction electron hybridization.

DOI: 10.1103/PhysRevB.90.081114 PACS number(s): 71.27.+a, 75.30.Kz, 71.10.−w

Introduction. The discovery of spin-triplet superconductivity (SC) inside the ferromagnetic (FM) phase of the heavy fermion compound UGe_2 [1] sparked an intense discussion about the cause of such a coexistence. Although the spin-triplet paired phase has been known to appear in condensed ^{3}He [2] and most likely in Sr_2RuO_4 [3], until its discovery in UGe_2 there was no convincing example for a strongly FM material hosting SC.

Specifically, the phase diagram for UGe_2 on the temperature-pressure (T-p) plane contains both SC and two FM phases, with stronger and weaker magnetization [4], usually referred to as FM2 and FM1, respectively, as well as a paramagnetic phase (PM), with first-order phase transitions between them at low temperature, $T \lesssim 7$ K [5]. The FM-SC coexistence is strongly suggestive of a single mechanism based on magnetic correlations which is responsible for the appearance of both FM and SC and thus should be treated on equal footing, as, e.g., in UGe_2 both phases disappear at the same pressure [1,4]. Another indication of the coupled nature of both phases is that the SC dome on the T-p plane coincides with the phase transition between FM2 and FM1 [4]. Thus, we address here in detail the question of the microscopic origin of the observed ferromagnetism, as it should bring us closer to determining the mechanism of superconductivity. The question related to the inclusion of SC requires a separate study [6,7] (see the discussion at the end).

Experimental observations suggest that the ferromagnetism in UGe_2 has an itinerant nature [1,8,9] and is mediated by the uranium $5f$ electrons [1,10,11]. Delocalization of the $5f$ electrons can be interpreted as resulting from the hybridization of the original $5f$ atomic states with those from the conduction band [8] derived from p states due to Ge and d-s states due to U. This is supported by a noticeable difference in the effective paramagnetic moment per uranium atom in this compound with respect to the corresponding atomic value for either the f^3 or f^2 configurations [1], as well as from a fractional value of the magnetization relative to the atomic-moment saturation. This means that the Hund's rule coupling in the atomic sense is broken, and the itineracy of the $5f$ electrons is the source of the band ferromagnetism in which Hund's ferromagnetic interaction plays a role, in combination with a stronger intra-atomic Coulomb interaction. Thus, f-electron orbital degeneracy is not essential, but the role of hybridization is.

Apart from other theories concerning the origin of FM in the considered class of materials [12,13], there exists [14] a phenomenological explanation of the magnetic properties within a rigid-band Stoner approach, which requires introduction of an *ad hoc* two-peaked structure of the density of states (DOS) near the Fermi surface (FS). Our purpose is to invoke a microscopic description starting from the Anderson-lattice model (ALM) which is appropriately adapted to the heavy fermion compound UGe_2. This comprises a relatively simple quasi-two-dimensional electronic structure [15–17]. From such a starting point an effective nonrigid two-band description arises naturally and allows for a detailed explanation of the magnetic and electronic properties, at least on a semiquantitative level. Additionally, as the correlations among $5f$ electrons are sizable, an emergence of the Stoner-like picture of FM can be accounted for only with the inclusion of specific features coming from the electronic correlations. Although the resulting explanation of the physical properties is semiquantitative in nature, it provides, in our view, a coherent picture of a number of properties [4,10,11,18,19].

Model. We base our predictions for the ALM on a variational treatment with the Gutzwiller wave function $|\psi_G\rangle = \prod_{\mathbf{i}} \hat{P}_{\mathbf{i}} |\psi_0\rangle$, where $\hat{P}_{\mathbf{i}}$ is the operator projecting out part of the double occupancies from the uncorrelated ground state $|\psi_0\rangle$ at site $\mathbf{i}$. We have extended the standard approach [20–22] to the *statistically consistent form* [23] [statistically consistent Gutzwiller approximation (SGA) method]. Explicitly, we start with the ALM Hamiltonian, with an applied magnetic field introduced via the Zeeman term ($h \equiv \frac{1}{2} g \mu_B H$), i.e.,

$$\begin{aligned}\hat{\mathcal{H}} - \mu \hat{N} = {} & {\sum_{\mathbf{i},\mathbf{j},\sigma}}' t_{\mathbf{ij}} \hat{c}^{\dagger}_{\mathbf{i},\sigma} \hat{c}_{\mathbf{j},\sigma} - \sum_{\mathbf{i},\sigma} (\mu + \sigma h) \hat{n}^{c}_{\mathbf{i},\sigma} \\ & + \sum_{\mathbf{i},\sigma} (\epsilon_f - \mu - \sigma h) \hat{n}^{f}_{\mathbf{i},\sigma} + U \sum_{\mathbf{i}} \hat{n}^{f}_{\mathbf{i},\uparrow} \hat{n}^{f}_{\mathbf{i},\downarrow} \\ & + V \sum_{\mathbf{i},\sigma} (\hat{f}^{\dagger}_{\mathbf{i},\sigma} \hat{c}_{\mathbf{i},\sigma} + \hat{c}^{\dagger}_{\mathbf{i},\sigma} \hat{f}_{\mathbf{i},\sigma}), \end{aligned} \tag{1}$$

*marcin.wysokinski@uj.edu.pl
†marcin.abram@uj.edu.pl
‡ufspalek@if.uj.edu.pl

where the primed sum denotes summation over all lattice sites $\mathbf{i} \neq \mathbf{j}$, and $\hat{f}$ and $\hat{c}$ are operators related to f and c orbitals, respectively, with spin $\sigma = \uparrow, \downarrow$. We have also defined the total number of electrons operator as $\hat{N}$, and for the respective orbitals and spins as $\hat{n}^f_{\mathbf{i},\sigma} \equiv \hat{f}^\dagger_{\mathbf{i},\sigma}\hat{f}_{\mathbf{i},\sigma}$, $\hat{n}^c_{\mathbf{i},\sigma} \equiv \hat{c}^\dagger_{\mathbf{i},\sigma}\hat{c}_{\mathbf{i},\sigma}$. In our model, we consider the finite intra-f-orbital Coulomb interaction U, the on-site interorbital hybridization $V < 0$, the hopping amplitude between the first (t) and the second ($t' = 0.25\ |t|$) nearest neighboring sites, and the atomic level for f states placed at $\epsilon_f = -3|t|$. In the following $|t|$ is used as the energy unit.

First, we would like to evaluate the ground-state energy, $E_G \equiv \langle\psi_G \mid \hat{\mathcal{H}} \mid \psi_G\rangle / \langle\psi_G \mid \psi_G\rangle$. Applying the usual procedure [21,22], called the Gutzwiller approximation (GA), we simplify the projection to the local sites on which the operators from (1) act. In that manner one obtains the effective single-particle Hamiltonian in a momentum space with renormalized hybridization by the Gutzwiller narrowing factor q_σ [24–26], namely,

$$\hat{\mathcal{H}}_{\mathrm{GA}} \equiv \sum_{\mathbf{k},\sigma} \Psi^\dagger \begin{pmatrix} \epsilon^c_{\mathbf{k}} - \sigma h - \mu & \sqrt{q_\sigma}\, V \\ \sqrt{q_\sigma}\, V & \epsilon_f - \sigma h - \mu \end{pmatrix} \Psi + \Lambda U d^2, \tag{2}$$

where we have defined $\Psi^\dagger \equiv (\hat{c}^\dagger_{\mathbf{k},\sigma}, \hat{f}^\dagger_{\mathbf{k},\sigma})$, and $\epsilon^c_{\mathbf{k}}$ is the starting conduction band energy, Λ denotes the number of lattice sites, and d^2 is the probability of a having doubly occupied f orbital that we optimize variationally. In order to ensure that variationally calculated polarization and the f-level occupancy would coincide with those coming from the self-consistent procedure [23], we modify our effective Hamiltonian (2) by introducing additional constraints on the polarization (m_f) and the number (n_f) of f electrons via the Lagrange-multiplier method. The effective Hamiltonian with the constraints now takes the form

$$\begin{aligned} &\hat{\mathcal{H}}_{\mathrm{SGA}} \\ &\equiv \hat{\mathcal{H}}_{\mathrm{GA}} - \lambda^f_n \left(\sum_{\mathbf{k},\sigma} \hat{n}^f_{\mathbf{k},\sigma} - \Lambda n_f \right) - \lambda^f_m \left(\sum_{\mathbf{k},\sigma} \sigma \hat{n}^f_{\mathbf{k},\sigma} - \Lambda m_f \right) \\ &= \sum_{\mathbf{k},\sigma} \Psi^\dagger \begin{pmatrix} \epsilon^c_{\mathbf{k}} - \sigma h - \mu & \sqrt{q_\sigma} V \\ \sqrt{q_\sigma} V & \epsilon_f - \sigma\left(h + \lambda^f_m\right) - \lambda^f_n - \mu \end{pmatrix} \Psi \\ &\quad + \Lambda\left(U d^2 + \lambda^f_n n_f + \lambda^f_m m_f\right). \end{aligned} \tag{3}$$

Those constraint parameters λ^f_n and λ^f_m are also determined variationally. They play the role of nonlinear self-consistent fields acting on the charge and the spin degrees of freedom, respectively. Diagonalization of (3) in this spatially homogeneous case leads to four branches of eigenenergies, $E^\pm_{\mathbf{k}\sigma}$ representing two spin-split hybridized bands $E^\pm$. In order to determine the equilibrium properties of the system, we need to find the minimum of the generalized Landau grand-potential functional $\mathcal{F}$,

$$\frac{\mathcal{F}}{\Lambda} = -\frac{1}{\Lambda\beta} \sum_{\mathbf{k}\sigma b} \ln\left[1 + e^{-\beta E^b_{\mathbf{k}\sigma}}\right] + \left(\lambda^f_n n_f + \lambda^f_m m_f + U d^2\right), \tag{4}$$

where $b = \pm$. Effectively, it leads to the set of five nonlinear equations, $\partial\mathcal{F}/\partial\vec{\lambda} = 0$ for $\vec{\lambda} \equiv \{d, n_f, m_f, \lambda^f_n, \lambda^f_m\}$. However, due to the fact that the total number of electrons remains constant when pressure or the magnetic field is applied, we need also to satisfy the equation for the chemical potential μ via the condition

$$n = \frac{1}{\Lambda} \sum_{\mathbf{k}b\sigma} f\left(E^b_{\mathbf{k}\sigma}\right), \tag{5}$$

with f being the Fermi distribution. The equilibrium thermodynamic potential functional defines also the ground-state energy $E_G = \mathcal{F}|_0 + \Lambda\mu_0 n$, where the subscript 0 denotes the optimal values. After carrying out the minimization, we can also calculate the total spin polarization from

$$m \equiv m_c + m_f = \frac{1}{\Lambda} \sum_{\mathbf{k}b\sigma} \sigma f\left(E^b_{\mathbf{k}\sigma}\right). \tag{6}$$

Numerical calculations with a precision of at least 10^{-7} were carried out for a two-dimensional square lattice of $\Lambda = 512 \times 512$ size, and for low temperatures $\beta \equiv 1/k_B T \geqslant 1500$, emulating the $T \to 0$ limit.

Results. First, we analyze FM and PM solutions in the absence of field. In Fig. 1 we draw a phase diagram on the total filling–hybridization strength plane. For weak hybridization, FM phases are favored due to the negative balance between the increase of the kinetic and decrease of the Coulomb energies, caused by a relative shift of the spin-resolved DOS.

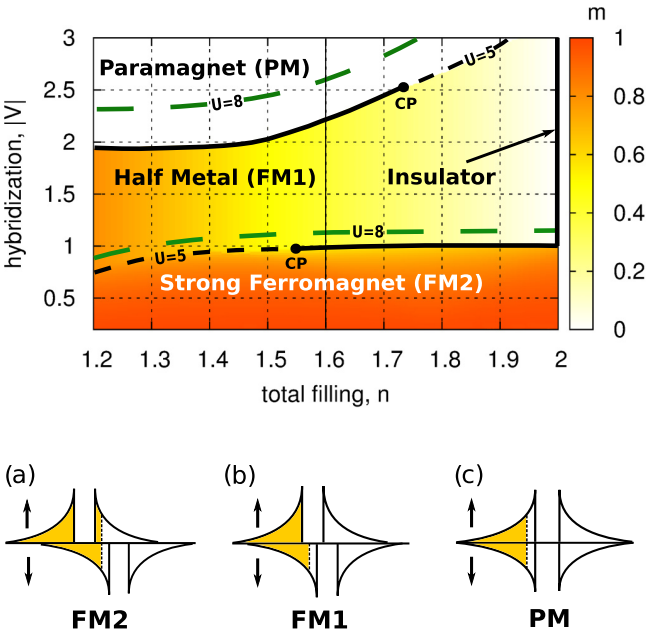

FIG. 1. (Color online) Top: Phase diagram on the plane total filling–hybridization strength for the zero field, containing both FM and PM phases for $U = 5$. The color scale denotes total spin polarization m. Phases are divided by the dashed and the solid lines. Dashed lines denote the second-order transition, whereas the solid denotes the first-order transition with the critical points, CP. Fine dashed lines mark how the phase borders would change for $U = 8$. (a)–(c) depict a schematic spin-resolved density of states corresponding to the phase sequence appearing along the solid vertical line (from bottom to top).

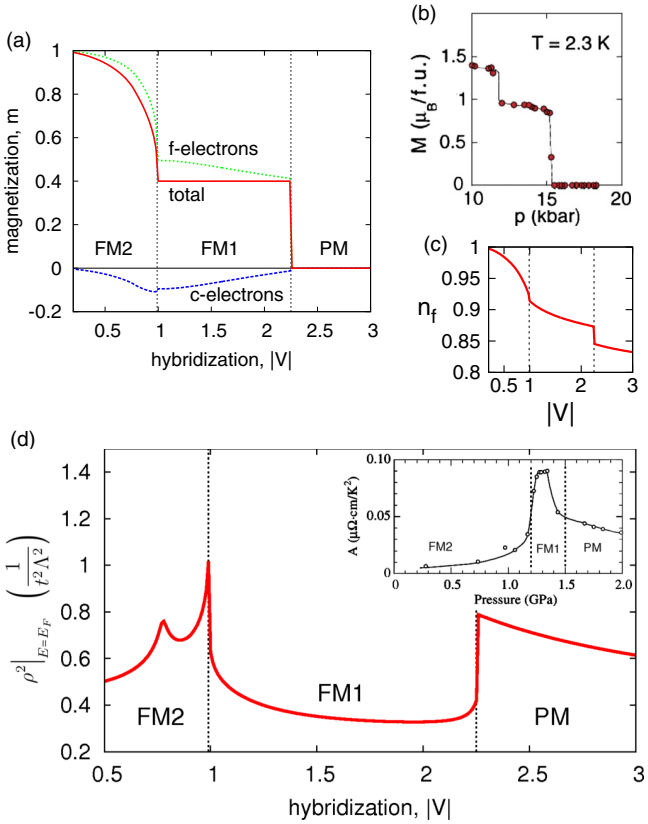

FIG. 2. (Color online) (a) Magnetization as a function of hybridization strength for the band filling $n = 1.6$, and the Coulomb repulsion $U = 5$. Both phase transitions induced by the hybridization change are of first order. (b) Corresponding experimental results from Ref. [4]. (c) f-orbital filling as a function of hybridization. (d) Square of DOS at the Fermi level vs $|V|$ through the phase sequence. Inset: Experimentally measured T^2-term coefficient A of the resistivity vs pressure from Ref. [18].

This is visualized by the diminution of the spin-subband overlap up to the FS—cf. Figs. 1(a) and 1(b). The appearance of a spontaneous polarization, as a result of a competition between the kinetic and the Coulomb energies, is in fact the feature of the Stoner mechanism for the band FM onset. In comparison to the usual single-band (e.g., Hubbard) model, we can distinguish in a natural manner between the two FM phases. The first (FM1) appears when the chemical potential is placed in the hybridization gap, between the spin subbands of the lower hybridized band, which is characterized also by magnetization equal to $m = 2 - n$ [cf. Fig. 1(b)]. In that situation, only the spin-minority carriers are present at and near the FS. The second phase (FM2) emerges when we further lower the hybridization and thus the chemical potential enters the majority spin-subband DOS [cf. Fig. 1(a)], giving rise to a step (discontinuous) increase in magnetization [cf. Fig. 2(a)]. In the limit of strong hybridization, for a fixed total filling, when the correlations weaken due to lowering of the f-orbital average occupancy [$n_f \lesssim 0.85$, cf. Fig. 2(c)], the kinetic energy gain outbalances a subsequent reduction of the average Coulomb interaction and the PM phase is energetically favorable. A similar mechanism for the formation of FM and, in particular, the characterization of phases, was studied before in Refs. [24–27].

In UGe_2 the spacing between Ge and U atoms decreases with increasing pressure, resulting in an enlargement of their orbital overlap. Even though other parameters may also be altered (e.g., ϵ_f), we presume that the main effect of the pressure exerted on the material can be modeled by a generally nonlinear concomitant strengthening of the hybridization amplitude. Thus, from Fig. 1 it can be seen that for the total filling n in the range 1.55–1.75, the sequence of phases and the order of the transitions are the same, as those found experimentally for UGe_2 by increasing the pressure [4,8]. As a representative band filling we have selected $n = 1.6$, marked by the vertical line in Fig. 1. In fact, as we compare the magnetization versus hybridization along the traced line [cf. Fig. 2(a)] with the corresponding experimental data [4] [cf. Fig. 2(b)], we find a good qualitative resemblance. Moreover, the magnetization differentiation among the orbitals [cf. Fig. 2(a)] is in agreement with the neutron scattering data [10,11] at ambient pressure (in our model $|V| \simeq 0.5$), where it was found that, almost exclusively, electrons from uranium atoms (f orbital) contribute to the ferromagnetism. In our picture it results from the fact that the competition between Coulomb repulsion and hybridization-induced itineracy concerns mainly the f electrons. Furthermore, as for low hybridization (in the FM2 phase) we obtain a small compensating polarization due to the c electrons, we suggest that the experimentally observed small negative magnetization between the uranium atoms at ambient pressure [11] may come from the delocalized cloud of conduction electrons.

Our microscopic description of the phase transitions induced by the change of the FS topology also compares favorably with the electronic-state features of UGe_2 derived from de Haas–van Alphen oscillations [18,19]. In Ref. [18] it is suggested that the majority spin FS disappears in the FM1 phase, in complete accord with the character of DOS presented in Fig. 1(b). We also reproduce the feature of an abrupt change of the FS at the FM1-PM phase transition [18,19] [cf. Fig. 2(d)]. Namely, here it corresponds to the step change of the chemical potential position merging into both bands. Furthermore, in the experimental data at the metamagnetic phase transition there is an observed significant enhancement of the quasiparticle mass renormalization [19]. As it is proportional to the DOS at Fermi level, in Fig. 2(d) we provide the corresponding behavior, which can be understood within our model by the chemical potential crossing the high hybridization peak in the majority spin subband. The transition then leads to a step change of FS only in the majority spin subband, while the minority subband evolves rather continuously, which is also seen experimentally [19].

For the sake of completeness, we have shown in the inset in Fig. 2(d) the pressure dependence of the T^2 term of resistivity [18] as it should have roughly the same dependence as the squared DOS at the FS, versus $|V|$ (we assume that the Kadowaki-Woods scaling holds). However, the jump that we obtain at the FM1-PM transition has not been observed in the resistivity measurements [18].

In the applied field, our model is also in good agreement with available experimental data for UGe_2. In Fig. 3(a) we display a phase diagram on the hybridization–applied-

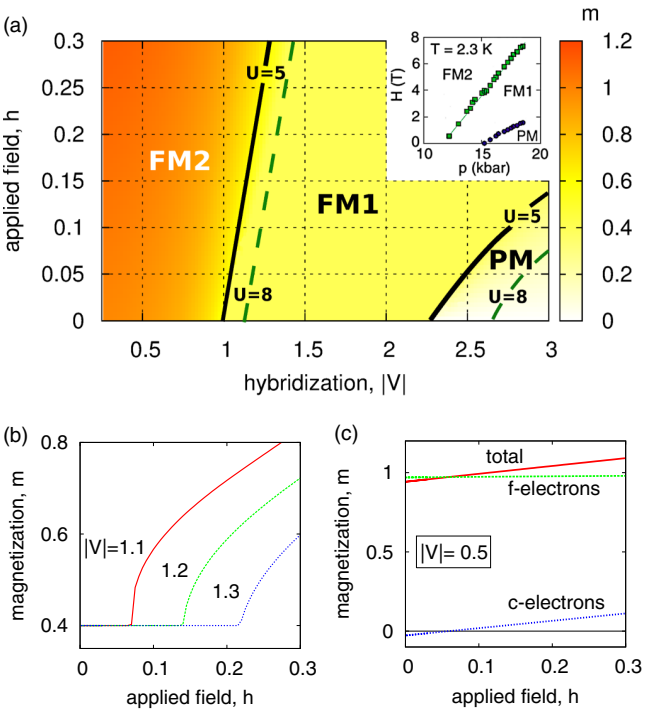

FIG. 3. (Color online) (a) Phase diagram on the applied field–hybridization strength plane for $n = 1.6$ and $U = 5$. The color scale denotes total spin polarization. The dashed lines mark the phase stability thresholds for $U = 8$. In the inset we show experimental results [4]. (b) Magnetization vs applied field for selected hybridization strengths when the system is entering into the FM1 to FM2 phase-transition regime. (c) Evolution of orbital-resolved magnetization with the field for low hybridization, $|V| = 0.5$ (mimicking ambient pressure). Note the very small c-electron polarization up to $h \simeq 0.1$.

magnetic-field plane that corresponds to that determined experimentally [4] [cf. the inset of Fig. 3(a)]. Similarly, as in Ref. [4], the magnetization at the phase transition between FM1 and FM2 triggered by the applied magnetic field starts from the same baseline, independently of the hybridization strength [cf. Fig. 3)]. However, one should note that, due to the fact that pressure not only changes the hybridization magnitude but also other microscopic parameters, we are not able to reproduce the magnetization cascade with increasing magnetic field when crossing the transitions.

The next feature found in UGe_2 at ambient pressure is an initial lack of measurable polarization on the germanium atoms with increasing magnetic field, as inferred from the neutron scattering data [10]. In our model we find a similar trend. For low hybridization ($|V| \simeq 0.5$ emulating ambient pressure), c-electron polarization increases slowly, and even up to $h \approx 0.1$ it is negligible [cf. Fig. 3(c)].

Remarks. With the simple but powerful technique based on the generalized Gutzwiller ansatz (SGA method), applied to the Anderson lattice model, we have constructed a microscopic model of FM in UGe_2. Namely, we are able to reproduce the main experimental features observed at low temperature, by applying either pressure or magnetic field [cf. Figs. 2(a) and 3(a)]. FM properties can be explained within the simplest hybridized two-orbital model, without taking into account the f-orbital degeneracy, i.e., by effectively incorporating both the Coulomb and the Hund's rule interaction into an effective interaction U, as would also be the case in the Hartree-Fock approximation [7].

To determine the stability of SC inside the FM phase, the present approach should be extended to account for the Hund's rule interaction explicitly, which can be crucial for the formation of the unconventional triplet SC [6,7,28,29]. If this is the case, it can be triggered even by a purely repulsive Coulomb interaction in conjunction with the residual Hund's rule coupling, as discussed in Refs. [28,29]. This issue requires a separate analysis. Another path for discussing the coexistence of SC with FM could be going beyond the Gutzwiller approximation, where we account also for the more distant correlations when determining the effective Hamiltonian [30,31]. Here, the central question is whether the spin-triplet pairing should be treated on the same footing as ferromagnetism, i.e., does it already appear in a direct space formulation [6,7,28,29] or is it mediated by collective spin fluctuations in the ferromagnetic phase [14,32–34] among already well defined quasiparticles. A crossover from the latter to the former approach is expected to take place with the increasing strength of the repulsive Coulomb interaction U.

Acknowledgments. The work has been partially supported by the Foundation for Polish Science (FNP) under the Grant TEAM, as well as by the National Science Centre (NCN) under the Grant MAESTRO, No. DEC-2012/04/A/ST3/00342. We would like to thank J. Kaczmarczyk for discussions and a critical reading of the manuscript.

[1] S. S. Saxena, P. Agarwal, K. Ahilan, F. M. Grosche, R. K. W. Haselwimmer, M. J. Steiner, E. Pugh, I. R. Walker, S. R. Julian, P. Monthoux, G. G. Lonzarich, A. Huxley, I. Sheikin, D. Braithwaite, and J. Flouquet, Nature (London) **406**, 587 (2000).

[2] A. J. Leggett, Rev. Mod. Phys. **47**, 331 (1975).

[3] J. F. Annett, B. L. Györffy, and K. I. Wysokiński, New J. Phys. **11**, 055063 (2009); K. I. Wysokiński, J. F. Annett, and B. L. Györffy, Phys. Rev. Lett. **108**, 077004 (2012); M. Gradhand, K. I. Wysokiński, J. F. Annett, and B. L. Györffy, Phys. Rev. B **88**, 094504 (2013).

[4] C. Pfleiderer and A. D. Huxley, Phys. Rev. Lett. **89**, 147005 (2002).

[5] V. Taufour, D. Aoki, G. Knebel, and J. Flouquet, Phys. Rev. Lett. **105**, 217201 (2010).

[6] J. Spałek, Phys. Rev. B **63**, 104513 (2001).

[7] M. Zegrodnik and J. Spałek, Phys. Rev. B **86**, 014505 (2012).

[8] C. Pfleiderer, Rev. Mod. Phys. **81**, 1551 (2009), Sec. III A.

[9] D. Aoki and J. Flouquet, J. Phys. Soc. Jpn. **81**, 011003 (2012).

[10] A. Huxley, I. Sheikin, E. Ressouche, N. Kernavanois, D. Braithwaite, R. Calemczuk, and J. Flouquet, Phys. Rev. B **63**, 144519 (2001).

[11] N. Kernavanois, B. Grenier, A. Huxley, E. Ressouche, J. P. Sanchez, and J. Flouquet, Phys. Rev. B **64**, 174509 (2001).
[12] K. Hirohashi and K. Ueda, J. Phys. Soc. Jpn. **73**, 1576 (2004).
[13] D. Belitz, T. R. Kirkpatrick, and J. Rollbühler, Phys. Rev. Lett. **94**, 247205 (2005).
[14] K. G. Sandeman, G. G. Lonzarich, and A. J. Schofield, Phys. Rev. Lett. **90**, 167005 (2003).
[15] A. B. Shick and W. E. Pickett, Phys. Rev. Lett. **86**, 300 (2001).
[16] V. H. Tran, S. Paschen, R. Troć, M. Baenitz, and F. Steglich, Phys. Rev. B **69**, 195314 (2004).
[17] Y. Onuki, I. Ukon, S. Won Yun, I. Umehara, K. Satoh, T. Fukuhara, H. Sato, S. Takayanagi, M. Shikama, and A. Ochiai, J. Phys. Soc. Jpn. **61**, 293 (1992).
[18] R. Settai, M. Nakashima, S. Araki, Y. Haga, T. C. Kobayashi, N. Tateiwa, H. Yamagami, and Y. Onuki, J. Phys.: Condens. Matter **14**, L29 (2002).
[19] T. Terashima, T. Matsumoto, C. Terakura, S. Uji, N. Kimura, M. Endo, T. Komatsubara, and H. Aoki, Phys. Rev. Lett. **87**, 166401 (2001).
[20] D. Vollhardt, Rev. Mod. Phys. **56**, 99 (1984).
[21] T. M. Rice and K. Ueda, Phys. Rev. Lett. **55**, 995 (1985).
[22] P. Fazekas and B. H. Brandow, Phys. Scr. **36**, 809 (1987).
[23] Approach derived in J. Jędrak, J. Kaczmarczyk, and J. Spałek, arXiv:1008.0021; J. Jędrak and J. Spałek, Phys. Rev. B **81**, 073108 (2010); **83**, 104512 (2011); J. Kaczmarczyk and J. Spałek, *ibid.* **84**, 125140 (2011); M. Wysokiński, J. Jędrak, J. Kaczmarczyk, and J. Spałek, in *Lectures on the Physics of Strongly Coreelated Sysytems XVI: Sixteenth Training Course in the Physics of Strongly Correlated Systems*, edited by A. Avella and F. Mancini, AIP Conf. Proc. Vol. 1485 (AIP, Melville, NY, 2012), p. 319; M. Abram, J. Kaczmarczyk, J. Jędrak, and J. Spałek, Phys. Rev. B **88**, 094502 (2013); O. Howczak, J. Kaczmarczyk, and J. Spałek, Phys. Status Solidi B **250**, 609 (2013); A. P. Kądzielawa, J. Spałek, J. Kurzyk, and W. Wójcik, Eur. Phys. J. B **86**, 252 (2013); M. M. Wysokiński and J. Spałek, J. Phys.: Condens. Matter **26**, 055601 (2014).
[24] R. Doradziński and J. Spałek, Phys. Rev. B **56**, R14239 (1997).
[25] R. Doradziński and J. Spałek, Phys. Rev. B **58**, 3293 (1998).
[26] O. Howczak and J. Spałek, J. Phys.: Condens. Matter **24**, 205602 (2012).
[27] K. Kubo, Phys. Rev. B **87**, 195127 (2013).
[28] M. Zegrodnik, J. Spałek, and J. Bünemann, New J. Phys. **15**, 073050 (2013).
[29] M. Zegrodnik, J. Bünemann, and J. Spałek, New J. Phys. **16**, 033001 (2014).
[30] J. Kaczmarczyk, J. Spałek, T. Schickling, and J. Bünemann, Phys. Rev. B **88**, 115127 (2013).
[31] J. Kaczmarczyk, J. Bünemann, and J. Spałek, New J. Phys. **16**, 073018 (2014).
[32] D. Fay and J. Appel, Phys. Rev. B **22**, 3173 (1980).
[33] T. R. Kirkpatrick, D. Belitz, T. Vojta, and R. Narayanan, Phys. Rev. Lett. **87**, 127003 (2001).
[34] R. Roussev and A. J. Millis, Phys. Rev. B **63**, 140504 (2001).

3.4 Article A.3, Criticalities in the itinerant ferromagnet UGe_2

In this work we have extended our previous modeling of UGe_2 properties by the Anderson lattice model within the SGA method to nonzero temperature. We have found that in accord with the experimental observations [111], the first order metamagnetic phase transition is terminated at the critical ending point (CEP) and changes its character to the crossover behavior. This behavior is explained as follows. The thermal motion smears out the initially sharp hybridization gap. As a result, the magnetization of the FM2 and FM1 phases at the metamagnetic transition are bending towards each other, eventually leading to the change of the 1st order transition into the crossover behavior at a single point (CEP). Moreover, our model also predicts that the first-order FM to PM transition for higher temperatures changes its character into the second-order transition line at the tricritical point (TCP). It is explained as the effect of magnetization of the FM1 phase bending towards zero where finally, for the specific critical temperature, vanishes and thus the transition becomes second order. The mentioned classical critical point is of the tricritical nature, since in the space spanned by the temperature T, hybridization $|V|$ and field h, tricritical wings (surfaces of the first-order transitions) emerge from this point and terminate in a pair of quantum critical ending points (QCEP) depending on the direction of the applied magnetic field. For the same total number of electrons, $n = 1.6$ as in the previous work (Article A.2), we have found that the mutual relation between critical temperatures of CEP and TCP agrees with that determined experimentally. By this correspondence we have assigned physical units to the reduced microscopic parameters used in our model. We have verified our model by comparing resulting second order transition line connecting TCP with QCEP projected onto magnetic field - temperature plane with the experimental data [111, 112] and found an excellent agreement. We have also determined position of QCEP to be around 30 T, in variance with value 18 T estimated by means of the extrapolation in the Ref. [112].

Additionally to the quantitative description of the all criticalities observed in UGe_2, our model predicts existence of a new quantum critical point (QCP) of the Lifshitz type in the vicinity of the superconducting dome. It can be reached by evolving CEP at the metamagnetic transition down to $T = 0$ by changing both electron concentration and pressure. We have modeled the applied pressure by the increasing hybridization strength. At this QCP the ferromagnetic quantum critical fluctuations may come as a source of the spin-triplet pairing. however, this last point requires a separate study.

PHYSICAL REVIEW B **91**, 081108(R) (2015)

Criticalities in the itinerant ferromagnet UGe_2

Marcin M. Wysokiński,[1,*] Marcin Abram,[1,†] and Józef Spałek[1,2,‡]

[1]*Marian Smoluchowski Institute of Physics, Jagiellonian University, Łojasiewicza 11, PL-30-348 Kraków, Poland*

[2]*Academic Centre for Materials and Nanotechnology (ACMiN), AGH University of Science and Technology, Al. Mickiewicza 30, PL-30-059 Kraków, Poland*

(Received 28 November 2014; revised manuscript received 28 January 2015; published 20 February 2015)

We provide a microscopic description of the magnetic properties of UGe_2 and, in particular, of its both classical and quantum critical behavior. Namely, we account for all the critical points: the critical ending point (CEP) at the metamagnetic phase transition, the tricritical point, and the quantum critical end point at the ferromagnetic to paramagnetic phase transition. Their position agrees quantitatively with experiment. Additionally, we predict that the metamagnetic CEP can be traced down to zero temperature and becomes quantum critical point by a small decrease of both the total electron concentration and the external pressure. The system properties are then determined by the quantum critical fluctuations appearing near the instability point of the Fermi surface topology.

DOI: 10.1103/PhysRevB.91.081108 PACS number(s): 71.27.+a, 75.30.Kz, 71.10.−w

Introduction. Attempts to determine the quantum critical behavior and the corresponding critical points (QCPs) have attracted much attention due to the unique phenomena with singular physical properties associated with them as temperature $T \to 0$ and other parameters (pressure p, applied field H, or electron concentration n) are varied [1–3]. Additionally, in the canonical case—the heavy fermion systems—unconventional superconductivity often appears near those QCPs making the quantum critical fluctuations the primary pairing inducing factor. Also, the classical critical points (CCPs) and their evolution towards QCP provide the testing ground for study of detailed quantitative behavior of different systems [4,5].

UGe_2, in this respect, is one of the unique materials that exhibit all the above features. Therefore, the explanation of the magnetic phase diagram and intimately connected critical points within a single theoretical framework would provide a complete understanding of this remarkable quantum material [4,6–9]. The phase diagram on the pressure-temperature (p-T) plane comprises two ferromagnetic phases, of weaker (FM1) and stronger (FM2) magnetization, paramagnetic phase (PM), as well as the spin-triplet superconducting phase (SC) [4,6,10]. SC disappears at the same pressure as FM [6] and the maximum of the superconducting critical temperature T_s coincides with the critical pressure for the FM2-FM1 phase transition [7]. Thus, it is strongly suggestive that FM and SC are strongly intertwined as described by some theoretical approaches [11–15].

The p-T-H phase diagram for UGe_2 comprises the characteristic *wing shape* [8,9]. Such structure was theoretically obtained by Belitz *et al.* [16] within mean-field approach for a single-band itinerant ferromagnet. However, this approach cannot account for the two different ferromagnetic phases appearing in UGe_2, as well as for the critical ending point (CEP), separating the region with a discontinuous drop in magnetization from a crossover regime [8,17].

In this work we provide a quantitative microscopic description of all magnetic critical properties of UGe_2 within the framework of the Anderson lattice model (ALM) treated by a modified Gutzwiller approach [18], called *the statistically consistent Gutzwiller approximation* (SGA) (for a description of the method and a detailed comparison to the slave-boson approach, see Ref. [19]; for its applications, see Refs. [20]). Validity of this model in the context of UGe_2 [18] is based on earlier results: first, on band structure calculations [21,22] and second, on experimental observations [4,6,23]. The first feature is a quasi-two-dimensional topology of the Fermi surface (FS) [21,22] which justifies calculations for a two-dimensional square lattice. On the other hand, despite the circumstance that the distance between uranium atoms is above the Hill limit [4], the experimental value of the paramagnetic moment per U atom is different from that for either f^3 or f^2 configurations [6,24]. This speaks for the presence of a sizable hybridization between the initially localized f electrons and those from the conduction band. For strong enough hybridization, f electrons contribute essentially to the heavy itinerant quasiparticle states and play a dominant role in the magnetic properties [6,10,24].

We provide a coherent explanation of FM and PM phase appearances as driven by a competition between the hybridization from one side and the f-f Coulomb local repulsive interaction from the other [18]. Specifically, we obtain two different FM phases [15,18,25–28] by varying the predetermined position of the chemical potential with respect to the peaks in the quasiparticle density of states (DOS) including the spin-split subbands. Although, Gutzwiller ansatz in certain regimes favors antiferromagnetism over FM [25–27,29,30], we restrict our discussion to the latter phase, because in the considered range of electron concentration, $n \simeq 1.6$, FM phase turned out to have the lowest energy [25,26].

In Fig. 1 we draw schematically the respective DOS for considered phases. It can be seen clearly that the shape of the FS (limiting the filled parts) will be vastly different in each of the phases. Within our approach, most of the properties of UGe_2 at $T = 0$ can be explained [18] in agreement with related experiments of magnetization [7], neutron scattering [10,24], and the de Haas–van Alphen oscillations [31,32]. The character of the FM1 phase, which we obtain as a half-metallic type [cf. Fig. 1(b)], is also supported by the band-structure calculations [22].

In the present work we extend our previous approach [18] to nonzero temperature and on this basis we determine the

*marcin.wysokinski@uj.edu.pl
†marcin.abram@uj.edu.pl
‡ufspalek@if.uj.edu.pl

character of all phase transitions on the p-T-H diagram of UGe_2, as well as discuss the nature of all the classical and quantum critical points. We also show that by a small decrease of electron concentration (by $\sim$7%), the system can reach another quantum criticality via a metamagnetic transition upon changing the pressure. We also predict the corresponding change in FS topology distinguishing the two phases of significantly different magnetic susceptibility.

Model. We start from ALM with the Zeeman term included ($h \equiv \frac{1}{2} g \mu_0 \mu_B H$) in the Hamiltonian

$$\hat{\mathcal{H}} - \mu \hat{N} = {\sum_{\mathbf{i},\mathbf{j},\sigma}}' t_{\mathbf{ij}} \hat{c}^{\dagger}_{\mathbf{i},\sigma} \hat{c}_{\mathbf{j},\sigma} - \sum_{\mathbf{i},\sigma} (\mu + \sigma h) \hat{n}^{c}_{\mathbf{i},\sigma} + \sum_{\mathbf{i},\sigma} (\epsilon_f - \mu - \sigma h) \hat{n}^{f}_{\mathbf{i},\sigma} + U \sum_{\mathbf{i}} \hat{n}^{f}_{\mathbf{i},\uparrow} \hat{n}^{f}_{\mathbf{i},\downarrow} + V \sum_{\mathbf{i},\sigma} (\hat{f}^{\dagger}_{\mathbf{i},\sigma} \hat{c}_{\mathbf{i},\sigma} + \hat{c}^{\dagger}_{\mathbf{i},\sigma} \hat{f}_{\mathbf{i},\sigma}), \quad (1)$$

which comprises dispersive conduction (c) band electrons and f electrons coming from atomic f shell located at $\epsilon_f < 0$. In the model we include specifically the nearest- ($t < 0$) and the second-nearest- ($t' = 0.25|t|$) neighbor hopping amplitudes between c electrons, f level at $\epsilon_f = -3|t|$, sizable $f - f$ Coulomb repulsion $U = 5|t|$, and the $c - f$ hybridization V of the on-site form.

To obtain an effective single particle picture from the many-body Hamiltonian (1) we use the extended Gutzwiller approximation (GA) called the SGA (for details, see [19]). The method was successfully applied to a number of problems [20]. Formally, we add to the effective Hamiltonian obtained in GA [33,34], $\hat{\mathcal{H}}_{\mathrm{GA}}$, additional constraints on the number of f electrons and their magnetization by means of the Lagrange multipliers. It leads to the new effective Hamiltonian $\hat{\mathcal{H}}_{\mathrm{SGA}}$ of the form

$$\hat{\mathcal{H}}_{\mathrm{SGA}} \equiv \hat{\mathcal{H}}_{\mathrm{GA}} - \lambda^{f}_{n} \left(\sum_{\mathbf{k},\sigma} \hat{n}^{f}_{\mathbf{k},\sigma} - \Lambda n_f \right) - \lambda^{f}_{m} \left(\sum_{\mathbf{k},\sigma} \sigma \hat{n}^{f}_{\mathbf{k},\sigma} - \Lambda m_f \right) \equiv \sum_{\mathbf{k},\sigma} \hat{\Psi}^{\dagger}_{\mathbf{k}\sigma} \begin{pmatrix} \epsilon^{c}_{\mathbf{k}} - \sigma h - \mu & \sqrt{q_\sigma} V \\ \sqrt{q_\sigma} V & \epsilon_f - \sigma (h + \lambda^{f}_{m}) - \lambda^{f}_{n} - \mu \end{pmatrix} \hat{\Psi}_{\mathbf{k}\sigma} + \Lambda \left(U d^2 + \lambda^{f}_{n} n_f + \lambda^{f}_{m} m_f \right), \quad (2)$$

where $\hat{\Psi}^{\dagger}_{\mathbf{k}\sigma} \equiv (\hat{c}^{\dagger}_{\mathbf{k},\sigma}, \hat{f}^{\dagger}_{\mathbf{k},\sigma})$. Furthermore, q_σ is the hybridization narrowing factor in the standard form [18,20], and Λ is a number of lattice sites.

At nonzero temperature, one needs to minimize the generalized Landau grand-potential functional

$$\frac{\mathcal{F}}{\Lambda} = -\frac{1}{\Lambda \beta} \sum_{\mathbf{k}\sigma b} \ln \left[1 + e^{-\beta E^{b}_{\mathbf{k}\sigma}} \right] + \left(\lambda^{f}_{n} n_f + \lambda^{f}_{m} m_f + U d^2 \right), \quad (3)$$

where $E^{b}_{\mathbf{k}\sigma}$ are four eigenvalues of the effective Hamiltonian (2) labeled with the spin (σ) and band (b) indices. λ^{f}_{n} and λ^{f}_{m} are the Lagrange multipliers assuring the correct statistical consistency of equations for n_f and m_f and play the role of correlation-induced effective fields [20]. Minimization of $\mathcal{F}$ is carried out with respect to the set of all parameters $\vec{\lambda} \equiv \{d, n_f, m_f, \lambda^{f}_{n}, \lambda^{f}_{m}\}$. Additionally, as the number of particles in the system is conserved we have to determine the chemical potential and adjust it to each of the phases according to the condition $n = 1/\Lambda \sum_{\mathbf{k}b\sigma} f(E^{b}_{\mathbf{k}\sigma})$, with $f(E)$ being the Fermi-Dirac function. In effect, the model is described by set of six algebraic equations which are solved with the help of the GSL library, with typical accuracy 10^{-11}.

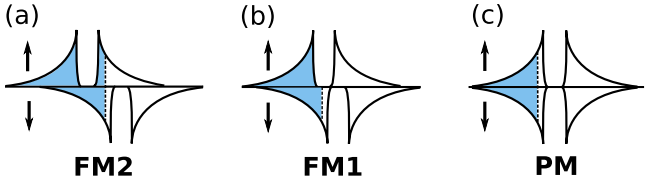

FIG. 1. (Color online) Schematic characterization of phases by their spin-resolved density of states. The arrows label the spin subbands and the dotted line marks the position of the chemical potential.

The Landau grand-potential functional for the equilibrium values of the parameters, $\mathcal{F}_0$, has the meaning of the physical grand potential Ω which is the proper quantity for studying the system at any temperature, $\mathcal{F}_0 \equiv \Omega \equiv U - TS - \mu N$. Therefore, the free energy of the system is defined by $F = \mathcal{F}_0 + \mu N$ and the ground-state energy is $E_G \equiv F(T = 0)$.

Results. We assume that the main effect of the applied pressure is emulated by an increase of the hybridization amplitude $|V|$, even though other parameters (e.g., ϵ_f) may also change. However, as our previous results indicate, hybridization change is the principal factor of the pressure dependencies observed in UGe_2 [18].

In Fig. 2 we plot the phase diagram on the $|V| - T$ plane. In the low-T regime we are able to reproduce the correct evolution of both metamagnetic (left) and ferromagnetic to paramagnetic (right) phase transitions observed in experiment (cf. inset), together with the respective critical behavior [7–9,17]. The position of the CCPs is very sensitive to the selected total band filling, $n = n_f + n_c$. Our fitting constraint is the ratio of the corresponding critical temperatures, $T_{\mathrm{CEP}}/T_{\mathrm{TCP}} \approx 7\ \mathrm{K}/24\ \mathrm{K}$ [8]. Consequently, for the band filling $n = 1.6$, selected in our previous analysis at $T = 0$ [18], we obtain agreement of our calculated ratio under the proviso that experimental values of the critical temperatures are determined with accuracy ± 0.25 K.

Our model does not account for correct curvatures of phase transitions above CCPs (cf. Fig. 2). This discrepancy can be attributed to the fact that also other microscopic parameters can alter when applying pressure, e.g., ϵ_f, and to additional

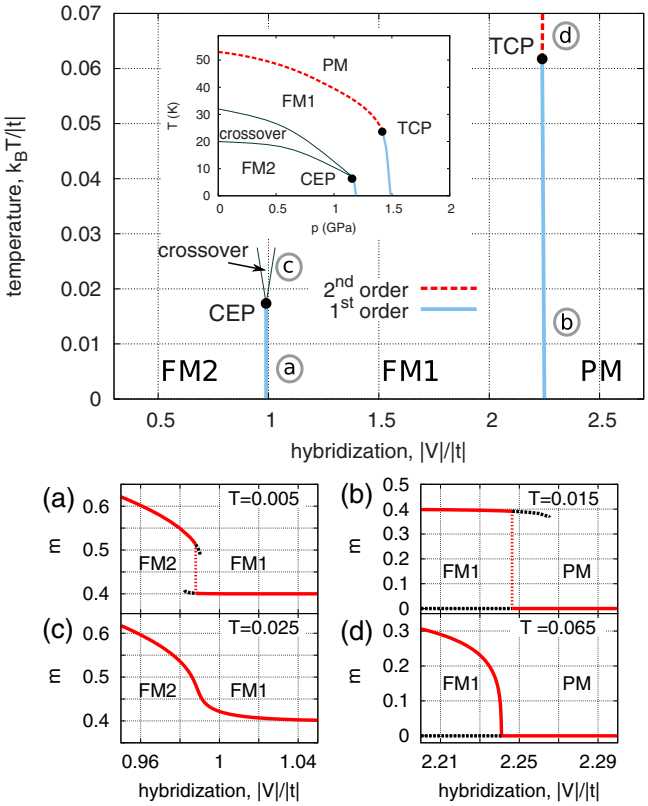

FIG. 2. (Color online) Top: Phase diagram on hybridization strength-reduced temperature plane encompassing both FM and PM phases for total band filling $n = 1.6$. The correct character of phase transitions and positions of critical points in UGe_2 [7–9,17] is reproduced. For comparison, we present in the inset the experimental p-T phase diagram of UGe_2 (cf. [7,8]). In (a)–(d) we draw the magnetization change with the increasing hybridization strength when the system undergoes phase transition at points indicated with respective encircled letters ⓐ–ⓓ. Solid red lines denote energetically favorable solution, whereas dashed black lines denote the unstable solutions.

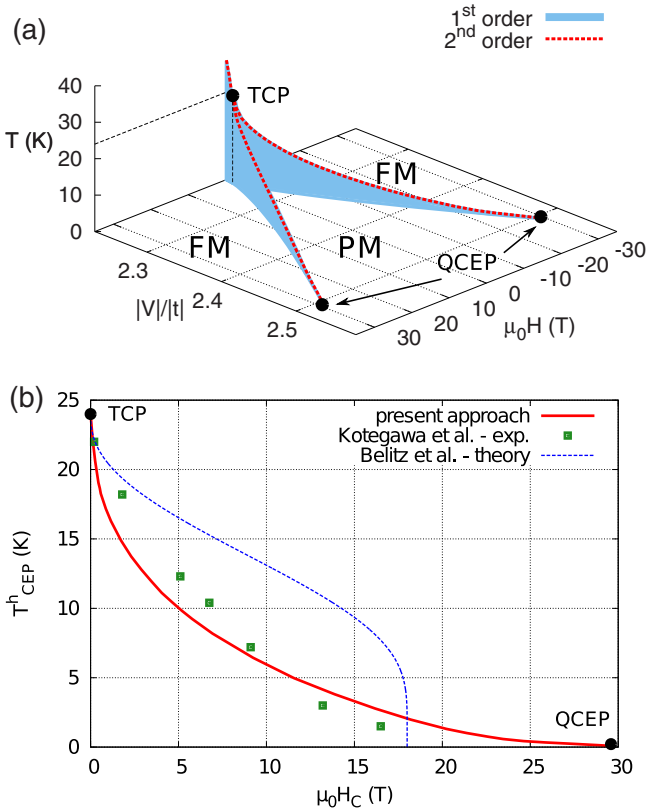

FIG. 3. (Color online) (a) Wing structure of the phase transition planes derived from our model. (b) Comparison of the calculated dependence of the temperature vs applied magnetic field at the critical end point (CEP) with the experimental points adopted from [9]. For comparison, we include also the prediction by Belitz *et al.* [16], with the fitting parameters selected on the basis [9]: $H_{\rm QCEP} = 18$ T and $T_{\rm TCP} = 24$ K.

entropic factors important in the case of $T > 0$ Gutzwiller projection [35,36].

In our calculations we have used reduced temperature $k_BT/|t|$. We rescale it to the physical units by relating it to the experimentally measured values at CCPs [7–9,17]. Accordingly, we also rescale the reduced field $\frac{1}{2}g\mu_B\mu_0H/|t|$ to Tesla units.

At the metamagnetic (FM2-FM1) phase transition we obtain CEP separating the discontinuous-transition line from the crossover regime. At low T both solutions with the weaker and the stronger magnetization coexist in the limited range of the hybridization strength [cf. Fig. 2(a)]. As the system approaches the transition from the FM1 side, FS changes drastically only in one spin subband, in which the chemical potential crosses the hybridization gap, resulting also in a discontinuous jump of the total moment $m = m_f + m_c$. With the increasing temperature, the edges of the gap are gradually smeared out. This leads to a deviation from the pure half-metallic type of the FM1 phase. The magnetization is *bending* towards the trend observed in the FM2 phase, and eventually at CEP it is changing to a crossover line [cf. Fig. 2(c)].

In the case of FM to PM transition the situation is different [cf. Figs. 2(b) and 2(d)]. At low temperature, the magnetization of this *half-metallic* FM1 phase discontinuously drops to zero [cf. Fig. 2(b)]. However, with the increasing temperature, the ferromagnetic solution departs from a sharp half-metallic type and slowly *bends* over towards the paramagnetic solution, eventually reaching the critical point by changing the transition character to that of second order [cf. Fig. 2(d)]. The just described critical point is of tricritical character (TCP). This is because its evolution can be followed by applying the magnetic field down to $T = 0$, where it turns into the quantum critical ending point (QCEP) [cf. Fig. 3(a)]. In this manner, we have achieved a full characteristic at the *wing-shape* p-T-H phase diagram [8,9]. As the detailed form of the hybridization change with applied pressure is unknown, and in principle nonlinear, we compare our predicted shape of wings by tracing the evolution of CEP on the temperature-magnetic field T^h_{CEP}-μ_0H_C plane [cf. Fig. 3(b)] and comparing it to the experimental data [9]. We obtain a satisfactory quantitative agreement with the experimental points, as well as recover its proper curvature. For comparison, the results from the

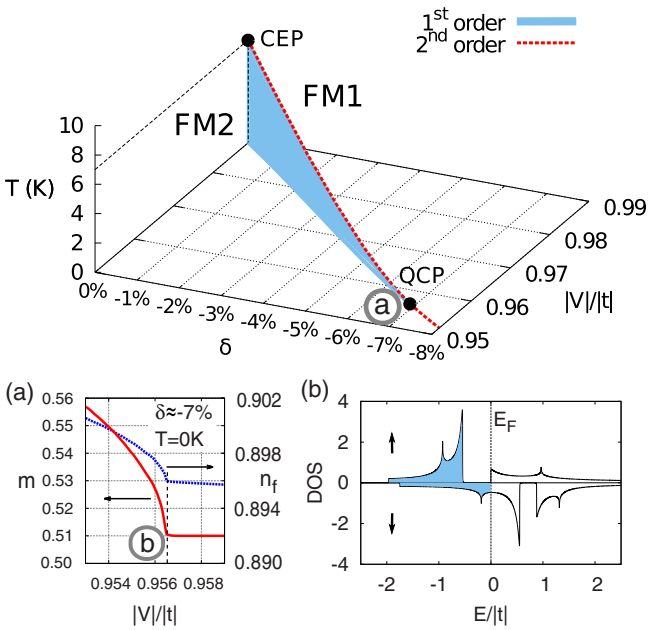

FIG. 4. (Color online) Top: Evolution of CEP on the $|V|$-T-δ plane down to $T = 0$ and QCP (see main text). Bottom: (a) Change of magnetization and f electron number as the system undergoes quantum critical transition. (b) Density of states at QCP. Note the intermediate character of FS between FM2 and FM1 of the state at QCP. Encircled letter ⓐ at top diagram refers to the position of the curves in panel (a), and respectively ⓑ at panel (a) to the position of the DOS in (b).

mean-field approach to the single-band case by Belitz *et al.* [16] are also drawn, as is universal explanation of tricritical behavior of itinerant ferromagnets. Nevertheless, as suggested by the authors in Ref. [9], the crucial element determining for UGe_2 the correct shape of the wings is the change of FS, present in our two-band ALM model. We also predict that the curve of the T^h_{CEP} vs $\mu_0 H_C$ dependence has a longer tail than that estimated in Ref. [9], i.e., that QCEP should be located at fields around 30 T. Our estimate thus calls for a more precise determination of the QCEP position.

In fitting to the data in Fig. 3 we have assumed that the g factor for f electrons $g_f = 2$ (the same as for c electrons). This assumption is based on the presumption that for itinerant electrons the crystal-field multiplet structure is washed out. Parenthetically, taking g_f significantly different provides a worse agreement, but the curvature character remains unchanged.

In Fig. 4 we draw the evolution of CEP at the metamagnetic transition with the decrease of both the hybridization and the electron concentration. The latter quantity is characterized by the parameter $\delta = \frac{n_x - n}{n} 100\%$, where $n = 1.6$ is initial and n_x is the actual concentration. On the V-T-δ phase diagram the CEP can be followed down to zero temperature, where it joins the second-order transition line [cf. Fig. 4(a)]. At this second-order transition the Fermi level for the majority spin subband is exactly at the border of the gap [cf. Fig. 4(b)]. It means that along this line quantum critical fluctuations of FS topology are present. In other terms, we have a strong indication that in the vicinity of the SC dome maximum this compound exhibits a *Lifshitz* type of quantum critical behavior. This quantum critical transition can be associated also with the specific valence change [cf. Fig. 4(a)]. However, here the average f electron number changes continuously in contrast to the discontinuous drop originating from the f-c electron repulsion [37]. The difference in the origin of *Lifshitz* type of ferromagnetic QCP with respect to that considered before [38,39] is that here it results from the two-band model and separates different FM phases.

Summary. We have described the phase diagram of UGe_2 at nonzero temperature and have determined the location of the critical points, as well as proposed an additional quantum critical point for UGe_2. With the help of the Anderson lattice model we are able to reproduce quantitatively all the principal features of the magnetism in this compound. We also have determined the location of experimentally observed critical and quantum critical points, together with a correct order of the phase transitions related to them.

Although our mean-field approach seems to capture all the features concerning details of the p-T-H phase diagram of UGe_2, we should note that, in principle, fluctuations of order parameters can bring quantitative changes to our results. However, as the phase transitions are induced by the drastic changes of the Fermi surface, the effect of the fluctuations should be minor (except near the predicted QCP—cf. Fig. 4) and may lead to a correction of the CEP and TCP positions.

It should be noted that we have employed an orbitally nondegenerate ALM. Accounting for the degenerate one would imply inclusion of the residual Hund's rule interaction present in the degenerate ALM model which could be important in inducing the spin-triplet pairing [40].

Acknowledgments. The work was partly supported by the Foundation for Polish Science (FNP) under the Grant TEAM and partly by the National Science Centre (NCN) under MAESTRO, Grant No. DEC-2012/04/A/ST3/00342. Access to the supercomputer located at Academic Centre for Materials and Nanotechnology of the AGH University of Science and Technology in Kraków is also acknowledged.

[1] H. v. Löhneysen, A. Rosch, M. Vojta, and P. Wölfle, Rev. Mod. Phys. **79**, 1015 (2007).

[2] Q. Si, P. Gegenwart, and F. Steglich, *Understanding Quantum Phase Transitions*, edited by L. D. Carr (CRC Press, Boca Raton, 2011), Chaps. 8, 18, pp. 193–216, 445–468.

[3] A. Ślebarski and J. Spałek, Phys. Rev. Lett. **95**, 046402 (2005).

[4] C. Pfleiderer, Rev. Mod. Phys. **81**, 1551 (2009) (Sec. III.A).

[5] J. Spalek, A. Datta, and J. M. Honig, Phys. Rev. Lett. **59**, 728 (1987); J. Spałek, Phys. Status Solidi B **243**, 78 (2006).

[6] S. S. Saxena, P. Agarwal, K. Ahilan, F. M. Grosche, R. K. W. Haselwimmer, M. J. Steiner, E. Pugh, I. R. Walker, S. R. Julian, P. Monthoux, G. G. Lonzarich, A. Huxley, I. Sheikin, D. Braithwaite, and J. Flouquet, Nature (London) **406**, 587 (2000).

[7] C. Pfleiderer and A. D. Huxley, Phys. Rev. Lett. **89**, 147005 (2002).
[8] V. Taufour, D. Aoki, G. Knebel, and J. Flouquet, Phys. Rev. Lett. **105**, 217201 (2010).
[9] H. Kotegawa, V. Taufour, D. Aoki, G. Knebel, and J. Flouquet, J. Phys. Soc. Jpn. **80**, 083703 (2011).
[10] A. Huxley, I. Sheikin, E. Ressouche, N. Kernavanois, D. Braithwaite, R. Calemczuk, and J. Flouquet, Phys. Rev. B **63**, 144519 (2001).
[11] T. R. Kirkpatrick, D. Belitz, T. Vojta, and R. Narayanan, Phys. Rev. Lett. **87**, 127003 (2001).
[12] K. Machida and T. Ohmi, Phys. Rev. Lett. **86**, 850 (2001).
[13] A. A. Abrikosov, J. Phys: Condens. Matter **13**, L943 (2001).
[14] D. Sa, Phys. Rev. B **66**, 140505 (2002).
[15] K. G. Sandeman, G. G. Lonzarich, and A. J. Schofield, Phys. Rev. Lett. **90**, 167005 (2003).
[16] D. Belitz, T. R. Kirkpatrick, and J. Rollbühler, Phys. Rev. Lett. **94**, 247205 (2005).
[17] F. Hardy, C. Meingast, V. Taufour, J. Flouquet, H. v. Löhneysen, R. A. Fisher, N. E. Phillips, A. Huxley, and J. C. Lashley, Phys. Rev. B **80**, 174521 (2009).
[18] M. M. Wysokiński, M. Abram, and J. Spałek, Phys. Rev. B **90**, 081114(R) (2014).
[19] J. Jędrak, J. Kaczmarczyk, and J. Spałek, arXiv:1008.0021.
[20] J. Jędrak and J. Spałek, Phys. Rev. B **83**, 104512 (2011); J. Kaczmarczyk and J. Spałek, *ibid.* **84**, 125140 (2011); O. Howczak, J. Kaczmarczyk, and J. Spałek, Phys. Status Solidi B **250**, 609 (2013); A. P. Kądzielawa, J. Spałek, J. Kurzyk, and W. Wójcik, Eur. Phys. J. B **86**, 252 (2013); M. Abram, J. Kaczmarczyk, J. Jędrak, and J. Spałek, Phys. Rev. B **88**, 094502 (2013); M. Zegrodnik, J. Spałek, and J. Bünemann, New J. Phys. **15**, 073050 (2013); M. M. Wysokiński and J. Spałek, J. Phys.: Condens. Matter **26**, 055601 (2014).
[21] A. B. Shick and W. E. Pickett, Phys. Rev. Lett. **86**, 300 (2001).
[22] M. Samsel-Czekała, M. Werwiński, A. Szajek, G. Chełkowska, and R. Troć, Intermetallics **19**, 1411 (2011).
[23] V. H. Tran, S. Paschen, R. Troć, M. Baenitz, and F. Steglich, Phys. Rev. B **69**, 195314 (2004).
[24] N. Kernavanois, B. Grenier, A. Huxley, E. Ressouche, J. P. Sanchez, and J. Flouquet, Phys. Rev. B **64**, 174509 (2001).
[25] R. Doradziński and J. Spałek, Phys. Rev. B **56**, R14239 (1997).
[26] R. Doradziński and J. Spałek, Phys. Rev. B **58**, 3293 (1998).
[27] O. Howczak and J. Spałek, J. Phys: Condens. Matter **24**, 205602 (2012).
[28] K. Kubo, Phys. Rev. B **87**, 195127 (2013).
[29] G. Kotliar and A. E. Ruckenstein, Phys. Rev. Lett. **57**, 1362 (1986).
[30] V. Dorin and P. Schlottmann, Phys. Rev. B **46**, 10800 (1992).
[31] T. Terashima, T. Matsumoto, C. Terakura, S. Uji, N. Kimura, M. Endo, T. Komatsubara, and H. Aoki, Phys. Rev. Lett. **87**, 166401 (2001).
[32] R. Settai, M. Nakashima, S. Araki, Y. Haga, T. C. Kobayashi, N. Tateiwa, H. Yamagami, and Y. Onuki, J. Phys: Condens. Matter **14**, L29 (2002).
[33] T. M. Rice and K. Ueda, Phys. Rev. Lett. **55**, 995 (1985).
[34] P. Fazekas and B. H. Brandow, Phys. Scr. **36**, 809 (1987).
[35] W.-S. Wang, X.-M. He, D. Wang, Q.-H. Wang, Z. D. Wang, and F. C. Zhang, Phys. Rev. B **82**, 125105 (2010).
[36] M. Sandri, M. Capone, and M. Fabrizio, Phys. Rev. B **87**, 205108 (2013).
[37] K. Miyake and S. Watanabe, J. Phys. Soc. Jpn. **83**, 061006 (2014).
[38] R. Roussev and A. J. Millis, Phys. Rev. B **63**, 140504 (2001).
[39] D. Fay and J. Appel, Phys. Rev. B **22**, 3173 (1980).
[40] M. Zegrodnik, J. Bünemann, and J. Spałek, New J. Phys. **16**, 033001 (2014); J. Spałek and M. Zegrodnik, J. Phys.: Condens. Matter **25**, 435601 (2013).

3.5 Article A.4, Tricritical wings in UGe_2: A microscopic interpretation

In the work [120] we have studied the shape of the tricritical wings on the basis of the model developed in the previous papers (Articles A.2 [113] and A.3 [114]) with respect to the assumed change of the electron concentration and f-electron Landé factor. We have shown that by changing total filling away from $n = 1.6$ both, mutual relation of the temperatures of CEP and TCP and second order transition line joining TCP with QCEP immediately looses its agreement with the experimental findings, pointing to the sensitivity of obtained results. We argue that it is in fact argument that our excellent fit discussed in Article A.3 is not fortuitous. We have also commented on the theory for the tricriticality from Refs. [146, 147] and compared it with our mechanism.

Inspired by the experimental works on the dual nature of the $5f$ electrons in UGe_2 [148] we have checked whether taking Landé g_f factor for f electrons different from the free electron value can provide a better agreement of the tricritical wings borders, as it would suggest partially localized nature, in variance with the claims of their full itinerancy [20]. We have found that g-factor for f electrons close to the free-electron value, $g_f = 2$, provides the best fit, suggesting that the multiplet structure is washed out be the itineracy of f-electrons.

Journal of Magnetism and Magnetic Materials ∎ (∎∎∎∎) ∎∎∎–∎∎∎

Contents lists available at ScienceDirect

Journal of Magnetism and Magnetic Materials

journal homepage: www.elsevier.com/locate/jmmm

Tricritical wings in UGe_2: A microscopic interpretation

Marcin Abram*, Marcin M. Wysokiński, Józef Spałek

Marian Smoluchowski Institute of Physics, Jagiellonian University, ulica Łojasiewicza 11, PL-30-348 Kraków, Poland

ARTICLE INFO

Article history:
Received 20 June 2015
Received in revised form
3 July 2015
Accepted 10 July 2015

Keywords:
Ferromagnetism
Heavy fermions
Critical points
UGe_2

PACS:
71.27.+a
75.30.kz
71.10.-w

ABSTRACT

In the present work we analyze the second order transition line that connects the tricritical point and the quantum critical ending point on the temperature–magnetic-field plane in UGe_2. For the microscopic modeling we employ the Anderson lattice model recently shown to provide a fairly complete description of the full magnetic phase diagram of UGe_2 including all the criticalities. The shape of the so-called tricritical wings, i.e. surfaces of the first-order transitions, previously reported by us to quantitatively agree with the experimental data, is investigated here with respect to the change of the total filling and the Landé factor for f electrons which can differ from the free electron value. The analysis of the total filling dependence demonstrates sensitivity of our prediction when the respective positions of the critical ending point at the metamagnetic transition and tricritical point are mismatched as compared to the experiment.

1. Motivation and overview

Quantum critical phenomena have captured general attention due to their unique singular properties observed at low temperature ($T \to 0$) and near the quantum critical point (QCP) which is frequently accompanied by the unconventional superconductivity (SC) [1]. From this perspective, f-electron compound UGe_2 is a system with phase diagram comprising coexistence of spin-triplet SC and ferromagnetism (FM) [2–6], as well as an abundance of critical points (CPs), either of quantum and classical nature [7]. Experimental studies among others have revealed existence of the two characteristic classical CPs in the absence of the field (cf. Fig. 1): (i) the critical ending point (CEP) at 7 K at the metamagnetic transition separating strong (FM2) and weak magnetization (FM1) regions [8–10], and (ii) the tricritical point (TCP) at the FM to paramagnetic (PM) phase transition located at $T=24$ K. Additionally, with the applied magnetic field the second order transition line starting from TCP can be followed to $T=0$ where it is expected to terminate in a quantum critical ending point (QCEP) [9,10]. In effect the magnetic phase boundaries in UGe_2 reflect the so-called tricritical wing shape.

Such a complex magnetic phase diagram with all the above criticalities, both classical and quantum, is particularly challenging in terms of theoretical modeling. One of the first approaches, based on the single-band model describing tricritical wings, was the work by Belitz et al. [11]. However, the microscopic description of the magnetic phase diagram with all the CPs including also CEP at the metamagnetic transition, as observed in UGe_2, has been missing until our recent works [13,14].

Our analysis is based on the (two-orbital) Anderson lattice model (ALM) [13,14], often referred to as the periodic Anderson model. Findings for UGe_2, both from first principle calculations and experiments are the following: the quasi-two-dimensional character of the Fermi surface [15], a uniaxial anisotropy for magnetization [16], U–U interatomic distance above the so-called Hill limit [1], and the paramagnetic moment per U atom different from that expected for either f^3 or f^2 atomic configurations [2,17]. We show in the following that all of these findings can be coherently explained within our two-orbital model starting with originally localized f-states and subsequently being strongly hybridized with the conduction (c) band states on a two dimensional lattice and with the applied magnetic field accounted for by the Zeeman term only.

Ferromagnetic order in our model arises from effect of competing hybridization and the f–f interatomic Coulomb repulsion. The emergence of two distinct ferromagnetic phases is in our model driven by the changing topology of the Fermi surface [18–21] which in turn is induced by a relative motion of hybridized and spin split subbands with the increasing f–c hybridization. The results obtained from such picture [13] qualitatively agree with the

* Corresponding author.
E-mail addresses: marcin.abram@uj.edu.pl (M. Abram), marcin.wysokinski@uj.edu.pl (M.M. Wysokiński), ufspalek@if.uj.edu.pl (J. Spałek).

http://dx.doi.org/10.1016/j.jmmm.2015.07.017
0304-8853/

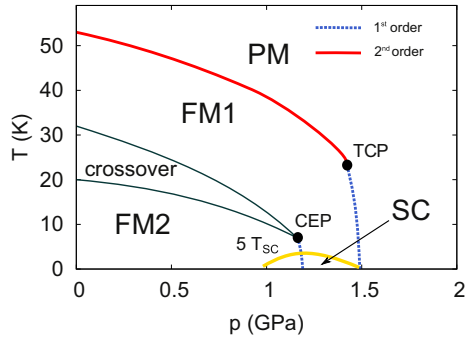

Fig. 1. Schematic magnetic phase diagram of UGe_2 on pressure–temperature plane drawn on the basis of the experimental results [9].

majority of UGe_2 magnetic and electronic properties, as seen in neutron scattering [17], de Haas–van Alphen oscillations [22,23], and magnetization measurements [8]. Also, a semi-metallic character of the weak FM1 phase is supported by the band-structure calculations [24]. A similar idea concerning the emergence of two distinct FM phases in UGe_2 was also obtained earlier within the phenomenological picture based on the Stoner theory incorporating a two-peak structure of the density of states in a single band [25]. In brief, our microscopic model extended to the case of $T > 0$ [14] describes well emergence of all CPs on the magnetic phase diagram of UGe_2 [8–10] in the semiquantitative manner [14]. Here we compare in detail our results with the experimental data, namely predicted second order transition line joining the TCP with the corresponding QCEP. In particular, we determine the influence of the following factors: (i) the total band filling n, and (ii) the value of the Landé factor g_f for f states, on the position of this second-order line. The influence of factor (i) has the following importance. For exemplary filling $n=1.6$ we have shown [14] that the relative position of the TCP and CEP (cf. Fig. 1) is the same as that seen in the experiments [9,10]. The important question is whether such a mutual alignment of those two critical points is necessary to achieve a good fit and to what extent the proper curvature of the line joining TCP and QCEP is robust with respect to the selected band filling. The discussion of the dependence on (ii) has its justification in the not fully resolved nature of magnetism in heavy-fermion systems in general and UGe_2 in particular. Although it is assumed and widely accepted to be fully itinerant [2], there is evidence for a partially localized contribution [24,26]. In such a case, the influence of the orbital effects and their coupling to the spin should have an influence on g_f value.

2. Model and approach

We begin with the orbitally nondegenerate Anderson-lattice model (ALM) on square lattice and with applied magnetic field accounted for via the Zeeman splitting (i.e., with the effective field is $h \equiv \frac{1}{2} g\mu_0\mu_B H$), so that the starting Hamiltonian is

$$\hat{\mathcal{H}}_0 = \sum_{\mathbf{i},\mathbf{j},\sigma}{}' t_{\mathbf{ij}} \hat{c}^{\dagger}_{\mathbf{i}\sigma}\hat{c}_{\mathbf{j}\sigma} - \sum_{\mathbf{i},\sigma} \sigma h \hat{n}^{c}_{\mathbf{i}\sigma} + \sum_{\mathbf{i},\sigma}\left(\epsilon_f - \frac{g_f}{g}\sigma h\right)\hat{n}^{f}_{\mathbf{i}\sigma} + U\sum_{\mathbf{i}} \hat{n}^{f}_{\mathbf{i}\uparrow}\hat{n}^{f}_{\mathbf{i}\downarrow} + V\sum_{\mathbf{i},\sigma}(\hat{f}^{\dagger}_{\mathbf{i}\sigma}\hat{c}_{\mathbf{i}\sigma} + \hat{c}^{\dagger}_{\mathbf{i}\sigma}\hat{f}_{\mathbf{i}\sigma}), \tag{1}$$

where the onsite hybridization is of magnitude $V < 0$ and the Landé factor for f electrons is g_f (the free electron value is $g=2$).

The model describes a two-orbital system with the conduction (c) band arising from the nearest (t) and the second-nearest (t') neighbor hoppings, and the strong f–f Coulomb interaction is of magnitude U. If it is not stated otherwise, we set $t' = 0.25|t|$, $U = 5|t|$, $\epsilon_f = -3|t|$, $g_f = g = 2$, and $n \equiv \sum_\sigma \langle \hat{n}^{c}_{\mathbf{i}\sigma} + \hat{n}^{f}_{\mathbf{i}\sigma}\rangle = 1.6$.

We also add to the Hamiltonian (1) the usual term with the chemical potential μ, i.e.,

$$\hat{\mathcal{H}} \equiv \hat{\mathcal{H}}_0 - \mu \sum_{\mathbf{i},\sigma}(\hat{n}^{c}_{\mathbf{i}\sigma} + \hat{n}^{f}_{\mathbf{i}\sigma}). \tag{2}$$

The model is solved here by means of *statistically consistent Gutzwiller approximation* (SGA) [27–29]. The method was successfully applied to the number of problems [30,31]. It is characterized with the physical transparency and flexibility that it could be also incorporated into other methods such as EDABI [32,33].

We introduce the Gutzwiller projection acting onto uncorrelated wave function $|\psi_0\rangle$ in the following manner:

$$|\psi_G\rangle = \prod_{\mathbf{i}} P_{G;\mathbf{i}}\,|\psi_0\rangle, \tag{3}$$

where $|\psi_G\rangle$ is the wave function of the correlated ground state. In effect, we map many-particle correlated Hamiltonian (1) onto an effective single-particle Hamiltonian $\hat{\mathcal{H}}_{SGA}$ acting on uncorrelated wave function $|\psi_0\rangle$, that, after taking the space Fourier transform, is as follows:

$$\hat{\mathcal{H}}_{SGA} \equiv \hat{\Psi}^{\dagger}_{\mathbf{k}\sigma}\begin{pmatrix} \epsilon^{c}_{\mathbf{k}} - \sigma h - \mu & \sqrt{q_\sigma}V \\ \sqrt{q_\sigma}V & \epsilon_f - \sigma\frac{g_f}{g}h - \mu \end{pmatrix}\hat{\Psi}_{\mathbf{k}\sigma} - \lambda^{f}_{n}\left(\sum_{\mathbf{k},\sigma}\hat{n}^{f}_{\mathbf{k}\sigma} - \Lambda n_f\right) - \lambda^{f}_{m}\left(\sum_{\mathbf{k},\sigma}\sigma\hat{n}^{f}_{\mathbf{k}\sigma} - \Lambda m_f\right) + \Lambda U d^2 \tag{4}$$

where $\hat{\Psi}^{\dagger}_{\mathbf{k}\sigma} \equiv (\hat{c}^{\dagger}_{\mathbf{k},\sigma}, \hat{f}^{\dagger}_{\mathbf{k},\sigma})$, Λ is the number of the system sites, q_σ is the hybridization narrowing factor, and $d^2 \equiv \langle \hat{n}^{f}_{\mathbf{i}\uparrow}\hat{n}^{f}_{\mathbf{i}\downarrow}\rangle_0$ [31]. Necessary constraints for the f electron number and their magnetic moment [29] are incorporated by means of the Lagrange multipliers λ^{f}_{n} and λ^{f}_{m}, respectively. Hamiltonian (4) can be straightforwardly diagonalized with the resulting four eigenvalues $\{E^{b}_{\mathbf{k}\sigma}\}$ labeled with the spin ($\sigma = \pm 1$) and hybridized-band ($b = \pm 1$) indices. For $T > 0$ we construct a generalized Landau grand-potential functional according to

$$\frac{\mathcal{F}}{\Lambda} = -\frac{1}{\Lambda\beta}\sum_{\mathbf{k}\sigma b}\ln[1 + e^{-\beta E^{b}_{\mathbf{k}\sigma}}] + (\lambda^{f}_{n} n_f + \lambda^{f}_{m} m_f + U d^2), \tag{5}$$

which is next minimized with respect to the set of following parameters assembled to a vector, $\vec{\lambda} \equiv \{d, n_f, m_f, \lambda^{f}_{n}, \lambda^{f}_{m}\}$. Additionally, we adjust self-consistently the chemical potential from the condition of fixing the total number of electrons, $n = 1/\Lambda\sum_{\mathbf{k}b\sigma} f(E^{b}_{\mathbf{k}\sigma})$, where $f(E)$ is the Fermi–Dirac function. Finally the ground state energy is defined by

$$E_G = \mathcal{F}|_0 + \mu N, \tag{6}$$

where $\mathcal{F}|_0$ means that the value of $\mathcal{F}$ is taken at minimum for the parameters $\vec{\lambda}$.

Please cite this article as: M. Abram, et al., Journal of Magnetism and Magnetic Materials (2015), http://dx.doi.org/10.1016/j.jmmm.2015.07.017

3. Results and discussion

We start our analysis with the discussion on the proper assignment of the physical units to the microscopic parameters provided so far in dimensionless units (i.e. scaled by $|t|$) to make the quantitative comparison with the observed UGe_2 characteristics. To do so, we have adjusted them [14] by matching the relative positions of the two classical CPs: TCP and CEP at the ferromagnetic transition, as well as attributing the experimentally measured critical temperatures. Matching the results in physical units by fixing the position of two critical points we would call a *strong fitting*, whereas by fixing the position of just a single of them a *weak fitting*.

In our previous works [13,14] we have found that for the total filling $n=1.6$ we could coherently and quantitatively describe the UGe_2 phase diagram. Although, there is no direct experimental evidence in UGe_2 for choosing this particular filling, we have first matched for chosen n TCP and CEP temperatures according to the experiment [14] – strong fitting condition –, and second, we have verified our prediction obtaining agreement of the second-order transition line joining TCP with QCEP [10] with that measured. Additionally, the comparison has provided among others the estimate of the QCEP appearance about 30 T, i.e., higher than that suggested in Ref. [10] which is 18 T.

A natural question arises if this test is sensitive to the choice of n. We show in Fig. 2 that the second-order transition line joining TCP and QCEP determined for a slightly different total filling than $n=1.6$ deviates significantly from the trend of the experimental data [10]. Hence indeed, the comparison is very sensitive to the choice of n. Thus, together with equally sensitive adjustment of T_{TCP} and T_{CEP} with respect to the choice of n [14], it is unlikely that our excellent agreement for the single value of parameter n is fortuitous.

For the sake of completeness and reference to other related works we include in Fig. 2 the (dashed) curve predicted by the one of the most successful approaches describing the general tricritical behavior in itinerant magnetic systems [11,12]. In that procedure, the necessary inputs are the positions of the two CPs, namely TCP and QCEP, leading in fact to the *strong fitting*, but with different pairs of CPs. However, such fitting can be associated with an error as the position of the QCEP, in contrast to TCP and CEP, is not experimentally determined but only extrapolated to 18 T, following Ref. [10]. Note that this condition in our modeling is satisfied for the total filling around $n \simeq 1.55$ (cf. Fig. 2) if we take the extrapolated value of the critical field. In this case, the comparison with results for UGe_2 [10] is worse than e.g. for $n=1.6$ and the temperature of the CEP is much lower than that determined in experiments [8].

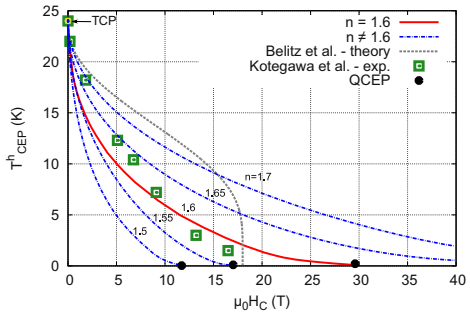

Fig. 2. The second-order transition line joining TCP and QCEP for selected values of total filling, n. Solid curve is replotted from the results reported in Ref. [14]. Experimental points are extracted from pictures in Ref. [10]. Short-dashed curve predicted by the theory formulated by Belitz et al. [11] is shown for comparison (see main text).

It is worth mentioning that the model employed by us belongs to the class discussed earlier by Kirkpatrick and Belitz [12] to reflect the generic tricriticality in the case of metallic magnets. Namely, systems in which the conduction electrons are not a source of the magnetism themselves couple to the magnetically ordered localized electrons in a second band. The origin of the first-order transition at low temperature described within the mean-field theory developed in the Refs. [11,12] is based on the effect of the soft fermionic modes coupled to the magnetization fluctuations, and thus differs from our approach. Here the mechanism for ferromagnetism is due to the coupling of the conduction electrons with localized f states by hybridizing with them and competing with the f–f Coulomb interaction. This competition in the Stoner-like manner induces phase transitions associated with the abrupt changes of the Fermi surface topology.

The simplest verification of our analysis can be carried out by means of chemical alloying, i.e., by changing the electron concentration in the system. However, the lack of known isostructural compounds to UGe_2 may be an apparent obstacle for such test. Though, the determination of the tail of the 2nd order line joining TCP and QCEP for the field larger than 16 T should provide an insight on the issue whether our model correctly predicts the appearance of QCEP around 30 T [14].

If our model is to be used to understand the magnetism of other ferromagnetic superconductors: URhGe [34] and UCoGe [35], it would provide a perfect testing ground of our model as those compounds have been frequently studied by means of the chemical substitution [1,3–6].

Finally, we provide a brief analysis of the impact of the Landé factor value for f electrons, g_f, i.e., in the situation when the z component of the total spin of the system does not commute with Hamiltonian. In Fig. 3 we present the curves for three different values of g_f. The curve for $g_f=2$ is plotted as the reference curve and is based on the results of Ref. [14]. Value of g_f is not known for UGe_2 and generally, for complex compounds has a tensor character which depends on the magnitude of the spin–orbit coupling. For that reason we restrict our discussion to the comparison when g_f is equal to the free electron value $g_f=2$, and subsequently when is lower and higher (cf. Fig. 3) [36]. Specifically, the lower value of Landé factor $g_f = 6/7$ is motivated by that for the Ce-based compounds, where it can be derived for the spin $S = 1/2$ and angular momentum $L=3$, oriented antiparallel and where, strictly speaking, our model is also generally valid, as long as we do not account for the orbital degeneracy of f states of the uranium-based materials. As presented in Fig. 3, it seems that any value of g factor for f states which deviates considerably from the free-electron value provides much worse agreement with experimental data [10]. In conclusion, due to predominantly itinerant nature of f electrons in UGe_2 [26], it is very likely that any crystal-field derived multiplet

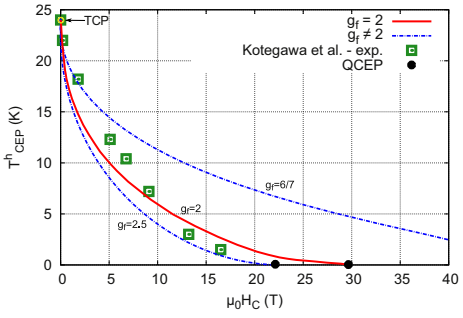

Fig. 3. The second-order transition line joining TCP and QCEP for selected values of Landé factor for f electrons, g_f. Solid curve for $g_f=2$ is replotted from the results reported in Ref. [14]. Experimental points are extracted from Ref. [10].

Please cite this article as: M. Abram, et al., Journal of Magnetism and Magnetic Materials (2015), http://dx.doi.org/10.1016/j.jmmm.2015.07.017

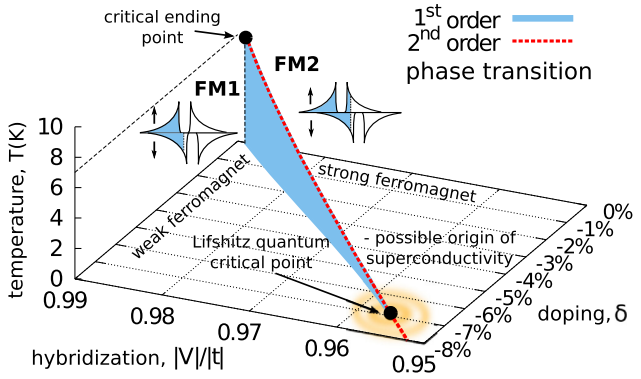

Fig. 4. Evolution of the critical temperature of CEP towards Lifshitz QCP driven by changing total filling, n, and hybridization, V, reproduced after [14].

structure is washed out and hence the value $g_f \simeq 2$ should be regarded as realistic value. Nevertheless, the problem of double localized-itinerant nature of f-electrons [24,26] may arise as the system evolves with the increasing temperature, in comparison to the pressure evolution at low temperature studied in detail here.

4. Outlook

In the present work we have employed the Anderson lattice model [13,14] to provide a fairly complete description of the magnetic phase diagram (p–T–h profiles) of UGe_2 including all the criticalities for this compound. In particular, we study the effect of the choice of the total filling on the quality of the fit, based on our model, to the experimental data [10] concerning the second-order transition line joining the critical points TCP and QCEP. We have found that our prediction is very sensitive to the change of n, which leads also to a mismatch of critical temperatures of TCP and CEP at the metamagnetic transition as compared to the experiment. We infer from this result that our excellent agreement for the single value of n is unlikely fortuitous. We have also analyzed the effect of the Landé factor g_f value for f electrons. In this case, any sizable deviation from the free electron value $g_f=2$ shifts the theoretical curves away from the experimental points. Thus treating f electrons as truly itinerant electrons in UGe_2 seems to be fully justified.

Our final remark addresses the problem of the spin-triplet superconductivity (SC) origin occurring in UGe_2 [1,2]. We have predicted in our previous work [14] the appearance of QCP in the vicinity of the SC dome. It have been proposed that CEP (cf. Fig. 1) at the metamagnetic phase boundary can be followed down to the $T=0$ by changing both the electron concentration and the hybridization magnitude $|V|$ (cf. Fig. 4). The proposed quantum critical point is of Lifshitz type as it separates states with two distinct Fermi-surface topologies. Quantum critical fluctuations or the residual f–f Hund's rule interaction (neglected here) can become the possible source of the spin-triplet superconductivity [37–41]. A detailed and quantitative discussion of the pairing requires a separate analysis.

Acknowledgements

The work was supported by the National Science Centre (NCN) under the Grant MAESTRO, no. DEC-2012/04/A/ST3/00342.

References

[1] C. Pfleiderer, Rev. Mod. Phys. 81 (2009) 1551.
[2] S.S. Saxena, P. Agarwal, K. Ahilan, F.M. Grosche, R.K.W. Haselwimmer, M. J. Steiner, E. Pugh, I.R. Walker, S.R. Julian, P. Monthoux, G.G. Lonzarich, A. Huxley, I. Sheikin, D. Braithwaite, J. Flouquet, Nature 406 (2000) 587.
[3] D. Aoki, J. Flouquet, J. Phys. Soc. Jpn. 81 (2012) 011003.
[4] D. Aoki, A. Gourgout, A. Pourret, G. Bastien, G. Knebel, J. Flouquet, C. R. Phys. 15 (2014) 630.
[5] D. Aoki, J. Flouquet, J. Phys. Soc. Jpn. 83 (2014) 051011.
[6] A.D. Huxley, Physica C 514 (2015) 368.
[7] Coexistence of FM and SC was observed for the first time by A. Kolodziejczyk for the weak itinerant ferromagnets Y_9Co_7 [42–44]. However, SC was found there to be of spin-singlet nature and strongly competing with FM, in contrast to the UGe_2 case, where it is of the spin-triplet character and its coexsitence with FM seems to be strongly cooperative as e.g. both phases disappear at the same pressure.
[8] C. Pfleiderer, A.D. Huxley, Phys. Rev. Lett. 89 (2002) 147005.
[9] V. Taufour, D. Aoki, G. Knebel, J. Flouquet, Phys. Rev. Lett. 105 (2010) 217201.
[10] H. Kotegawa, V. Taufour, D. Aoki, G. Knebel, J. Flouquet, J. Phys. Soc. Jpn. 80 (2011) 083703.
[11] D. Belitz, T.R. Kirkpatrick, J. Rollbühler, Phys. Rev. Lett. 94 (2005) 247205.
[12] T.R. Kirkpatrick, D. Belitz, Phys. Rev. B 85 (2012) 134451.
[13] M.M. Wysokiński, M. Abram, J. Spałek, Phys. Rev. B 90 (2014) 081114(R).
[14] M.M. Wysokiński, M. Abram, J. Spałek, Phys. Rev. B 91 (2015) 081108(R).
[15] A.B. Shick, W.E. Pickett, Phys. Rev. Lett. 86 (2001) 300.
[16] A. Huxley, I. Sheikin, E. Ressouche, N. Kernavanois, D. Braithwaite, R. Calemczuk, J. Flouquet, Phys. Rev. B 63 (2001) 144519.
[17] N. Kernavanois, B. Grenier, A. Huxley, E. Ressouche, J.P. Sanchez, J. Flouquet, Phys. Rev. B 64 (2001) 174509.
[18] R. Doradziński, J. Spałek, Phys. Rev. B 56 (1997) R14239.
[19] R. Doradziński, J. Spałek, Phys. Rev. B 58 (1998) 3293.
[20] O. Howczak, J. Kaczmarczyk, J. Spałek, Phys. Status Solidi B 250 (2013) 609.
[21] K. Kubo, Phys. Rev. B 87 (2013) 195127.
[22] T. Terashima, T. Matsumoto, C. Terakura, S. Uji, N. Kimura, M. Endo, T. Komatsubara, H. Aoki, Phys. Rev. Lett. 87 (2001) 166401.
[23] R. Settai, M. Nakashima, S. Araki, Y. Haga, T.C. Kobayashi, N. Tateiwa, H. Yamagami, Y. Onuki, J. Phys: Condens. Matter 14 (2002) L29.
[24] M. Samsel-Czekała, M. Werwiński, A. Szajek, G. Chełkowska, R. Troć, Intermetallics 19 (2011) 1411.
[25] K.G. Sandeman, G.G. Lonzarich, A.J. Schofield, Phys. Rev. Lett. 90 (2003) 167005.
[26] R. Troć, Z. Gajek, A. Pikul, Phys. Rev. B 86 (2012) 224403.
[27] T.M. Rice, K. Ueda, Phys. Rev. Lett. 55 (1985) 995.
[28] P. Fazekas, B.H. Brandow, Phys. Scr. 36 (1987) 809.
[29] J. Jędrak, J. Kaczmarczyk, J. Spałek, arXiv:1008.0021.
[30] M. Abram, J. Kaczmarczyk, J. Jędrak, J. Spałek, Phys. Rev. B 88 (2013) 094502.
[31] M.M. Wysokiński, J. Spałek, J. Phys.: Condens. Matter 26 (2014) 055601.
[32] A.P. Kądzielawa, J. Spałek, J. Kurzyk, W. Wójcik, Eur. Phys. J. B 86 (2013) 252.
[33] A.P. Kądzielawa, Acta Phys. Pol. A 126 (2014) A58.
[34] D. Aoki, A. Huxley, E. Ressouche, D. Braithwaite, J. Flouquet, J.-P. Brison, E. Lhotel, C. Paulsen, Nature 413 (2001) 613.
[35] N.T. Huy, A. Gasparini, D.E. de Nijs, Y. Huang, J.C.P. Klaasse, T. Gortenmulder, A. de Visser, A. Hamann, T. Görlach, H.v. Löhneysen, Phys. Rev. Lett. 99 (2007) 067006.
[36] P. Quinet, E. Biémont, At. Data Nucl. Data Tables 87 (2004) 207.
[37] M. Zegrodnik, J. Spałek, Phys. Rev. B 86 (2012) 014505.
[38] M. Zegrodnik, J. Spałek, J. Bünemann, New J. Phys. 15 (2013) 073050.
[39] J. Spałek, M. Zegrodnik, J. Phys.: Condens. Matter 25 (2013) 435601.
[40] M. Zegrodnik, J. Bünemann, J. Spałek, New J. Phys. 16 (2014) 033001.
[41] J. Spałek, Phys. Rev. B 63 (2001) 104513.
[42] A. Kołodziejczyk, B.V. Sarkissian, B.R. Coles, J. Phys. F 10 (1980) L333.
[43] A. Kołodziejczyk, Physica B 130 (1985) 189.
[44] K. Rogacki, A. Kołodziejczyk, L. Bochenek, T. Cichorek, Philos. Mag. 95 (2015) 503.

Please cite this article as: M. Abram, et al., Journal of Magnetism and Magnetic Materials (2015), http://dx.doi.org/10.1016/j.jmmm.2015.07.017

3.6 Article A.5, Gutzwiller wave-function solution for Anderson lattice model: Emerging universal regimes of heavy quasiparticle states

In the work[1] [118] we have developed analytic formulation of the variational technique called the *Diagrammatic Expansion for Gutzwiller Wave Function* (DE-GWF) and have applied it to the Anderson lattice model. As already discussed, the method enables for a systematic evaluation of the expectation values with the full Gutzwiller wave function (GWF) (cf. Sec. 2.2). We have shown that for ALM the method converges very fast and for example the density of states converges already in the third order of the expansion.

We have focused on the principal properties of the paramagnetic state, particularly connected with the features of the density of states. First, we have shown that by inclusion of the higher orders of the expansion the hybridization peaks are essentially enhanced. This has direct consequences for the effective mass renormalization which should correspond to the density of states at the Fermi level. The spectacular enhancement of this parameter has been obtained in the close vicinity of the Kondo insulating state and the van Hove singularity, in addition to the strongly correlated regime of the small hybridization and f-electron number close to unity.

Moreover, our method leads to the formation of the effective f band out of initially localized states, as a combined effect of both hybridization and Coulomb interaction. The incorporation of the effect of U in the hopping parameters in the effective Hamiltonian leads to the formation of the f band. Therefore, one could imply that due to the correlations f electrons separately acquire dispersion (k-dependence). We have associated the value of the emerging f-bandwidth with a measure of direct itineracy of f electrons. On the total number of electrons - hybridization plane, we have singled out three distinct regions with significantly widened f band that we have identified as corresponding to the the frequently considered regimes within separate models, namely **(i)** mixed-valence regime, **(ii)** almost-Kondo/Kondo insulator regime, and **(iii)** Kondo-lattice limit when the f-electron occupancy is very close to the f electrons half-filling, $n_f \to 1$. In this manner we can describe all the universal heavy fermion regimes within a single framework.

Additionally, our analysis of the effective Hamiltonian resulting from ALM provides a direct microscopic rationalization of the narrow dispersive f-band, assumed *ad-hoc* in the phenomenological picture in Refs. [149, 101, 102]. In those latter works, when dealing with the description of normal and superconducting states in $CeCoIn_5$, a finite width of the f-band has been assumed. Our theory leads to the formation of this band in a natural manner. Thus the f-electron itineracy may be necessary feature for the unconventional superconductivity to emerge within this model.

[1] preprint as of August 10, 2015

Gutzwiller Wave-Function Solution for Anderson Lattice Model: Emerging Universal Regimes of Heavy Quasiparticle States

Marcin M. Wysokiński,[1,*] Jan Kaczmarczyk,[1,2,†] and Jozef Spałek[1,‡]

[1] *Marian Smoluchowski Institute of Physics, Jagiellonian University, ulica Łojasiewicza 11, PL-30-348 Kraków, Poland*

[2] *Institute of Science and Technology Austria, Am Campus 1, A-3400 Klosterneuburg, Austria*

(Dated: August 11, 2015)

The recently proposed diagrammatic expansion (DE) technique for the full Gutzwiller wave function (GWF) is applied to the Anderson lattice model. This approach allows for a systematic evaluation of the expectation values with full Gutzwiller wave function in the finite dimensional systems. It introduces results extending in an essential manner those obtained by means of standard Gutzwiller approximation (GA) scheme which is variationally exact only in infinite dimensions. Within the DE-GWF approach we discuss principal paramagnetic properties and their relevance to the heavy fermion systems. We demonstrate the formation of an effective, narrow f-band originating from atomic f-electron states and subsequently interpret this behavior as a *direct itineracy* of f-electrons; it represents a combined effect of both the hybridization and the correlations reduced by the Coulomb repulsive interaction. Such feature is absent on the level of GA which is equivalent to the zeroth order of our expansion. Formation of the hybridization- and electron-concentration-dependent narrow f-band rationalizes common assumption of such dispersion of f levels in the phenomenological modeling of the band structure of $CeCoIn_5$. Moreover, it is shown that the emerging f-electron *direct itineracy* leads in a natural manner to three physically distinct regimes within a single model, that are frequently discussed for $4f$- or $5f$- electron compounds as separate model situations. We identify these regimes as: (i) mixed-valence regime, (ii) Kondo-insulator border regime, and (iii) Kondo-lattice limit when the f-electron occupancy is very close to the f-states half-filling, $\langle \hat{n}_f \rangle \to 1$. The nonstandard features of emerging correlated quantum liquid state are stressed.

PACS numbers: 71.27.+a, 71.10.-w, 71.28.+d, 71.10.Fd

I. INTRODUCTION AND MOTIVATION

Heavy fermion systems (HFS) belong to the class of quantum materials with strongly correlated $4f$ or $5f$ electrons. They exhibit unique properties resulting from their universal electronic features (e.g. very high density of states at the Fermi level) almost independent of their crystal structure. Among those unique properties are: (i) enormous effective masses in the Fermi-liquid state, as demonstrated through the linear specific heat coefficient[1–5] and their direct spin-dependence in the de Haas-van Alphen measurements[6–8], (ii) Kondo-type screening of localized or almost localized f-electron magnetic moments by the conduction electrons[9,10], (iii) unconventional superconductivity, appearing frequently at the border or coexisting with magnetism[11], and (iv) abundance of quantum critical points and associated with them non-Fermi (non-Landau) liquid behavior[12–14].

The Anderson lattice model (ALM), also frequently referred to as periodic Anderson model, and its derivatives: the Kondo[15–17] and the Anderson-Kondo[18,19] lattice models, capture the essential physics of HFS. Although, the class of exact solutions is known for this model[20–23], they are restricted in the parameter space. Thus, for thorough investigation of the model properties the approximate methods are needed. One of the earliest theoretical approaches for the models with a strong Coulomb repulsion was the variational Gutzwiller wave function (GWF) method[24–29]. However, despite its simple and physically transparent form, a direct analytic evaluation of the expectation values with full GWF cannot be carried out rigorously for arbitrary dimension and spatially unbound systems.

One of the ways of overcoming this difficulty is the so-called Gutzwiller Approximation (GA), in which only local two-particle correlations are taken into account when evaluating the expectation values. GA provides already a substantial insight into the overall properties of strongly correlated systems[9,10,26,30–35]. Moreover, this approach has been reformulated recently to the so-called *statistically-consistent Gutzwiller approximation* (SGA) scheme and successfully applied to a number of problems involving correlated electron systems[19,36–43]. Among those, a concrete application has been a microscopic description of the fairly complete magnetic phase diagram of UGe_2[42,43] which provided quantitatively correct results, even without taking into account the $5f$-orbital degeneracy due to uranium atoms.

An advanced method of evaluating the expectation values for GWF is the variational Monte Carlo technique (VMC)[44–52]. However, this method is computationally expensive and suffers from the system-size limitations. Though, one must note that the VMC method allows for extension of GWF by including e.g. Jastrow intersite factors[53].

Here we use an alternative method of evaluating the expectation values for GWF, namely a systematic dia-

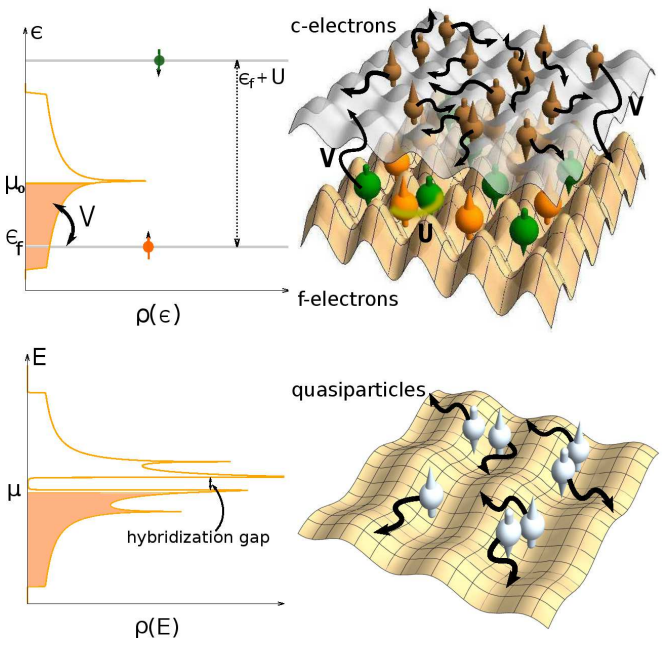

FIG. 1: (Color online) Upper part: Schematic representation of the two-orbital Anderson lattice model with initially localized f- and delocalized c-electrons, and hybridization between them. Bottom part: Emerging quasiparticle states in the hybridized bands of correlated particles. On the left: the shapes of the density of states in the respective situations.

grammatic expansion for the Gutzwiller wave function (DE-GWF)[54–58]. This method was formulated initially for the Hubbard model in two dimensions in the context of Pomeranchuk instability[54], and applied subsequently to the description of high-temperature superconductivity for the Hubbard[55,58] and the t-J[56] models. In the zeroth order of the expansion this approach straightforwardly reduces to the GA[56]. For the one-dimensional Hubbard model it converges[54] to the exact GWF results. Within DE-GWF a larger variational space can be sampled than within the alternative VMC technique because the long-range components of the effective Hamiltonian are accounted for naturally. The DE-GWF method (truncated to match the variational spaces) reproduces the results of VMC with improved accuracy (as shown for the t-J[56] and the Hubbard models[55]). Additionally, the method works also in the thermodynamic limit. In effect, the approach is well suited to capture subtle effects, e.g. those related to the topology of the Fermi surface in the correlated state[54] or the investigated here formation of a narrow f-electron band.

In this study, we extend the DE-GWF approach to discuss principal paramagnetic properties within ALM. The emergence of the quasiparticle picture is schematically illustrated in Fig.1. Explicitly, we investigate the shape of the quasiparticle density of states (DOS, $\rho(E)$), evolving with the increasing order of the expansion, k. For $k > 0$ the hybridization gap widens up with respect to that in GA ($k = 0$ case) and DOS peaks are significantly pronounced. Moreover, we investigate the DOS at the Fermi level ($\rho(E_F)$) evolution with the increasing the hybridization strength $|V|$ – total electron concentration n, plane, as it is a direct measure of the heavy-quasiparticle effective mass. We find that this parameter is significantly enhanced for $k > 0$, mainly in the low hybridization limit and at the border of the Kondo-insulating state. Furthermore, we trace the contribution coming from the originally localized f-electrons (cf. Fig. 1 - upper part) to the quasiparticle spectrum with the increasing order of the expansion. For $k > 0$, f-quasiparticles effectively acquire a nonzero bandwidth (up to 6% of the conduction bandwidth) as a combined effect of both interelectronic correlations and hybridization.

Assumption of a narrow f band existence has recently been made in a phenomenological modeling of the heavy fermion compound $CeCoIn_5$ band structure[59–61]. We show that the emergence of such a band, absent in GA ($k = 0$), is an evidence of the f-electron direct itineracy explained later. To quantify this itineracy we introduce the parameter w_f - the width of the effective, narrow f-band. On the hybridization strength – total electron concentration, $|V|$ – n plane, w_f is significantly enlarged in the three distinct regimes, which we identify respectively as the mixed-valence, Kondo/almost Kondo insulating, and the Kondo-lattice regimes (when f-electron concentration is close to the half-filling, i.e., when $\langle \hat{n}_f \rangle \to 1$). These physically distinct regimes are frequently discussed and identified in various experiments[2,11,62–66] and in theory[19,33,67,68].

The structure of the paper is as follows. In Sec. II we describe the ALM Hamiltonian and define the Gutzwiller variational wave function in a nonstandard manner. In Sec. III we derive the DE-GWF method for ALM and determine the effective single-particle two-band Hamiltonian. In Sec. IV we present results concerning paramagnetic properties: the quasiparticle spectrum, the resultant density of states at the Fermi level, and formation of an effective narrow f-electron band out of initially localized states. In Appendix A we discuss the equivalence of the zeroth-order DE-GWF approach with GA. In Appendix B we present some technical details of DE-GWF technique.

II. MODEL HAMILTONIAN AND GUTZWILLER WAVE FUNCTION

Our starting point is the Anderson lattice model (ALM) with the chemical potential μ and expressed through Hamiltonian

$$\hat{\mathcal{H}} = \sum_{\mathbf{i},\mathbf{j},\sigma} t_{\mathbf{ij}} \hat{c}^{\dagger}_{\mathbf{i}\sigma} \hat{c}_{\mathbf{j}\sigma} - \sum_{\mathbf{i},\sigma} \mu \hat{n}^{c}_{\mathbf{i}\sigma} + \sum_{\mathbf{i},\sigma} (\epsilon_f - \mu) \hat{n}^{f}_{\mathbf{i}\sigma} + U \sum_{\mathbf{i}} \hat{n}^{f}_{\mathbf{i}\uparrow} \hat{n}^{f}_{\mathbf{i}\downarrow} + \sum_{\mathbf{i},\mathbf{j},\sigma} (V_{\mathbf{ij}} \hat{f}^{\dagger}_{\mathbf{i}\sigma} \hat{c}_{\mathbf{j}\sigma} + V^{*}_{\mathbf{ij}} \hat{c}^{\dagger}_{\mathbf{i}\sigma} \hat{f}_{\mathbf{j}\sigma}), \quad (1)$$

where $\mathbf{i} = (i_x, i_y)$ (and similarly $\mathbf{j}$) is the two-dimensional site index, $\hat{f}_{\mathbf{i}\sigma}$ ($\hat{f}^\dagger_{\mathbf{i}\sigma}$) and $\hat{c}_{\mathbf{i}\sigma}$ ($\hat{c}^\dagger_{\mathbf{i}\sigma}$) are the annihilation (creation) operators related to f- and c- orbitals respectively, and $\sigma = \uparrow, \downarrow$ is the z-component direction of the spin. We assume that the hopping in the conduction band takes place only between the nearest neighboring sites, $t_{\mathbf{ij}} \equiv t\delta_{|\mathbf{i}-\mathbf{j}|,1}$, the hybridization has the simplest onsite character[69], $V_{\mathbf{ij}} = V\delta_{\mathbf{i},\mathbf{j}}$, the local Coulomb repulsion on the f orbital has the amplitude U, and the initially atomic f states are located at the energy ϵ_f. In the following $|t|$ is used as the energy unit.

Gutzwiller wave function (GWF) is constructed from the uncorrelated Slater determinant $|\psi_0\rangle$ by projecting out fraction of the local double f-occupancies by means of the Gutzwiller projection operator $\hat{P}_G$,

$$|\psi_G\rangle \equiv \hat{P}_G|\psi_0\rangle \equiv \prod_{\mathbf{i}} \hat{P}_{G;\mathbf{i}}|\psi_0\rangle. \tag{2}$$

In the GA approach when only a single f orbital (in the present case) is correlated the projection operator can be defined by

$$\hat{P}_{G;\mathbf{i}} \equiv 1 - (1-g)\hat{n}^f_{\mathbf{i}\uparrow}\hat{n}^f_{\mathbf{i}\downarrow}, \tag{3}$$

where g is a variational parameter. Such form allows for interpolating between the fully correlated ($g = 0$) and the uncorrelated ($g = 1$) limits. Equivalently one can consider average number of doubly occupied states, $\langle \hat{n}^f_{\mathbf{i}\uparrow}\hat{n}^f_{\mathbf{i}\downarrow}\rangle \equiv d^2$ as a variational parameter.

The Gutzwiller projection operator can be selected differently as proposed in Ref. 70, namely

$$\hat{P}^\dagger_{G;\mathbf{i}}\hat{P}_{G;\mathbf{i}} \equiv \hat{P}^2_{G;\mathbf{i}} = \mathbf{1} + x\hat{d}^{HF}_{\mathbf{i}}. \tag{4}$$

In the above relation x is a variational parameter and for the paramagnetic and translationally invariant system we define Hartree-Fock (HF) operators of the form

$$\hat{d}^{HF}_{\mathbf{i}} \equiv \hat{n}^{HF}_{\mathbf{i}\uparrow}\hat{n}^{HF}_{\mathbf{i}\downarrow} = (\hat{n}^f_{\mathbf{i}\uparrow} - n_{0f})(\hat{n}^f_{\mathbf{i}\downarrow} - n_{0f}), \tag{5}$$

where n_{0f} denotes average occupation of a single f state and spin σ in the uncorrelated state, $|\psi_0\rangle$, i.e., $n_{0f} = \langle \hat{f}^\dagger_{\mathbf{i}\sigma}\hat{f}_{\mathbf{i}\sigma}\rangle_0$. Hereafter the shortened notation for the expectation values is used, i.e., $\langle\psi_0|...|\psi_0\rangle \equiv \langle ...\rangle_0$. Strictly speaking, although, $\hat{d}^{HF}_{\mathbf{i}}$ has not the Hartree-Fock form of the double occupancy operator, the HF superscript has its meaning as the property, $\langle \hat{d}^{HF}_{\mathbf{i}}\rangle_0 \equiv 0$ is preserved.

On the other hand, the Gutzwiller projection operator can be defined in general form as

$$\hat{P}_{G;\mathbf{i}} = \sum_{\Gamma} \lambda_\Gamma \mid \Gamma\rangle_{\mathbf{i}}\langle\Gamma \mid_{\mathbf{i}}, \tag{6}$$

with variational parameters $\lambda_\Gamma \in \{\lambda_0, \lambda_\uparrow, \lambda_\downarrow, \lambda_d\}$ that characterize the possible occupation probabilities for the four possible atomic Fock f-states $\mid \Gamma\rangle_{\mathbf{i}} \in \{\mid 0\rangle_{\mathbf{i}}, |\uparrow\rangle_{\mathbf{i}}, |\downarrow\rangle_{\mathbf{i}}, |\uparrow\downarrow\rangle_{\mathbf{i}}\}$.

Relation (4) couples λ_Γ and x, reducing the number of independent variational parameters to one. Explicitly, we may express the parameters λ_Γ by the coefficient x,

$$\begin{aligned} \lambda_0^2 &= 1 + xn_{0f}^2, \\ \lambda_\sigma^2 = \lambda_{\bar{\sigma}}^2 \equiv \lambda_s^2 &= 1 - xn_{0f}(1-n_{0f}), \\ \lambda_d^2 &= 1 + x(1-n_{0f})^2. \end{aligned} \tag{7}$$

As the parameters λ_Γ and x are coupled by the conditions (7), there is a freedom of choice of the variational parameter; in this work we have selected x. The parameter x covers the same variational space as g in GA. Additionally, the projector (4) leads to much faster convergence than (3) (cf. Ref. 54). From (4) it is clear that $x = 0$ corresponds to the uncorrelated limit. The other extremity, the fully correlated state is reached for $x = \max\{x(\lambda_d = 0), x(\lambda_0 = 0)\}$. This leads to the bounds $\max\{\frac{-1}{(1-n_{0f})^2}, \frac{-1}{(n_{0f})^2}\} \leq x \leq 0$. The minimal value is $x = -4$ for $n_{0f} = 0.5$.

The method is suitable for an arbitrary filling of the f orbital. However, due to the fact that present work is mainly addressed to the description of the Ce-based compounds, we study the regime in which the f-orbital filling either does not exceed unity or is only slightly larger. Precisely, in the all figures presented here the f-orbital filling is never larger than 1.05.

III. DE-GWF METHOD

A. General scheme

In this section we present general implementation of the DE-GWF method. The procedure is composed of the following steps:

1. Choice of initial state $|\psi_0\rangle$.
2. Evaluation of $\langle\hat{\mathcal{H}}\rangle_G \equiv \frac{\langle\psi_G|\hat{\mathcal{H}}|\psi_G\rangle}{\langle\psi_G|\psi_G\rangle}$ for selected $|\psi_0\rangle$ - cf. Sec. III B.
3. Minimization of $\langle\hat{\mathcal{H}}\rangle_G$ with respect to the variational parameter (here x).
4. Construction of the effective single particle Hamiltonian determined by $\delta\hat{\mathcal{H}}^{\text{eff}}(|\psi_0\rangle) = \delta\hat{\mathcal{H}}(|\psi_0\rangle)$ - cf. Sec. III C.
5. Determination of $|\psi_0'\rangle$ as a ground state of the effective Hamiltonian - cf. Sec. III D.
6. Execution of the self-consistent loop: starting again from the step 1 with $|\psi_0'\rangle$ until a satisfactory convergence, i.e., $|\psi_0'\rangle = |\psi_0\rangle$, is reached.

Steps 4 and 5 ensure that the final form of $|\psi_0\rangle$ represents the optimal choice which minimizes the ground state energy $\langle\hat{\mathcal{H}}\rangle_G$. The DE-GWF method with respect to other related methods, GA and VMC, introduces a

new technique for evaluating the expectation value of the correlated Hamiltonian with GWF (step 2 of the above procedure). In particular, it provides an important improvement as, e.g., for GA only single sites in the lattice contain the projection whereas the remaining environment does not. GA leads e.g. to the inability of obtaining the superconducting phase in the Hubbard model[55]. On the other hand, the VMC method tackles that problem properly, but at the price of extremely large computing power needed. This leads to the lattice size limitations (typically up to 20x20 sites) and a limited distance of real space intersite correlations taken into account.

In this respect, DE-GWF introduces, in successive orders of the expansion, correlations to the environment of individual sites (beyond GA), as well as converges in a systematic manner to the full GWF solution. Also, DE-GWF was shown to provide results of better accuracy than VMC[56], and additionally, is free from the finite-size limitations. It also demands definitely less computational power than VMC. Thus in general, this method is capable of treating more complex problems with GWF. On the other hand, DE-GWF is tailored specifically for GWF, while VMC allows for starting from different forms of variational wave function e.g., adding the Jastrow factors[52,53].

B. Diagrammatic expansion

The key point of the variational procedure is the calculation of the expectation value of Hamiltonian (1) with GWF $|\psi_G\rangle$ (point 1 from the scheme in Sec. III A), by starting from the expression

$$\langle\hat{\mathcal{H}}\rangle_G \equiv \frac{\langle\psi_G \mid \hat{\mathcal{H}} \mid \psi_G\rangle}{\langle\psi_G \mid \psi_G\rangle} = \frac{\langle\psi_0 \mid \hat{P}_G\hat{\mathcal{H}}\hat{P}_G \mid \psi_0\rangle}{\langle\psi_0 \mid \hat{P}_G^2 \mid \psi_0\rangle}. \quad (8)$$

We use the DE-GWF technique[54–57], based on the expansion of the expectation values appearing in Eq. (8) in the power series in variational parameter x, with the highest power representing number of correlated vertices assumed to be correlated in the environment - besides local ones. This method is systematic in the sense that the zeroth order corresponds to GA[47], whereas with the increasing order the full GWF solution is approached. Explicitly, we determine expectation values with respect to GWF of any product operator originating from the starting Hamiltonian (1) $\hat{\mathcal{O}}_{\mathbf{i(j)}} = \{\hat{c}^\dagger_{\mathbf{i}\sigma}\hat{c}_{\mathbf{j}\sigma}, \hat{n}^c_{\mathbf{i}\sigma}, \hat{n}^f_{\mathbf{i}\sigma}, \hat{n}^f_{\mathbf{i}\uparrow}\hat{n}^f_{\mathbf{i}\downarrow}, \hat{f}^\dagger_{\mathbf{i}\sigma}\hat{c}_{\mathbf{j}\sigma}, \hat{c}^\dagger_{\mathbf{i}\sigma}\hat{f}_{\mathbf{j}\sigma}\}$. This is executed by first accounting for the projection part on the site $\mathbf{i(j)}$ - *external* vertices (e.g., computing $\hat{\mathcal{O}}^G_{\mathbf{i(j)}} \equiv \hat{P}_{G;\mathbf{i}}(\hat{P}_{G;\mathbf{j}})\hat{\mathcal{O}}_{\mathbf{i(j)}}(\hat{P}_{G;\mathbf{j}})\hat{P}_{G;\mathbf{i}}$, see below) and then, including one-by-one correlations (terms) to the other sites $\mathbf{l} \neq \mathbf{i}, \mathbf{j}$ - *internal* vertices.

Formally, the procedure starts in effective power expansion in x of all relevant expectation values

$$\begin{aligned}\langle\psi_G \mid \hat{\mathcal{O}}_{\mathbf{i(j)}} \mid \psi_G\rangle &= \Big\langle \hat{\mathcal{O}}^G_{\mathbf{i(j)}} \prod_{\mathbf{l}\neq\mathbf{i},\mathbf{j}} \hat{P}^2_{G;l} \Big\rangle_0 \\ &= \sum_{k=0}^{\infty} \frac{x^k}{k!} {\sum_{\mathbf{l}_1,\ldots,\mathbf{l}_k}}' \langle \hat{\mathcal{O}}^G_{\mathbf{i(j)}} \hat{d}^{HF}_{\mathbf{l}_1,\ldots,\mathbf{l}_k}\rangle_0,\end{aligned} \quad (9)$$

where $\hat{d}^{HF}_{\mathbf{l}_1,\ldots,\mathbf{l}_k} \equiv \hat{d}^{HF}_{\mathbf{l}_1}\cdots\hat{d}^{HF}_{\mathbf{l}_k}$. The prime in the multiple summation denotes restrictions: $\mathbf{l}_p \neq \mathbf{l}_{p'}$, and $\mathbf{l}_p \neq \mathbf{i}, \mathbf{j}$ for all p, p'. k is the order of the expansion. Note that for $k = 0$ we obtain $\langle\psi_G|\hat{\mathcal{O}}_{\mathbf{i(j)}}|\psi_G\rangle = \langle\hat{\mathcal{O}}^G_{\mathbf{i(j)}}\rangle_0$. This means that the projection operators act only locally (i.e., only the sites $\mathbf{i}$ and $\mathbf{j}$ are affected) and in this case we recover the GA results (for a details discussion of the equivalence see Appendix A). Expectation values in (9) can now be calculated by means of the Wick's theorem in its real-space version, as they involve only products averaged with $|\psi_0\rangle$. Such power expansion in x allows for taking into account long-range correlations between k *internal* sites $(\mathbf{l}_1, ..., \mathbf{l}_k)$ and the *external* ones $(\mathbf{i}, \mathbf{j})$. It must be noted that it is not a perturbative expansion with respect to the small parameter x. Instead, the expansion should be understood as an analytic series with the order determined by the number of correlated *internal vertices* taken in the nonlocal environment. For $k = \infty$, the full GWF solution would be obtained. However, on the basis of our results, a satisfactory results for the expansion in ALM case are reached already starting from $k = 3$.

As said above, the expectation values $\langle ...\rangle_0$ in Eq. (9) can be evaluated by means of the Wick's theorem. Then, the terms with k *internal* sites can be visualized as diagrams with k internal and 1 (or 2) *external* vertices. The lines connecting those vertices are defined as,

$$\begin{aligned} C_{\mathbf{ij}} &\equiv \langle\hat{c}^\dagger_{\mathbf{i}\sigma}\hat{c}_{\mathbf{j}\sigma}\rangle_0, \\ W_{\mathbf{ij}} &\equiv \langle\hat{f}^\dagger_{\mathbf{i}\sigma}\hat{c}_{\mathbf{j}\sigma}\rangle_0, \\ F_{\mathbf{ij}} &\equiv \langle\hat{f}^\dagger_{\mathbf{i}\sigma}\hat{f}_{\mathbf{j}\sigma}\rangle_0 - \delta_{\mathbf{ij}}n_{0f}. \end{aligned} \quad (10)$$

By constructing the projector operator (4), we have eliminated all the diagrams with the local f-orbital contractions ($\langle\hat{f}^\dagger_{\mathbf{i}\sigma}\hat{f}_{\mathbf{i}\sigma}\rangle_0$), the so-called *Hartree bubbles*. This procedure, as discussed explicitly in Ref. 54, leads to significantly faster convergence than that with the usual Gutzwiller projector, with the variational parameter g[71]. It constitutes the main reason for the efficiency of the DE-GWF method. Finally, all the expectation values with respect to GWF are normalized by $\langle\psi_G|\psi_G\rangle$ (cf. Eq. (8)). However, through the linked-cluster theorem[72], the terms coming from expansion of $\langle\psi_G|\psi_G\rangle \equiv \langle\psi_0|\hat{P}_G^2|\psi_0\rangle$ cancel out with all disconnected diagrams appearing in the numerator of Eq. (8). In effect, the expectation values can be expressed in the closed form by the diagrammatic sums $S \in \{T^{cc(1,1)}_{\mathbf{ij}}, T^{fc(1,1)}, T^{fc(3,1)}, I^{c(2)}, I^{f(2)}, I^{f(4)}\}$, defined in Appendix B, what leads to the following resultant ex-

pression for the ground state energy:

$$\begin{aligned}\frac{\langle\hat{\mathcal{H}}\rangle_G}{L} &= \frac{2}{L}\sum_{\mathbf{i},\mathbf{j}} t_{\mathbf{ij}} T^{cc(1,1)}_{\mathbf{ij}} - 2\mu I^{c(2)} \\ &+2(\epsilon_f-\mu)\left(n_{0f}+(1+xm)I^{f(2)}+\gamma I^{f(4)}\right) \\ &+U\lambda_d^2\left(d_0+2n_{0f}I^{f(2)}+(1-xd_0)I^{f(4)}\right) \\ &+4V\left(\alpha T^{fc(1,1)}+\beta T^{fc(3,1)}\right),\end{aligned} \tag{11}$$

where the trivial sums $\sum_\sigma = 2$ and $\sum_{\mathbf{i}} = L$ have already been included. Parameters $\{\alpha, \beta, \gamma, m, d_0\}$ are all functions of n_{0f} and x (cf. Appendix B, Eq. (B2)). For $k = 0$, only the diagrammatic sums $T^{cc(1,1)}_{\mathbf{ij}}$, $I^{c(2)}$ and $T^{fc(1,1)}$ do not vanish and we reproduce the standard GA result; the Coulomb energy reduces to $U\lambda_d^2 d_0$ and hybridization to $4V\alpha\langle\hat{f}^\dagger_{\mathbf{i}}\hat{c}_{\mathbf{i}}\rangle_0$, whereas the diagrammatic sums for c-band only are trivial (cf. the discussion in Appendix A).

The expectation value $\langle\hat{\mathcal{H}}\rangle_G$ calculated diagrammatically is minimized next with respct to the variational parameter x (step 3 in the scheme in Sec. III A).

C. Effective quasiparticle Hamiltonian

The next step in our procedure (step 4 in the scheme in Sec. III A) is the mapping of the correlations contained in $\langle\psi_G|\hat{\mathcal{H}}|\psi_G\rangle/\langle\psi_G|\psi_G\rangle$ onto the corresponding uncorrelated expectation value $\langle\psi_0|\hat{\mathcal{H}}^{\rm eff}|\psi_0\rangle$. It is realized via the condition that the minima of the expectation values of both Hamiltonians coincide for the same equilibrium values of lines (10) and n_{0f}, which define $|\psi_0\rangle$. Note that the present formulation of this step of our minimization procedure is equivalent to those previously used[54–58]. Explicitly,

$$\begin{aligned}&\delta\langle\hat{\mathcal{H}}^{\rm eff}\rangle_0(C,F,W,n_{0f}) = \delta\langle\hat{\mathcal{H}}\rangle_G(C,F,W,n_{0f}) \\ &= \frac{\partial\langle\hat{\mathcal{H}}\rangle_G}{\partial C}\delta C + \frac{\partial\langle\hat{\mathcal{H}}\rangle_G}{\partial W}\delta W + \frac{\partial\langle\hat{\mathcal{H}}\rangle_G}{\partial F}\delta F + \frac{\partial\langle\hat{\mathcal{H}}\rangle_G}{\partial n_{0f}}\delta n_{0f},\end{aligned} \tag{12}$$

where skipping lattice indices for lines means that we consider each of them separately. It leads directly to the following form of the effective single-particle two-band Hamiltonian with non-local interband hybridization, i.e,

$$\begin{aligned}\hat{\mathcal{H}}^{\rm eff} &= \sum_{\mathbf{i},\mathbf{j},\sigma} t^c_{\mathbf{ij}}\hat{c}^\dagger_{\mathbf{i}\sigma}\hat{c}_{\mathbf{j}\sigma} + \sum_{\mathbf{i},\mathbf{j},\sigma} t^f_{\mathbf{ij}}\hat{f}^\dagger_{\mathbf{i}\sigma}\hat{f}_{\mathbf{j}\sigma} \\ &+\sum_{\mathbf{i},\mathbf{j},\sigma}(V^{fc}_{\mathbf{ij}}\hat{c}^\dagger_{\mathbf{i}\sigma}\hat{f}_{\mathbf{j}\sigma} + \text{H.c.}),\end{aligned} \tag{13}$$

where the effective hopping and hybridization parameters are derivatives with respect to lines,

$$\begin{aligned}t^c_{\mathbf{ij}} &= \frac{\partial\langle\hat{\mathcal{H}}\rangle_G}{\partial C_{\mathbf{ij}}}, \qquad V^{fc}_{\mathbf{ij}} = \frac{\partial\langle\hat{\mathcal{H}}\rangle_G}{\partial W_{\mathbf{ij}}}, \\ t^f_{\mathbf{ij}} &= \frac{\partial\langle\hat{\mathcal{H}}\rangle_G}{\partial F_{\mathbf{ij}}}, \qquad t^f_{\mathbf{ii}} = \frac{\partial\langle\hat{\mathcal{H}}\rangle_G}{\partial n_{0f}}.\end{aligned} \tag{14}$$

D. Determination of $|\psi_0'\rangle$

In this section we determine $|\psi_0'\rangle$ as a ground state of $\hat{\mathcal{H}}^{\rm eff}$ (point 5 from the scheme in Sec. III A).

In order to obtain the effective dispersion relations for c- and f-electrons and the $\mathbf{k}$-dependent hybridization we use the lattice Fourier transform

$$\begin{aligned}\epsilon^{c(f)}_{\mathbf{k}} &= \frac{1}{L}\sum_{\mathbf{i},\mathbf{j}} e^{i(\mathbf{i}-\mathbf{j})\mathbf{k}} t^{c(f)}_{\mathbf{ij}}, \\ V^{cf}_{\mathbf{k}} &= \frac{1}{L}\sum_{\mathbf{i},\mathbf{j}} e^{i(\mathbf{i}-\mathbf{j})\mathbf{k}} V^{fc}_{\mathbf{ij}}.\end{aligned} \tag{15}$$

In this manner, we reduce the many-body problem to the effective single-quasiparticle picture (cf. Fig. 1) described by the effective two-band Hamiltonian. The 2x2 -matrix representation of Eq. (13) resulting from such a transform, has the following form

$$\begin{aligned}\hat{\mathcal{H}}^{\rm eff} &= \sum_{\mathbf{k},\sigma}(\hat{c}^\dagger_{\mathbf{k}\sigma}\ \hat{f}^\dagger_{\mathbf{k}\sigma})\begin{pmatrix}\epsilon^c_{\mathbf{k}} & V^{cf}_{\mathbf{k}} \\ V^{cf}_{\mathbf{k}} & \epsilon^f_{\mathbf{k}}\end{pmatrix}\begin{pmatrix}\hat{c}_{\mathbf{k}\sigma} \\ \hat{f}_{\mathbf{k}\sigma}\end{pmatrix} \\ &= \sum_{\mathbf{k},\sigma}(\hat{c}^\dagger_{\mathbf{k}\sigma}\ \hat{f}^\dagger_{\mathbf{k}\sigma})\mathcal{T}^\dagger\begin{pmatrix}E_{\mathbf{k}+} & 0 \\ 0 & E_{\mathbf{k}-}\end{pmatrix}\mathcal{T}\begin{pmatrix}\hat{c}_{\mathbf{k}\sigma} \\ \hat{f}_{\mathbf{k}\sigma}\end{pmatrix},\end{aligned} \tag{16}$$

where the eigenvalues, $E_{\mathbf{k}\pm}$ of the above Hamiltonian are

$$E_{\mathbf{k}a} = \xi^+_{\mathbf{k}} + a\sqrt{(\xi^-_{\mathbf{k}})^2 + (V^{cf}_{\mathbf{k}})^2}, \tag{17}$$

where $a \equiv \pm 1$ differentiates between the two hybridized bands. For convenience, we have defined

$$\xi^+_{\mathbf{k}} \equiv \frac{\epsilon^c_{\mathbf{k}} + \epsilon^f_{\mathbf{k}}}{2} \quad \text{and} \quad \xi^-_{\mathbf{k}} \equiv \frac{\epsilon^c_{\mathbf{k}} - \epsilon^f_{\mathbf{k}}}{2}. \tag{18}$$

$\mathcal{T}$ in Eq. (16) is the unitary transformation matrix to the basis in which $\hat{\mathcal{H}}^{\rm eff}$ is diagonal, defined as

$$\mathcal{T} = \begin{pmatrix}u_+ & u_- \\ u_- & -u_+\end{pmatrix}, \tag{19}$$

where

$$u_\pm = \sqrt{\frac{1}{2}\left(1 \pm \frac{\xi^-_{\mathbf{k}}}{\sqrt{(\xi^-_{\mathbf{k}})^2 + (V^{cf}_{\mathbf{k}})^2}}\right)}. \tag{20}$$

It is now straightforward to obtain the principal correlation functions (lines), i.e.

$$\begin{aligned}\langle\hat{c}^\dagger_{\mathbf{k}\sigma}\hat{c}_{\mathbf{k}\sigma}\rangle_0 &= u_+^2\Theta(E_{\mathbf{k}+}) + u_-^2\Theta(E_{\mathbf{k}-}), \\ \langle\hat{f}^\dagger_{\mathbf{k}\sigma}\hat{c}_{\mathbf{k}\sigma}\rangle_0 &= u_+u_-\big(\Theta(E_{\mathbf{k}+}) - \Theta(E_{\mathbf{k}-})\big), \\ \langle\hat{f}^\dagger_{\mathbf{k}\sigma}\hat{f}_{\mathbf{k}\sigma}\rangle_0 &= u_-^2\Theta(E_{\mathbf{k}+}) + u_+^2\Theta(E_{\mathbf{k}-}),\end{aligned} \tag{21}$$

where $\Theta(E)$ denotes the Heaviside step function and plays the role of an energy cutoff for respective quasiparticle bands energies (17). Using the reverse Fourier transformation we obtain self-consistent equations for lines

and n_{0f},

$$
\begin{aligned}
C_{\mathbf{ij}} &= \frac{1}{L}\sum_{\mathbf{k}a}\langle \hat{c}^{\dagger}_{\mathbf{k}\sigma}\hat{c}_{\mathbf{k}\sigma}\rangle_0 \; e^{i(\mathbf{i}-\mathbf{j})\mathbf{k}}, \\
W_{\mathbf{ij}} &= \frac{1}{L}\sum_{\mathbf{k}a}\langle \hat{f}^{\dagger}_{\mathbf{k}\sigma}\hat{c}_{\mathbf{k}\sigma}\rangle_0 \; e^{i(\mathbf{i}-\mathbf{j})\mathbf{k}}, \\
F_{\mathbf{ij}} &= \frac{1}{L}\sum_{\mathbf{k}a}\langle \hat{f}^{\dagger}_{\mathbf{k}\sigma}\hat{f}_{\mathbf{k}\sigma}\rangle_0 \; e^{i(\mathbf{i}-\mathbf{j})\mathbf{k}}, \\
n_{0f} &= \frac{1}{L}\sum_{\mathbf{k}a}\langle \hat{f}^{\dagger}_{\mathbf{k}\sigma}\hat{f}_{\mathbf{k}\sigma}\rangle_0 .
\end{aligned}
\tag{22}
$$

To determine the properties of the model, we solve in the self-consistent loop the system of Eqs. (14) and (22)[54–58] (point 6 from the scheme in Sec. III A)

Finally, the ground state energy E_G is defined by

$$
E_G = \langle \hat{\mathcal{H}}\rangle_G|_0 + n\mu, \tag{23}
$$

where $\langle \hat{\mathcal{H}}\rangle_G|_0$ denotes the expectation value (11) of the starting Hamiltonian for the equilibrium values of the lines and the total number of particles is defined by $n \equiv 2\langle \hat{n}^f_{\mathbf{i}\sigma} + \hat{n}^c_{\mathbf{i}\sigma}\rangle_G$. The f-orbital filling separately is defined by $n_f \equiv 2\langle \hat{n}^f_{\mathbf{i}\sigma}\rangle_G$.

IV. RESULTS AND DISCUSSION

A. System description and technical remarks

In our analysis we consider a square, translationally invariant, and infinite ($L \to \infty$) lattice, with two orbitals (f and c) per site. The square lattice consideration is justified by the common quasi-two-dimensional layered structure of f atoms in the elementary cell of many Ce-based heavy fermion systems[2,11] that our studies are relevant to.

While proceeding with the diagrammatic expansion (DE), in principle two approximations need to be made.

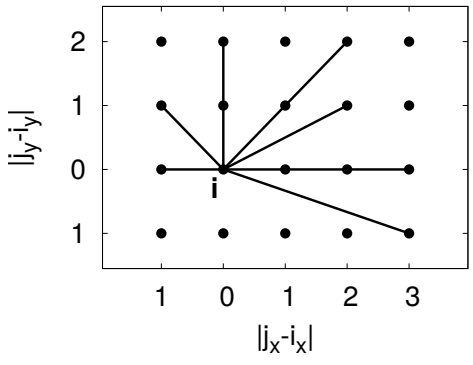

FIG. 2: Schematic illustration of the real-space cutoff on the lattice. The solid lines denote exemplary, in terms of distance, correlation functions (referred to as *lines*) taken into account between **i**-site (in the center) and the **j**-sites (on the periphery). Farther connections are not considered.

First, only the lines (10) satisfying the relation $|\mathbf{i}-\mathbf{j}|^2 = (i_x-j_x)^2+(i_y-j_y)^2 \leq 10$ are taken into account (i.e., we make a real-space cutoff - cf. Fig. 2). For comparison, in VMC only rarely lines farther than these connecting nearest neighboring sites (more precisely, only the lines corresponding to the hopping term range of the starting Hamiltonian) are taken into account[49,50]. From our numerical calculations it follows that the nearest- and the second-nearest neighbor contractions compose the dominant contributions (cf. Fig. 7b).

The second limitation in DE is the highest order of the expansion, k, taken into account. Asymptotic behavior starting from $k = 3$, of some properties such as the density of states (DOS) at the Fermi level (FL), $\rho(E_f)$, and the width of the effective f band, w_f (cf. Figs.4, 5c and 6), speak in favor of the calculation reliability, achieved already in that order. Therefore, if not specified otherwise, the expansion is carried out up to the third order ($k = 3$), i.e., with the three internal vertices taken into account. We stress again that the zeroth-order approximation ($k = 0$) is equivalent to the GA approach (cf. Appendix A for details). The results of GA are regarded here as a reference point for determining a systematic evolution, including both qualitative and quantitative changes, when the higher-order contributions are implemented.

The parameters of the ALM Hamiltonian (1) are taken in units of $|t|$: a strong Coulomb repulsion is taken as $U = 10$, the reference energy for f-electrons, $\epsilon_f = -3$, the onsite hybridization is assumed negative and varies in the range $|V| \in (0.8, 2.5)$, and the total band filling ($n \equiv 2\langle \hat{n}^f_{\mathbf{i}\sigma} + \hat{n}^c_{\mathbf{i}\sigma}\rangle_G$) is in the range allowed by the condition that the f level occupancy per site ($n_f \equiv 2\langle \hat{n}^f_{\mathbf{i}\sigma}\rangle_G$) roughly does not exceed unity. The reason for consideration of this regime is the circumstance that for interesting us Ce-based compounds the concentration of f electrons per cerium should not exceed 1 (i.e., with the Ce^{3+} and Ce^{4+} configurations only). However, from the construction of the method the regime for $n_f > 1$ is fully accessible and physically correct. In carrying out the DE-GWF procedure we adjust the chemical potential $\mu \equiv E_F$ for the fixed total filling n. Numerical integration of Eq. (22) and the self-consistent loop were both performed with precision of the order of 10^{-6} or better with the help of Gnu Scientific Library (GSL) procedures[73].

B. Correlated Fermi liquid

Before the detailed analysis is carried out, a methodological remark is in place. The effective Hamiltonian (13) is of single-particle form, but coupled to the self-consistent procedure of evaluating the relevant averages (22). However, this does not compose the full picture. The physical quantities are those obtained with a projected wave function. For example, $n_f \equiv \sum_\sigma \langle \psi_G|\hat{f}^{\dagger}_{\mathbf{i}\sigma}\hat{f}_{\mathbf{i}\sigma}|\psi_G\rangle = \sum_\sigma \langle \mathcal{P}_G\hat{n}^f_{\mathbf{i}\sigma}\mathcal{P}_G\rangle_0$, which in general

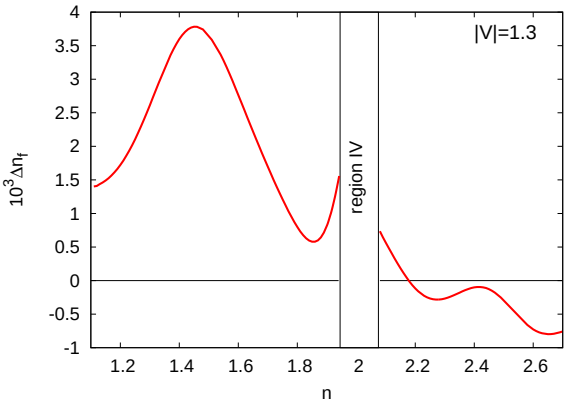

FIG. 3: Difference between uncorrelated and correlated f-electron number, $\Delta n_f \equiv \sum_\sigma \langle \hat{n}^f_{\mathbf{i}\sigma}\rangle_G - \sum_\sigma \langle \hat{n}^f_{\mathbf{i}\sigma}\rangle_0$ along the line of constant hybridization, $|V| = 1.3$, with respect to changing total filling. The specific character of the region IV is explained in Sec. IV.

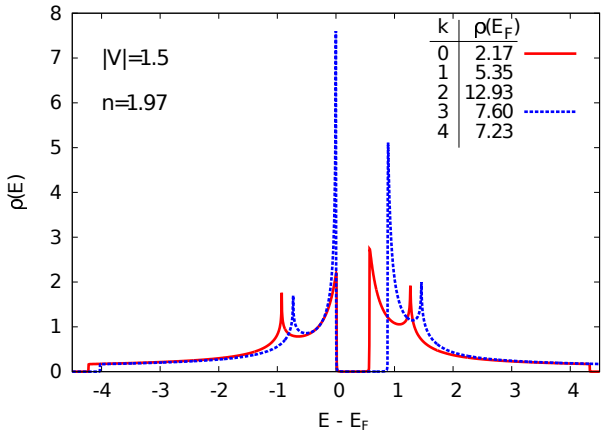

FIG. 4: (Color online) Density of states (DOS) near the half-filling ($n = 1.97$) at $|V| = 1.5$ for selected orders of the diagrammatic expansion ($k = 0, 3$). Explicit values of $\rho(E_F)$ are also listed in the inset Table (for $0 \le k \le 4$). For $k = 3$ a satisfactory convergence of the expansion is reached. The $k = 1, 2, 4$ plots are not included for clarity as, apart from peak heights, they are practically the same as the plot for $k = 3$. For $k > 0$ (beyond GA) the hybridization peaks are more pronounced (large DOS at the Fermi level $\rho(E_F)$), which is related directly to the increased by correlation effective-mass enhancement for quasiparticles.

is slightly different from $\sum_\sigma \langle \hat{n}^f_{\mathbf{i}\sigma}\rangle_0$. The situation is illustrated explicitly in Fig. 3. In effect, the quasiparticle picture is amended with the nonstandard features of this *correlated* (*quantum*) *liquid* (CL). Parenthetically, the same difference will appear when considering magnetic and superconducting states, where the magnetic moments, $\langle \hat{S}^z_{\mathbf{i}}\rangle_G$ vs. $\langle \hat{S}^z_{\mathbf{i}}\rangle_0$, and the superconducting gaps, $\langle \hat{\Delta}_{\mathbf{ij}}\rangle_G$ and $\langle \hat{\Delta}_{\mathbf{ij}}\rangle_0$ will be different. So, we have a mapping of the correlated onto quasiparticle states, but not of the physical properties. In brief, we have to distinguish between the correlated and the uncorrelated f-electron occupancy or other property even though, from the way of constructing (13), the density of quasiparticle states (coming from (13)), represents that in the correlated state.

C. Quasiparticle Density of States

We start with analysis of the quasiparticle DOS emerging from the DE-GWF method in successive orders of the expansion (cf. Fig. 4). For $k > 0$ and the total filling $n = 1.97$ (i.e., near the half filling), the hybridization peaks become more pronounced (cf. Fig.4-the inset Table) and the hybridization gap increases.

For $k > 0$ the overall shape of DOS changes only quantitatively (cf. Fig. 4). However, the value of the DOS at the Fermi level, $\rho(E_F)$, changes remarkably (cf. the inset to Fig. 4). Although for $k = 1$ it is underestimated and for $k = 2$ overestimated, for $k = 4$ we see no significant difference with respect to the $k = 3$ case. For this reason, if not specified explicitly, the subsequent analysis is proceeded in the third order, $k = 3$.

The value of $\rho(E_F)$ is of crucial importance. This parameter is a measure of the quasiparticle effective mass, as the latter is inversely proportional to the second derivative of the energy, $\nabla^2_{\mathbf{k}} E_{\mathbf{k}}$, at the Fermi surface, and thus is determined by $\rho(E_F)$.

In Fig. 5a we draw the value of $\rho(E_F)$ on the plane hybridization – total electron number (per site), $V - n$. This quantity is particularly strongly enhanced near the half filling ($n \simeq 2$). In comparison to the lowest value $\rho(E_F) \approx 0.75$, the maximal enhancement is of the order of 40. In Fig. 5b we present evolution of $\rho(E_F)$ on the logarithmic scale with the decreasing total filling and approaching $n = 2$ (vertical arrow in Fig. 5a marked by the encircled letter b). The extrapolated value of $\rho(E_F)$ may reach extremely high values of 1000 and even more (dashed line in Fig. 5b) in the region IV. Such feature could explain extremely high mass renormalization in some of HFS for large but finite value of the Coulomb interaction U.

The region where $\rho(E_F)$ is enhanced strongly, is that with low hybridization $|V|$ values and for the total filling $n \simeq 1$. This region is strictly correlated with the position of the second pronounced peak in DOS (cf. Fig. 4) which therefore has its meaning as the Van Hove singularity. Additionally, for $n_f \simeq 1$, where the effects of correlations are the strongest, we observe also a large value of $\rho(E_F)$. In that limit the stability of magnetic phases should be studied separately[18,19].

As marked in Fig. 5a, near the total half-filling, $n \simeq 2$, we could not obtain a satisfactory convergence of our self-consistent procedure. This is attributed to the position of the chemical potential extremely close to the hybridization-induced peaks (significant when $n_f \gtrsim 0.9$). Technically, this leads to extreme fluctuations (out of our

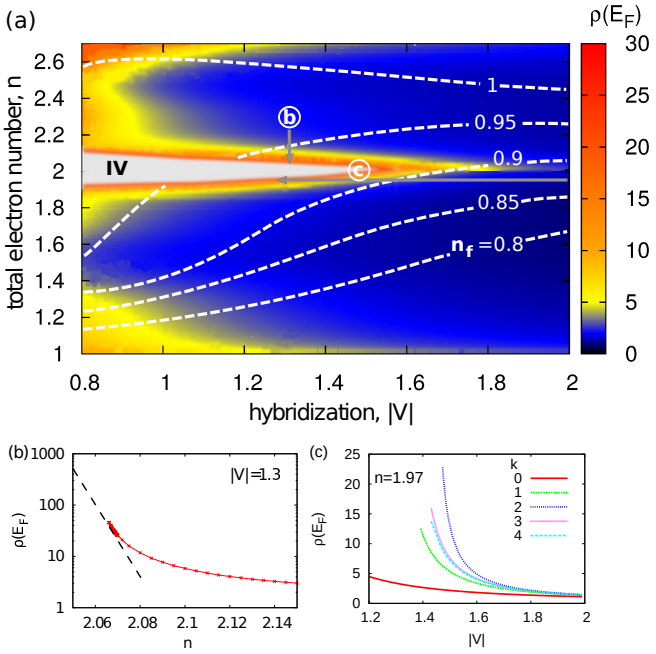

FIG. 5: (Color online) (a) Density of states at the Fermi level $\rho(E_F)$ on the hybridization strength – total electron concentration plane, $|V|$ – n. Additionally (not marked), for $n = 2$ we obtain always the Kondo insulating state. By IV (for consistency with Fig.7) we have marked a V-shaped region where we have no numerical convergence due to the presence of singular hybridization peaks for low $|V|$ and with n near the half filling (see main text). (b) Evolution of $\rho(E_F)$ in the half-logarithmic scale near the region IV (along the vertical arrow with the letter b). By extrapolation (dashed line in (b)), for the almost half-filled situation, $\rho(E_F)$ can be enhanced even by factor of 1000 relative to its lowest values on the $|V|$ – n plane. (c) Evolution of $\rho(E_F)$ with the decreasing $|V|$ (along the horizontal arrow with letter c), within successive orders of the expansion ($k \leq 4$). For large $|V| \gtrsim 1.8$, GA ($k = 0$ order) provides already realistic values of $\rho(E_F)$.

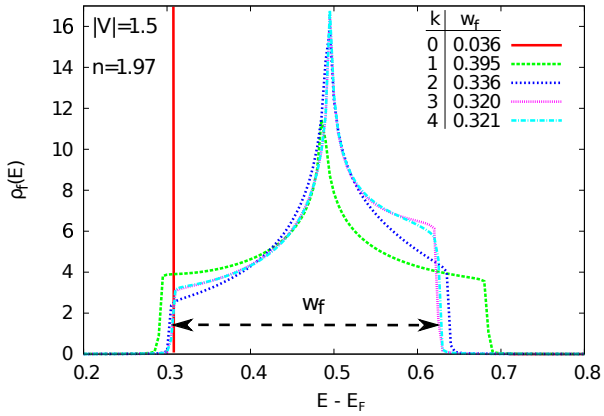

FIG. 6: (Color online) f-electron density of states $\rho_f(E)$ within successive orders of expansion ($k \leq 4$). For $k = 1$ and higher, formation of the effective f-band can be clearly observed. For $k = 3$ the final shape of $\rho_f(E)$ and the value of f-band width w_f stabilize.

numerical precision) of the filling, effective hopping parameters, and the lines coming from the effective Hamiltonian (13), as they are sensitive to a slight change of the chemical potential position. For $n = 2$ and nonzero hybridization, we obtain always the Kondo insulating state. However, strictly speaking, the true Kondo-type compensated state is demonstrated explicitly only if magnetic structure is taken into account explicitly[9,10,18].

In Fig. 5c we depict the $\rho(E_F)$ evolution with the decreasing hybridization amplitude $|V|$ for $k \leq 4$. Our results show that for large $|V|$, GA ($k = 0$) already is reasonable approximation. The situation changes as we approach the low-$|V|$ regime near the half-filling, where inclusion of higher-order contributions leads to a strong enhancement of $\rho(E_F)$, as discussed above.

In summary, the quasiparticle mass is enhanced spectacularly near $n = 2$ and in the regime of small hybridization $|V|$. The f-state occupancy is then $n_f \gtrsim 0.9$. This is the regime associated with the heavy-fermion and the Kondo-insulating states. We discuss those states in detail in what follows.

D. f-electron direct itineracy

As stated already, the DE-GWF method is used here to map the correlated (many-body) system, described by the original Hamiltonian (1) with the help of the Gutzwiller wave function $|\psi_G\rangle$, onto that described by the effective quasiparticle Hamiltonian (13) with an uncorrelated wave function $|\psi_0\rangle$. By constructing the effective Hamiltonian it is possible to extract the explicit contribution to the quasiparticle picture as coming from a direct hopping between the neighboring f sites. By contrast, in GA ($k = 0$) case, the f electrons itineracy is only due to the admixture of c-states when the quasiparticle states are formed. Once we proceed with the diagrammatic expansion to higher order ($k > 0$), they start contributing to the quasiparticle spectrum in the form of a dispersive f-band (cf. Fig. 6). The resulting band is narrow, $w_f \leq 0.5$, whereas the starting conduction (c) band has the width of $w_c = 8$. As was mentioned in the Sec. I, we interpret the parameter w_f as a measure of emerging degree of *direct itineracy*, i.e., presence of a direct hoppings between the neighboring f states in the effective Hamiltonian.

Again, a methodological remark is in place here on the numerical convergence of the results with respect to k. Namely, the f-bandwidth appears already for $k = 1$, but both its width and the curvature stabilizes only starting from $k = 3$.

In the recent phenomenological modeling of $CeCoIn_5$[59–61] the band structure used is the hybridized-two-band independent-particle model with dispersive f-band, even though the Ce $4f$ states can be placed well above the so-called Hill limit, where there should not be any direct hopping between the original neighboring f

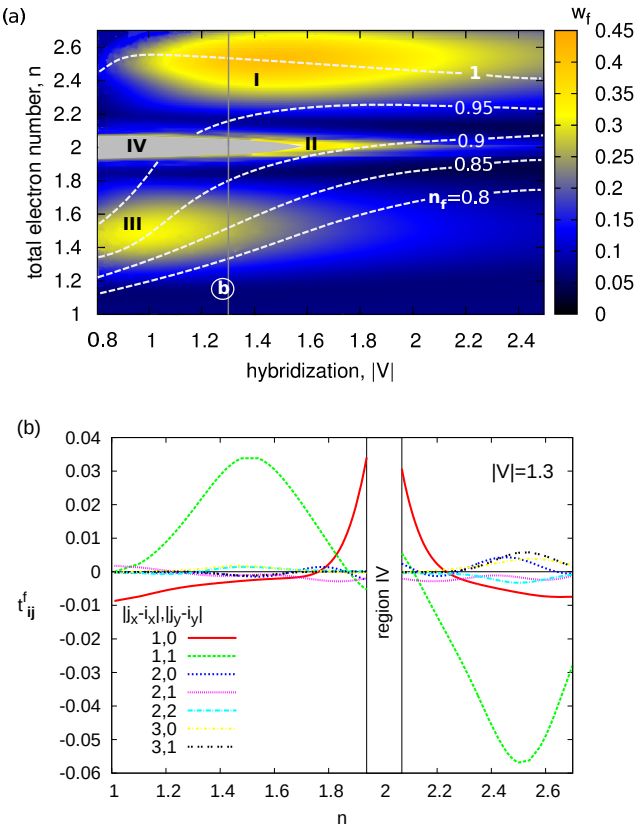

FIG. 7: (Color online) (a) Effective bandwidth of f-states, w_f, on the hybridization strength $|V|$ – electron concentration n plane. w_f is regarded as a measure of direct itineracy of f-electron states. Three separate disjoint regions (light color) are regarded as universal and frequently discussed as separate limits, both in theory and experiment. Namely, the mixed valence regime (III), the Kondo/almost Kondo-insulating regime (II), and the Kondo-lattice regime (I) with $n_f \to 1-\delta$, $\delta \ll 1$. (b) Effective f-electron intersite hoppings $t^f_{\mathbf{ij}}$ along the marked vertical line of the diagram for $|V| = 1.3$. The energy dispersion for f quasiparticles is determined mainly by the nearest and the second nearest hoppings $t^f_{\mathbf{ij}}$. Region IV, near $n = 2$ is marked separately due to the lack of convergence of the numerical results (see main text).

states. The fit presented there provides w_f of the same order of magnitude as that obtained here. As those phenomenological models do not include the Coloumb interaction, the ground state is determined by the uncorrelated wave function. Hence, our analysis of the effective Hamiltonian resulting from ALM provides a direct microscopic rationalization of the narrow dispersive f-band presence assumed *ad-hoc* in the fitting procedure in Ref. 59–61.

In Fig. 7a we display diagram comprising the width of f-band w_f on $|V|$ – n plane, with contours of constant values of n_f. We observe the appearance of regions, where the f quasiparticles have a sizable bandwidth (bright color) and other, where they remain localized (dark regimes). We expect that in the regions, where f electrons are forming a band, a nontrivial unconventional superconductivity and/or magnetism may appear. These topics should be treated separately as they require a substantial extension of the present approach (incorporating new type of lines)[55–58].

With the help of the width w_f we may single out three physically distinct regimes (cf. Fig. 7a). We identify those regions as the mixed-valence regime (III), the Kondo/almost Kondo insulating regime (II), and the Kondo-lattice regime (I) with $n_f \to 1-\delta$, with $\delta \ll 1$ (cf. Fig. 7a). These universal regions are usually discussed independently within different specific models and methods. In regime I the role of f-c Coulomb interactions (the Falicov-Kimball term) may be needed for completeness (cf. Ref. 74), whereas in the Kondo-lattice regime the transformation to the Anderson-Kondo model is appropriate (cf. Refs. 18,19). In the extreme situation, the heavy-fermion states are modeled by pure Kondo-lattice model[75–77]. However, strictly speaking, the last model applies only in the limit of localized f electrons ($n_f = 1$), since then the total numbers of f and c electrons are conserved separately.

In Fig. 7b we present the effective hopping parameters for f states for $|V| = 1.3$, i.e., along the marked vertical line in Fig. 7a. This line crosses three singled out regions of the itineracy. The leading contribution to the f-electron band energy arises from the nearest- and the second nearest-neighbor hoppings. Such circumstance confirms that our earlier assumption about the real-space cutoff shown in Fig. 2 has been selected properly. Moreover, it points to the importance of including also the components beyond those of the starting Hamiltonian, only rarely taken into account within the VMC method[49,50].

In Fig. 8 we show the contributions to the effective hybridization. The initial (bare) local hybridization acquires momentum dependence. Nevertheless, the local part is still dominant since the nonlocal terms are at least two orders of magnitude smaller.

The emerging in our model f-band introduces a new definition of the f-electron itineracy as it is not so much connected to the Fermi-surface size[78], but with the appearance of a direct hoppings between f sites. This difference is highly nontrivial, especially in the limit $n_f = 1$, where we obtain the largest bandwidth w_f. Such behavior is attributed to the specific character of our approach. Namely, we consider here the processes within our initial Hamiltonian (1), but under the assumption that the neighboring sites are also correlated. This, as we have shown directly, leads also to the finite f-band in the effective single particle Hamiltonian (13). The results thus throw a new light on the longstanding issue of the dual localized-itinerant nature of f electrons in HFS[79,80]. While the magnetism can be attributed to the almost localized nature of f electrons, an unconventional superconductivity requires their itineracy in an explicit manner, as will be discussed elsewhere[81]

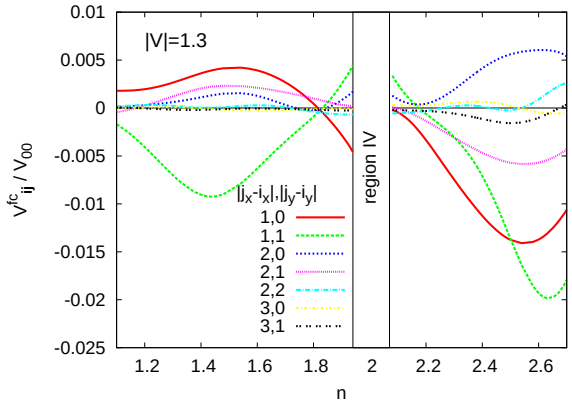

FIG. 8: (Color online) Spatial contributions $V^{cf}_{\mathbf{ij}}$ to the effective hybridization normalized by the first onsite ($\mathbf{i} = \mathbf{j}$) V_{00} term along the marked vertical line of the diagram in Fig.7a for $|V| = 1.3$. Note that due to correlation initially local, onsite hybridization acquires effectively momentum dependence. However, the nonlocal contributions constitute only up to 2% of the local one.

V. SUMMARY

We have applied a recently developed diagrammatic technique (DE-GWF) of evaluating the expectation values with the full Gutzwiller wave function for the case of two-dimensional Anderson lattice. We have analyzed properties of the model by discussing the most important features of the heavy fermion systems in the paramagnetic state. We have also shown that by approaching in successive orders of the expansion the full Gutzwiller-wavefunction solution, we obtain a systematic convergence. In the zeroth order of expansion our method reduces to the standard Gutzwiller Approximation (GA).

In difference with GA, DE-GWF does not overestimate the hybridization narrowing factor. Furthermore, our method produces unusually enhanced peaks at the Fermi level in the density of states, particularly near the half-filling, $n \to 2$. This in turn, is connected to the value of effective mass and by analyzing in detail this region we can explain a very large mass enhancement observed in heavy fermion systems as described by ALM with large, but finite Coulomb-interaction value, here $U = 10|t|$. The regions of sizable $\rho(E_F)$ enhancement are also found in the small-hybridization limit and are connected to the presence of both the Van Hove singularity and the strong correlations in the limit of $n_f \to 1$.

The f-electron contribution to the full quasiparticle spectrum is analyzed in detail. For nonzero order of the expansion ($k > 0$) we observe a systematic formation of the effective f-band with the increasing k. In spite of the fact that the bare electrons are initially localized, f quasiparticles contribute to the total density of states as they become itinerant. We interpret this property as the emerging *direct* f-electron *itineracy*. As a measure of this behavior, we introduce the the width w_f of effective f-band. Formation of such narrow f-band rationalizes e.g. the recent phenomenological modeling of the $CeCoIn_5$ band structure[59–61].

The nonstandard character of the resultant *correlated* Fermi *liquid* (CL) which differs from either the Landau *Fermi liquid* (FL) and the *spin liquid* (SL), should be stressed. FL represents a weakly correlated state (no localization) and SL represents a fully correlated state. Our CL state in this respect has an intermediate character. Namely, the quasiparticle states are formed (as exemplified by e.g. density of states), but the physical properties such as the occupancy n_f, the magnetic moment $\langle \hat{S}^z_{\mathbf{i}} \rangle$ or the pairing gap in real space $\langle \hat{\Delta}_{\mathbf{ij}} \rangle$ are strongly renormalized by the correlations. Such situation is often termed as that of an almost localized Fermi-liquid state[4,9,10,16,17].

By analyzing the results on the hybridization strength $|V|$ – total band filling n plane, we single out explicitly three physically distinct regions, which we regard as three separate universality limits. Namely, we have linked those disjoint regions with the regimes frequently discussed as separate classes in the heavy fermion systems: the mixed-valence regime, the Kondo/almost Kondo insulating regime, and the Kondo-lattice regime for $n_f \to 1$. We suggest, that the regions of significant f-electron itineracy can be connected to the unconventional heavy fermion superconductivity which would require separate studies.

We have also commented on the longstanding issue of a dual localized-itinerant nature of f electrons in the heavy fermion systems. The new definition of itineracy is in accord with their (almost) localized nature.

Acknowledgements

We are grateful for discussions with Jörg Bünemann. The work was partly supported by the National Science Centre (NCN) under the Grant MAESTRO, No. DEC-2012/04/A/ST3/00342. Access to the supercomputer located at Academic Center for Materials and Nanotechnology of the AGH University of Science and Technology in Kraków is also acknowledged. MW acknowledges also the hospitality of the Institute of Science and Technology Austria during the final stage of development of the present work, as well as a partial financial support from Society - Environment - Technology project of the Jagiellonian University for that stay. JK acknowledges support from the People Programme (Marie Curie Actions) of the European Union's Seventh Framework Programme (FP7/2007-2013) under REA grant agreement n° [291734].

Appendix A: Equivalence of the k=0 order DE-GWF expansion and the Gutzwiller approximation (GA)

Here we show the equivalence of the zeroth order DE-GWF and the standard Gutzwiller approximation (GA).

In both methods (DE-GWF in the zeroth order of expansion $k = 0$) the effect of the projection can be summarized by the expressions for evaluating following expectation values: $\langle \hat{n}_{\mathbf{i}\uparrow}\hat{n}_{\mathbf{i}\downarrow}\rangle_G$ and $\langle \hat{f}^\dagger_{\mathbf{i}\sigma}\hat{c}_{\mathbf{i}\sigma} + \text{H.c.}\rangle_G$. The remaining averages in ALM are unchanged under the projection.

Explicitly, in the DE-GWF for $k = 0$ the resulting averages are expressed as follows

$$\langle \hat{n}_{\mathbf{i}\uparrow}\hat{n}_{\mathbf{i}\downarrow}\rangle_G^{(k=0)} = \lambda_d^2 n_{0f}^2 \tag{A1a}$$

$$\langle \hat{f}^\dagger_{\mathbf{i}\sigma}\hat{c}_{\mathbf{i}\sigma} + \text{H.c.}\rangle_G^{(k=0)} = \alpha\langle \hat{f}^\dagger_{\mathbf{i}\sigma}\hat{c}_{\mathbf{i}\sigma} + \text{H.c.}\rangle_0, \tag{A1b}$$

where parameter α (see also Appendix B: Eqs. (B1) and (B2)) is defined as

$$\alpha \equiv (1 - n_{0f})\lambda_0\lambda_s + n_{0f}\lambda_d\lambda_s. \tag{A2}$$

On the other hand, in GA the resulting averages are expressed as[26]

$$\langle \hat{n}_{\mathbf{i}\uparrow}\hat{n}_{\mathbf{i}\downarrow}\rangle_G^{(GA)} = \langle n^f_{\mathbf{i}\uparrow}\hat{n}^f_{\mathbf{i}\downarrow}\rangle_0 \equiv d^2, \tag{A3a}$$

$$\langle \hat{f}^\dagger_{\mathbf{i}\sigma}\hat{c}_{\mathbf{i}\sigma} + \text{H.c.}\rangle_G^{(GA)} = \sqrt{q}\langle \hat{f}^\dagger_{\mathbf{i}\sigma}\hat{c}_{\mathbf{i}\sigma} + \text{H.c.}\rangle_0, \tag{A3b}$$

where the parameter d^2 is the double occupancy probability, and q is the so-called Gutzwiller factor reducing the hybridization amplitude, which for the equal number of particles for each spin is defined as

$$\sqrt{q} = \frac{\sqrt{(n_{0f} - d^2)(1 - 2n_{0f} + d^2)} + \sqrt{(n_{0f} - d^2)d^2}}{\sqrt{n_{0f}(1 - n_{0f})}}. \tag{A4}$$

If we identify double occupancy probabilities expressed by both methods in (A3a) and (A1a) to be equal, yielding $d^2 = \lambda_d^2 n_{0f}^2$, then the parameter α (A2) exactly reduces to the parameter $\sqrt{q}$ (A4).

GA procedure results in the effective single-particle Hamiltonian of the form

$$\hat{\mathcal{H}}_{GA} \equiv \sum_{\mathbf{k},\sigma} \hat{\Psi}^\dagger_{\mathbf{k}\sigma} \begin{pmatrix} \epsilon^c_{\mathbf{k}} - \mu & \sqrt{q_\sigma}V \\ \sqrt{q_\sigma}V & \epsilon_f - \mu \end{pmatrix} \hat{\Psi}_{\mathbf{k}\sigma} + LUd^2$$
$$-\lambda^f_n\Big(\sum_{\mathbf{k},\sigma}\hat{n}^f_{\mathbf{k},\sigma} - Ln_{0f}\Big) - \lambda^f_m\Big(\sum_{\mathbf{k},\sigma}\sigma\hat{n}^f_{\mathbf{k},\sigma} - Lm_f\Big). \tag{A5}$$

In the above Hamiltonian it is necessary to add constraints for f-electron concentration and their magnetization in order to satisfy consistency of the procedure[27,82]. In effect, the whole variational problem is reduced to minimization of the ground state energy with respect to d^2, n_{0f}, m_f, and respective Lagrange multipliers λ^f_n and λ^f_m, playing the role of the effective molecular fields[82]. However, the effect of constraint for f-electron magnetization is relevant only in the case of magnetism consideration either as intrinsic[42,43] or induced by applied magnetic field[41]. Here, as we discuss paramagnetic state $m^f = \lambda^f_m = \lambda^f_n = 0$.

The DE-GWF method by construction guarantees that the variationally obtained f-electron occupancy number n_f coincides with that obtained self-consistently[57]. We have thus provided analytical argument for the equivalence of the DE-GWF method for $k = 0$ and the standard GA procedure. Also, by an independent numerical cross-check we have verified that all the observables calculated within both methods indeed coincide.

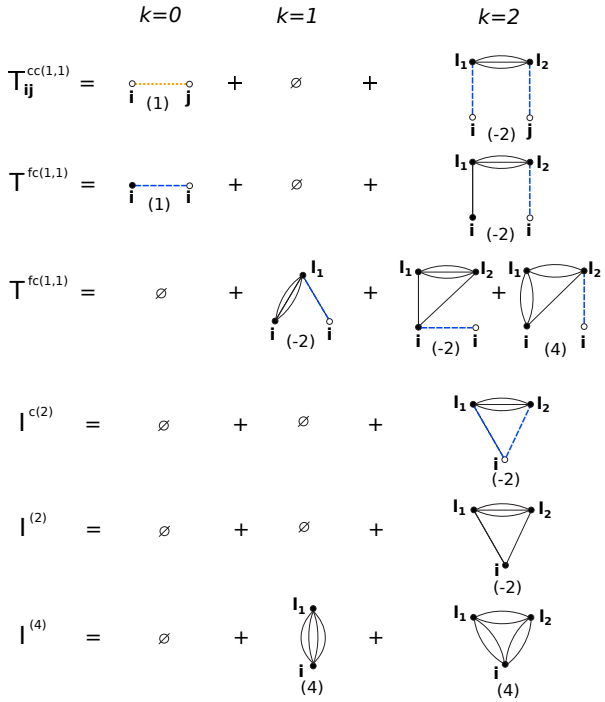

FIG. 9: (Color online) Diagrammatic sums to the second order, $k = 2$. c- and f- orbital sites are denoted with empty and filled circles respectively. Solid, dashed (blue) and dotted (orange) connections represent F, W, and C lines respectively (cf. Eq. (10)). The numbers in brackets under diagrams stand for their multiplicity resulting from the Wick's theorem. Note that by construction of our sums we have no diagrams with so-called "Hartree bubbles", namely loop-lines within the same site and orbital.

Appendix B: Diagrammatic sums

We start with expressions for the following projected operators originating from ALM Hamiltonian (1), namely

$$\hat{P}_{G;\mathbf{i}}\hat{d}_{\mathbf{i}}\hat{P}_{G;\mathbf{i}} = \lambda_d^2[2n_{0f}\hat{n}^{HF}_{\mathbf{i}} + (1 - xd_0)\hat{d}^{HF}_{\mathbf{i}} + d_0\hat{P}^2_{G;\mathbf{i}}],$$
$$\hat{P}_{G;\mathbf{i}}\hat{n}_{\mathbf{i}\sigma}\hat{P}_{G;\mathbf{i}} = (1 + xm)\hat{n}^{HF}_{\mathbf{i}} + \gamma\hat{d}^{HF}_{\mathbf{i}} + n_{0f}\hat{P}^2_{G;\mathbf{i}},$$
$$\hat{P}_{G;\mathbf{i}}\hat{f}^{(\dagger)}_{\mathbf{i}\sigma}\hat{P}_{G;\mathbf{i}} = \alpha\hat{f}^{(\dagger)}_{\mathbf{i}\sigma} + \beta\hat{f}^{(\dagger)}_{\mathbf{i}\sigma}\hat{n}^{HF}_{\mathbf{i}}, \tag{B1}$$

where additionally we have defined

$$\begin{aligned} \hat{n}_{\mathbf{i}}^{HF} &\equiv \hat{n}_{\mathbf{i}\sigma}^{HF} = \hat{n}_{\mathbf{i}\bar{\sigma}}^{HF}, \\ \beta &\equiv \lambda_s(\lambda_d - \lambda_0), \\ \alpha &\equiv \lambda_s\lambda_0 + \beta n_{0f}, \\ \gamma &\equiv x(1-2n_{0f}), \\ d_0 &\equiv n_{0f}^2, \\ m &\equiv n_{0f}(1-n_{0f}). \end{aligned} \tag{B2}$$

As mentioned in the main text, such form of the projected operators significantly speeds up the convergence of the numerical results[54], since by construction all two-operator averages for a single site and f-orbital, the so-called *Hartree bubbles*, vanish. The above operator algebra leads to the compact definition of the diagrammatic sums: $S \in \{T_{\mathbf{ij}}^{cc(1,1)}, T_{\mathbf{ij}}^{fc(1,1)}, T_{\mathbf{ij}}^{fc(3,1)}, I^{c(2)}, I^{(2)}, I^{(4)}\}$ in Eq. (11),

$$S = \sum_{k=0}^{\infty} \frac{x^k}{k!} S(k). \tag{B3}$$

with the k-th order contributions

$$\begin{aligned} T_{\mathbf{ij}}^{cc(1,1)}(k) &\equiv \sum_{\mathbf{l}_1,\ldots,\mathbf{l}_k} \langle \hat{c}_{\mathbf{i}\sigma}^{\dagger} \hat{c}_{\mathbf{j}\sigma} \hat{d}_{\mathbf{l}_1,\ldots,\mathbf{l}_k}^{HF} \rangle_0^c, \\ T^{fc(1[3],1)}(k) &\equiv \sum_{\mathbf{l}_1,\ldots,\mathbf{l}_k} \langle [\hat{n}_{\mathbf{i}}^{HF}] \hat{f}_{\mathbf{i}\sigma}^{\dagger} \hat{c}_{\mathbf{i}\sigma} \hat{d}_{\mathbf{l}_1,\ldots,\mathbf{l}_k}^{HF} \rangle_0^c, \\ I^{c(2)}(k) &\equiv \sum_{\mathbf{l}_1,\ldots,\mathbf{l}_k} \langle \hat{n}_{\mathbf{i}\sigma}^{c} \hat{d}_{\mathbf{l}_1,\ldots,\mathbf{l}_k}^{HF} \rangle_0^c, \\ I^{(2)}(k) &\equiv \sum_{\mathbf{l}_1,\ldots,\mathbf{l}_k} \langle \hat{n}_{\mathbf{i}}^{HF} \hat{d}_{\mathbf{l}_1,\ldots,\mathbf{l}_k}^{HF} \rangle_0^c, \\ I^{(4)}(k) &\equiv \sum_{\mathbf{l}_1,\ldots,\mathbf{l}_k} \langle \hat{d}_{\mathbf{i}}^{HF} \hat{d}_{\mathbf{l}_1,\ldots,\mathbf{l}_k}^{HF} \rangle_0^c. \end{aligned} \tag{B4}$$

Superscript c in the expectation values means that only the connected diagrams are to be included. Note that in (B4) there are no summation restrictions, due to the linked cluster theorem[72]. The resulting diagrammatic sums for S up to second order ($k = 2$) are depicted in Fig. 9.

* Electronic address: marcin.wysokinski@uj.edu.pl
† Electronic address: jan.kaczmarczyk@ist.ac.at
‡ Electronic address: ufspalek@if.uj.edu.pl

[1] K. Andres, J. E. Graebner, and H. R. Ott, Phys. Rev. Lett. **35**, 1779 (1975).
[2] G. R. Stewart, Rev. Mod. Phys. **56**, 755 (1984).
[3] N. Grewe and F. Steglich, *in Handbook on the Physics and Chemistry of Rare Earths*, vol. 14 (Northe-Holland, Amsterdam, 1991).
[4] P. Fulde, J. Keller, and G. Zwicknagl, *in Solid State Physics*, vol. 41 (Academic Press, New York, 1988).
[5] H. R. Ott, *in Progress in Low Temperature Physics*, vol. XI (North-Holland, Amsterdam, 1987).
[6] R. Citro, A. Romano, and J. Spałek, Physica B **259-261**, 213 (1999).
[7] I. Sheikin, A. Gröger, S. Raymond, D. Jaccard, D. Aoki, H. Harima, and J. Flouquet, Phys. Rev. B **67**, 094420 (2003).
[8] A. McCollam, S. R. Julian, P. M. C. Rourke, D. Aoki, and J. Flouquet, Phys. Rev. Lett. **94**, 186401 (2005).
[9] R. Doradziński and J. Spałek, Phys. Rev. B **56**, R14239 (1997).
[10] R. Doradziński and J. Spałek, Phys. Rev. B **58**, 3293 (1998).
[11] C. Pfleiderer, Rev. Mod. Phys. **81**, 1551 (2009).
[12] G. R. Stewart, Rev. Mod. Phys. **73**, 797 (2001).
[13] H. v. Löhneysen, A. Rosch, M. Vojta, and P. Wölfle, Rev. Mod. Phys. **79**, 1015 (2007).
[14] G. Lonzarich, Nature Physics **1**, 5 (2005).
[15] C. Lacroix and M. Cyrot, Phys. Rev. B **20**, 1969 (1979).
[16] A. C. Hewson, *The Kondo Problem to Heavy Fermions* (Cambridge University Press, 1993).
[17] A. Auerbach and K. Levin, J. Appl. Phys. **61**, 3162 (1987).
[18] O. Howczak and J. Spałek, J. Phys.: Condens. Matter **24**, 205602 (2012).
[19] O. Howczak, J. Kaczmarczyk, and J. Spałek, Phys. Status Solidi (b) **250**, 609 (2013), ISSN 1521-3951.
[20] P. Gurin and Z. Gulácsi, Phys. Rev. B **64**, 045118 (2001).
[21] Z. Gulácsi, Phys. Rev. B **66**, 165109 (2002).
[22] Z. Gulácsi and D. Vollhardt, Phys. Rev. Lett. **91**, 186401 (2003).
[23] Z. Gulácsi and D. Vollhardt, Phys. Rev. B **72**, 075130 (2005).
[24] C. M. Varma, W. Weber, and L. J. Randall, Phys. Rev. B **33**, 1015 (1986).
[25] Z. Gulácsi, R. Strack, and D. Vollhardt, Phys. Rev. B **47**, 8594 (1993).
[26] T. M. Rice and K. Ueda, Phys. Rev. Lett. **55**, 995 (1985).
[27] T. M. Rice and K. Ueda, Phys. Rev. B **34**, 6420 (1986).
[28] K. Miyake, S. Schmitt-Rink, and C. M. Varma, Phys. Rev. B **34**, 6554 (1986).
[29] P. Fazekas, *Electron Correlation and Magnetism* (World Scientific, Singapore, 1999).
[30] G. Kotliar and A. E. Ruckenstein, Phys. Rev. Lett. **57**, 1362 (1986).
[31] J. Spałek, A. Datta, and J. M. Honig, Phys. Rev. Lett. **59**, 728 (1987).
[32] F. Gebhard, Phys. Rev. B **44**, 992 (1991).
[33] V. Dorin and P. Schlottmann, Phys. Rev. B **46**, 10800 (1992).
[34] V. Dorin and P. Schlottmann, Phys. Rev. B **47**, 5095 (1993).
[35] J. Bünemann, W. Weber, and F. Gebhard, Phys. Rev. B **57**, 6896 (1998).
[36] J. Jędrak and J. Spałek, Phys. Rev. B **83**, 104512 (2011).
[37] J. Kaczmarczyk and J. Spałek, Phys. Rev. B **84**, 125140 (2011).
[38] M. Abram, J. Kaczmarczyk, J. Jędrak, and J. Spałek, Phys. Rev. B **88**, 094502 (2013).
[39] A. P. Kądzielawa, J. Spałek, J. Kurzyk, and W. Wójcik, Eur. Phys. J. B **86**, 252 (2013).
[40] M. Zegrodnik, J. Bünemann, and J. Spałek, New J. Phys.

16, 033001 (2014).
[41] M. M. Wysokiński and J. Spałek, J. Phys.: Condens. Matter **26**, 055601 (2014).
[42] M. M. Wysokiński, M. Abram, and J. Spałek, Phys. Rev. B **90**, 081114(R) (2014).
[43] M. M. Wysokiński, M. Abram, and J. Spałek, Phys. Rev. B **91**, 081108(R) (2015).
[44] B. Edegger, V. N. Muthukumar, and C. Gros, Phys. Rev. B **74**, 165109 (2006).
[45] M. Lugas, L. Spanu, F. Becca, and S. Sorella, Phys. Rev. B **74**, 165122 (2006).
[46] M. Raczkowski, M. Capello, D. Poilblanc, R. Frésard, and A. M. Oleś, Phys. Rev. B **76**, 140505 (2007).
[47] B. Edegger, V. N. Muthukumar, and C. Gros, Advances in Physics **56**, 927 (2007).
[48] C.-P. Chou, F. Yang, and T.-K. Lee, Phys. Rev. B **85**, 054510 (2012).
[49] J. Liu, J. Schmalian, and N. Trivedi, Phys. Rev. Lett. **94**, 127003 (2005).
[50] T. Watanabe, H. Yokoyama, K. Shigeta, and M. Ogata, New J. Phys. **11**, 075011 (2009).
[51] M. Z. Asadzadeh, F. Becca, and M. Fabrizio, Phys. Rev. B **87**, 205144 (2013).
[52] H. Watanabe, K. Seki, and S. Yunoki, Phys. Rev. B **91**, 205135 (2015).
[53] R. Jastrow, Phys. Rev. **98**, 1479 (1955).
[54] J. Bünemann, T. Schickling, and F. Gebhard, Eur. Phys. Lett. **98**, 27006 (2012).
[55] J. Kaczmarczyk, J. Spałek, T. Schickling, and J. Bünemann, Phys. Rev. B **88**, 115127 (2013).
[56] J. Kaczmarczyk, J. Bünemann, and J. Spałek, New J. Phys. **16**, 073018 (2014).
[57] J. Kaczmarczyk, Phil. Mag. **95**, 563 (2015).
[58] J. Kaczmarczyk, T. Schickling, and J. Bünemann, Phys. Status Solidi B. (2015).
[59] P. Aynajian, E. H. da Silva Neto, A. Gyenis, R. E. Baumbach, J. D. Thompson, Z. Fisk, E. D. Bauer, and A. Yazdani, Nature **486**, 201 (2012).
[60] M. P. Allan, F. Massee, D. K. Morr, J. S. Dyke, A. W. Rost, A. P. Mackenzie, C. Petrovic, and J. C. S. Davis, Nature Physics **9**, 468 (2013).
[61] J. S. Dyke, F. Massee, M. P. Allan, J. C. S. Davis, C. Petrovic, and D. K. Morr, Proc. Natl. Acad. Sci. **111**, 11663 (2014).
[62] A. T. Holmes, D. Jaccard, and K. Miyake, Phys. Rev. B **69**, 024508 (2004).
[63] A. Ślebarski and J. Spałek, Phys. Rev. Lett. **95**, 046402 (2005).
[64] A. Ślebarski, J. Spałek, M. Fijałkowski, J. Goraus, T. Cichorek, and L. Bochenek, Phys. Rev. B **82**, 235106 (2010).
[65] M. Szlawska, D. Kaczorowski, A. Ślebarski, L. Gulay, and J. Stępień-Damm, Phys. Rev. B **79**, 134435 (2009).
[66] D. Kaczorowski and A. Ślebarski, Phys. Rev. B **81**, 214411 (2010).
[67] S. Watanabe and K. Miyake, Phys. Rev. Lett. **105**, 186403 (2010).
[68] H. Tsunetsugu, M. Sigrist, and K. Ueda, Rev. Mod. Phys. **69**, 809 (1997).
[69] In principle, the hybridization can have an intersite character[83].
[70] F. Gebhard, Phys. Rev. B **41**, 9452 (1990).
[71] Z. Gulácsi, M. Gulácsi, and B. Jankó, Phys. Rev. B **47**, 4168 (1993).
[72] A. L. Fetter and J. D. Walecka, *Quantum Theory of Many-Particle Systems* (Dover Publications, New York, 2003).
[73] M. Galassi, J. Davies, J. Theiler, B. Gough, G. Jungman, P. Alken, M. Booth, and F. Rossi, GNU Scientific Library Reference Manual (3rd Ed.), ISBN 0954612078.
[74] K. Miyake and Y. Onishi, J. Phys. Soc. Jpn. **69**, 355 (2000).
[75] J. Spałek, Phil. Mag. **95**, 661 (2015).
[76] S. Doniach, Phys. Rev. B **35**, 1814 (1987).
[77] B. Coqblin, C. Lacroix, M. A. Gusmão, and J. R. Iglesias, Phys. Rev. B **67**, 064417 (2003).
[78] S. Hoshino and Y. Kuramoto, Phys. Rev. Lett. **111**, 026401 (2013).
[79] T. Park, M. J. Graf, L. Boulaevskii, J. L. Sarrao, and J. D. Thompson, Proc. Natl. Acad. Sci. **105**, 6825 (2008).
[80] R. Troć, Z. Gajek, and A. Pikul, Phys. Rev. B **86**, 224403 (2012).
[81] M. M. Wysokiński, J. Kaczmarczyk, and J. Spałek, unpublished.
[82] J. Jędrak, J. Kaczmarczyk, and J. Spałek, arXiv:1008.0021.
[83] P. Ghaemi, T. Senthil, and P. Coleman, Phys. Rev. B **77**, 245108 (2008).

3.7 Article A.6, Correlation-driven d-wave superconductivity in Anderson lattice model

The work[2] [121] provides the originally planned goal, namely the appearance of an unconventional superconductivity as solely due to the electronic correlations. For that purpose we have extended the DE-GWF method to incorporate the superconducting correlations in the Anderson lattice model (cf. Sec. 2.2). We have considered d-wave symmetry of the order parameter as such pairing symmetry is expected [100, 101, 102] in the presence of strong electronic correlations. We have determined the regions of its stability against paramagnetism by presenting the results on the hybridization - total number of electrons plane. Our results reflect several features observed in heavy fermion superconductors, especially in $CeCoIn_5$: the dominant $d_{x^2-y^2}$ symmetry of the order parameter, reasonable value of the pairing condensation energy, and two different superconducting gaps within different bands (in our case one is due to interband component of the SC order). As this work is first of its kind, it is planned to be elaborated in detail in the near future.

[2] preprint as of August 10, 2015

Correlation-driven d-wave superconductivity in Anderson lattice model

Marcin M. Wysokiński,[1,*] Jan Kaczmarczyk,[1,2,†] and Jozef Spałek[1,‡]

[1] *Marian Smoluchowski Institute of Physics, Jagiellonian University, ulica prof. S. Łojasiewicza 11, PL-30-348 Kraków, Poland*

[2] *Institute of Science and Technology Austria, Am Campus 1, A-3400 Klosterneuburg, Austria*

(Dated: August 12, 2015)

We present solution of the Anderson lattice model treated by means of a systematic Diagrammatic Expansion for the Guzwiller Wave Function which leads to the stable and correlation-driven multiband superconducting (SC) groundstate of dominant $d_{x^2-y^2}$-wave symmetry. Such state has been observed in heavy fermion compound $CeCoIn_5$, but it may also appear in other Ce-based superconductors. We also draw some conclusions about the common features of the pairing proposed here for heavy fermion systems with those for an analogous approach to high-temperature superconductivity.

Motivation. Starting form the first observation of superconductivity (SC) in the heavy fermion system(HFS) $CeCu_2Si_2$[1, 2], there is an ongoing discussion concerning the microscopic mechanism(s) of pairing in this class of *unconventional superconductors* [3–6]. The first issue here is how to incorporate essential electronic correlations among f electrons, induced by the strong Coulomb repulsion between them, into an emergent quasiparticle picture resulting from f-c hybridization of the originally atomic f electron states with the band (c) states. Those quasiparticle states, when possible to form [7, 8], must incorporate the strong f-f Coulomb interactions of magnitude U which represents by far the largest energy scale in the system and thus minimally renormalizes strongly the hybridization leading to f-c state coherence. The second issue is the appearance of magnetism, often concomitant with localization of f electrons, that either coexist or competes with SC.

Over thirty of HFS are known to be superconducting [9], either magnetic or not, but all have similar properties. This circumstance justifies the assumption almost universally made [3, 5, 6, 10] that the pairing may have origin in the common principal features of electronic structure. Here we analyze the Anderson lattice model (ALM), regarded as encompassing those principal features for orbitally nondegenerate f states of Ce-based compounds and show that a stable SC state of dominant $d_{x^2-y^2}$-wave character, can be triggered by purely repulsive f-f interactions in the strongly correlated state. As a method of approach we have selected recently proposed by us [11–15] a systematic *Diagrammatic Expansion for the Gutzwiller Wave Function* (DE-GWF). It should be noted at the start that this method reproduces in zeroth order the Gutzwiller approximation which nonetheless does not lead to a stable SC solution as it includes only the local correlations. Therefore, the role of nonlocal correlations, inherent in DE-GWF approach, is regarded as the essential factor which leads to the non-BCS type of SC state, as discussed in detail below. The method of approach allows for a direct comparison with an analogous approach to the high temperature superconductivity (HTS) [12–15] and on this basis to draw conclusions about universal features of pairing in those two systems.

Previous considerations of pairing in HFS of correlation-driven and of purely electronic origin involve related models such as the Kondo lattice (KL) model [16–19], the Anderson-Kondo lattice (AKL) model [20–23] or ALM with the Falicov-Kimball term to discuss the valence-fluctuation induced pairing [24]. A separate class of models is based on the spin-fluctuation pairing among uncorrelated electrons [5, 10, 25]. The treatments based on the KL neglect direct f-c hybridization and therefore can be regarded as a limit of AKL when the renormalized hybridization is negligible and the pairing is solely due to exchange processes. Additionally, in KL the numbers of f and c electrons are conserved separately and the formation of f-c pairs states comes only form treating f electrons as fermions and decoupling properly the Kondo-exchange term which breaks this conservation law. All of these considerations (apart from the spin fluctuation

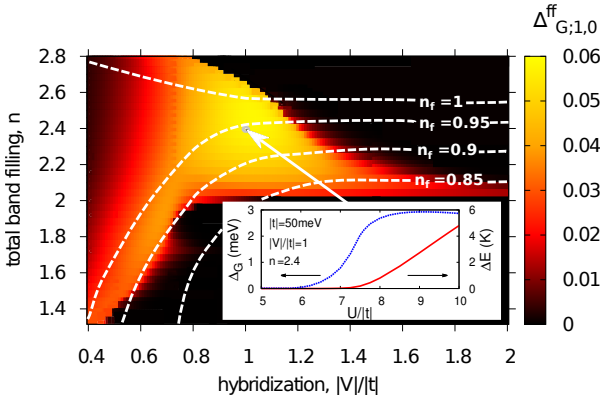

FIG. 1. Phase diagram on the band filling-hybridization magnitude plane with the dominant, $d_{x^2-y^2}$-wave superconducting order parameter for f electrons, $\Delta^{ff}_{G;1,0}$ (see main text). The dashed lines mark selected f-orbital isovalents. In the inset we show for the selected point ($n = 2.4$, $|V|/|t| = 1$) that SC appears with the increasing Coulomb interaction $U/|t|$ and is prominent near $n_f \sim 1$, i.e in the heavy fermion regime.

mechanism) start from a real-space picture in which correlations and local pairing have been introduced. Thus, it seems natural to address the problem directly within ALM, in which the pairing appears as a direct product of strong correlations. This is the aim of this work.

Model and method of approach. Our starting point is ALM

$$\hat{\mathcal{H}} = \sum_{\mathbf{i},\mathbf{j},\sigma} t_{\mathbf{ij}} \hat{c}^{\dagger}_{\mathbf{i}\sigma} \hat{c}_{\mathbf{j}\sigma} - \mu \sum_{\mathbf{i},\sigma} \hat{n}^{c}_{\mathbf{i}\sigma} + (\epsilon_f - \mu) \sum_{\mathbf{i},\sigma} \hat{n}^{f}_{\mathbf{i}\sigma} + U \sum_{\mathbf{i}} \hat{n}^{f}_{\mathbf{i}\uparrow} \hat{n}^{f}_{\mathbf{i}\downarrow} + \sum_{\mathbf{i},\mathbf{j},\sigma} (V_{\mathbf{ij}} f^{\dagger}_{\mathbf{i}\sigma} \hat{c}_{\mathbf{j}\sigma} + V^{*}_{\mathbf{ij}} c^{\dagger}_{\mathbf{i}\sigma} \hat{f}_{\mathbf{j}\sigma}), \tag{1}$$

on a two dimensional (2D), translationally invariant square lattice, with the chemical potential μ, and with the usual notation, where $\mathbf{i},\mathbf{j}$ and σ denote site and spin indices, respectively. Hamiltonian (1) comprises dispersive conduction (c) band and f electrons, initially in their atomic states of eigenenergy ϵ_f.

Ground state properties of (1) are obtained variationally with the GWF, $|\psi_G\rangle$, constructed from the uncorrelated-single Slater determinant, $|\psi_0\rangle$, by projecting out fraction of the local double occupancies within the f orbital by means of Gutzwiller operator: $|\psi_G\rangle = \hat{\mathcal{P}}_G|\psi_0\rangle \equiv \prod_{\mathbf{i}} \hat{\mathcal{P}}_{G;\mathbf{i}}|\psi_0\rangle$. The method and the normal state of ALM have been discussed in detail elsewhere [26]. The operator $\hat{\mathcal{P}}_G$ is defined by [27] $\hat{\mathcal{P}}^{\dagger}_{G;\mathbf{i}}\hat{\mathcal{P}}_{G;\mathbf{i}} \equiv \mathbf{1} + x\hat{d}^{HF}_{\mathbf{i}}$, where x is a variational parameter and $\hat{d}^{HF}_{\mathbf{i}} \equiv \hat{n}^{HF}_{\mathbf{i}\uparrow}\hat{n}^{HF}_{\mathbf{i}\downarrow} = (\hat{n}^{f}_{\mathbf{i}\uparrow} - n^{f}_{0})(\hat{n}^{f}_{\mathbf{i}\downarrow} - n^{f}_{0})$, with $n^{f}_{0} \equiv \langle \hat{n}^{f}_{\mathbf{i}\sigma}\rangle_0$, where we use shortened notation $\langle ...\rangle_{G(0)} \equiv \frac{\langle \psi_{G(0)}|...|\psi_{G(0)}\rangle}{\langle \psi_{G(0)}|\psi_{G(0)}\rangle}$.

The main difficulty of the approach is in determining the expectation values of Hamiltonian (1) with GWF, $\langle \hat{\mathcal{H}}\rangle_G = \frac{\langle \hat{\mathcal{P}}_G \hat{\mathcal{H}} \hat{\mathcal{P}}_G\rangle_0}{\langle \hat{\mathcal{P}}^2_G\rangle_0}$. As the complete evaluation cannot be executed in one step, the intersite correlations are systematically accounted for in consecutive orders. Formally, for any product operator, $\hat{\mathcal{O}}_{\mathbf{i}(\mathbf{j})}$ acting on the site $\mathbf{i}$ (and $\mathbf{j}$), the procedure starts with a power series expansion in x of its expectation value with GWF

$$\langle \hat{\mathcal{O}}_{\mathbf{i}(\mathbf{j})}\rangle_G = \Big\langle \hat{\mathcal{O}}^{G}_{\mathbf{i}(\mathbf{j})} \prod_{\mathbf{l}\neq\mathbf{i},\mathbf{j}} \hat{\mathcal{P}}^{2}_{G;\mathbf{l}} \Big\rangle_0 = \sum_{k=0}^{\infty} \frac{x^k}{k!} {\sum_{\mathbf{l}_1,...,\mathbf{l}_k}}' \langle \hat{\mathcal{O}}^{G}_{\mathbf{i}(\mathbf{j})} \hat{d}^{HF}_{\mathbf{l}_1,...,\mathbf{l}_k}\rangle_0, \tag{2}$$

where we have defined $\hat{\mathcal{O}}^{G}_{\mathbf{i}(\mathbf{j})} \equiv \hat{\mathcal{P}}_{G;\mathbf{i}}(\hat{\mathcal{P}}_{G;\mathbf{j}})\hat{\mathcal{O}}_{\mathbf{i}(\mathbf{j})}(\hat{\mathcal{P}}_{G;\mathbf{j}})\hat{\mathcal{P}}_{G;\mathbf{i}}$ and $\hat{d}^{HF}_{\mathbf{l}_1,...,\mathbf{l}_k} \equiv \hat{d}^{HF}_{\mathbf{l}_1}\cdots\hat{d}^{HF}_{\mathbf{l}_k}$. The prime summation denotes the following restrictions $\mathbf{l}_p \neq \mathbf{l}_{p'}$, and $\mathbf{l}_p \neq \mathbf{i},\mathbf{j}$ for all p, p'. Power series in x allows for a systematic incorporation of the long-range correlations among k non-local sites $(\mathbf{l}_1, ..., \mathbf{l}_k)$ and the local ones $(\mathbf{i},\mathbf{j})$. The resulting expectation values with the Slater determinant $|\psi_0\rangle$ can be evaluated by applying the Wick's theorem, this time in real space. Namely, all resulting products of two-operator contractions can be visualized as *diagrams* of lines connecting vertices (sites) linked by the respective averages [13, 26]. Here we allow for both the paramagnetic and superconducting contractions (lines) defined respectively as

$$P^{\alpha,\beta}_{\mathbf{l},\mathbf{l}'} \equiv \langle \hat{\alpha}^{\dagger}_{\mathbf{l}\sigma}\hat{\beta}_{\mathbf{l}'\sigma}\rangle_0 - \delta_{\alpha f}\delta_{\beta f}\delta_{\mathbf{l}\mathbf{l}'}n_{0f}, \quad S^{\alpha,\beta}_{\mathbf{l},\mathbf{l}'} \equiv \langle \hat{\alpha}^{\dagger}_{\mathbf{l}\sigma}\hat{\beta}^{\dagger}_{\mathbf{l}'\bar{\sigma}}\rangle_0, \tag{3}$$

where $\alpha,\beta \in \{c, f\}$ and $\mathbf{l},\mathbf{l}'$ are the lattice indices. For an infinite lattice, we introduce a real space cutoff, namely we consider only the lines satisfying relation $|\mathbf{l}-\mathbf{l}'|^2 \equiv (l_x - l'_x)^2 + (l_y - l'_y)^2 \leq 10$. The resulting expectation value of the Hamiltonian then can be expressed by the diagrammatic sums (for details see Refs. [13, 26, 28]). In that manner, the average depends on the variational parameter x and correlation functions (lines) (3) only.

The iterative procedure for obtaining the physical ground state of (1) is as follows:
1. $\langle \hat{\mathcal{H}}\rangle_G$ is evaluated diagrammatically for selected $|\psi_0\rangle$.
2. $\langle \hat{\mathcal{H}}\rangle_G$ is minimized with respect to x.
3. The effective single particle Hamiltonian $\hat{\mathcal{H}}^{\text{eff}}$ for the uncorrelated wave function $|\psi_0\rangle$ is determined.
4. New trial $|\psi'_0\rangle$ is obtained from $\hat{\mathcal{H}}^{\text{eff}}$. The points 1-4 are repeated in a self-consistent loop until a satisfactory convergence, i.e., the condition $|\psi_0\rangle = |\psi'_0\rangle$ is reached to a good accuracy.

The effective single particle Hamiltonian $\hat{\mathcal{H}}^{\text{eff}}$ for the uncorrelated wave function $|\psi_0\rangle$ is determined from the condition that of its expectation value in the minimum for the equilibrium lines coincides with $\langle \hat{\mathcal{H}}\rangle_G$, namely

$$\delta\langle \hat{\mathcal{H}}^{\text{eff}}\rangle_0(P^{\alpha,\beta}_{\mathbf{l},\mathbf{l}'}, S^{\alpha,\beta}_{\mathbf{l},\mathbf{l}'}, n_{0f}) = \delta\langle \hat{\mathcal{H}}\rangle_G(P^{\alpha,\beta}_{\mathbf{l},\mathbf{l}'}, S^{\alpha,\beta}_{\mathbf{l},\mathbf{l}'}, n_{0f}) = \sum_{\mathbf{l},\mathbf{l}'} \Big(\frac{\partial\langle \hat{\mathcal{H}}\rangle_G}{\partial P^{\alpha,\beta}_{\mathbf{l},\mathbf{l}'}} \delta P^{\alpha,\beta}_{\mathbf{l},\mathbf{l}'} + \frac{\partial\langle \hat{\mathcal{H}}\rangle_G}{\partial S^{\alpha,\beta}_{\mathbf{l},\mathbf{l}'}} \delta S^{\alpha,\beta}_{\mathbf{l},\mathbf{l}'} \Big) + \frac{\partial\langle \hat{\mathcal{H}}\rangle_G}{\partial n_{0f}} \delta n_{0f}. \tag{4}$$

Explicitly, the effective single particle Hamiltonian reads,

$$\hat{\mathcal{H}}^{\text{eff}} = \sum_{\mathbf{i},\mathbf{j},\sigma} \Big(t^{cc}_{\mathbf{ij}} \hat{c}^{\dagger}_{\mathbf{i}\sigma}\hat{c}_{\mathbf{j}\sigma} + t^{ff}_{\mathbf{ij}} \hat{f}^{\dagger}_{\mathbf{i}\sigma}\hat{f}_{\mathbf{j}\sigma} + t^{cf}_{\mathbf{ij}} (\hat{c}^{\dagger}_{\mathbf{i}\sigma}\hat{f}_{\mathbf{j}\sigma} + \text{h.c.}) \Big) + \sum_{\mathbf{i},\mathbf{j},\sigma} \Delta^{cf}_{\mathbf{ij}} (\hat{c}^{\dagger}_{\mathbf{i}\sigma}\hat{f}^{\dagger}_{\mathbf{j}\bar{\sigma}} + \text{h.c.}) + \sum_{\mathbf{i},\mathbf{j}} \Delta^{ff}_{\mathbf{ij}} (\hat{f}^{\dagger}_{\mathbf{i}\uparrow}\hat{f}^{\dagger}_{\mathbf{j}\downarrow} + \text{h.c.}), \tag{5}$$

with effective microscopic parameters determined by the conditions

$$t^{\alpha\beta}_{\mathbf{ij}} = \frac{\partial\langle \mathcal{H}\rangle_G}{\partial P^{\alpha,\beta}_{\mathbf{i},\mathbf{j}}}, \quad \Delta^{\alpha\beta}_{\mathbf{ij}} = \frac{\partial\langle \mathcal{H}\rangle_G}{\partial S^{\alpha,\beta}_{\mathbf{i},\mathbf{j}}}, \quad t^{ff}_{\mathbf{ii}} = \frac{\partial\langle \mathcal{H}\rangle_G}{\partial n_{0f}}. \tag{6}$$

From the construction of GWF, which introduces correlations within the f orbital only, there is no effective pairing between the c-electrons, since there are no lines $S^{c,c}_{\mathbf{i},\mathbf{j}}$ in the diagrams visualizing the Wick's contractions in (2). By means of the Fourier transform to the momentum space, the effective Hamiltonian is reformulated to the Bogoliubov - de Gennes - Nambu form [29],

$$\hat{\mathcal{H}}^{\text{eff}} = \sum_{\mathbf{k}} \Psi^{\dagger}_{\mathbf{k}} \begin{pmatrix} \epsilon^{cc}_{\mathbf{k}} & 0 & \epsilon^{fc}_{\mathbf{k}} & \Delta^{fc}_{\mathbf{k}} \\ 0 & -\epsilon^{cc}_{\mathbf{k}} & \Delta^{fc}_{\mathbf{k}} & -\epsilon^{fc}_{\mathbf{k}} \\ \epsilon^{fc}_{\mathbf{k}} & \Delta^{fc}_{\mathbf{k}} & \epsilon^{ff}_{\mathbf{k}} & \Delta^{ff}_{\mathbf{k}} \\ \Delta^{fc}_{\mathbf{k}} & -\epsilon^{fc}_{\mathbf{k}} & \Delta^{ff}_{\mathbf{k}} & -\epsilon^{ff}_{\mathbf{k}} \end{pmatrix} \Psi_{\mathbf{k}}, \tag{7}$$

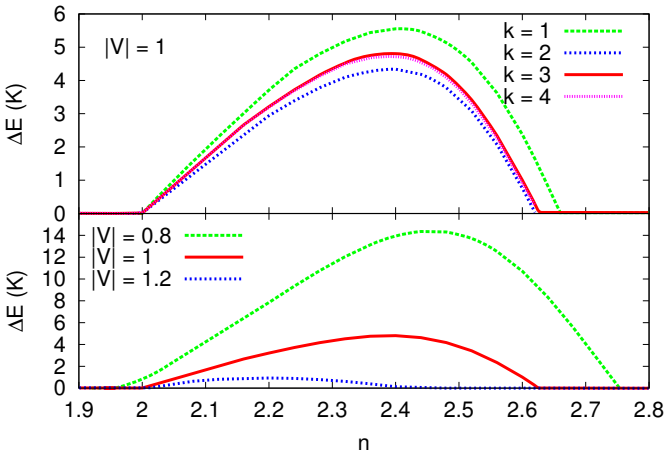

FIG. 2. Top: Order (k) dependence of the condensation energy ΔE for $|V| = 1$. The $k = 3$ and $k = 4$ plots are practically the same, so the satisfactory convergence is already reached. Bottom: ΔE along the selected constant $|V|$.

where we have defined $\Psi^\dagger \equiv (\hat{c}^\dagger_{\mathbf{k}\uparrow}, \hat{c}_{-\mathbf{k}\downarrow}, \hat{f}^\dagger_{\mathbf{k}\uparrow}, \hat{f}_{-\mathbf{k}\downarrow})$ and $\epsilon^{\alpha\beta}_{\mathbf{k}}(\Delta^{\alpha\beta}_{\mathbf{k}}) = (1/L)\sum_{\mathbf{ij}} t^{\alpha\beta}_{\mathbf{ij}}(\Delta^{\alpha\beta}_{\mathbf{ij}})e^{i(\mathbf{i}-\mathbf{j})\mathbf{k}}$. By L we denote the number of lattice sites. Hamiltonian (7) can be easily transformed into its diagonal form by the unitary transformation matrix $\mathcal{T}$ composed from the normalized eigenvectors. The respective averages of components from Ψ and $\Psi^\dagger$ can be expressed as $\langle \Psi^\dagger_n \Psi_m \rangle = \sum_j \mathcal{T}_{jn}\mathcal{T}_{jm}\Theta(E_j)$, where E_j is j-th eigenvalue to the eigenvector $\phi_j = (\mathcal{T}_{j1},\ \mathcal{T}_{j2},\ \mathcal{T}_{j3},\ \mathcal{T}_{j4})$ of Hamiltonian (7). By the inverse Fourier transform, the formulas for the new lines read

$$P^{\alpha,\beta}_{\mathbf{i},\mathbf{j}}\left(S^{\alpha,\beta}_{\mathbf{i},\mathbf{j}}\right) = \frac{1}{L}\sum_{\mathbf{k}} \langle \hat{\alpha}^\dagger_{\mathbf{k}}\hat{\beta}_{\mathbf{k}}\rangle_0 \left(\langle \hat{\alpha}^\dagger_{\mathbf{k}}\hat{\beta}^\dagger_{\mathbf{k}}\rangle_0\right) e^{i(\mathbf{i}-\mathbf{j})\mathbf{k}}. \quad (8)$$

Effectively, to determine equilibrium properties of the model the system of Eqs. (6) and (8) need to be solved self-consistently, together with the minimization of $\langle \hat{\mathcal{H}}\rangle_G$ with respect to x [11–14, 28]. We also adjust the chemical potential as the total filling n is fixed. Finally, the physical ground state energy of the system is obtained as $E_G = \langle \hat{\mathcal{H}}\rangle_G|_0 + n\mu$, where $|_0$ denotes the equilibrium value and $n \equiv 2\langle \hat{n}^f_{\mathbf{i}\sigma} + \hat{n}^c_{\mathbf{i}\sigma}\rangle_G$ is the total electron concentration. Likewise, we define f orbital filling, $n_f = 2\langle \hat{n}^f_{\mathbf{i}\sigma}\rangle_G$.

Our variational scheme allows for determination of both $\hat{\mathcal{H}}^{\text{eff}}$ and $|\psi_0\rangle$. The latter, in turn, enables us for computing the SC order parameters

$$\Delta^{\alpha\beta}_{G;i_x-j_x,i_y-j_y} \equiv \langle \hat{\alpha}^\dagger_{\mathbf{i}}\hat{\beta}^\dagger_{\mathbf{j}}\rangle_G = \langle \hat{\mathcal{P}}_G\hat{\alpha}^\dagger_{\mathbf{i}}\hat{\beta}^\dagger_{\mathbf{j}}\hat{\mathcal{P}}_G\rangle_0. \quad (9)$$

Although there is no pairing term between the c electrons in the effective Hamiltonian (5), the corresponding superconducting correlation functions are nonzero.

Results. We have selected values of the microscopic parameters realistic for the Ce-based HFS, namely c-electron band emerging from the nearest-neighbor hopping, $t = -1$ (reference energy) and second nearest-neighbor, $t' = 0.25|t|$, f-electron atomic level position $\epsilon_f = -3|t|$, and f–f Coulomb repulsion, $U = 10|t|$. The c–f hybridization is considered of variable and the nearest-neighbor origin with $V < 0$. The energy units are scaled to Kelvins by assuming $|t| = 50meV$ (see e.g. [6, 8]). We have restricted our results to the f orbital filling not exceeding unity or slightly larger (but here never $n_f > 1.05$) to model possible local f^{3+}, f^{4+} or f^{2+} configurations. The diagrammatic expansion, if not stated otherwise, has been carried out up to the third order of expansion, $k = 3$. The convergence issue would be elaborated later.

In Fig. 1 we draw the phase diagram characterized by the value of the f-f electron $d_{x^2-y^2}$ component of the order parameter, $\Delta^{ff}_{G;1,0}$ on the total filling n - hybridization magnitude $|V|$ plane, with the f-state filling n_f marked. The values of the remaining d-wave contributions, $\Delta^{\alpha\beta}_{G;i_x-j_x,i_y-j_y}$ are less than 20% of the dominant $\Delta^{ff}_{G;1,0}$. In the inset we draw the SC gap magnitude and the condensation energy $\Delta E = E_{PM} - E_{SC}$ vs. U, where E_{PM} and E_{SC} are the ground state energies for the paramagnetic (normal) and SC states, respectively. It explicitly shows the emergence of the superconductivity as driven by the increasing electronic correlations. The superconductivity is suppressed in three limits on the $|V|$-n plane. First, SC disappears for low n and large $|V|$, as the f-orbital is not filled enough for correlations to matter; we need $n_f \gtrsim 0.8 - 0.85$ for that. Second, for low $|V|$ the superconductivity disappears as f electrons are loosing their itineracy induced by the coupling to the conduction band. Third, for large $|V|$, SC is suppressed because the correlations are again too weak.

In Fig. 2, top we show the order depednence of diagrammatic expansion on the example of the condensation energy along selected $|V| = 1$–direction (cf. also Fig. 1). As the $k = 3$ and $k = 4$ plots are practiclly the same, the satisfactory convergence is reached already in the third order ($k = 3$).

In Figs. 2 bottom and 3 top, we plot the condensation energy for the constant $|V|$ and n values. The lines in Fig. 3 are terminated for low $|V|$, as we could not obtain there a satisfactory numerical convergence for the self-consistent loop for the paramagnetic solution due to the presence of extremely enhanced hybridization peaks (cf. with Ref. [26]). The obtained condensation energy is large but reasonable for the heavy fermion systems. Nevertheless, the condensation energy can be suppresed by introducing frustrated hybridization, namely taking both the intersite and the onsite contributions. In the Fig. 3, bottom we show that considered by us correlation-driven superconductivity for low values of hybridization is of the non-BCS origin as we gain in the kinetic energy in SC with respect to the paramagnetic (normal) state.

For more precise reference to the experimental data, we address the case of $CeCoIn_5$ [6–8]. The Fermi level in this compound is placed lower in energy that the middle point

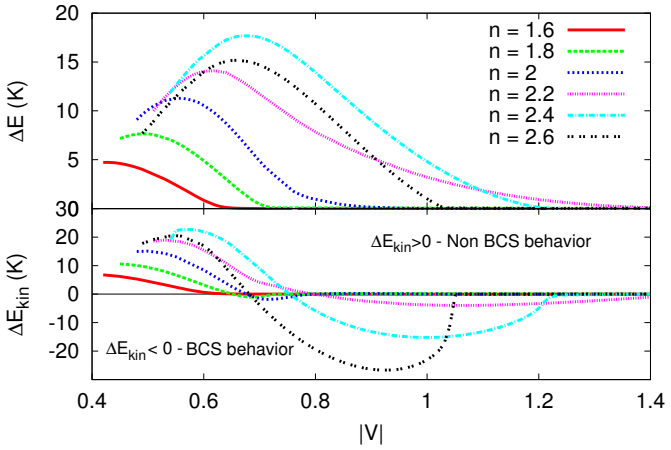

FIG. 3. Top: ΔE along the fixed $|V|$-directions. Bottom: Kinetic-energy difference for the same cases; $\Delta E_{kin} > 0$ marks a non-BCS behavior.

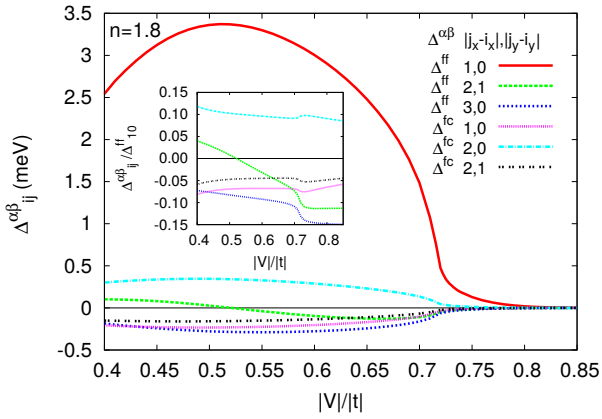

FIG. 4. Effective gap components with the leading d_{x-y^2}-wave symmetry of f-f order parameter. The components of relative amplitude $\Delta^{\alpha\beta}_{i_x-j_x,i_y-j_y}/\Delta^{ff}_{i_x-j_x,i_y-j_y} < 5\%$ are not included.

of the emergent hybridization gap, thus the regime of $n < 2$ in our model is suitable in this case. In this regime, the condensation energy for the non-BCS superconductivity is of the same order of magnitude as that for the $CeCoIn_5$ critical temperature ($T_s = 2.2K$) and e.g., for $n = 1.8$ and $|V| \simeq 0.65$ is explicitly the same (cf. Fig. 3, top).

For a further comparison with the experimental data for $CeCoIn_5$, in Fig. 4 we show the effective superconducting pairing components (lines) along $n = 1.8$ direction. Note that our effective Hamiltonian can serve as a direct rationalization of the phenomenological model used in Refs. [6–8]. The dominant line is that joining the f-f sites and of the $d_{x^2-y^2}$-wave symmetry, $\Delta^{ff}_{1,0}$. What is more important, our model also predicts a multiband superconductivity with the similar relation between the component gap magnitudes as proposed in recent experiments [6–8] (in the experiment $\sim 20\%$, here $\sim 10-15\%$ - cf. Fig. 4, inset).

Summary. The Anderson lattice model was solved here by the DE-GWF approach which includes intrinsic correlation-driven microscopic mechanism for superconductivity. Obtained superconducting state has several properties, recently found to exhibit by $CeCoIn_5$ [6–8] and most probably by other Ce-based superconductors [5, 9]: (i) The superconductivity is of non-BCS (the gain in the kinetic energy) and multiband (f-f and f-c pairing) character; (ii) The leading gap component is that for f-f pairing and $d_{x^2-y^2}$-wave symmetry; (iii) The values of condensation energy are in the reasonable range for the description of f-electron compounds superconducting critical temperatures.

The results incorporate SC as an intrinsic property of ALM as modeling heavy fermion compounds. This completes the full picture of ALM describing all, the most important emergent phenomena observed in heavy fermion systems.

The developed framework can be extended to the description of different symmetries of the superconducting order parameter and its spatial modulation (e.g. FFLO state), as well as study a coexistence or competition with magnetism.

Acknowledgements We are grateful for stimulating discussions with Jörg Bünemann. The work has been partially supported (MMW and JS) by the National Science Centre (NCN) under the Grant MAESTRO, No. DEC-2012/04/A/ST3/00342. JK acknowledges support from the People Programme (Marie Curie Actions) of the European Union's Seventh Framework Programme (FP7/2007-2013) under REA grant agreement n° [291734].

* marcin.wysokinski@uj.edu.pl
† jan.kaczmarczyk@uj.edu.pl
‡ ufspalek@if.uj.edu.pl

[1] F. Steglich, H. Aarts, C. Bredl, W. Lieke, D. Meschede, W. Franz, and H. Schäfer, Phys. Rev. Lett. **43**, 1892 (1979).
[2] F. Steglich, Phys. Stat. Solidi (b) **242**, 392 (2005).
[3] P. Riseborough, G. Schmiedeshoff, and J. L. Smith, *in The Physics of Superconductors*, Vol. II (Springer, Berlin, 2004) Chap. 10.
[4] J. D. Thompson and Z. Fizk, J. Phys. Soc. Jpn. **81**, 011002 (2012).
[5] D. J. Scalapino, Rev. Mod. Phys. **84**, 1383 (2012).
[6] J. S. Dyke, F. Massee, M. P. Allan, J. C. S. Davis, C. Petrovic, and D. K. Morr, Proc. Natl. Acad. Sci. **111**, 11663 (2014).
[7] B. B. Zhou, S. Misra, E. H. da Silva Neto, P. Aynajian, R. E. Baumbach, J. D. Thompson, E. D. Bauer, and A. Yazdani, Nature Physics **9**, 474 (2013).
[8] M. P. Allan, F. Massee, D. K. Morr, J. S. Dyke, A. W. Rost, A. P. Mackenzie, C. Petrovic, and J. C. S. Davis,

Nature Physics **9**, 468 (2013).
[9] C. Pfleiderer, Rev. Mod. Phys. **81**, 1551 (2009).
[10] P. Monthoux, D. Pines, and G. G. Lonzarich, Nature **450**, 1177 (2007).
[11] J. Bunemann, T. Schickling, and F. Gebhard, Eur. Phys. Lett. **98**, 27006 (2012).
[12] J. Kaczmarczyk, J. Spałek, T. Schickling, and J. Bünemann, Phys. Rev. B **88**, 115127 (2013).
[13] J. Kaczmarczyk, J. Bünemann, and J. Spałek, New J. Phys. **16**, 073018 (2014).
[14] J. Kaczmarczyk, Phil. Mag. **95**, 563 (2014).
[15] J. Kaczmarczyk, T. Schickling, and J. Bünemann, Phys. Status Solidi B. (2015), 10.1002/pssb.201552082.
[16] R. Flint and P. Coleman, Phys. Rev. Lett. **105**, 246404 (2010).
[17] O. Bodensiek, R. Žitko, M. Vojta, M. Jarrell, and T. Pruschke, Phys. Rev. Lett. **110**, 146406 (2013).
[18] M. Z. Asadzadeh, F. Becca, and M. Fabrizio, Phys. Rev. B **87**, 205144 (2013).
[19] M. Z. Asadzadeh, M. Fabrizio, and F. Becca, Phys. Rev. B **90**, 205113 (2014).
[20] J. Spałek, Phys. Rev. B **38**, 208 (1988).
[21] H. Weber and M. Vojta, Phys. Rev. B **77**, 125118 (2008).
[22] O. Howczak, J. Kaczmarczyk, and J. Spałek, Phys. Stat. Solidi (b) **250**, 609 (2013).
[23] K. Masuda and D. Yamamoto, Phys. Rev. B **87**, 014516 (2013).
[24] A. T. Holmes, D. Jaccard, and K. Miyake, J. Phys. Soc. Jpn. **76**, 051002 (2007).
[25] K. Miyake, S. Schmitt-Rink, and C. M. Varma, Phys. Rev. B **34**, 6554 (1986).
[26] M. M. Wysokiński, J. Kaczmarczyk, and J. Spałek, unpublished (2015).
[27] F. Gebhard, Phys. Rev. B **41**, 9452 (1990).
[28] J. Kaczmarczyk, T. Schickling, and J. Bünemann, Phys. Status Solidi b (2015).
[29] P. G. de Gennes, *Superconductivity in Metals and Alloys* (W. A. Benjamin, New York, 1966).

3.8 Additional project: Transport through the superconducting hybrid junctions

During my PhD studies I have pursued additional project [122, 123, 124] not connected with the strongly correlated systems, however related with the part of the topic of this Thesis, namely concerning superconductivity.

Blonder, Tinkham and Klapwijk (BTK) in their seminal work [150] have developed approach based on the Bogoliubov - de Gennes equations for the electric transport including Andreev reflection processes through the conventional superconductor - normal conductor ballistic junction under assumption of the dirty contact modeled by the scattering potential at the interface. This straightforward and transparent approach has successfully explained observed experimental conductance characteristics for the case of conventional s-wave symmetry of the superconducting order parameter[151]. The theory was generalized also to account for the different symmetries, e.g., d-wave [152]. It turned out to be important tool for the interpretations of the spectroscopic measurements reveling the nature of superconductors itself.

Due to the symmetry of the superconducting state and the assumed constant density of states close to the Fermi energy BTK formalism gives no thermoelectric power in the standard case. This transport coefficient is very important parameter and many controversies exist about its measurements in the superconductors and the structures containing superconductors [153]. One of the attempts to obtain nonzero thermoelectric signal was the consideration of the energy dependent superconducting gap, $\Delta(E)$ [154] as suggested for the hole superconductivity.

3.8.1 Article B.1. Thermoelectric Effect in the Normal Conductor - Superconductor Junction: A BTK Approach

In Article B.1 [122] we have developed the theory intimately based on the BTK approach which give rise to the nonzero thermopower and is based on the explicit consideration of the energy dependent density of states. It was explicitly calculated for the free electron gas in different dimensional situations as well as for the case where Fermi level was near the Van Hove singularity. Thermopower was found to be the strongest when the Fermi level is placed close to the band bottom, e.g., as in the case of the heavy fermion systems.

Thermoelectric Effect in the Normal Conductor–Superconductor Junction: A BTK Approach

M.M. Wysokiński*

Marian Smoluchowski Institute of Physics, Jagiellonian University, W.S. Reymonta 4, 30-059 Kraków, Poland

(Received August 17, 2012)

The thermopower of the junction between normal conductor and s-wave superconductor has been investigated. For this purpose we have analyzed in detail a simple generalization of the Blonder–Tinkham–Klapwijk theory by taking into account explicitly an energy dependence of the density of states near the Fermi level. Both linear and nonlinear thermopowers have been calculated for 3D free electron gas, 3D Fermi liquid, and the case with Van Hove singularity in the vicinity of the Fermi level. In the linear regime, for all models, the thermopower as function of temperature has a clear maximum with its position and the value depending strongly on the junction barrier strength. In the nonlinear regime, we have found very large values of the thermopower (up to $8k_{\rm B}/e$) and strongly asymmetric behavior with respect to the change of the temperature gradient sign.

PACS: 74.45.+c, 74.25.fg, 73.23.Ad

1. Introduction

Tunneling spectroscopy between normal and superconducting (NS) materials is one of the most effective tools to study the nature of the superconducting state [1, 2]. Despite the existence of energy gap in superconductor (SC), quantum transport is still possible for energies below the gap value by means of reflection of the incident electron as a hole with the opposite charge and momentum, as predicted by Andreev [3, 4]. Currents flowing across the junction of an arbitrary transparency were theoretically analyzed in the seminal paper of Blonder, Tinkham, and Klapwijk (BTK) [5]. They have discussed a continuous transition from the tunneling limit to the metallic regime. The theory was shown to be successful in describing experimental data of the current–voltage characteristics in point contacts [6–8].

There were many extensions of this theory, related to incorporating different nature of superconducting state: d-wave symmetry of the order parameter [9], the Fulde–Ferrell–Larkin–Ovchinnikov state [10, 11], hole superconductivity [12], two-band superconductivity [13], dimensionality of the problem [14, 15], as well as different type of the non-superconducting material of the junction: ferromagnet [16], semiconductor [17], graphene [18]. The theory was also successfully adapted to the molecular junctions [19]. The main strength of the BTK approach is its simplicity and possibility of studying exotic features in a straightforward manner.

Nonetheless, the electrical conductance does not provide the full understanding of the system. For example, it is important to look into the thermodynamic properties of particular materials and their electrical response to the temperature gradient. In general, the problem of thermoelectric phenomenon in superconductors and in the superconductive junctions was studied extensively both theoretically [20–31] and experimentally [32–34] with an astonishing precision. Namely, the temperature and the voltage is measured to the order of mK and μV, respectively. Also, in majority of those papers the thermoelectric effect was analyzed using the Green function approach. Explicitly, the Eilenberger–Usadel equations [35] were used, as they seem to be the most effective modern tool in the description of thermoelectric properties of superconductive systems. However, despite the great progress achieved in the field during last two decades, the thermopower of such systems is still not fully understood [36]. In the words of the recent review [36]: "a significant advance in the theory is required before the thermopower of mesoscopic proximity-coupled systems is understood".

In view of the successes of the BTK theory to describe conductance of the system it is of interest to study the thermopower also within this intuitive approach. Although it was employed earlier in some special cases [12, 37] in its simple form leads to zero thermopower irrespectively of the temperature difference over the junction. Here we propose a simple extension of the theory to include thermodynamic properties of the quantum fluids on both sides of the junction, particularly non-trivial density of states naturally gives rise to the Seeback effect.

* e-mail: marcin.wysokinski@uj.edu.pl

Additionally, as in the case of conductance, this approach can be further generalized to take into account specific features of some exotic materials (e.g., those with non-standard band mass distribution, nontrivial gap symmetry, realistic dimensionality of the system).

Usually, the effect of density of states (DOS) energy dependence in the NS junctions current characteristics is ignored. Even though, it is negligible when conductance is studied, in the case of the thermopower it has turned out to be crucial. Therefore this modification to the BTK approach would complete the picture of the thermoelectric effect in planar NS junctions. The effect of the DOS in the similar manner was also considered earlier by Mazin [38] in the context of measuring the spin polarization of the ferromagnet in the ferromagnet–superconductor junction, and by Kupka [15] in the context of realistic three-dimensional geometry of NS junction.

Here we present the general framework which allows to obtain a nonzero Seebeck effect within the extended BTK approach, and applied to the simplest case of the normal metal–s-wave superconductor junction. Namely, we include explicitly the effect of the non-constant DOS around the Fermi level and apply it to the following selected situations: 3D free electron gas and 3D Fermi liquid. This inclusion gives rise to the nonzero thermoelectric effect, and results in large thermopower value across the junction. Particular set of parameters, leading to the large value of the thermopower, can possibly be realized in heavy fermion systems, where a small Fermi velocity implies a large value of dimensionless parameter modeling the barrier strength. Additionally, we have also discussed the effect of the logarithmic Van Hove singularity (VHS) present in the vicinity of the Fermi energy that gives possibility to study the thermopower also in the case of negative slope of DOS.

The paper is organized as follows. In Sect. 2 we discuss BTK theory with an explicit inclusion of energy dependent DOS, as well as refer to the previous works on the thermoelectric effect in NS junction. In Sect. 3 we derive the modified BTK formula for the case of 3D free electron gas and present results concerning the thermopower, both in the linear and the nonlinear regimes. Additionally we apply this approach to the Fermi liquid case. In Sect. 4 we extend our analysis to the case of DOS with VHS represented by a logarithmic function. Finally, in Sect. 5, we provide a brief summary.

2. Model and Approach

2.1. Modified Blonder–Tinkham–Klapwijk formalism

The BTK theory [5] describes electrical current through the NS junction. The starting point are the Bogoliubov–de Gennes equations [39] describing a two-component wave function $\begin{pmatrix} u \\ v \end{pmatrix}$ for s-wave superconductor with a constant superconducting gap Δ:

$$\begin{pmatrix} \mathcal{H} & \Delta \\ \Delta^* & -\mathcal{H}^\dagger \end{pmatrix} \begin{pmatrix} u \\ v \end{pmatrix} = E \begin{pmatrix} u \\ v \end{pmatrix}, \tag{1}$$

where the Hamiltonian for free electron gas reads $\mathcal{H} = -\frac{\hbar^2\nabla^2}{2m} - \mu(x) + V(x)$. The potential, utilized in the form $V(x) = K\delta(x)$, models the interfacial scattering. For convenience we also introduce dimensionless barrier strength $Z = K/\hbar v_{\mathrm{F}}$. In BTK formalism, one considers incident electron which is scattered by different processes at the interface with a finite transparency: it can be reflected, reflected as a hole (Andreev reflection — AR) or transmitted as a quasiparticle. For the states taking part in the tunneling processes, employing plane wave approximation, the corresponding multicomponent wave function is constructed. For simplicity we assume that all of particles have the same value of the momentum equal to the Fermi momentum. Applying the standard boundary conditions, i.e., by demanding continuity of the wave functions and their spatial derivatives at the interface, one can derive the probabilities of all the processes. Using those probabilities, following BTK, the net current formula is obtained in the following form [5]:

$$\begin{aligned} I_{\mathrm{NS}} = 2N(0)ev_{\mathrm{F}}\mathcal{A}\int_{-\infty}^{\infty}\Big\{&\big[1-B(E)\big]f^{\mathrm{N}}(E-eV) \\ &- A(E)f^{\mathrm{N}}(E+eV) \\ &- \big[1-A(E)-B(E)\big]f^{\mathrm{S}}(E)\Big\}\,\mathrm{d}E, \end{aligned} \tag{2}$$

where $N(0)$ denotes DOS at the Fermi level, v_{F} is the Fermi velocity, $\mathcal{A}$ is the area of contact, and f^{N}, f^{S} are the Fermi distribution functions for the NC and SC, respectively. Functions $A(E)$ and $B(E)$ are the tunneling probabilities of the hole (Andreev) reflection and the usual reflection of the incident electron, respectively. For simplicity, we also define the transfer probability

$$\begin{aligned} T(E) \equiv{}& (1-B)f^{\mathrm{N}}(E-eV) - Af^{\mathrm{N}}(E+eV) \\ &- (1-A-B)f^{\mathrm{S}}(E). \end{aligned} \tag{3}$$

BTK approach has been generalized to realistic 3-dimensional geometry, where $T(E)$ depends also on the angle of incidence, as shown in a number of papers [14, 15]. However, the main contribution to the current is provided for angles of incidence close to zero, effectively similar to one-dimensional geometry (for justification, see Ref. [15] and references therein).

In the one-dimensional case, the product of the DOS ($\sim \partial k/\partial E_k$) and the charge carriers velocity ($\sim \partial E_k/\partial k$) is constant. In more general case, this assumption is well justified for calculating current–voltage characteristics, but it is insufficient for more subtle effects such as the thermoelectricity considered here. Also, it is important to include the effect of energy-dependent DOS in the study of spin-polarization of the ferromagnet in the case of the ferromagnet–superconductor junction [38].

In BTK approach [5], electrons contributing to the current are only those whose velocities are directed towards the junction i.e. those with $v_x > 0$. The current (2) through junction of area $\mathcal{A}$ can be rewritten in the spirit of the Landauer–Büttiker approach to the elec-

tronic transport as

$$I_{\rm NS} = e\mathcal{A}\sum_{k,\sigma} v_x T(E_k), \tag{4}$$

with $T(E_k)$ given by (3). In higher-dimension geometries, the energy dependence of DOS does not cancel out with that of the group velocity. In those cases, we have to take into account explicitly the product of DOS and velocity in the net current formula, i.e., start from the formula

$$I_{\rm NS} = 2e\mathcal{A}\int_0^\infty {\rm d}E T(E) \oint_{v_x>0} \frac{{\rm d}S(E)}{|\nabla_k E|} v_x. \tag{5}$$

In this formula we treat DOS rather as a "number of conductance channels". This concept is based on the assumption of not taking into account the fact that the hole retracing electron path is on the opposite side of the Fermi surface and therefore, feels different DOS. We also neglect the shift of DOS due to non-zero voltage over the junction, since it rather weakly influences the current characteristics. The resulting integral over the equi-energy surfaces can be solved by introducing the explicit energy dependence. This simple effect, in turn modifies the final BTK formula. In Sect. 3 we present our calculations of the thermopower taking into account the parabolic dispersion relation in the 3D free electron gas and linear dispersion relation around the Fermi energy for 3D Fermi liquid [40].

2.2. Thermopower definition

As said above, in the standard BTK approach there is no nonzero thermopower due to the symmetry in expression (2) irrespectively of the temperature difference. However, the assumptions introduced in more specific models give rise to the non-zero thermopower in NS junctions. The only works exploring thermoelectric properties of the NS junction via BTK formalism is that by Hirsch [12, 37]. He explored thermoelectric phenomena by including the energy dependent superconducting gap function [12] observed in the hole-superconductivity model, as well as by considering a more realistic rectangular barrier of finite width [37]. The latter case was also investigated in the case of ferromagnet–superconductor Andreev point contacts [41]. Here, the source of the thermoelectric effect in the NS junction is the energy dependence of v_x and of DOS, as expressed in (5). This feature does not alter much the conductivity, but gives rise to the thermoelectric phenomena.

By keeping the two electrodes at different temperature or applying voltage, we obtain a non-zero current through the junction. If both the voltage V and the temperature difference δT are small, we can write that the total current as

$$I_{\rm e} = L_{11}V + L_{12}\delta T. \tag{6}$$

The quantity that measures the thermoelectric effect is the thermopower or the Seebeck coefficient S, which is defined as the voltage driving to zero the current flowing in response to the temperature difference. This means that

$$S \equiv -\left(\frac{V}{\delta T}\right)_{\rm I=0} = \frac{L_{12}}{L_{11}}. \tag{7}$$

3. 3D Free-electron-gas case

For 3D free electron gas, the integral in (5) can be carried out analytically and is equal to

$$\oint_{v_x>0} \frac{{\rm d}S(E)}{|\nabla_k E|} v_x = \frac{k^2}{\hbar}\int_{\frac{-\pi}{2}}^{\frac{\pi}{2}} {\rm d}\theta \int_{\frac{-\pi}{2}}^{\frac{\pi}{2}} {\rm d}\phi \cos^2(\theta)\cos(\phi) = \frac{2m\pi E}{\hbar^3}. \tag{8}$$

We have obtained linear energy dependence, which in turns modifies the BTK net-current formula in the following manner:

$$I_{\rm NS} = \frac{1+Z^2}{eE_{\rm F}R_{\rm N}}\int_{-E_{\rm F}}^{\infty} (E+E_{\rm F})T(E)\,{\rm d}E. \tag{9}$$

As in the BTK papers [5], we have set the chemical potential equal to zero and thus, in the final result have shifted energies by the Fermi energy. Also, the current is normalized by the resistance of the NN junction [5] ($R_{\rm N}$). Let us note that in all numerical calculations discussed in the next sections we have taken the Fermi energy equal to $E_{\rm F} = 150\Delta$.

3.1. Linear regime

In Fig. 1 we draw schematically the NS junction. The black rectangle represents the barrier and the gray regions in it mark the regime of energies, for which the probability $A(E)$ is large ≈ 1. The dashed line show the chemical potential, taken as zero of energy. The bias is applied to the normal metal only. The black lines are the Fermi distributions on the cold and the warm sides of the junction. δT is the temperature difference across the junction.

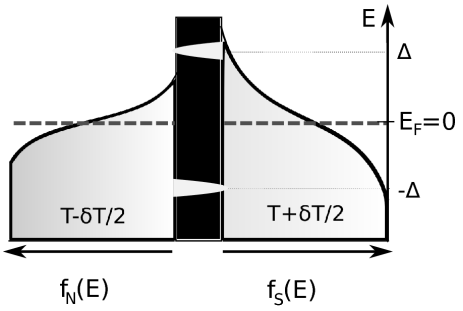

Fig. 1. Schematic diagram showing energetic properties of the NS junction in the limit of strong barrier, where the NC is colder than SC. The black rectangle represents the barrier. Heavy black lines show the Fermi functions. Dashed line denotes (common) Fermi energy, and thin lines on the right indicate positions of energy gap ($\pm\Delta$).

In the linear regime and very small temperature difference and voltage, δT, $V \to 0$, we expand the Fermi functions in the Taylor series, which to the first order are

$$f^{\mathrm{N}} = f_{T-\delta T/2}(E - eV) = f_T(E) - eV\frac{\partial f}{\partial E} + \frac{\delta T}{2T}E\frac{\partial f}{\partial E},$$

$$f^{\mathrm{S}} = f_{T+\delta T/2}(E) = f_T(E) - \frac{\delta T}{2T}E\frac{\partial f}{\partial E}. \qquad (10)$$

Substituting those forms to Eq. (5) we obtain the explicit formula for the thermopower

$$S = \frac{\int \frac{\partial f}{\partial E}E(E+E_{\mathrm{F}})(1-B-A)\,\mathrm{d}E}{k_{\mathrm{B}}T\int \frac{\partial f}{\partial E}(E+E_{\mathrm{F}})(1-B+A)\,\mathrm{d}E}\frac{k_{\mathrm{B}}}{e}. \qquad (11)$$

In Fig. 2 we present temperature dependence of the thermopower in the linear regime for selected values of the barrier strength, Z. The tendency is similar to that obtained by Hirsch [12]. Namely, with the increase of the barrier strength the thermopower increases. Also, for sufficiently high barrier strengths we have obtained a clear maximum of the thermopower as a function of temperature. The temperature dependence remains similar in the nonlinear regime (for larger temperature difference, δT), with slightly changed position of the thermopower maximum. What is worth mentioning the character of the thermopower temperature dependence for larger barrier strengths qualitatively agrees with the corresponding thermopower dependence calculated within the Usadel-equation framework [27].

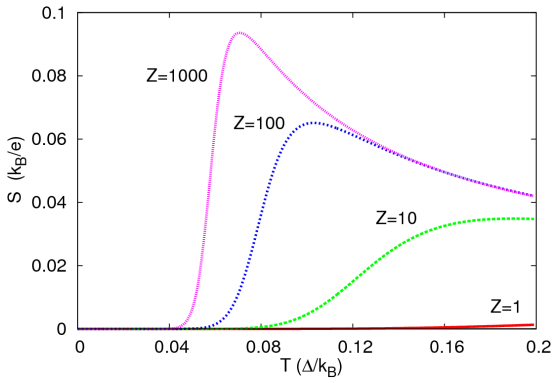

Fig. 2. Temperature dependence of the linear thermopower for selected barrier strength values, Z. The case of 3D free electron gas is considered.

The relevant energies of the junction are schematically presented as the diagram in Fig. 1. Probability of AR, $A(E)$, is equal to 1 for energies $\pm\Delta$, irrespectively of the value of the barrier strength [5]. Therefore, in the large barrier strength limit, $Z \to \infty$, the transport is almost blocked for all energies except for those close to $\pm\Delta$. Due to this circumstance, we obtain practically zero thermopower for temperatures less than $T = 0.05\Delta/k_{\mathrm{B}}$. In this limit, thermal excitations do not reach the upper channel of transmission around $+\Delta$ and there are fully occupied states on both sides of the junction for $E = -\Delta$. Once the temperature crosses this limit, we reach a maximum for the thermopower and subsequently the part T^{-1} starts dominating for all barrier strengths. The highest temperature shown in Fig. 2 is $T = 0.2\Delta/k_{\mathrm{B}}$, as we do not take into account the temperature dependence of the superconducting gap.

3.2. Nonlinear regime

In this section we present numerical results in the nonlinear regime. The thermopower depends on the barrier strength Z, temperature T, and the temperature difference δT. We have obtained asymmetric behavior of the thermopower (Fig. 3b–d) as a function of temperature difference δT, despite of the symmetric behavior of the zero-voltage current (Fig. 3a). For the positive sign of the temperature difference, we have obtained large values of the thermopower (up to $8k_{\mathrm{B}}/e$) in spite of a relatively small currents.

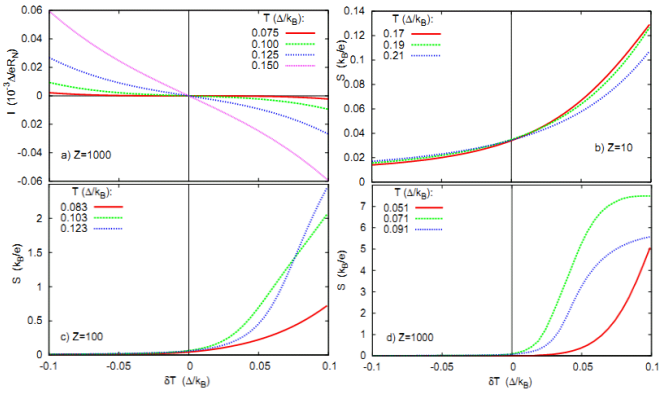

Fig. 3. Nonlinear zero-voltage current as a function of temperature difference, δT for selected values of the average temperature (T) in the system, for the barrier strength parameter $Z = 1000$ (part (a)) and nonlinear thermopower as a function of the temperature difference (δT) for selected temperatures (T) of the junction (around the temperature of the maximal linear thermopower, cf. Fig. 2) and selected values of barrier strength parameter $Z = 10, 100, 1000$ (parts (b), (c), and (d), respectively). 3D free electron gas is considered.

The asymmetry can be understood via a simple picture (cf. Fig. 1). For any temperature difference when at least one of the temperatures is high enough for thermal excitations to reach the transmission channel ($+\Delta$), a relatively large current is flowing through the junction. Consider the temperature difference of a positive sign, so the thermal smearing in SC is higher than in NC, such as thermal excitations in the former reach the energy equal to Δ. The voltage, applied to NC in order to have zero net current, shifts the Fermi energy in the NC with respect to the Fermi energy in the SC.

Large voltages are required to compensate for thermally induced currents. Therefore, we have a relatively high thermopower. The opposite happens for the negative sign of the temperature difference. In that situation even small shift of the Fermi energy in the NC results in the large change of the flowing current, and one gets small thermopower.

In a similar manner, we may argue about the behavior of the thermopower as a function of the barrier strength,

observed clearly in the linear regime. With the increasing parameter Z, the main transmission channels around energies $\pm\Delta$ are narrower. For that reason, we have to shift the Fermi level by a larger voltage to have zero net current over the junction.

3.3. 3D Fermi-liquid case

It was shown first by Landau [42] that a more accurate description of electrons in metals is the theory of the Fermi liquid taking into account interaction between particles near the Fermi energy. This theory assumes linear dispersion relation in the vicinity of the Fermi level, i.e.

$$E_k - E_{\rm F} = \hbar v_{\rm F}(k - k_{\rm F}), \tag{12}$$

with the Fermi velocity $v_{\rm F} = \hbar k_{\rm F}/m^*$, where $k_{\rm F}$ is the Fermi momentum and m^* the enhanced effective mass. Since the Fermi liquid is considered to be more realistic description of electrons in metals, we have calculated analytically the product of the DOS and velocity within this model in three dimensions

$$\oint_{v_x>0} \frac{{\rm d}S(E)}{|\nabla_k E|} v_x = \frac{k^2}{\hbar} \int_{\frac{-\pi}{2}}^{\frac{\pi}{2}} {\rm d}\theta \int_{\frac{-\pi}{2}}^{\frac{\pi}{2}} {\rm d}\phi \cos^2(\theta)\cos(\phi)$$
$$= \frac{(E+E_{\rm F})^2\pi}{\hbar^3 v_{\rm F}^2}. \tag{13}$$

The energy dependence is explicitly quadratic and different from the corresponding linear dependence for 3D free electron gas, cf. Eq. (8). The numerical results, however, both in linear and nonlinear regime differ only slightly from those shown for a 3D free electron gas and we do not present them here.

4. Effect of the Van Hove singularity

In Sects. 3 and 4 we have presented a consistent argument for the importance of the DOS shape on the thermopower in the 3D free electron gas, and in the 3D Fermi liquid. For the sake of completeness, we have investigated the thermopower within the model, in which we include in the integrand (5) the form of DOS with Van Hove singularity (VHS). We model the VHS by logarithmic function of energy with fitting parameters taken from the two-dimensional tight-binding model [43], namely:

$$N(E) = b_1 \ln\left|\frac{E}{b_2}\right|, \tag{14}$$

with $b_1 = -0.04687|t|^{-1}$, and $b_2 = 21.17796|t|$, where t is hopping, taken as $|t| = 100\Delta$.

This model corresponds to the assumption of constant velocity and realistic DOS. In the linear regime, thermopower can be expressed as

$$S = \frac{\int \frac{\partial f}{\partial E} E\left(\ln|\frac{E-\alpha}{b_2}|\right)(1-B-A)\,{\rm d}E}{k_{\rm B}T\int \frac{\partial f}{\partial E}\left(\ln|\frac{E-\alpha}{b_2}|\right)(1-B+A)\,{\rm d}E}\frac{k_{\rm B}}{e}, \tag{15}$$

where α denotes a relative shift (chosen arbitrarily) of the Fermi energy with respect to VHS. There were experiments in which the Fermi energy was found in a very close vicinity of the VHS [44, 45], or moved appreciably relative to it.

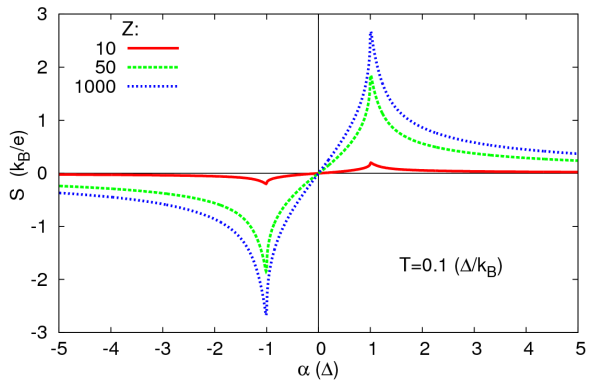

Fig. 4. The dependence of the linear thermopower on the relative shift of the Fermi energy with respect to Van Hove singularity α for a few values of barrier strength parameter Z. The average temperature in the system is taken as $T = 0.1\Delta/k_{\rm B}$.

The results of the linear thermopower as a function of parameter α for different values of barrier strengths for the fixed temperature $T = 0.1\Delta/k_{\rm B}$, are presented in Fig. 4. The maximum of the thermopower is well pronounced and fixed to the particular value of the shift of the Fermi energy with respect to the VHS, $\alpha = \Delta$. Therefore, we have studied the linear temperature dependence of the thermopower and nonlinear effects, particularly for $\alpha = \Delta$. The behavior of temperature dependence of the linear thermopower (not shown) is similar as that for 3D gas and for the Fermi liquid, but the values are larger than in the previous cases. The interesting feature of this model is that when the Fermi energy crosses the VHS, thermopower changes sign. This behavior of the thermopower is very different from that found by Hirsch who postulated universality of the thermopower sign for the hole theory of SC [12]. This observation seems to be very promising for the future experimental verification.

5. Conclusions

In this paper we have extended the Blonder, Tinkham, Klapwijk approach [5] to the tunneling spectroscopy between normal metal and superconducting materials of s-wave type. Our contribution is to go beyond the approximation of the constant product of the density of states (DOS) and the group velocity of charge carriers. Inspired by the papers of Mazin [38] and Kupka [15] we have introduced to the BTK current formula an explicit energy dependence of the product of DOS and the velocity. For the case of 3D free-electron gas, the product was found to be linear in energy, whereas within the Fermi liquid theory, quadratic. This modification virtually does not affect the current–voltage characteristics or conductance of the NS junction, but it gives rise to the thermoelectric effect. Previously only Hirsch [12, 37] examined the thermopower in NS junction via BTK approach in special cases by introducing either the energy-dependent

superconducting gap function [12] (in the so-called model of the hole superconductivity) or by invoking the barrier with finite width [37].

Both linear and nonlinear regimes of thermopower were studied for the cases of free electron gas, the Fermi liquid, and for the model with the logarithmic Van Hove singularity. With the increase of the barrier strength the thermopower increases. We believe that heavy fermion systems are promising for the experimental verification of our theoretical predictions, since low values of the Fermi velocity should result in high value of the effective barrier strength.

We have found a maximum of the thermopower as a function of average junction temperature (Fig. 2). Behavior is qualitatively similar to that obtained via the Usadel–Eilenberger equations [27]. In the nonlinear regime, we have investigated additionally its dependence on the temperature difference, where we have found a spectacular asymmetry of the thermopower with respect to δT sign inversion (Fig. 3b–d), irrespectively of the fact that the zero-voltage current is completely symmetric (Fig. 3a). This can be attributed to the asymmetry of the system, where by applying the voltage one shifts the Fermi energy of the normal conductor with respect to the superconducting gap in the superconductor.

The approach can be applied also for the studies of 2D systems. The integral in (5) leads to either $\sqrt{E}$ or E dependence of the velocity times DOS function for 2D free electrons and the Landau–Fermi liquid, respectively.

Studies of the thermopower in the case of DOS with Van Hove singularity intuitively shows that the thermopower has different sign on the negative and positive slope of DOS (Fig. 4). Similar behavior of the thermopower can be expected for the Kondo insulators. In those systems one observes a sharp minimum in the DOS at the Fermi level which is sometimes considered to be a small semiconducting-like gap between the bands. Let us note that BTK theory predicts extremely large values of the barrier strength parameter Z in heavy fermion systems resulting from the small value of the Fermi velocity (this is also the case for large differences between the Fermi velocities on the both sides of the junction interface [1]). However, this would require an extension of the present approach to the situation with strongly correlated electrons [46–48].

Acknowledgments

The work has been partially supported by the Foundation for Polish Science (FNP) under the TEAM program. The author greatly appreciates the stimulating discussion with Professor Józef Spałek resulting in proposition of taking into consideration Fermi liquid case and critical reading of the manuscript.

References

[1] G. Deutscher, *Rev. Mod. Phys.* **77**, 109 (2005).

[2] D. Daghero, R.S. Gonnelli, *Supercond. Sci. Technol.* **23**, 043001 (2010).

[3] A. Andreev, *Sov. Phys.-JETP* **19**, 1228 (1964).

[4] A. Andreev, *Zh. Eksp. Teor. Fiz.* **46**, 1823 (1964).

[5] G.E. Blonder, M. Tinkham, T.M. Klapwijk, *Phys. Rev. B* **25**, 4515 (1982).

[6] G.E. Blonder, M. Tinkham, *Phys. Rev. B* **27**, 112 (1983).

[7] G.J. Strijkers, Y. Ji, F.Y. Yang, C.L. Chien, J.M. Byers, *Phys. Rev. B* **63**, 104510 (2001).

[8] J.Y.T. Wei, N.-C. Yeh, D.F. Garrigus, M. Strasik, *Phys. Rev. Lett.* **81**, 2542 (1998).

[9] C. Bruder, *Phys. Rev. B* **41**, 4017 (1990).

[10] J. Kaczmarczyk, M. Sadzikowski, J. Spałek, *Phys. Rev. B* **84**, 094525 (2011).

[11] J. Kaczmarczyk, M. Sadzikowski, J. Spałek, *Physica C* **471**, 193 (2011).

[12] J.E. Hirsch, *Phys. Rev. B* **50**, 5 (1994).

[13] V. Lukic, E.J. Nicol, *Phys. Rev. B* **76**, 144508 (2007).

[14] N.A. Mortensen, K. Flensberg, A.P. Jauho, *Phys. Rev. B* **59**, 10176 (1999).

[15] M. Kupka, *J. Phys., Condens. Matter* **2**, 10599 (1990).

[16] I.I. Mazin, A.A. Golubov, B. Nadgorny, *J. Appl. Phys.* **89**, 7576 (2001).

[17] M. Veldhorst, A. Brinkman, *Phys. Rev. Lett.* **105**, 107002 (2010).

[18] J. Linder, A. Sudbo, *Phys. Rev. B* **77**, 064507 (2008).

[19] T. Domański, A. Donabidowicz, K.I. Wysokiński, *Phys. Rev. B* **78**, 144515 (2008).

[20] V.L. Ginzburg, *Zh. Eksp. Teor. Fiz.* **14**, 177 (1944).

[21] Y. Galperin, V. Gurevich, V. Kozub, *JETP Lett.* **17**, 476 (1973).

[22] Y. Galperin, V. Gurevich, V. Kozub, *Zh. Eksp. Teor. Fiz.* **17**, 687 (1973).

[23] Y.G.V.G.A.G. Aronov, V. Kozub, *Adv. Phys.* **30**, 539 (1981).

[24] Y.M. Galperin, V.L. Gurevich, V.I. Kozub, A.L. Shelankov, *Phys. Rev. B* **65**, 064531 (2002).

[25] N.R. Claughton, C.J. Lambert, *Phys. Rev. B* **53**, 6605 (1996).

[26] R. Seviour, A.F. Volkov, *Phys. Rev. B* **62**, R6116 (2000).

[27] P. Virtanen, T. Heikkilaä, *Appl. Phys. A* **89**, 625 (2007).

[28] A.F. Volkov, V.V. Pavlovskii, *Phys. Rev. B* **72**, 014529 (2005).

[29] K.I. Wysokiński, *Phys. Rev. B* **82**, 115423 (2010).

[30] J.E. Hirsch, *Phys. Rev. Lett.* **72**, 558 (1994).

[31] A. Bardas, D. Averin, *Phys. Rev. B* **52**, 12873 (1995).

[32] J. Eom, C. Chien, V. Chandrasekhar, *Phys. Rev. Lett.* **81**, 437 (1998).

[33] D.A. Dikin, S. Jung, V. Chandrasekhar, *Phys. Rev. B* **65**, 012511 (2001).

[34] A. Parsons, I.A. Sosnin, V.T. Petrashov, *Phys. Rev. B* **67**, 140502 (2003).

[35] K.D. Usadel, *Phys. Rev. Lett.* **25**, 507 (1970).

[36] V. Chandrasekhar, *Supercond. Sci. Technol.* **22**, 083001 (2009).

[37] J.E. Hirsch, *Phys. Rev. B* **58**, 8727 (1998).

[38] I.I. Mazin, *Phys. Rev. Lett.* **83**, 1427 (1999).

[39] P.G. de Gennes, *Superconductivity in Metals and Alloys*, W.A. Benjamin, New York 1966, Ch. 5.

[40] J.B. Ketterson, S.N. Song, *Superconductivity*, Cambridge University Press, Cambridge 1999, Ch. 24.

[41] P. Wójcik, A. Naylor, M. Wołoszyn, B.J. Hickey, B.J. Spisak, J. Adamowski, *J. Supercond. Novel Magn.* **24**, 939 (2011).

[42] L.D. Landau, *Sov. Phys.-JETP* **8**, 70 (1959).

[43] R. Szczesniak, M. Mierzejewski, J. Zielinski, P. Entel, *Solid State Commun.* **117**, 369 (2001).

[44] D.H. Lu, M. Schmidt, T.R. Cummins, S. Schuppler, F. Lichtenberg, J.G. Bednorz, *Phys. Rev. Lett.* **76**, 4845 (1996).

[45] A. Piriou, N. Jenkins, C. Berthod, I. Maggio-Aprile, F.O., *Nature Commun.* **2**, 221 (2011).

[46] A reliable mean-field approach in the form of statistically consistent renormalized mean-field theory has been formulated in [47, 48].

[47] J. Kaczmarczyk, J. Spałek, *Phys. Rev. B* **84**, 125140 (2011).

[48] J. Jędrak, J. Spałek, *Phys. Rev. B* **83**, 104512 (2011).

3.8.2 Article B.2. Seebeck effect in the graphene-superconductor junction

In Article B.2 [123] we have accounted for the explicit energy dependence for the graphene density of states and within the framework of the Dirac-Bogoliubov-de Gennes equations [155] we have studied Seebeck effect. According to the predictions obtained for the conventional superconductors, we have obtained that large values of the thermopower are for the situation where the Fermi level is not much shifted from zero (Dirac point) and roughly does not exceed the specular Andreev reflection regime.

JOURNAL OF APPLIED PHYSICS **113**, 163905 (2013)

Seebeck effect in the graphene-superconductor junction

Marcin M. Wysokiński[1,a)] and Jozef Spałek[1,2,b)]
[1]*Marian Smoluchowski Institute of Physics, Jagiellonian University, Reymonta 4, PL-30-059 Kraków, Poland*
[2]*Faculty of Physics and Applied Computer Science, AGH University of Science and Technology, Reymonta 19, PL-30-059 Kraków, Poland*

(Received 19 February 2013; accepted 3 April 2013; published online 25 April 2013)

Thermopower of graphene-superconductor (GS) junction is analyzed within the extended Blonder-Tinkham-Klapwijk formalism. Within this approach, we have also calculated the temperature dependence of the zero-bias conductance for GS junction. Both quantities reflect quasi-relativistic nature of massless Dirac fermions in graphene. Both the linear and the non-linear regimes are considered. © *2013 AIP Publishing LLC*. [http://dx.doi.org/10.1063/1.4802503]

I. INTRODUCTION

Graphene is one of the most remarkable new materials. Not only has its discovery[1] violated in same sense Landau's theory of the thermodynamical instability of a two-dimensional structure[2] but also due to the peculiar band structure it has provided us with an invaluable opportunity to test relativistic quantum electrodynamics in the desktop laboratory.[3] For that reason, much effort has been put into understanding of the phenomena associated with this material.

Since the graphene-based devices are usually considered as a mesoscopic systems, the Landauer approach is widely utilized to study the ballistic transport in them.[4–6] Even though this approach does not account in the simplest form for all the features of the material, it provides a good overall description of the electric transport. This approach was extended by Blonder, Tinkham, and Klapwijk[7] (BTK) to the case of standard normal metal-superconductor (NS) junction, and in this manner yielded a very good description of the experimental data.[8] Their method has been widely used for different specific situations[9–17] and finally adapted for graphene-superconductor (GS) hybrid systems.[18–22] One of the most peculiar properties predicted in such systems is the specular Andreev reflection and deviations of the conductance spectra[18] from those predicted by BTK for normal metals.[7]

Landauer formalism has also been successfully adapted for thermoelectrical transport in mesoscopic devices.[23–25] In the case of standard NS junctions, BTK formula also turned out to be useful technique for predicting effects concerning thermal properties of electric and heat currents.[11,13,17,26] This method has also been used for the graphene-based superconducting hybrid structures for obtaining the thermal conductance.[20,27–29] However, the thermopower has not been studied so far. This topic is addressed in this article.

In this work, we provide systematic study of the effect of the temperature on the charge current in the GS junction using a generalized BTK formalism for the specific case of graphene. We present results concerning the temperature dependence of the zero-bias conductance and the Seebeck coefficient in the linear regime. For the sake of completeness, we also discuss the non-linear thermopower.

The paper is organized as follows. In Sec. II (and in Appendix), we present briefly a generalized BTK approach for the charge current through the GS junction. The linear transport coefficients are discussed: in particular, the zero-bias conductance and the thermopower. We also briefly comment on the effect of non-linear corrections on the Seebeck coefficient. Finally, we conclude in Sec. IV.

II. MODEL

We consider a ballistic limit for graphene based junction composed of the normal region and induced by means of the proximity effect superconducting region (cf. Fig. 1). For the description of the unconventional quasiparticle states, we utilize Dirac-Bogoliubov-de Gennes equations for the two-dimensional (2D) sheet of graphene in the form[18,30]

$$\begin{pmatrix} H_j - E_F\mathbf{1} & \Delta \\ \Delta^\dagger & E_F\mathbf{1} - H_j \end{pmatrix}\begin{pmatrix} u \\ v \end{pmatrix} = \epsilon\begin{pmatrix} u \\ v \end{pmatrix}, \tag{1}$$

where the index j can be either $+$ or $-$, which refers to the two inequivalent valleys K and K′ in the Brillouin zone. The single particle Hamiltonian is given by

$$H_\pm = -i\hbar v_F(\sigma_x\partial_x \pm \sigma_y\partial_y) + U, \tag{2}$$

where v_F is the energy independent Fermi velocity for the graphene, and $\{\sigma_i\}$ denote respective Pauli matrices. Because of the valley degeneracy, one can effectively do the calculation for the one valley only. We assume that in the geometry, where the interface is determined by the y-axis, the pair potential with the s-wave symmetry changes step-like in the x-axis direction

$$\Delta(\mathbf{r}, T) = \begin{cases} 0 & x < 0, \\ \Delta(T)e^{i\phi} & x > 0, \end{cases} \tag{3}$$

where the temperature dependence of the gap function can be deduced from the usual BCS theory[31] and is taken in the following form:

$$\frac{\Delta(T)}{\Delta_0} = \tanh\left(\sqrt{1.76\cdot\sqrt{\frac{T_c}{T}-1}}\right). \tag{4}$$

[a)]Electronic address: marcin.wysokinski@uj.edu.pl
[b)]Electronic address: ufspalek@if.uj.edu.pl

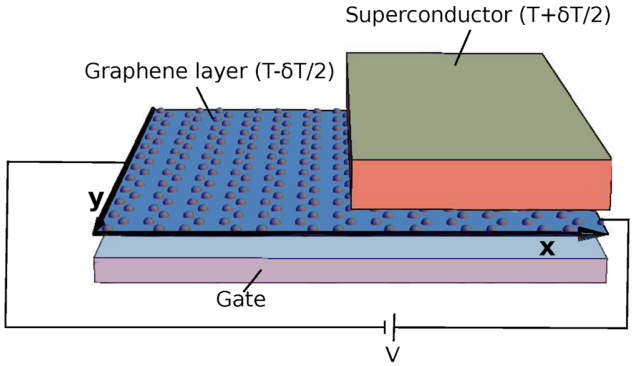

FIG. 1. Proposed schematic, experimental setup considered in our modeling.

The BCS theory of the superconductivity based on the requirement that the coherence length is large when compared to the Fermi wavelength. Under that condition, we can assume that the additional potential U has the form

$$U(\mathbf{r}) = \begin{cases} 0 & x < 0, \\ -U_0 & x > 0, \end{cases} \tag{5}$$

with large U_0 ($E_F + U_0 \gg \Delta_0$) and for the simplicity we define $E_F' = E_F + U_0$. In numerical calculations, we set $E_F' = 1000\Delta_0$.

In the spirit of the BTK scheme (by matching the wave functions at the boundary ($x = 0$)), we obtain expressions for the amplitudes of the Andreev hole reflection (AR) ($a(\epsilon, \theta)$) and the normal reflection ($b(\epsilon, \theta)$) of the incident electron—see Appendix for details of the method. Note that there is no intrinsic barrier at the GS junction, and thus the Fermi vector mismatch is the source of the normal reflection. The transmission probability, averaged over the angles, takes the following form:[7,14]

$$\mathcal{T}(\epsilon) = \int_{-\pi/2}^{\pi/2} d\theta \frac{\cos\theta}{2} \left(1 - |b(\epsilon,\theta)|^2 + \frac{\mathrm{Re}[e^{i\theta_A}]}{\cos\theta} |a(\epsilon,\theta)|^2\right). \tag{6}$$

The BTK formalism combined with the specific transmission probability derived for graphene defines charge current through the GS interface as[7,18]

$$I_e = \frac{4e}{h} \int_{-\infty}^{\infty} d\epsilon N(\epsilon) \mathcal{T}(\epsilon) \left(f^G(\epsilon - eV) - f^S(\epsilon)\right), \tag{7}$$

where f^G and f^S are the Fermi distribution functions for the normal (G) and the superconducting (S) region of GS junction, respectively, and

$$N(\epsilon) = \frac{|E_F + \epsilon| W}{\pi \hbar v_F}, \tag{8}$$

is the energy dependent number of transverse modes in the graphene sheet of width W.[18] However, formula (7) is not always accurate. The additional assumption is needed, that for each mode carrying incident electron, having energy $E_F + \epsilon$ and being Andreev reflected there is always enough modes at the level $E_F - \epsilon$ for this process to happen. However, away from perfect Andreev reflection regime ($|a(\epsilon)|^2 \neq 1$), as in our case, formula (7) remains rigorous.

The quantity describing thermoelectric properties of the system is thermopower, or Seebeck coefficient (S) measuring the voltage driving to zero the current flowing in response to the temperature difference, namely

$$S \equiv -\left(\frac{V}{\delta T}\right)_{I_e = 0}. \tag{9}$$

III. CHARGE TRANSPORT

A. Linear regime

Expansion of the Fermi functions in the normal and superconducting regions to the first (linear) order in both the bias and the temperature difference, with the average temperature T, i.e.,

$$\begin{aligned} f^G &\equiv f_{T-\delta T/2}(\epsilon - eV) \simeq f_T(\epsilon) - eV \frac{\partial f}{\partial \epsilon} + \frac{\delta T}{2T} \epsilon \frac{\partial f}{\partial \epsilon}, \\ f^S &\equiv f_{T+\delta T/2}(\epsilon) \simeq f_T(\epsilon) - \frac{\delta T}{2T} \epsilon \frac{\partial f}{\partial \epsilon}, \end{aligned} \tag{10}$$

enables to decouple Eq. (7) in the form

$$I_e = GV + I_e^T \delta T. \tag{11}$$

The resulting from it the linear transport coefficients can be thus rewritten in the following closed forms:

$$\begin{aligned} G &= -\frac{4e^2}{h} \int_{-\infty}^{\infty} d\epsilon \frac{\partial f}{\partial \epsilon} N(\epsilon) \mathcal{T}(\epsilon), \\ I_e^T &= \frac{4e}{hT} \int_{-\infty}^{\infty} d\epsilon \frac{\partial f}{\partial \epsilon} \epsilon N(\epsilon) \mathcal{T}(\epsilon). \end{aligned} \tag{12}$$

The temperature gradient and the bias are set as positive with respect to x coordinate. For the temperature in the system approaching zero, the expression for the electric conductance (G) reduces to the well-known BTK zero-bias conductance formula[7]

$$G_{T\to 0} = \frac{4e^2}{h} N(0) \mathcal{T}(0). \tag{13}$$

In Fig. 2, we have plotted the zero-bias differential conductance (calculated from Eq. (12)) as a function of temperature, normalized by the ballistic conductance g_0 with having N transverse modes in a sheet of graphene of width W and given by

$$g_0 = \frac{4e^2}{h} \int_{-\infty}^{\infty} d\epsilon \frac{\partial f}{\partial \epsilon} N(\epsilon). \tag{14}$$

For relatively high position of the Fermi level in graphene (roughly $E_F \gtrsim 5\Delta_0$), the influence of the increasing temperature (up to the approximately $T/T_c = 0.5$) on the conductance is almost negligible (cf. Fig. 2). The origin of this behavior is strictly connected with the relatively

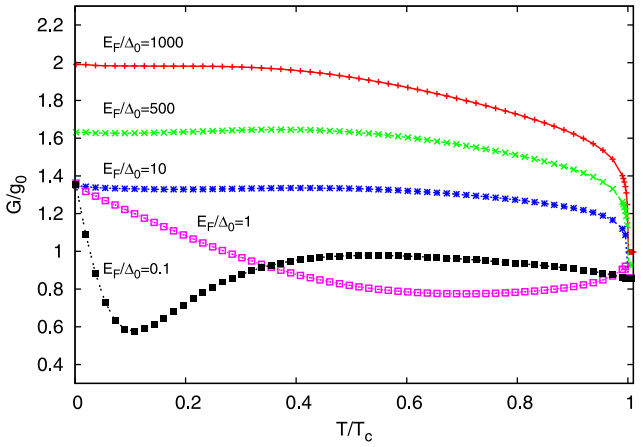

FIG. 2. Normalized zero-bias conductance as a function of temperature for various Fermi vector mismatch.

slow variation of the transmission probability $\mathcal{T}(\epsilon)$ for the subgap energies in this temperature regime, and thus does not differ qualitatively from the standard NS case.[7] In the low doping regime ($E_F \lesssim 5\Delta_0$), the linear differential conductance as a function of the temperature vastly differs from the standard NS case and reflects the specific electronic nature of graphene, as well as the impact of a crossover from the retro to the specular AR limit.

The non-trivial behavior of the Dirac fermions in graphene has also its influence on the linear thermopower. From Eqs. (9) and (11), formula for this quantity reads

$$S = \frac{I_e^T}{G} = -\frac{1}{k_B T}\frac{\int_{-\infty}^{\infty} d\epsilon\, \epsilon |\epsilon + E_F| \frac{\partial f}{\partial \epsilon}\mathcal{T}(\epsilon)}{\int_{-\infty}^{\infty} d\epsilon\, |\epsilon + E_F| \frac{\partial f}{\partial \epsilon}\mathcal{T}(\epsilon)}\frac{k_B}{e}. \qquad (15)$$

Results obtained by the numerical integration are presented in the Fig. 3. The low temperature regime differs from the one obtained for the NS junction.[11] Contrary to the NS case, for the graphene-based structure the thermopower does not vanish for non-zero temperatures. This is due to the relativistic nature of charge carriers in graphene, where AR does not vanish even for the high effective barrier (in our case effective barrier is only due to the Fermi level mismatch) for the subgap energies (for the normal incidence AR happens always with certainty[18]). Furthermore, in the low doping regime ($E_F \lesssim \Delta_0$), the Seebeck coefficient for the GS junction is around one order of magnitude larger than even for high effective barrier value (which as a phenomenological parameter can incorporate also the Fermi velocity mismatch[8]) in the NS case.[11]

In this regime, we observe a clear maximum in the temperature dependence of the Seebeck coefficient in the superconducting state. The maximum roughly corresponds to the minimum in the zero-bias conductance as a function of

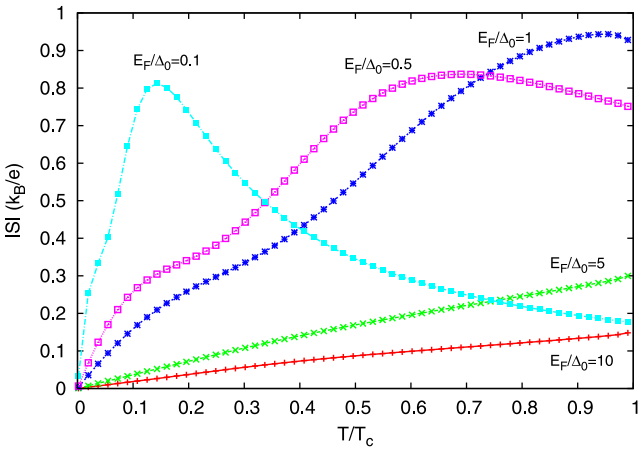

FIG. 3. Linear thermopower as a function of temperature in the system for various Fermi vector mismatch.

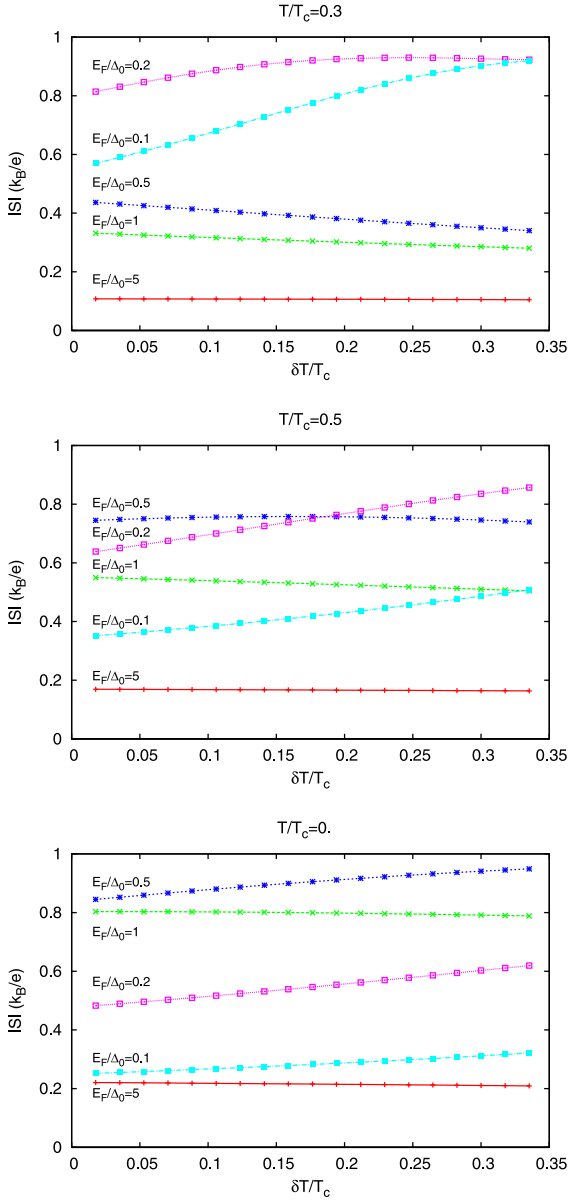

FIG. 4. Nonlinear thermopower as a function of the temperature gradient set over the junction for various Fermi energies in graphene. The net temperature in the system is marked above each plot.

temperature (cf. Fig. 2). The source of the significant enhancement of the thermopower in the low doping regime ($E_F \lesssim \Delta_0$) should be understood as an effect of being partly in the specular AR limit, where the transmission probability spectrum drops to zero for energy corresponding to the Fermi level position.[18] This feature affects the zero-bias conductance as a function of temperature and in turns is responsible for the thermopower increase in the specular AR limit. Therefore, in this regime, the thermopower is large and reaches values up to $1k_B/e$. This suggests that there is a potential for the application of this setup for cooling of various nanostructures.

B. Effect of the non-linearity

We have also studied numerically the effect of the non-linearity in our system. The thermopower in the non-linear regime can be calculated as a ratio between the bias voltage and the temperature gradient, when no charge current is flowing (c.f. Eq. (9)). The results in the non-linear regime are presented in Fig. 4. We have found that the non-linearity influences the thermopower in a not systematical manner with changing Fermi level position and the average temperature of the system. However, the change is not as dramatic as in the NS case[11] and is almost unnoticeable in the doped regime $E_F \gtrsim 5\Delta_0$.

IV. CONCLUSIONS

In this work, we have analyzed the thermoelectric charge transport in the graphene junction consisting of the normal and the superconducting parts. In the linear regime, we have calculated the temperature dependence of the zero-bias conductance and the thermopower. We have found deviations of these quantities from the standard normal metal-superconductor junction case that are caused by the relativistic nature of electrons in graphene. In the specular Andreev reflection regime, Seebeck coefficient is strongly enhanced for specific temperatures.

We have also studied the effect of non-linearity on the thermopower and we have found that for a high Fermi level positions ($E_F \gtrsim \Delta_0$) it stays almost unaffected and in the low Fermi level regime is noticeably enhanced with the increase of the temperature gradient.

ACKNOWLEDGMENTS

The authors greatly appreciate the stimulated discussion with Adam Rycerz, Jan Kaczmarczyk, and Marcin Abram. The work has been partially supported by the Foundation for Polish Science (FNP) under the TEAM program. We also acknowledge the Grant MAESTRO from the National Science Center (NCN).

APPENDIX: BTK FOR GRAPHENE

The wave function in the normal part of graphene (NG) ψ_N and in the superconducting region (SG) ψ_S, look, respectively, as follows:

$$\begin{aligned}\psi_N &= \psi_N^{e+} + b\psi_N^{e-} + a\psi_N^{h-}\\ \psi_S &= c\psi_S^{e+} + d\psi_S^{h+},\end{aligned} \tag{A1}$$

where the superscripts e and h refer to electron and hole in NG and electronlike and holelike excitation in SG, and the superscripts $+$ and $-$ to right and left moving particle, respectively.

Spinors resulting from Eq. (1) are expressed in the similar manner as in the Ref. 19, i.e., in the form

$$\begin{aligned}\psi_N^{e\pm} &= [1, \pm e^{\pm i\theta}, 0, 0]^T e^{\pm ik^e x\cos\theta},\\ \psi_N^{h-} &= [0, 0, 1, e^{-i\theta_A}]^T e^{-ik^h x\cos\theta_A},\\ \psi_S^{e+} &= [u, ue^{i\theta_S^e}, ve^{-i\phi}, ve^{i(\theta_S^e-\phi)}]^T e^{iq^e x\cos\theta_S^e},\\ \psi_S^{h-} &= [v, -ve^{-i\theta_S^h}, ue^{-i\phi}, -ue^{-i(\theta_S^h+\phi)}]^T e^{-iq^h x\cos\theta_S^h},\end{aligned} \tag{A2}$$

where for the sake of clarity we do not include phase factor $e^{ik_y y}$ since it corresponds to conservation of momentum in $\hat{\mathbf{y}}$ direction. The corresponding wave vectors are defined as follows:

$$k^{e(h)} = \frac{\epsilon + (-)E_F}{\hbar v_F}, \quad q^{e(h)} = \frac{E_F' + (-)\sqrt{\epsilon^2 - \Delta^2}}{\hbar v_F}, \tag{A3}$$

and the coherence factors are given by

$$u = \sqrt{\frac{1}{2}\left(1 + \frac{\sqrt{\epsilon^2 - \Delta^2}}{\epsilon}\right)}, \quad v = \sqrt{\frac{1}{2}\left(1 - \frac{\sqrt{\epsilon^2 - \Delta^2}}{\epsilon}\right)}. \tag{A4}$$

The conservation of momentum at the interface and along $\hat{\mathbf{y}}$ direction enables us to obtain mutual relations for the specific angles, namely

$$k^e \sin\theta = k^h \sin\theta_A = q^e \sin\theta_S^e = q^h \sin\theta_S^h. \tag{A5}$$

The system must also satisfy the continuity condition at the interface, $\psi_{\sigma L}(0) = \psi_{\sigma R}(0)$. The Hamiltonian is linear therefore is no need in matching derivatives. The resulting wave function amplitudes take the form

$$\begin{aligned}a(\epsilon,\theta) &= \frac{2\cos\theta(e^{-i\theta_S^h} + e^{i\theta_S^e})uv}{(e^{-i\theta_A} + e^{-i\theta_S^h})(e^{-i\theta} + e^{i\theta_S^e})u^2 - (e^{-i\theta} - e^{-i\theta_S^h})(e^{-i\theta_A} - e^{i\theta_S^e})v^2},\\ b(\epsilon,\theta) &= \frac{2\cos\theta[(e^{i\theta_S^e} - e^{-i\theta_A})v^2 + (e^{-i\theta_S^h} + e^{-i\theta_A})u^2]}{(e^{-i\theta_A} + e^{-i\theta_S^h})(e^{-i\theta} + e^{i\theta_S^e})u^2 - (e^{-i\theta} - e^{-i\theta_S^h})(e^{-i\theta_A} - e^{i\theta_S^e})v^2} - 1.\end{aligned} \tag{A6}$$

[1]K. S. Novoselov, A. K. Geim, S. V. Morozov, D. Jiang, M. I. Katsnelson, I. V. Grigorieva, S. V. Dubonos, and A. A. Firosov, Nature **438**, 197 (2005).
[2]L. D. Landau and J. M. Lifshitz, *Statistical Physics* (Pergamon, Oxford, 1980).
[3]C. W. J. Beenakker, Rev. Mod. Phys. **80**, 1337 (2008).
[4]J. Tworzydło, B. Trauzettel, M. Titov, A. Rycerz, and C. W. J. Beenakker, Phys. Rev. Lett. **96**, 246802 (2006).
[5]I. Snyman and C. W. J. Beenakker, Phys. Rev. B **75**, 045322 (2007).
[6]Y. Xing, Q. Sun, and J. Wang, Phys. Rev. B **80**, 235411 (2009).
[7]G. E. Blonder, M. Tinkham, and T. M. Klapwijk, Phys. Rev. B **25**, 4515 (1982).
[8]G. E. Blonder and M. Tinkham, Phys. Rev. B **27**, 112 (1983).
[9]J. Kaczmarczyk, M. Sadzikowski, and J. Spałek, Phys. Rev. B **84**, 094525 (2011).
[10]J. Kaczmarczyk, M. Sadzikowski, and J. Spałek, Physica C **471**, 193 (2011).
[11]M. M. Wysokiński, Acta Phys. Pol. A **122**, 758 (2012).
[12]G. Annunziata, H. Enoksen, J. Linder, M. Cuoco, C. Noce, and A. Sudbø, Phys. Rev. B **83**, 144520 (2011).
[13]A. Bardas and D. Averin, Phys. Rev. B **52**, 12873 (1995).
[14]N. A. Mortensen, K. Flensberg, and A. P. Jauho, Phys. Rev. B **59**, 10176 (1999).
[15]Y. Tanaka and S. Kashiwaya, Phys. Rev. Lett. **74**, 3451 (1995).
[16]V. Lukic and E. J. Nicol, Phys. Rev. B **76**, 144508 (2007).
[17]J. E. Hirsch, Phys. Rev. B **50**, 3165 (1994).
[18]C. W. J. Beenakker, Phys. Rev. Lett. **97**, 067007 (2006).
[19]J. Linder and A. Sudbø, Phys. Rev. B **77**, 064507 (2008).
[20]T. Yokoyama, J. Linder, and A. Sudbø, Phys. Rev. B **77**, 132503 (2008).
[21]Q. Zhang, D. Fu, B. Wang, R. Zhang, and D. Y. Xing, Phys. Rev. Lett. **101**, 047005 (2008).
[22]M. Titov and C. W. J. Beenakker, Phys. Rev. B **74**, 041401 (2006).
[23]U. Sivan and Y. Imry, Phys. Rev. B **33**, 551 (1986).
[24]P. N. Butcher, J. Phys.: Condens. Matter **2**, 4869 (1990).
[25]H. van Houten, L. W. Molenkamp, C. W. J. Beenakker, and C. T. Foxon, Semicond. Sci. Technol. **7**, B215 (1992).
[26]I. A. Devyatov, M. Yu Romashka, and A. V. Burmistrova, JETP Lett. **91**, 297 (2010).
[27]M. Titov, A. Ossipov, and C. W. J. Beenakker, Phys. Rev. B **75**, 045417 (2007).
[28]M. Salehi, M. Alidoust, and G. Rashedi, J. Appl. Phys. **108**, 083917 (2010).
[29]M. Salehi, M. Alidoust, Y. Rahnavard, and G. Rashedi, J. Appl. Phys. **107**, 123916 (2010).
[30]P. G. de Gennes, *Superconductivity in Metals and Alloys* (W. A. Benjamin, New York, 1966)
[31]J. B. Ketterson and S. N. Song, *Superconductivity* (Cambridge University Press, 1999).

3.8.3 Article B.3. Temperature Dependence of the Zero-Bias Conductance in the Graphene NIS Junction

In Article B.3 [124] we have investigated the effects of the nonzero temperature on the conductance oscillations in the graphene - insulator - superconductor junction with the change of the height of the insulating potential. We have shown the suppression of the oscillations amplitude with the increasing temperature for different model parameters.

Proceedings of the XVI National Conference on Superconductivity and Strongly Correlated Systems, Zakopane 2013

Temperature Dependence of the Zero-Bias Conductance in the Graphene NIS Junction

M.M. Wysokiński*

Marian Smoluchowski Institute of Physics, Jagiellonian University, W.S. Reymonta 4, 30-059 Kraków, Poland

The temperature dependence of the zero-bias conductance of the graphene-based, ballistic junction composed of the three consecutive regions: normal, with potential barrier ("insulating") and superconducting (NIS), is analyzed within the extended Blonder–Tinkham–Klapwijk approach. Within this approach we have found that oscillatory behavior of the conductance as a function of barrier strength is suppressed by the temperature – the amplitude diminishes with heating up the junction. Moreover, the subtle, although nontrivial feature of the system is reported: the average over the period of the oscillations of the zero-bias conductance for relatively small Fermi level mismatch behaves non-monotonically with the increase of the temperature with the maximum roughly at $T/T_c \approx 0.5$.

DOI: 10.12693/APhysPolA.126.A-36

PACS: 74.45.+c, 73.23.Ad

1. Introduction

The discovery of the graphene [1] opened up new opportunities in the material science for studying and designing electronic systems governed by relativistic quantum electrodynamics in the desktop laboratories. Shortly after, the field of quasi-relativistic physics has been enriched by the range of new materials where similar electronic structure to the graphene was found, such as silicon and germanium atoms arranged in a hexagonal lattice [2–4], and topological insulators [5] (surface states).

Despite similar energy dispersion, most of those new systems turned out to be significantly different from graphene. Especially, silicene was found to be intrinsically superconducting [6], contrary to the graphene, which has widened the freedom of experimental and theoretical studies on the superconducting, graphene-like systems.

One of the first concepts in this subfield was the junction based on the graphene, composed from normal and superconducting (induced by means of proximity effect) regions, proposed by Beenakker in his seminal work [7]. He found that due to the quasi-relativistic nature of the charge carriers, the conductance spectra differ significantly from the standard case [8]. Later, also other, more sophisticated ideas of electronic devices based on the interplay of the Dirac physics with the superconductivity were proposed [9–11].

In majority of articles concerning transport properties through the graphene-based superconducting hybrid structures the well-established extended Blonder–Tinkham–Klapwijk (BTK) formalism [8] has been used. Particularly this approach was proven to be successful for this class of systems in calculating e.g. conductance spectra [7, 12–14], heat conductance [9, 15–17] as well as thermopower [18] with the density of states explicitly taken into account [19].

Within this approach, the oscillatory behavior of the electric, as well as the heat conductance, as a function of the barrier strength was found in the graphene-based junction composed of normal and superconducting regions with the high external potential at the interface (NIS junction) [12, 13, 15]. This peculiar property of this system is a direct manifestation of the quasi-relativistic nature of charge carriers in the graphene.

The natural question that arises at this stage, that in particular we address in this work, is how the oscillatory behavior of the zero-bias conductance (ZBC) as a function of the barrier strength is affected by the increasing temperature. Particularly we have investigated temperature dependence of the amplitude, and the average over one period of the oscillations for different Fermi level mismatch (FLM) between normal and superconducting part of the junction.

The paper is organized as follows. In Sect. 2 we present briefly generalized BTK formalism for the calculating current through the NIS junction in the non-zero temperature. Then in Sect. 3 we discuss our results, mainly focused on the behavior of the conductance oscillations as a function of barrier strength with the raising temperature. Finally, we conclude in Sect. 4.

2. Model

We consider graphene-based junction composed of normal and superconducting regions with the energy potential of the width d and the height V_0 at the interface playing the role of the "insulating" barrier. Our starting point in the description of our system are Dirac–Bogoliubov–de Gennes equations for the two-dimensional (2D) sheet of graphene in the form [7, 20]:

$$\begin{pmatrix} \mathcal{H}_j - E_{\rm F}\mathbb{1} + U(\boldsymbol{r})\mathbb{1} & \Delta \\ \Delta^\dagger & E_{\rm F}\mathbb{1} - U(\boldsymbol{r})\mathbb{1} - \mathcal{H}_j \end{pmatrix} \psi = \epsilon\psi, \quad (1)$$

where the index j can be either $+$ or $-$ which refers to the two inequivalent valleys K and K' in the Brillouin zone, and the single particle Hamiltonian reads

*e-mail: marcin.wysokinski@uj.edu.pl

$$\mathcal{H}_j = -\mathrm{i}\hbar v_\mathrm{F}(\sigma_x\partial_x + \mathrm{sgn}(j)\sigma_y\partial_y), \quad (2)$$

with v_F standing for momentum independent velocity of charge carriers in graphene, and $\sigma_i\}$ denoting respective Pauli matrices. The potential $U(\boldsymbol{r})$ in Eq. (1) shifts Fermi energies in the normal, "insulating" and superconducting region and can be modeled as

$$U(\boldsymbol{r}) = -U_0\theta(x) + V_0\theta(-x)\theta(x+d). \quad (3)$$

We would treat the potential barrier at the interface of the junction in the limit of thin barrier ($d \to 0$) and high potential ($V_0 \to \infty$), at the same time keeping effective dimensionless barrier strength χ constant, defined similarly as in Refs. [12, 13, 15] as

$$\chi = \frac{V_0 d}{\hbar v_\mathrm{F}}. \quad (4)$$

The potential U_0 is used to tune effective Fermi level mismatch between normal and superconducting regions of the graphene sheet. In order to satisfy the mean-field condition for the superconductivity we set $\Delta_0 \ll (U_0 + E_\mathrm{F})$. Note that FLM can be also a source of the normal reflection. We have assumed the pairing potential with the s-wave symmetry changing step-like at the interface and having temperature dependence deduced from the usual BCS theory [21],

$$\Delta(\boldsymbol{r}, T) = \Delta_0\theta(x)\tanh\left(1.76\sqrt{\frac{T_\mathrm{c}}{T} - 1}\right). \quad (5)$$

Following the BTK formalism one should identify the relevant scattering processes and construct full wave functions for the normal (Ψ_N), "insulating" (Ψ_I) and superconducting (Ψ_S) regions, and force their continuity at the interfaces [12, 13]. Incoming electron (ψ^e_+) from the normal side of the graphene sheet can be backscattered either in the normal reflection process (ψ^e_-) or in so-called Andreev reflection process as a converted by the pair potential hole (ψ^h_-). In turn, in terms of the transmission it can be injected into the superconducting region as a Bogoliubov quasiparticle (ψ^Se_+, ψ^Sh_-). There are also bound electron and hole states in the "insulating" region (ψ^Ie_-, ψ^Ie_+, ψ^Ih_-, ψ^Ih_+). The respective full wave functions can be written in the following form:

$$\Psi_\mathrm{N} = \psi^\mathrm{e}_+ + r\psi^\mathrm{e}_- + r_a\psi^\mathrm{h}_-,$$

$$\Psi_\mathrm{I} = a_\mathrm{e}\psi^\mathrm{Ie}_+ + a_\mathrm{h}\psi^\mathrm{Ih}_+ + b_\mathrm{e}\psi^\mathrm{Ie}_- + b_\mathrm{h}\psi^\mathrm{Ih}_-,$$

$$\Psi_\mathrm{S} = t_\mathrm{e}\psi^\mathrm{Se}_+ + t_\mathrm{h}\psi^\mathrm{Se}_-. \quad (6)$$

Under the condition of the continuity at the boundaries of the global wave function,

$$\Psi_\mathrm{N}|_{x=-d} = \Psi_\mathrm{I}|_{x=-d}, \quad \Psi_\mathrm{I}|_{x=0} = \Psi_\mathrm{S}|_{x=0}, \quad (7)$$

one can derive respective wave functions amplitudes. Note that contrary to the standard case [8], due to the linearity of the Dirac–Weyl equation there is no need to match also derivatives of wave functions. The direct energy and angle of incidence dependence of the needed amplitudes r and r_a can be obtained after some straightforward algebra and are not shown here explicitly. For full formula and also explicit particles and quasi-particles wave function forms see e.g. Refs. [12, 13, 15].

The transmission probability through the NIS junction now can be expressed as [8]:

$$\mathcal{T}(\epsilon) = \int_{-\pi/2}^{\pi/2}\mathrm{d}\theta\frac{\cos\theta}{2} \times\left(1 - |r(\epsilon,\theta)|^2 + \frac{\mathrm{Re}[\mathrm{e}^{\mathrm{i}\theta_A}]}{\cos\theta}|r_a(\epsilon,\theta)|^2\right). \quad (8)$$

With the knowledge of the transmission probability in the spirit of the Landauer formalism one can write a full formula for the ballistic charge transport through the junction,

$$I_\mathrm{e}(V) = \frac{4e}{h}\int_{-\infty}^{\infty}\mathrm{d}\epsilon\; N(\epsilon)\mathcal{T}(\epsilon) \times\left(f^\mathrm{N}(\epsilon - eV) - f^\mathrm{S}(\epsilon)\right), \quad (9)$$

where functions $f^{(i)}$ denote Fermi–Dirac distributions with the superscript $\{i = \mathrm{N}, \mathrm{S}\}$ standing for the normal and superconducting region, respectively. The formula (9) holds for the biased junction with the voltage, V and accounts for the density of states in the graphene sheet of the width W,

$$N(\epsilon) = \frac{|E_\mathrm{F} + \epsilon|W}{\pi\hbar v_\mathrm{F}}. \quad (10)$$

The ZBC now can be obtained in a straightforward manner by linearizing Fermi functions with respect to the small voltage ($V \to 0$),

$$G = \frac{\partial I}{\partial V} = -\frac{4e^2}{h}\int_{-\infty}^{\infty}\mathrm{d}\epsilon\;\frac{\partial f}{\partial\epsilon}N(\epsilon)\mathcal{T}(\epsilon). \quad (11)$$

It is convenient to normalize above formula by the ballistic conductance of the same sheet of graphene without superconducting or external potential sources, kept in the same temperature,

$$g_0 = -\frac{4e^2}{h}\int_{-\infty}^{\infty}\mathrm{d}\epsilon\;\frac{\partial f}{\partial\epsilon}N(\epsilon). \quad (12)$$

3. Results

In all numerical calculations we have set shifted Fermi level in the superconducting region as $E'_\mathrm{F} = E_\mathrm{F} + U_0 = 100\Delta_0$.

The theoretical prediction of the oscillatory behavior of ZBC spectra (cf. Fig. 1) as a function of the effective barrier strength has been reported in the graphene NIS junction some time ago [12]. The issue mainly investigated here is how this quasi-relativistic behavior changes with increasing temperature. Therefore, we have analyzed the effect of the temperature, the effective barrier strength and the FLM on the normalized zero-bias conductance through the graphene NIS junction (calculated from Eq. (11)).

For $E'_\mathrm{F}/E_\mathrm{F} \geq 10$ the oscillations almost completely disappear (cf. Fig. 1), and in fact the effect of the barrier strength is negligible in this regime. Therefore in this limit NIS junction properties are similar to that of the NS junction in which case ZBC behaves non-trivially with the raising temperature (see Ref. [18]).

In the opposite regime, for $E'_\mathrm{F}/E_\mathrm{F} \leq 10$, by changing the barrier strength parameter, χ we can control to some

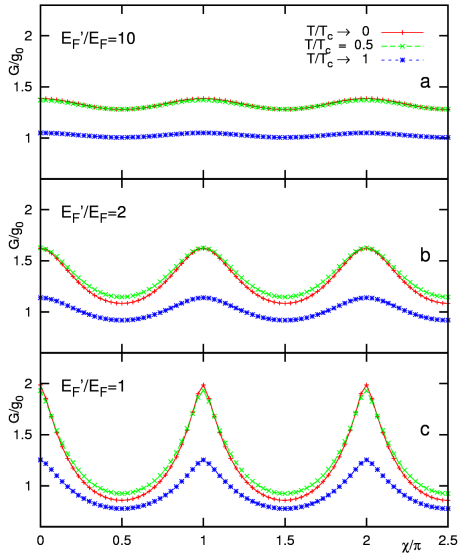

Fig. 1. Normalized ZBC as a function of the effective barrier strength, χ for selected temperatures. The plots in parts (a), (b), (c) differ with the FLM. The amplitude of the oscillations diminishes with the increase of the temperature (cf. inset in Fig. 3). Note that the average value of ZBC can slightly increase (cf. Fig. 3). At part (a) plots for $T/T_c \to 0$ and $T/T_c = 0.5$ are mostly overlapping.

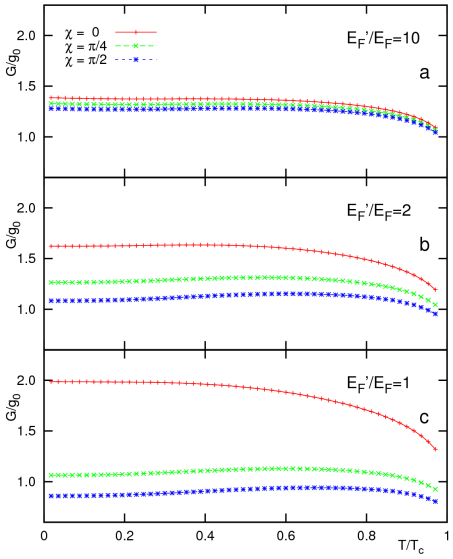

Fig. 2. Normalized ZBC as a function of the temperature for selected barrier strengths, χ. The plots in parts (a), (b), (c) differ with the FLM. For specific values of barrier strength, we obtain flat maximum (parts (b), (c)).

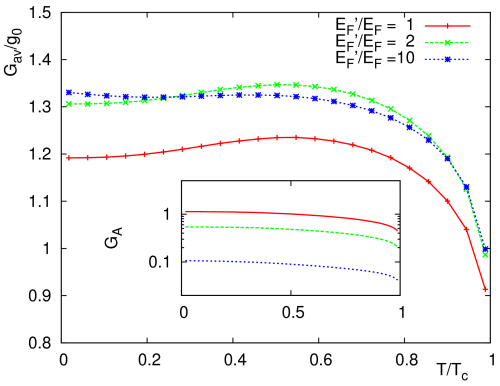

Fig. 3. The main plot presents averaged ZBC over the period of oscillations with respect to the change of the barrier strength as a function of the temperature for selected values of the FLM. In the inset we plot with the logarithmic scale the change of the oscillations amplitude (G_A) also as a function of the temperature. For relatively small FLM, the average ZBC changes non-monotonically with the temperature and has a maximum around $T/T_c \approx 0.5$, contrary to the monotonic decrease of the amplitude of ZBC oscillations.

larger extent the mutual relation between the probability of the Andreev and the normal reflection. However, with the increasing temperature the range of the manipulation diminishes which has a direct manifestation in the monotonic decrease of the ZBC oscillations amplitude (cf. inset of Fig. 3).

What is more, the upper limit of the oscillations (where the Andreev reflection dominates) is relatively less affected by the increase of the temperature than bottom limit approximately up to $T \approx 0.5T_c$ which is smooth boundary designated by the regime where thermal excitation are within the range of the superconducting gap. The situation reverses when the superconducting gap starts closing. This in turn gives rise to a non-monotonic change of the average ZBC, defined as:

$$G_{\rm av} = \frac{1}{\pi}\int_0^{\pi} G(\chi)\,{\rm d}\chi, \tag{13}$$

which in the low FLM regime ($E'_{\rm F}/E_{\rm F} \leq 10$) acquires maximum around $T \approx 0.5T_c$ (cf. Fig. 3). In comparison, ZBC of the graphene-based NS junction also has a non-monotonic behavior with the raising temperature but in the different regimes (i.e. for small position of the Fermi level in normal region of the junction) and of the different kind (cf. Ref. [18]). Also the origin of this behavior can be seen in the evolution of the ZBC with the increase of the temperature (cf. Fig. 2). For selected values of the barrier strength from the first period ($\chi = \frac{\pi}{2}, \frac{\pi}{4}$) ZBC is increasing up to a flat maximum approximately at the $T/T_c \approx 0.5$ (cf. Fig. 2b, c). In the same regime for $\chi = 0$ it drops slowly and remains almost unchanged.

4. Conclusions

In this work we have analyzed the temperature dependence of the zero-bias conductance of the graphene-based NIS ballistic junction. We have found that with the increasing temperature oscillations of the zero-bias conductance as a function of the barrier strength persist with

the monotonically decreasing amplitude. The interesting feature of the system is a non-monotonic change, of the average over the period of the oscillations of the zero-bias conductance (as a function of a barrier strength) with the increase of the temperature, with the maximum around $T/T_c \approx 0.5$ in the limit of a relatively small Fermi level mismatch ($E'_F/E_F \lesssim 10$).

Acknowledgments

The work has been supported by the Foundation for Polish Science (FNP) under the TEAM program. The author also greatly acknowledge financial support from the project DOCTUS.

References

[1] K.S. Novoselov, A.K. Geim, S.V. Morozov, D. Jiang, M.I. Katsnelson, I.V. Grigorieva, S.V. Dubonos, A.A. Firosov, *Nature* **438**, 197 (2005).

[2] G.G. Guzmán-Verri, L.C. Lew Yan Voon, *Phys. Rev. B* **76**, 075131 (2007).

[3] S. Lebègue, O. Eriksson, *Phys. Rev. B* **79**, 115409 (2009).

[4] S. Cahangirov, M. Topsakal, E. Aktürk, H. Şahin, S. Ciraci, *Phys. Rev. Lett.* **102**, 236804 (2009).

[5] X.-L. Qi, S.-C. Zhang, *Rev. Mod. Phys.* **83**, 1057 (2011).

[6] L. Chen, B. Feng, K. Wu, *Appl. Phys. Lett.* **102**, 081602 (2013).

[7] C.W.J. Beenakker, *Phys. Rev. Lett.* **97**, 067007 (2006).

[8] G.E. Blonder, M. Tinkham, T.M. Klapwijk, *Phys. Rev. B* **25**, 4515 (1982).

[9] M. Titov, C.W.J. Beenakker, *Phys. Rev. B* **74**, 041401 (2006).

[10] M. Titov, A. Ossipov, C.W.J. Beenakker, *Phys. Rev. B* **75**, 045417 (2007).

[11] S.-G. Cheng, Y. Xing, J. Wang, Q.-F. Sun, *Phys. Rev. Lett.* **103**, 167003 (2009).

[12] S. Bhattacharjee, K. Sengupta, *Phys. Rev. Lett.* **97**, 217001 (2006).

[13] J. Linder A. Sudbø, *Phys. Rev. B* **77**, 064507 (2008).

[14] Q. Zhang, D. Fu, B. Wang, R. Zhang, D.Y. Xing, *Phys. Rev. Lett.* **101**, 047005 (2008).

[15] T. Yokoyama, J. Linder, A. Sudbø, *Phys. Rev. B* **77**, 132503 (2008).

[16] M. Salehi, M. Alidoust, G. Rashedi, *J. Appl. Phys.* **108**, 083917 (2010).

[17] M. Salehi, M. Alidoust, Y. Rahnavard, G. Rashedi, *J. Appl. Phys.* **107**, 123916 (2010).

[18] M. Wysokiński, J. Spałek, *J. Appl. Phys.* **113**, 163905 (2013).

[19] M.M. Wysokiński, *Acta Phys. Pol. A* **122**, 758 (2012).

[20] P.G. de Gennes, *Superconductivity in Metals and Alloys*, W. A. Benjamin, New York 1966, Ch. 5.

[21] J.B. Ketterson, S.N. Song, *Superconductivity*, Cambridge University Press, Cambridge 1999.

Chapter 4

Summary and Conclusions

To conclude, we present in this Chapter a summary of our results, as well as sketch some of the research directions set by the topics analyzed in this Thesis. Particularly, we are here focused on (but not limit ourselves to) the heavy fermion systems (HFS), exhibiting unconventional magnetism and superconductivity, as described by the Anderson lattice model (ALM). Additionally, we have analyzed closed packed neutral fermions within the three-dimensional (3D) Hubbard model on the fcc lattice in the context of modeling properties of the canonical correlated system, normal liquid ^{3}He. In both model cases we have obtained our results based on the Gutzwiller wave function variational approach. Specifically, we summarize the analyzed problems concerning strongly correlated system in the following points:

- Within the statistically consistent Gutzwiller approximation (SGA) approach we have analyzed 3D Hubbard model in an applied magnetic field to describe the physical properties such as the spin-direction-dependent quasiparticle effective masses, the magnetization, and the specific heat. Additionally, we have made a quantitative comparison with the experimentally determined magnetization curve for liquid ^{3}He in the normal state [38].

- Within the same method (SGA), applied to ALM, we have provided the microscopic mechanism for the presence of two distinct ferromagnetic phases on the UGe_2 phase diagram at zero temperature. Our results agrees with the experimental data concerning the magnetization, the neutron scattering, and the de Haas - van Alphen oscillations [113].

- Nontrivial extension of the previous analysis to nonzero temperature has provided the explanation of the emergence of all the quantum and the classical critical points on the magnetic phase diagram of UGe_2. The existing so-called tricritical wing structure of the magnetic phase boundaries for this material's pressure - magnetic field - temperature phase diagram, compares with experimental data quantitatively [114].

- We have analyzed the stability of our quantitative fit of the tricritical wings of ferromagnetic to paramagnetic phase boundary in UGe_2 with respect to the changing band filling and the f-electron Landé-factor value. The results suggest that our fit to the experimental data is very sensitive to the numerical value of both the mentioned parameters. In the case of band filling, we have drawn the conclusion

that as ALM does not provide a good fit unless the position of all the critical points are matched. It is thus unlikely that our good comparison with experiment is fortuitous. In the case of f-electron Landé factor, a good fit when it is the same as that for free electron value, which suggests that in UGe_2 the multiplet structure is washed out by the f electrons itineracy [120].

- Within the diagrammatic expansion for Gutzwiller wave function (DE-GWF) method we have analyzed paramagnetic properties of ALM. We have obtained major physical observable of the heavy fermion systems that is the very large mass enhancement (as deduced from the density of states at the Fermi energy). We have additionally provided a non-magnetic phase diagram including disjoint the mixed-valence, the Kondo/almost-Kondo insulating, and the Kondo-lattice ($n_f \to 1$) regimes, distinguished by the emergence of direct f-f hopping out of originally atomic states [118].

- The same method, DE-GWF have been used for analysis of unconventional d-wave superconductivity in ALM driven by purely repulsive Coulomb interaction. We have found large region of paired state being favored against paramagnetism. The superconductivity exhibits several features in accord with the recent experimental findings for $CeCoIn_5$ [100, 101, 102], as e.g., its multiband character [121]. The result is the first of its kind and should be studied farther.

In the additional project we have analyzed tunnel metal - insulator - superconductor (NIS) junctions thermoelectric characteristics. For that reason, we have first developed the extended Blonder - Tinkham - Klapwijk formula accounting for explicit density of states energy dependence around the Fermi level [122]. The modified formula was used for the analysis of the graphene-based NS junction [123]. The temperature dependence of the conductance oscillations in the graphene-based NIS junctions have been also studied.

The results concerning heavy fermion systems obtained in this Thesis are all the more important, since they provide a strong basis for the future research. Namely, we have provided semi-complete microscopic interpretation of magnetic phase diagram of UGe_2 only lacking the spin-triplet superconductivity to make a full picture. The natural question is concerned with the extension of our model for particularly inclusion of the missing element of the predicted phase diagram: the spin-triplet superconductivity. Our model can be extended in several possible directions, that need further investigations:

- We have predicted [114] that in the close vicinity of the superconducting dome a Lifshitz quantum critical point may be placed. A tempting scenario behind the pairing origin has its source in the role of quantum critical fluctuations of the Fermi surface topology. However, a formal theory is still lacking.

- From the different perspective, as inclusion of the higher orders of expansion in the DE-GWF technique applied to ALM favors d-wave superconductivity against paramagnetism [121], it may happen that the equal-spin pairing coexisting with ferromagnetism would be favored against ferromagnetic-only state particular near the metamagnetic phase transition, what would complete our microscopic model for the description of UGe_2.

- ALM in the standard form does not account for the f-orbital degeneracy, which can be important for the case of UGe_2. Consideration of extended degenerate ALM

with the effective Hund's rule coupling may also lead to the onset of unconventional spin-triplet superconductivity driven by real space pairing [156, 157, 158, 159].

It is also of particular interest to investigate further the emerging superconductivity in ALM as treated by DE-GWF method for its interplay with either antiferro- or ferromagnetism, to reveal to what extend resulting phase diagram can describe the observed phases. As our results concerning superconductivity, are very promising in the light of the recent experiments for $CeCoIn_5$ [100, 101, 102], it would be also interesting to consider ALM in this specific situation by including principal features of a realistic band structure to allow for a quantitative comparison with experiment.

Bibliography

[1] W. L. Ginzburg and L. Landau, Zh. Eksp. Teor. Fiz. **20**, 1064 (1950).

[2] A. A. Abrikosov, Sov. Phys. JETP **5**, 1174 (1957).

[3] J. Bardeen, N. Cooper, and J. R. Scrieffer, Phys. Rev. **108**, 1175 (1957).

[4] P. G. de Gennes, *Superconductivity in Metals and Alloys* (W. A. Benjamin, New York, 1966).

[5] N. N. Bogoliubov, Sov. Phys. JETP **7**, 41 (1958).

[6] J. G. Valatin, Nuovo Cimento **7**, 843 (1958).

[7] L. P. Gor'kov, Sov. Phys. JETP **36**, 1364 (1959).

[8] G. M. Eliashberg, Sov. Phys. JETP **11**, 696 (1960).

[9] C. Pfleiderer, Rev. Mod. Phys. **81**, 1551 (2009), (chapter III. A).

[10] A. Drozdov, M. I. Eremets, I. A. Troyan, V. Ksenofontov, and S. I. Shylin, arXiv: 1506.08190 .

[11] F. Steglich, H. Aarts, C. Bredl, W. Lieke, D. Meschede, W. Franz, and h. Schäfer, Phys. Rev. Lett. **43**, 1892 (1979).

[12] K. A. Müller and J. G. Bednorz, Z. Phys. B **64**, 189 (1986).

[13] K. Bechgaard, K. Carneiro, M. Olsen, F. B. Rasmussen, and C. S. Jacobsen, Phys. Rev. Lett. **46**, 852 (1981).

[14] H. Takahasi, K. Igawa, K. Arii, M. Kamihara, Y. amd Hirano, and H. Hosono, Nature **453**, 376 (2008).

[15] J. Spałek and D. Goc-Jagło, Physica Scripta **86**, 048301 (2012).

[16] D. Pines, Phys. Rev. **109**, 280 (1958).

[17] A. Kołodziejczyk, B. V. Sarkissian, and B. R. Coles, J. Phys. F **10**, L333 (1980).

[18] A. Kołodziejczyk, Physica B **130**, 189 (1985).

[19] K. Rogacki, A. Kołodziejczyk, L. Bochenek, and T. Cichorek, Phil. Mag. **95**, 503 (2015).

[20] S. S. Saxena, P. Agarwal, K. Ahilan, F. M. Grosche, R. K. W. Haselwimmer, M. J. Steiner, E. Pugh, I. R. Walker, S. R. Julian, P. Monthoux, G. G. Lonzarich, A. Huxley, I. Sheikin, D. Braithwaite, and J. Flouquet, Nature **406**, 587 (2000).

[21] D. Aoki, A. Huxley, E. Ressouche, D. Braithwaite, J. Flouquet, J.-P. Brison, E. Lhotel, and C. Paulsen, Nature **413**, 613 (2001).

[22] N. T. Huy, A. Gasparini, D. E. de Nijs, Y. Huang, J. C. P. Klaasse, T. Gortenmulder, A. de Visser, A. Hamann, T. Görlach, and H. v. Löhneysen, Phys. Rev. Lett. **99**, 067006 (2007).

[23] D. Aoki and J. Flouquet, J. Phys. Soc. Jpn. **81**, 011003 (2012).

[24] D. Aoki and J. Flouquet, J. Phys. Soc. Jpn. **83**, 061011 (2014).

[25] D. Aoki, A. Gourout, A. Pourret, G. B. Bastien, G. Knebel, and J. Flouquet, C. R. Physique in press (2014).

[26] L. D. Landau and E. M. Lifshitz, *Quantum Mechanics: Non-Relativistic Theory* (Pergamon Press, Oxford, 1965).

[27] V. B. Berestetskii, E. M. Lifshitz, and L. P. Pitaevskii, *Relativistic Quantum Theory* (Pergamon Press, Oxford, 1971).

[28] J. Spałek, *Wstęp do fizyki materii skondensowanej* (PWN, Warszawa, 2015).

[29] F. London, *Superfluids, Vol. II* (Wiley, New York, ADDRESS, 1954).

[30] H. A. Mook, Phys. Rev. Lett. **55**, 2452 (1985).

[31] D. S. Greywall, Phys. Rev. B **27**, 2747 (1983).

[32] D. S. Greywall, Phys. Rev. B **33**, 7520 (1986).

[33] L. Landau, Sov. Phys. JETP **8**, 70 (1959).

[34] J. Hubbard, Proc. R. Soc. London, Ser. A **276**, 238 (1963).

[35] J. Hubbard, Proc. R. Soc. London, Ser. A **281**, 401 (1964).

[36] M. C. Gutzwiller, Phys. Rev. Lett. **10**, 159 (1963).

[37] J. Kanamori, Progr. Theor. Phys. **30**, 275 (1963).

[38] M. M. Wysokiński and J. Spałek, J. Phys.: Condens. Matter **26**, 055601 (2014).

[39] T. Kopp, F. J. Seco, S. Schiller, and P. Wölfle, Phys. Rev. B **38**, 11835 (1988).

[40] J. Spałek, P. Korbel, and W. Wójcik, Phys. Rev. B **56**, 971 (1997).

[41] N. F. Mott, Proc. Phys. Soc, Sec. A **62**, 416 (1949).

[42] N. F. Mott, *Metal-Insulator Transitions* (Taylor and Francis, London, 1990).

[43] F. Gebhard, *The Mott Metal-Insulator Transition* (Springer-Verlag, Berlin Heidelberg, 1997).

[44] M. Imada, A. Fujimori, and Y. Tokura, Rev. Mod. Phys. **70**, 1039 (1998).

[45] M. Moeckel and S. Kehrein, Phys. Rev. Lett. **100**, 175702 (2008).

[46] M. Eckstein, M. Kollar, and P. Werner, Phys. Rev. Lett. **103**, 056403 (2009).

[47] M. Schiró and M. Fabrizio, Phys. Rev. Lett. **105**, 076401 (2010).

[48] D. Vollhardt, Rev. Mod. Phys. **56**, 99 (1984).

[49] S. A. J. Wiegers, P. E. Wolf, and L. Puech, Phys. Rev. Lett. **66**, 2895 (1991).

[50] J. Spałek, A. Datta, and J. M. Honig, Phys. Rev. Lett. **59**, 728 (1987).

[51] J. Spałek, J. Solid State Chem. **88**, 70 (1990).

[52] E. Dagotto, Rev. Mod. Phys. **66**, 763 (1994).

[53] A. Damascelli, Z. Hussain, and Z.-X. Shen, Rev. Mod. Phys. **75**, 473 (2003).

[54] P. A. Lee, N. Nagaosa, and X.-G. Wen, Rev. Mod. Phys. **78**, 17 (2006).

[55] J. Kaczmarczyk, J. Spałek, T. Schickling, and J. Bünemann, Phys. Rev. B **88**, 115127 (2013).

[56] J. Spałek and A. M. Oleś, Physica B **86-88**, 375 (1977).

[57] K. A. Chao, J. Spałek, and A. M. Oleś, J. Phys. C **20**, 27 (1977).

[58] J. Spałek, A. M. Oleś, and K. A. Chao, Phys. Status Solidi B **108**, 329 (1981).

[59] J. Kaczmarczyk, J. Bünemann, and J. Spałek, New J. Phys. **16**, 073018 (2014).

[60] J. Jędrak and J. Spałek, Phys. Rev. B **83**, 104512 (2011).

[61] D. Eichenberger and D. Baeriswyl, Phys. Rev. B **76**, 180504 (2007).

[62] K. Haule and G. Kotliar, Phys. Rev. B **76**, 104509 (2007).

[63] M. Civelli, M. Capone, A. Georges, K. Haule, O. Parcollet, T. D. Stanescu, and G. Kotliar, Phys. Rev. Lett. **100**, 046402 (2008).

[64] E. Gull and A. J. Millis, Phys. Rev. B **86**, 241106 (2012).

[65] M. Abram, J. Kaczmarczyk, J. Jędrak, and J. Spałek, Phys. Rev. B **88**, 094502 (2013).

[66] K. Andres, J. E. Graebner, and H. R. Ott, Phys. Rev. Lett. **35**, 1779 (1975).

[67] G. R. Stewart, Rev. Mod. Phys. **56**, 755 (1984).

[68] G. G. Lonzarich, J. Mag. and Mag. Mat. **76**, 1 (1988).

[69] A. J. Leggett, Rev. Mod. Phys. **47**, 331 (1975).

[70] K. Kadowaki and S. B. Woods, Solid State Communications **58**, 507 (1986).

[71] M. J. Rice, Phys. Rev. Lett. **20**, 1439 (1968).

[72] A. Auerbach and K. Levin, J. Appl. Phys. **61**, 3162 (1987).

[73] A. C. Hewson, *The Kondo Problem to Heavy Fermions* (Cambridge University Press, ADDRESS, 1993).

[74] Q. Si and F. Steglich, Science **329**, 1161 (2010).

[75] S. Doniach, Physica B+C **91**, 231 (1977).

[76] F. Steglich, J. Arndt, O. Stockert, S. Friedemann, M. Brando, C. Klingner, C. Krellner, C. Geibel, S. Wirth, S. Kirchner, and Q. Si, J. Phys.: Condens. Matter **24**, 294201 (2012).

[77] J. Spałek, Phys. Rev. B **37**, 533 (1988).

[78] J. Spałek, Phys. Rev. B **38**, 208 (1988).

[79] K. Byczuk, J. Spałek, and W. Wójcik, Phys. Rev. B **46**, 14134 (1992).

[80] M. M. Maśka, M. Mierzejewski, J. Kaczmarczyk, and J. Spałek, Phys. Rev. B **82**, 054509 (2010).

[81] M. Z. Asadzadeh, F. Becca, and M. Fabrizio, Phys. Rev. B **87**, 205144 (2013).

[82] O. Howczak, J. Kaczmarczyk, and J. Spałek, Phys. Status Solidi (b) **250**, 609 (2013).

[83] K. Masuda and D. Yamamoto, Phys. Rev. B **87**, 014516 (2013).

[84] M. Z. Asadzadeh, M. Fabrizio, and F. Becca, Phys. Rev. B **90**, 205113 (2014).

[85] J. R. Schrieffer and P. A. Wolff, Phys. Rev. **149**, 491 (1966).

[86] W. Metzner and D. Vollhardt, Phys. Rev. Lett. **62**, 324 (1989).

[87] A. Georges and G. Kotliar, Phys. Rev. B **45**, 6479 (1992).

[88] K. Byczuk, W. Hofstetter, and D. Vollhardt, Phys. Rev. Lett. **94**, 056404 (2005).

[89] G. Kotliar, S. Y. Savrasov, K. Haule, V. S. Oudovenko, O. Parcollet, and C. A. Marianetti, Rev. Mod. Phys. **78**, 865 (2006).

[90] H. Aoki, N. Tsuji, M. Eckstein, M. Kollar, T. Oka, and P. Werner, Rev. Mod. Phys. **86**, 779 (2014).

[91] M. A. Ruderman and C. Kittel, Phys. Rev. **96**, 99 (1954).

[92] T. Kasuya, Prog. Theor. Phys. **16**, 45 (1956).

[93] K. Yoshida, Phys. Rev. **106**, 893 (1957).

[94] R. Doradziński and J. Spałek, Phys. Rev. B **58**, 3293 (1998).

[95] R. Doradziński and J. Spałek, Phys. Rev. B **56**, R14239 (1997).

[96] O. Howczak and J. Spałek, J. Phys.: Condens. Matter **24**, 205602 (2012).

[97] P. Gegenwart, Q. Si, and F. Steglich, Nature Physics **4**, 186 (2008).

[98] F. M. Grosche, P. Agarwal, S. R. Julian, N. J. Wilson, R. K. W. Haselwimmer, S. J. S. Lister, N. D. Mathur, F. V. Carter, S. S. Saxena, and G. G. Lonzarich, J. Phys.: Condens. Matter **12**, L533 (2000).

[99] P. Pagliuso, R. Movshovich, A. Bianchi, M. Nicklas, N. Moreno, J. Thompson, M. Hundley, J. Sarrao, and Z. Fisk, Physica B **312–313**, 129 (2002).

[100] B. B. Zhou, S. Misra, E. H. da Silva Neto, P. Aynajian, R. E. Baumbach, J. D. Thompson, E. D. Bauer, and A. Yazdani, Nature Physics **9**, 474 (2013).

[101] M. P. Allan, F. Massee, D. K. Morr, J. S. Dyke, A. W. Rost, A. P. Mackenzie, C. Petrovic, and J. C. S. Davis, Nature Physics **9**, 468 (2013).

[102] J. S. Dyke, F. Massee, M. P. Allan, J. C. S. Davis, C. Petrovic, and D. K. Morr, Proc. Natl. Acad. Sci. **111**, 11663 (2014).

[103] B. D. White, J. D. Thompson, and M. B. Maple, Physica C **514**, 246 (2015).

[104] H. Q. Yuan, F. M. Grosche, M. Deppe, C. Geibel, G. Sparn, and F. Steglich, Science **302**, 2104 (2003).

[105] A. T. Holmes, D. Jaccard, and K. Miyake, Phys. Rev. B **69**, 024508 (2004).

[106] K. Miyake and Y. Onishi, J. Phys. Soc. Jpn. **69**, 355 (2000).

[107] S. Watanabe and K. Miyake, Phys. Rev. Lett. **105**, 186403 (2010).

[108] H. Yamaoka, Y. Ikeda, I. Jarrige, N. Tsujii, Y. Zekko, Y. Yamamoto, J. Mizuki, J.-F. Lin, N. Hiraoka, H. Ishii, K.-D. Tsuei, T. C. Kobayashi, F. Honda, and Y. Ōnuki, Phys. Rev. Lett. **113**, 086403 (2014).

[109] C. Petrovic, P. G. Pagliuso, M. F. Hundley, R. Movshovich, J. L. Sarrao, J. D. Thompson, Z. Fisk, and P. Monthoux, J. Phys.: Condens. Matter **13**, L337 (2001).

[110] C. Pfleiderer and A. D. Huxley, Phys. Rev. Lett. **89**, 147005 (2002).

[111] V. Taufour, D. Aoki, G. Knebel, and J. Flouquet, Phys. Rev. Lett. **105**, 217201 (2010).

[112] H. Kotegawa, V. Taufour, D. Aoki, G. Knebel, and J. Flouquet, J. Phys. Soc. Jpn. **80**, 083703 (2011).

[113] M. M. Wysokiński, M. Abram, and J. Spałek, Phys. Rev. B **90**, 081114(R) (2014).

[114] M. M. Wysokiński, M. Abram, and J. Spałek, Phys. Rev. B **91**, 081108(R) (2015).

[115] J. Bunemann, T. Schickling, and F. Gebhard, EPL **98**, 27006 (2012).

[116] J. Kaczmarczyk, Philosophical Magazine **95**, 563 (2014).

[117] J. Kaczmarczyk, T. Schickling, and J. Bünemann, Phys. Status Solidi B. (2015).

[118] M. M. Wysokiński, J. Kaczmarczyk, and J. Spałek, arXiv:1505.07003 (2015).

[119] K. Masuda and D. Yamamoto, Phys. Rev. B **91**, 104508 (2015).

[120] M. Abram, M. M. Wysokiński, and J. Spałek, J. Mag. and Mag. Mat. (2015), accepted for publication.

[121] M. M. Wysokiński, J. Kaczmarczyk, and J. Spałek, in preparation (2015).

[122] M. M. Wysokiński, Acta Phys. Pol. A **122**, 758 (2012).

[123] M. Wysokiński and J. Spałek, J. Appl. Phys. **113**, 163905 (2013).

[124] M. M. Wysokiński, Acta Phys. Pol. A **126**, A (2014).

[125] P. Gurin and Z. Gulácsi, Phys. Rev. B **64**, 045118 (2001).

[126] Z. Gulácsi, Phys. Rev. B **66**, 165109 (2002).

[127] Z. Gulácsi and D. Vollhardt, Phys. Rev. Lett. **91**, 186401 (2003).

[128] Z. Gulácsi and D. Vollhardt, Phys. Rev. B **72**, 075130 (2005).

[129] T. M. Rice and K. Ueda, Phys. Rev. Lett. **55**, 995 (1985).

[130] J. Bünemann, W. Weber, and F. Gebhard, Phys. Rev. B **57**, 6896 (1998).

[131] T. Schickling, J. Bünemann, F. Gebhard, and W. Weber, New Journal of Physics **16**, 093034 (2014).

[132] G. Seibold and J. Lorenzana, Phys. Rev. Lett. **86**, 2605 (2001).

[133] J. Jędrak, J. Kaczmarczyk, and J. Spałek, arXiv: 1008.0021 .

[134] F. Gebhard, Phys. Rev. B **41**, 9452 (1990).

[135] A. L. Fetter and W. J. D., (Dover Publications, New York, ADDRESS, 2003).

[136] B. S. Shivaram, D. G. Hinks, M. B. Maple, M. A. deAndrade, and P. Kumar, Phys. Rev. B **89**, 241107 (2014).

[137] B. S. Shivaram, B. Dorsey, D. G. Hinks, and P. Kumar, Phys. Rev. B **89**, 161108 (2014).

[138] A. McCollam, S. R. Julian, P. M. C. Rourke, D. Aoki, and J. Flouquet, Phys. Rev. Lett. **94**, 186401 (2005).

[139] D. Aoki, W. Knafo, and I. Sheikin, Comptes Rendus Physique **14**, 53 (2013).

[140] M. Wysokiński, J. Jędrak, J. Kaczmarczyk, and J. Spałek, AIP Conf. Proc. **1485**, 319 (2012).

[141] M. M. Wysokiński, Master Thesis, Jagiellonian University (2011).

[142] A. B. Shick and W. E. Pickett, Phys. Rev. Lett. **86**, 300 (2001).

[143] R. Settai, M. Nakashima, S. Araki, Y. Haga, T. C. Kobayashi, N. Tateiwa, H. Yamagami, and Y. Onuki, J. Phys: Condens. Matter **14**, L29 (2002).

[144] A. Huxley, I. Sheikin, E. Ressouche, N. Kernavanois, D. Braithwaite, R. Calemczuk, and J. Flouquet, Phys. Rev. B **63**, 144519 (2001).

[145] N. Kernavanois, B. Grenier, A. Huxley, E. Ressouche, J. P. Sanchez, and J. Flouquet, Phys. Rev. B **64**, 174509 (2001).

[146] D. Belitz, T. R. Kirkpatrick, and J. Rollbühler, Phys. Rev. Lett. **94**, 247205 (2005).

[147] T. R. Kirkpatrick and D. Belitz, Phys. Rev. B **85**, 134451 (2012).

[148] R. Troć, Z. Gajek, and A. Pikul, Phys. Rev. B **86**, 224403 (2012).

[149] P. Aynajian, E. H. da Silva Neto, A. Gyenis, R. E. Baumbach, J. D. Thompson, Z. Fisk, E. D. Bauer, and A. Yazdani, Nature **486**, 201 (2012).

[150] G. E. Blonder, M. Tinkham, and T. M. Klapwijk, Phys. Rev. B **25**, 4515 (1982).

[151] G. E. Blonder and M. Tinkham, Phys. Rev. B **27**, 112 (1983).

[152] Y. Tanaka and S. Kashiwaya, Phys. Rev. Lett. **74**, 3451 (1995).

[153] V. L. Ginzburg, Rev. Mod. Phys. **76**, 981 (2004).

[154] J. E. Hirsch, Phys. Rev. B **58**, 8727 (1998).

[155] C. W. J. Beenakker, Phys. Rev. Lett. **97**, 067007 (2006).

[156] M. Zegrodnik and J. Spałek, Phys. Rev. B **86**, 014505 (2012).

[157] M. Zegrodnik, J. Spałek, and J. Bünemann, New J. Phys. **15**, 073050 (2013).

[158] J. Spałek and M. Zegrodnik, J. Phys.: Condens. Matter **25**, 435601 (2013).

[159] M. Zegrodnik, J. Bünemann, and J. Spałek, New J. Phys. **16**, 033001 (2014).